

The background is a grayscale scanning electron microscope (SEM) image showing numerous spherical, porous particles with a textured surface. A white outline of a bottle is centered at the top, and a white outline of a water drop is centered at the bottom. A white rectangular box with a thin border is positioned in the middle of the image, containing the title and subtitle.

Waste PET-MOF- Cleanwater

Waste PET-Derived Metal-Organic
Framework (MOFs) as Cost-effective
Adsorbents for Removal of Hazardous
Elements from Polluted Water

Jianwei Ren, Philiswa Nosizo Nomngongo
& Tien-Chien Jen (Editors)



Waste PET–MOF– Cleanwater

Waste PET-Derived Metal-Organic Framework
(MOFs) as Cost-effective Adsorbents for
Removal of Hazardous Elements from
Polluted Water

Jianwei Ren, Philiswa Nosizo Nomngongo &
Tien-Chien Jen (Eds)



UJ Press

*Waste PET-MOF-Cleanwater :
Waste PET-Derived Metal-Organic Framework (MOFs) as Cost-Effective Adsorbents for
Removal of Hazardous Elements from Polluted Water*

Published by UJ Press
University of Johannesburg
Library
Auckland Park Kingsway Campus
PO Box 524
Auckland Park
2006
<https://ujonlinepress.uj.ac.za/>

Compilation © Jianwei Ren, Philiswa Nosizo Nomngongo & Tien-Chien Jen 2022
Chapters © Individual contributors 2022
Published Edition © Jianwei Ren, Philiswa Nosizo Nomngongo & Tien-Chien Jen 2022
First published 2022

<https://doi.org/10.36615/9781776419463>

978-1-7764194-5-6 (Paperback)

978-1-7764194-6-3 (PDF)

978-1-7764194-7-0 (EPUB)

978-1-7764194-8-7 (XML)

This publication had been submitted to a rigorous double-blind peer-review process prior to publication and all recommendations by the reviewers were considered and implemented before publication.

Copy editor: Sigwabusuku Mafu

Cover design: Hester Roets, UJ Graphic Design Studio

Typeset in 10/13pt Merriweather Light





Contents

Preface	i
Jianwei Ren, Philiswa Nosizo Nomngongo & Tien-Chien Jen	
Chapter 1: More MOFs, less mess: State-of-art and MOFs application perspectives	1
Bożena Sartowska, Wojciech Starosta, Janwei Ren, Philiswa Nosizo Nomngongo	
Chapter 2: Synthesis of zirconium porous sorbents from waste PET flakes	19
Wojciech Starosta, Jianwei Ren, Philiswa Nosizo Nomngongo	
Chapter 3: Batch, fixed-bed column and hybrid microfiltration process studies of radiocesium removal from contaminated water by nanocomposite SiEA-KNiFe sorbent	33
Dagmara Chmielewska-Śmietanko, Agnieszka Miśkiewicz	
Chapter 4: MOF-assisted membrane process for removal of radionuclides and other hazardous elements from aqueous solutions	45
Agnieszka Miśkiewicz, Grażyna Zakrzewska-Kołtuniewicz, Wojciech Starosta	
Chapter 5: The production of prototypical MOFs from waste-PET provides a stepping-stone towards MOFs-based water-harvesting applications	57
Jianwei Ren, Tien-Chien Jen, Wojciech Starosta, Bożena Sartowska, Philiswa Nosizo Nomngongo	

Chapter 6: Nanocomposite membranes for the removal of dyes	79
Azile Nqombolo, Anele Mpupa, Jianwei Ren, Philiswa Nosizo Nomngongo	
Chapter 7: Application of various metal-organic frameworks in analytical methods: recent trends and future perspectives	93
Philiswa Nosizo Nomngongo, Azile Nqombolo, Jianwei Ren, Tien-Chien Jen, Wojciech Starosta, Bożena Sartowska	
Chapter 8: Post-synthetic modification of zirconium terephthalate sorbents and their application for sorption of selected toxic elements from water	125
Rafał Walczak, Iga Zuba, Wojciech Starosta, Jianwei Ren	
Chapter 9: Reuse of waste PET bottles through the production of activated carbon, an adsorbent to remove radionuclides from aqueous solutions	141
L. Fuks, I. Herdzik-Koniecko, M. Rogowski	
Chapter 10: Nanoporous carbon adsorbents derived from PET waste for the adsorption of environmental contaminants in aqueous matrices	159
Tshimangadzo S. Munonde, Philiswa Nosizo Nomngongo	
Chapter 11: Techno-economic feasibility assessment on the viability of using waste PET (trays and coloured bottles) to produce Metal-Organic Frameworks (MOFs)	171
Jianwei Ren, Tien-Chien Jen, Wojciech Starosta, Bożena Sartowska, Philiswa Nosizo Nomngongo	



Preface

Jianwei Ren , Philiswa Nosizo Nomngongo 
& Tien-Chien Jen 

University of Johannesburg

In counties like South Africa, the waste PET stream has posed a serious environmental problem, and the current recycling of waste PET remains as low as 30%. The waste PET recycling industries such as PETCO and Extrupet (South Africa) are struggling to implement innovative processes to operate profitably.

Furthermore, metal-organic frameworks (MOFs) are a new class of porous materials. The MOFs-based water treatment promises to provide cost-effective solutions to deal with polluted water. However, the high costs of MOFs production have created a challenge for its effective implementation. Regardless, cross-cutting advances in materials and engineering will help to solve these societal challenges. To maintain a world-class research and development associated with human capacity in South Africa, this multi-disciplinary and transdisciplinary work has been strengthened by the basic applied research continuum under the frame of South Africa (NRF)/Poland (NCBR) Joint Science and Technology Research Collaboration.

Since a circular economy refers to an economic system aimed at eliminating waste and the continual use of resources, this monograph will discuss the potential circular economy for waste PET towards water treatment through the elimination of the waste PET streams and continual use of recycled resources. It starts from the perspective on waste PET recycling in South Africa and the real market-driven needs. The concept of MOFs production from waste PET is approved through a series of process development and optimisation work. Then, application-oriented customisation is conducted based on the MOF materials with tailored properties.

Lastly, the techno-economic feasibility assessment on the viability of using waste PET (trays and coloured bottles) to produce MOFs materials is carried out. These interesting topics address some of the needs of the real world and provide new insights for readers, stakeholders, and decision-makers with the formation, characterisation, and utilisation of waste PET-derived MOFs materials. More importantly, this project can be

Waste PET-MOF-Cleanwater

a critical stepping-stone, enabling the wider MOFs-based practices in our real world.

Editors

Johannesburg, South Africa, 2022

Chapter 1

More MOFs, less mess: State-of-art and MOFs application perspectives

Bożena Sartowska ^a, Wojciech Starosta ^a, Janwei Ren ^b,
Philiswa Nosizo Nomngongo ^{c, d}

^a *Institute of Nuclear Chemistry and Technology,
Dorodna 16, 03-195 Warsaw, Poland*

^b *Department of Mechanical Engineering Science University of
Johannesburg, Cnr Kingsway and University Road, Auckland Park,
Johannesburg 2092, South Africa*

^c *Department of Chemical Sciences, University of Johannesburg,
Doornfontein Campus, P.O. Box 17011, Johannesburg,
2028, South Africa*

^d *Department of Science and Innovation–National Research Foundation
South African Research Chair Initiative (DSI–NRF SARChI), Nanotechnology for
Water, University of Johannesburg, Doornfontein 2028, South Africa*

Abstract

Metal-organic frameworks (MOFs) is a class of compounds consisting of metal ions or clusters coordinated to organic ligands to form one-, two-, or three - dimensional structures. MOFs are formed by anchoring metal-containing units or secondary-building units (SBUs) with organic linkers. Open frameworks that show exceptional features of permanent porosity, stable framework, enormous surface area, and pore volume are obtained. Due to these properties, MOFs are of interest for many different applications, including storage of gases, gas purification, gas separation, water remediation, and catalysis. They can also be used as conducting solids and supercapacitors. The wide range of different applications makes MOFs very important materials in our lives, for example, in areas of health, environment, and energy.

In this work, the set of MOFs information is presented.

1. Definitions

When you search for information: “What is metal-organic framework (MOF)?”, you can receive the answer: “Full text search our database of 158 300 titles for metal-organic framework (MOF) to find related research papers.” It means that metal-organic framework (MOF) is under immense investigation in various places around the world. Different definitions for the MOF abbreviation can be found.

1.1. O.M. YAGHI in *J. Am. Chem Soc.* 1996, 118, 295–296 (Yaghi & Li 1996: 295–296)

The successful assembly of extended frameworks from molecular building units has delivered a remarkable class of materials with a diverse architecture and function. These include metal-organic solids with open frameworks, having zeolite-like attributes, and others having important electronic and magnetic properties.

This definition was proved with the simplest strategies employed in the production of 3-D networks. In each case, the assembly is accompanied by the inclusion of a guest molecule G, which occupies the voids (Figure 1).

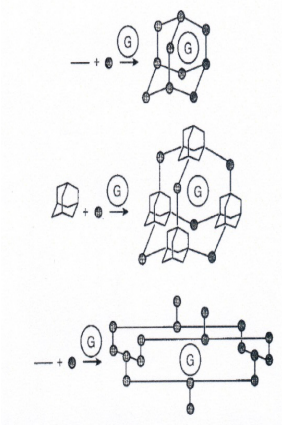


Figure 1: A schematic representation of the assembly of metal ions (dark spheres) and organic ligands (dark rods) or metal tetrahedral cluster to yield diamond-like frameworks (top and middle) or open frameworks with rectangular channels (bottom)

- 1.2. S.T. BATTEN in *Pure Applied Chemistry* 2013, 85, 8, 1715–1724 (Batten, Champness, Chen, Garcia-Martinez, Kitagawa, Ohrstrom, O’Keeffe, Suh & Reedijk 2013:1715–1724)

A metal-organic framework abbreviated as MOF, is a coordination network with organic ligands containing potential voids. This wording accounts for the fact that many systems are dynamic, and changes in structure and thus corresponding changes in potential porosity or solvent and/or guest-filled voids may occur depending on temperature, pressure, or other external factors. For these reasons, it is also not required for a MOF to be crystalline. Arguments based on both theory and experiment can suggest that some of these coordination polymers with direct anion-cation binding are more prone to form structures with open frameworks exhibiting permanent porosity than those forming positively charged networks. However, the grey zone between these extremes is large and increasing so that a definition based on such a charge distinction would be too restrictive. The archetypal MOFs structures are shown in Figure 2.

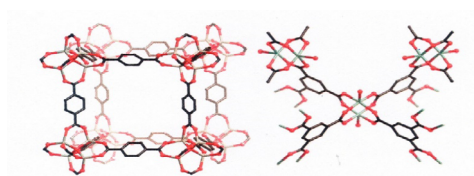


Figure 2: Archetypal MOFs: (left) the zinc and carboxylate-based MOF-5 where each $[Zn_4O]$ unit is bridged by six benzene-1,4 dicarboxylates; (right) HKUST-1 with copper paddlewheel dimers bridged by benzene-1,3,5-tricarboxylates. Colours description: light grey - Zn; turquoise - Cu; grey - C; red - O. Hydrogen atoms are not shown.

- 1.3. E. SHARMIN in *Introductory Chapter in Metal Organic Frameworks (MOFs)*, published by INTECH, 2016 (Sharmin & Zafar 2016:3–16)

MOFs as defined by Yaghi *et al.* are porous structures constructed from the coordinative bonding between metal ions and organic linkers or bridging ligands. The interesting feature is their porosity that allows the diffusion of guest molecules into the bulk structure. The shape and size of pores govern the shape and size selectivity of the guest to be incorporated. A simple MOF structure is shown in Figure 3.

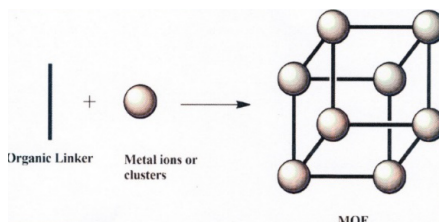


Figure 3: Structure of a MOF

1.4. Methods of MOFs naming

There are methods of naming the metal-organic frameworks (MOFs) structures. Nomenclature of metal-organic frameworks can be presented, for example, in the following ways:

1.4.1. Jemal Mohammed Yassin, Haramaya University

1. naming by Sequential Number of Synthesis; for example, MOF-n (metal-organic framework), RPF-n (Rare-earth Polymeric Framework), MPF-n (Metal Peptide Framework), etc.
2. naming by Initials of Institution or Place of Discovery; for example, HKUST-n, MIL-n, NU-n, NENU-n, SNU-n, JUC-n, CPO-n, and POST-n, etc.
3. naming by Sequence of Isostructural Synthesis, for example, IRMOF-n and also their other unclear mechanisms.

1.4.2. Andreas Schneemann, Technische Universität Dresden

Naming MOFs is completely up to a scientist; there is no real consensus in the literature. Some people use an abbreviation highlighting their university or place of origin (UiO, MIL, STAM, UMCM, SNU, or DUT) while some use an abbreviation describing the material (MOF, ZIF, MAF, PIZOF, CID, or PCN), and some people just use the formula unit (Fe_2dobdc , $\text{Zn}_2\text{bdc}_2\text{dabco}$, $\text{Fe}_2\text{dobdc}_n$, or $\text{Zn}_2\text{bdc}_2\text{dabco}_n$). The formula unit can be used if it is not complicated, so that everybody understands what it means. However, how a MOF is called upon publication is completely up to the scientist. As long as it makes sense, it is acceptable.

2. Structures

The presence of organic and inorganic primary building blocks (PBUs, i.e. organic linkers and metallic centres) in the structure of MOFs allows their potential application in several distinct fields due to the improved properties resulting from the symbiotic combination of these two different components. Porosity is undoubtedly the most desired property.

In this context, a great evolution has been observed concerning the pore/cage sizes leading to the isolation of several highly porous MOF structures. Examples are shown in Figure 4. Formed by the three-dimensional crystalline assembly of inorganic metal ions and organic ligand, MOFs enable a flexible structure design in which well-defined pore sizes, surfaces area and functionalities can be tailored by selecting different building blocks. This high degree of customisability of MOFs properties has attracted the interest of many researchers. To date, there are more than 20 000 different examples of structures of MOFs being reported and studied (Yap, Fow & Chen 2017:218–245), (Silva, Vilele, Tome & Paz 2015:6774–6803)

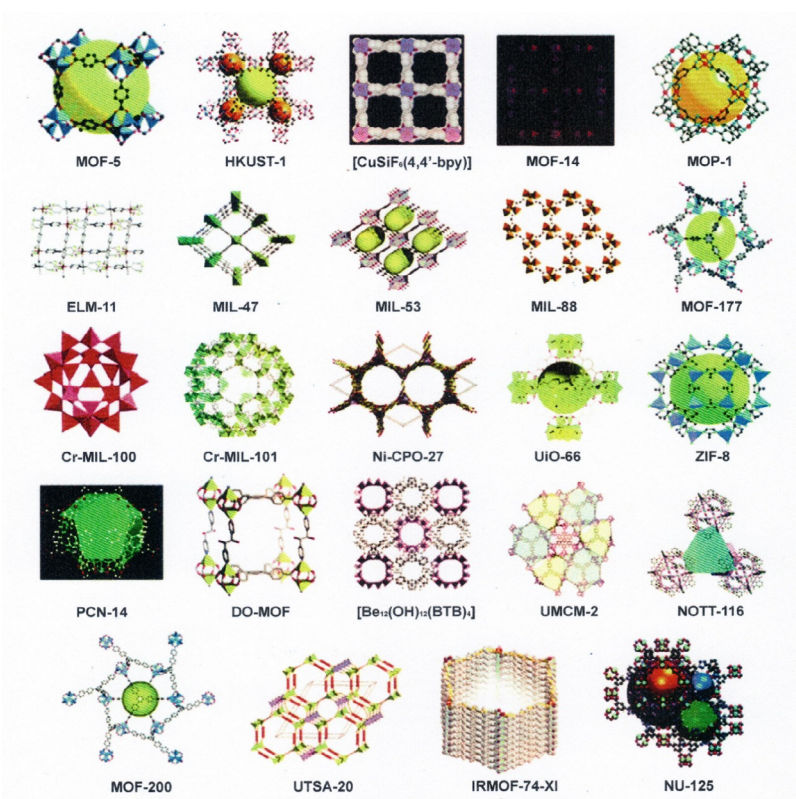


Figure 4: Porous MOFs prepared by several research groups aiming for accommodation or retention of chemical species in their pores/channels (Silva *et al* 2015:6774)

3. MOFs drop of history

Synthetic zeolites – comprised solely of inorganic components, such as silicates and aluminates – have been extensively studied since the 1940s. It was not until the late 1980s and early 1990s that the first crystalline porous materials with pore size larger than 1 and 2 nm were reported. In 1995, a unique class of crystalline porous materials termed “metal-organic frameworks (MOFs)” by Yaghi, emerged and has since distinguished itself with permanent porosity and high surface areas, due to the strong bonds between metal ions and charged organic ligands. The highly tunable inorganic and organic building units of MOFs have opened up a new chapter in design and applications of porous materials. In addition to the various possible combinations of inorganic and organic building units with different geometries and functionalities, MOFs offer unparalleled adaptability in isorecticular manipulation. While keeping the structural design and topology invariant, a vast number of alterations in their structures and functionalities can be readily accessed during synthesis or via post-synthetic modifications. Over the past few decades, over 100 000 structures have been reported in the “MOF subset” of the Cambridge Structural Database (CSD) and the number of MOF-related research publications has been continuously increasing. Figure 5 shows the number of MOFs structures and reports in defined years. Numerous representative high-porosity MOFs are indicated in the plot according to the year they were reported. The first use of supercritical CO₂ drying for activation MOFs is indicated in yellow (Zhang, Chen, Liu, Hanna, Wang, Taher-Ledar, Malek, Li & Farha 2020:7406–7427).

MOF chemistry is not a static field; new classes of MOFs are and will be constantly developed.

Authors try to develop transparent and objective criteria to quantify how different a novel material is with respect to the state of the art. For example, the pore geometry was selected as novelty and is presented in Figure 6. For each year, the average of relative distance in the geometry descriptor space to the MOFs reported in the Cambridge Structural database (CSD) in the preceding years is shown in red line. The MOFs with the largest distance for some of the peaks are shown in coordination polymers reported in CSD before the beginning of the MOF chemistry as a separate field of research, shown in red (Moosavi, Nandy, Jablonka, Ongari, Janet, Boyd, Lee, Smit & Kulik 2020:4068–4078).

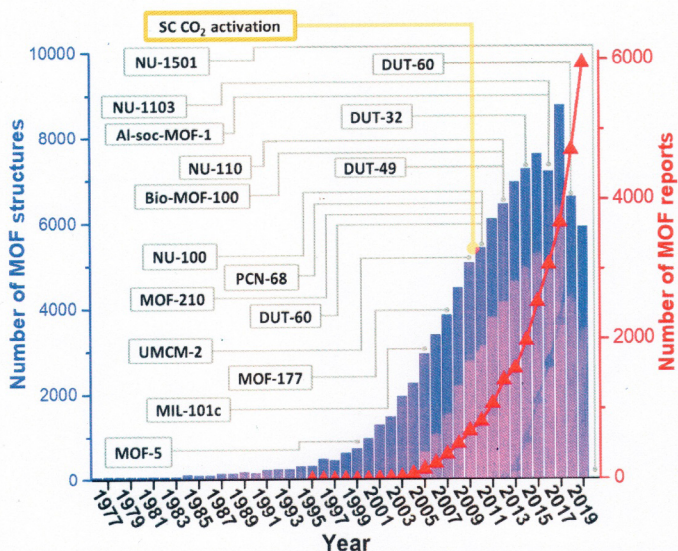


Figure 5: The number of MOFs in the Cambridge Structural Database (CSD) and MOF reports found in WoS, 1976–2019. The structural data was summarised from the MOF CSD subset of May 2020 (Zhang et al. 2020:7406)

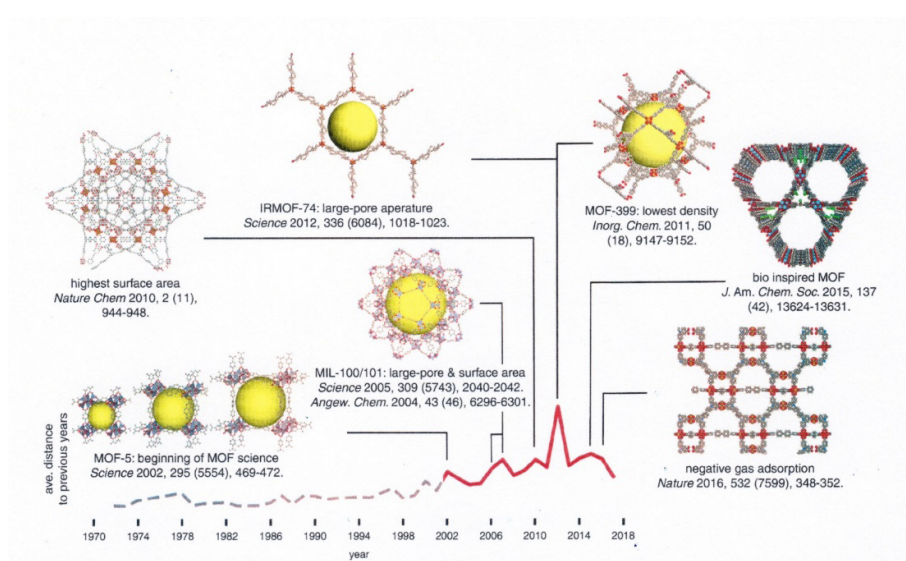


Figure 6: Timeline of evolution of MOF geometry (Moosavi et al. 2020:4068)

4. Methods of MOFs formation/production

Most of MOF synthesis are performed in the liquid state. The metal salt and ligand solvent are separately prepared and then mixed or metal salt and ligand are added to the solvent. In general, organic solvents, such as dimethylformamide, acetonitrile, acetone, diethylformamide, ethanol, and methanol are used. Since a solvent affects the properties of MOFs, it must be selected according to the desired characteristics of the targeted MOFs. The synthesis methods can be determined according to the solvent, the characteristics of the MOF, the required pore and particle size of the MOF, and laboratory conditions. The methods of synthesising MOFs are summarised in Figure 7 (Heo, Do, Ahn & Kim 2020:2061–2092).

4.1. Solvothermal synthesis

Solvothermal methods are the most common techniques of synthesizing MOFs with various morphologies. Organic solvent or a mixture of metal salt solution reacts with organic ligands. Solvothermal synthesis is performed at a temperature higher than the boiling point of the solvent, and a relatively high yield of MOF materials can be obtained. The solvothermal synthesis route has advantages of precisely controlling the morphologies, crystallinity, and the size of produced materials. On the other hand, the solvothermal method has disadvantages, because it is a complex process that requires the removal of solvent molecules from the pores.

4.2. Microwave-assisted synthesis

Microwave-assisted synthesis is widely used as a quick and simple method of generating MOFs. The driving force of this synthesis is microwave power. This synthesis method has a short reaction time and gives highly crystalline and porous textures and allows precise shape control and particle size reduction.

4.3. Slow evaporation

The slow evaporation method produces MOFs by gradually concentrating a precursor dissolved in a solvent or mixture of solvents by evaporation in an inert atmosphere. The slow evaporation method requires seven days to seven months of synthesis time without external energy.

4.4. Mechanochemical synthesis

Mechanochemical synthesis causes a chemical reaction that occurs due to the mechanical agitation and impact interactions between materials.

The reaction can proceed without the use of carcinogenic, toxic, or environmentally harmful organic solvent.

4.5. Sonochemical synthesis

This is a method of synthesising MOFs by utilising sonic waves. When the reactive mixture is exposed to ultrasonic waves, the molecules are chemically altered to produce compounds with new morphologies and unique properties.

4.6. Electrochemical synthesis

Since electrochemical synthesis does not require a metal salt, the anion associated with metal salt is not present; therefore, a high-purity substance can be obtained. In this method, metal ions are supplied through the oxidation of electrodes. When an appropriate voltage or current is applied, the metal dissolves and the metal ions necessary for MOF formation are released from the electrode surface. These metal ions immediately react with the linker present in the solution and a MOF is formed in proximity to the electrode surfaces.

Other ways of synthesizing MOFs include diffusion, spray drying, and ionothermal synthesis.

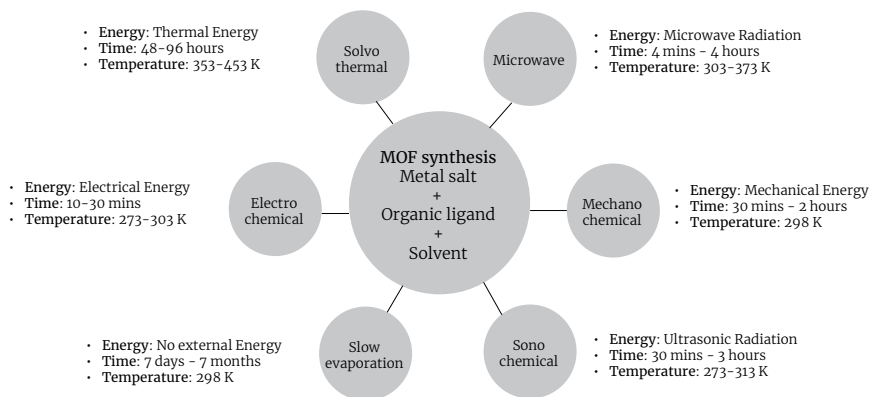


Figure 7: Summary of various MOF synthesis methods (Heo *et al.* 2020:2061)

5. Commercial MOFs

Besides scientific works on MOFs, there are some MOFs producers already. This means that MOFs required for specific applications are commercially available.

5.1. ProfMOF (Norway) (<https://profmof.com/>)

The company provides world-class metal-organic frameworks (MOFs) for industrial applications. Its MOFs can be applied to a wide array of industrial processes. The products have unique characteristics and provide high stability, high porosity, and functionalisation. The company offers some types of MOFs. For example:

1. UiO-66-ADC, Zr-acetylenedicarboxylate, $[\text{Zr}_6\text{O}_4(\text{OH})_4(\text{C}_4\text{O}_4)_{6-x}]$
SA (BET) = $648 \text{ m}^2 \text{ g}^{-1}$, pore volume = $0,30 \text{ cm}^3 \text{ g}^{-1}$, thermal stability = 300°C , particle size = $0,1-0,5 \mu\text{m}$
2. UiO-66-BDC, Zr-benededicarboxylate, $[\text{Zr}_6\text{O}_4(\text{OH})_4(\text{C}_8\text{H}_4\text{O}_4)_6]$
SA (BET) = $1266 \text{ m}^2 \text{ g}^{-1}$, pore volume = $0,52 \text{ cm}^3 \text{ g}^{-1}$, thermal stability = 400°C , particle size = $0,2-0,5 \mu\text{m}$

5.2. Merck (Germany) (<https://www.sigmaaldrich.com/PL/pl/technical-documents/technical-article/materials-science-and-engineering/photovoltaics-and-solar-cells/metal-organic-frameworks>)

The company offers MOFs under the tradename Basolite™. These materials provide a wide selection of different pore shapes and sizes, different metals (Al, Cu, Fe, and Zn), and different organic linkers (BDC, BTC, mIM). For example: Basolite® C 300, Cu-BTC MOF, HKUST-1, copper benzene-1,3,5-tricarboxylate with the empirical formula (Hill Notation): $\text{C}_{18} \text{H}_6 \text{Cu}_3 \text{O}_{12}$, can be found in their offer.

5.3. novoMOF (Switzerland) (<https://novomof.com/>)

The novoMOF is a company active in the field of advanced materials with a focus on synthesis and production of metal-organic frameworks (MOFs). The company produces any MOF at the required speed, scale, and quality. It scales the production of ordered metal-organic from grams to kilograms.

6. MOFs application areas

MOFs' important properties are: low density, high surface area, tunable pore functionality, and structural flexibility. These properties make MOFs useful in a wide area of prospective applications. Many of the studies performed on MOFs still focus on the possibility of adsorbing in the empty space and releasing molecules like hydrogen and carbon dioxide. Several studies are aimed at possible emerging applications, as listed below.

6.1. According to Pettinari *et al*, MOFs application can be divided into groups (Pettinari, Marchetti, Mosca, Tosi & Drozdov 2017:731–744). These are:

1. Gas storage and delivery
2. Biomedical applications
3. Catalytic applications
4. Luminescence properties
5. Sensing applications
6. Water, air, and fuel purification and horticulture
7. For magnetic materials
8. Electrochemical applications
9. MOFs membranes
10. Conductive MOFs
11. Polymer-MOF composites

6.2. According to Safaei, application of metal organic frameworks can be divided into groups (Safaei, Foroughi, Ebrahimipoor, Jahani, Omid & Khatami 2019:401–425)

1. Adsorption in aqua solutions, including biological compounds, antibiotics, and toxic pollution
2. Gas adsorption
3. Catalysts, including photocatalysts, electrocatalysts, and biocatalyst
4. Sensors, including electrochemical sensors, photoelectrochemical sensors, and biosensors
5. Electrochemical charge storage, including batteries, supercapacitors, and fuel cells
6. Drug delivery systems.

It is evident that there are similar points in Pettinari's and Safaei's works. These are:

1. Gas storage and delivery and gas adsorption
2. Water, air, and fuel purification and horticulture and toxic pollution remediation
3. Sensing applications and sensors

7. Gases applications area

As mentioned in point 6, MOFs applications in gases area are very important and needed.

7.1. Hydrogen storage

Hydrogen is a promising vehicle fuel due to its high specific energy, renewability, and its ability to be produced and oxidised without CO₂ emissions. But due to the low volumetric density of H₂ gas, the efficient and cost-effective storage of hydrogen remains a challenge. Storage in solid adsorbents has received significant attention as an alternative to compression in high-pressure tanks. Adsorbents have the potential to match or surpass the capacities typical for physical storage systems while doing so at lower pressures and with the potential to reduce costs. MOFs are perhaps the most intensively researched hydrogen adsorbents. Work was carried out to develop crystal structures of MOFs whose hydrogen was assessed experimentally following their identification by computational screening (Ahmed, Seth, Purewa, Wong-Foy, Veenstra, Matzger & Siege 2019:1568 –1577), (Ren, Musyoka, Langmi, Wartbooi, North & Mathe 2015:4617–4622).

7.2 Carbon capture

The energy demands of a global society are being met largely by combustion of fossil fuels, including coal, petroleum, and natural gas. A major greenhouse gas, carbon dioxide, is a key by-product of such combustion. The immense quantity of CO₂ emission has resulted in serious environmental issues, such as global warming, oceans acidification, extreme weather, and species extinction. The employment of MOFs in CO₂ capture and conversion applications has undergone three development stages:

1. the CO₂ adsorption capacity and selectivity of MOFs were tuned;
2. development of MOF-based materials and their use for the conversion of CO₂ to organic products; and
3. exploration and expansion of the scope of possible CO₂ transformation reactions involving MOF-based materials. MOF-based materials are already showing great potential as the next generation of CO₂ capture and conversion systems (Choe, Kim & Hong 2021:5172–5185), (Ding Flaig, Jiang & Yaghi 2019:2783–2830).

7.3. Gas separation

The separation and purification processes are critical for the modern chemical industry. The processes isolate pure components from chemical mixtures, which accounts for about half of industrial energy consumptions. Gas separation is widely involved in the production of bulk chemicals for manufacturing fuels, plastics, and polymers. A significant

number of important separations have been achieved by making use of MOFs as adsorber materials. Microporous MOFs for gas separation, pore engineering through the functionalisation strategies is confirmed as a powerful tool for efficient separation of different gases (Lin, Xiang, Xing, Zhou & Chen 2019:87–103). Examples of such uses/applications are listed below.

1. Separation of linear alkanes from their branched isomers can boost octane ratings in gasoline, which is a very important process in the petroleum industry.
2. Kinetic separation of D_2/H_2 ; deuterium is a stable isotope of hydrogen that has a number of commercial and scientific applications. The isotopic separation in deuterium is necessary for deuterium production due to its low abundance (0.0156% of all the naturally hydrogen).
3. Separation of C_2H_2/C_2H_4 ; ethylene (C_2H_4) is an essential raw chemical widely used in the manufacture of many polymers and useful chemicals. Acetylene is one important by-product/impurity of about 1% concentration. It can seriously affect the polymerisation of ethylene during production of polyethylene. Acetylene can be explosive in defined conditions. During the ethylene production, acetylene must be reduced to an acceptable low level.
4. Sulphur dioxide capture, the efficient capture of SO_2 is very important for gas purification processes, including flue and exhaust gases desulfurisation and natural gas purification
5. Separation of C_2H_2/CO_2 ; acetylene (C_2H_2) is an important source of many chemical products. CO_2 impurity during the production of C_2H_2 occurs and exists. Both compounds have almost identical sizes, shapes, and physical properties. The exploitation of efficient physical C_2H_2 adsorbent is demanded.

8. Water applications area

8.1. Desalination

Globally, the demand for fresh water is increasing due to population growth and water contamination. The portion of drinkable water on Earth is less than 1%, and seawater accounts for more than 97%. Desalination is the technology of separating salts from water to produce drinkable water and it is considered as one of the major solutions for water shortage. The desalination process also involves removing salt ions from the saline source to produce potable water or high purity water for industrial uses. MOFs can be applied for liquid separation and water treatment. The examples

of techniques and MOF contributions to this process are: capacitive deionisation, forward osmosis, adsorption desalination, reverse osmosis, MOF membranes, and membrane distillation (Kahdom & Deng 2018:219–230), (Lee, Hann & Park 2020:16319–16326).

8.2. Water vapour capture and dehumidification

Continuous globalisation of a better standard of living leads to the consumption of excessive amounts of energy, such as for indoor air-conditioning in regions with extreme temperatures. Air-conditioning devices based on thermally-driven adsorption heat pumps or desiccant cooling systems are considered to operate with moderate consumption of electric power. The working principle is governed by reversible exothermic adsorption and endothermic desorption of water in micro- or mesoporous solid materials. Porous materials with distinct water sorption and remarkable water uptake are ideal for humidity control in confined and poorly ventilated spaces. Advances in MOF chemistry have permitted several strategies for the synthesis of water-stable MOFs. Hydrolytically stable and recyclable MOFs with superior total water uptake remain a point of intensive research in MOF chemistry. MOF type materials stable in water can be mentioned here: Zr-MOFs, chromium-based MOFs, and Al (Cr)-soc-MOF-1 (Abtab, Alezi, Bhatt, Shkurenko, Balmabkhout, Aggarwal, Weselinski, Alsadun, Samin, Hedhili & Eddaoudi 2018:94–105).

8.3. Water purification

Clean and sustainable freshwater is a basic requirement for daily life and industrial activities. The rapid growth in the global population and the never-ending industrialisation have increased the consumption of clean water, directly produced a huge volume of wastewater, and caused severe pollution of water resources. The degree of overall water pollution largely exceeds the self-purification ability of the natural water ecosystem. Several water-stable MOFs have been demonstrated in recent years. These have been increasingly explored for water treatment, typically including the MIL family, UiO-66 series, zirconium, and pyrazole-based MOFs. These water-stable MOFs usually have strong coordination bonds which can prevent the potential destruction of metal-ligand bonds in water/moisture containing environment (Gu, Ng, Zhao & Wang 2020: 04092–040115).

9. Works performed in PET-MOF-CLEANWATER project

Project PET-MOF-CLEANWATER is realised in the frame of joint research programme between the National Research Foundation (NRF), South Africa

and the Polish National Centre for Research and Development (NCBR). The project is a cooperation in the area of water and green technology. The title of the project is: “The Studies on Waste PET-derived Metal-Organic Frameworks (MOFs) As Cost-effective Adsorbents for Removal of Hazardous Elements from Polluted Water.” The project acronym is: PET-MOF-CLEANWATER. It shows three parts of the project: (i) PET - Polyethylene terephthalate, (ii) MOF - Metal Organic Framework, (iii) CLEANWATER - clean water. This project is important for three reasons: (i) PET waste reduction, (ii) water purification from radioactive ions and heavy metals, and (iii) joint works with bilateral cooperation. More information on this project was shared during the first workshop organised on 16 October, 2019 at the Institute of Nuclear Chemistry and Technology in Warsaw. The presented information and results were shown in the PET-MOF-CLEANWATER project monography. The monography was edited by Wojciech Starosta and Bożena Sartowska, and published by the Institute of Nuclear Chemistry and Technology in 2020 (Starosta & Sartowska 2020)

10. Perspectives /possibility

10.1. New proposal

The BATMOF project is prepared and ready for use. Project title: “Evaluation of Metal-Organic Frameworks (MOFs)-mediated Process for Recycling Spent Li-ion Batteries”, with an acronym BATMOF. The subject is connected with the general topic: “Recycling and Re-use of End-of-Life Products”. Joint works were made with participants organised in the consortium: University of Johannesburg, South Africa; Institute of Nuclear Chemistry and Technology, Poland; National Institute for Cryogenics and Isotopic Technologies ICSI-Rm. Valcea ICSI Energy, Romania; ULENA Sp. z o.o., Poland; and the University of Limpopo, South Africa. The project objectives are:

1. Development and optimisation of the process using waste PET-derived organic linker as collector to selectively capture the particular metal ions (i.e. Mn) from the dissolved Li-ion batteries solution and form MOFs materials (i.e. Mn-MOF).
2. Process design and validation of using the waste PET-derived MOF membranes to selectively filter out raw materials in the dissolved Li-ion batteries solutions.
3. Numerical simulation and evaluation.

10.2. Possible PET-MOF-CLEANWATER continuation

A joint research programme between the National Research Foundation (NRF) of South Africa and the Polish National Centre for Research and Development (NCBR) is in progress. The aims of the programme are:

1. to support (through a co-funding model) joint research projects between South African and Polish researchers,
2. to facilitate the development of sustainable institutional links between partners of the two countries, and
3. to foster new linkages and engagements with small teams of young researchers for new links between South Africa and Poland. Areas of cooperation are: health sciences, agriculture, biosciences and biotechnology, environment and climate change, water and green technology, maritime economy, clean coal technology, and information and communication technology. According to this project history, in 2015 the first programme saw the acceptance of six projects accepted. In 2018, during the second programme, 10 projects were accepted. In 2022, the new joint research programme between the National Research Foundation (NRF) of South Africa and the Polish National Centre for Research and Development (NCBR) is expected.

We predict that MOF subjects mentioned above will be very interesting for our work's continuation and use of scientific teams' experience.

11. Conclusions

1. Metal-Organic Frameworks – MOFs – are considered as a new member of porous materials that have recently attracted attention to materials chemistry.
2. To date, there are more than 100 000 different structures of MOFs being reported and studied, as well as 50 000 modelled structures.
3. Five main areas are defined for the MOFs applications: adsorption, catalysts, sensors, electrochemical charge storage, and drug delivery systems. These examples are applicable and relevant to many other applications of MOFs.
4. Current and future MOFs structures are and can be applied in clearing away, cleaning up, tidying up, and putting in order our lives in different areas: environment, health and medicine, and science.
5. The phrase MORE MOFs – LESS MESS is true.

References

- Abtab SkMdT SM. 2018. Reticular Chemistry in Action: A Hydrolytically Stable MOF Capturing Twice Its Weight in Adsorbed Water. *Chem*, 4:94–105. <https://doi.org/10.1016/j.chempr.2017.11.005>
- Ahmed A. 2019. Exceptional hydrogen storage achieved by screening nearly half a million metal–organic frameworks. *Nature Communications*, 10:1568–1577. <https://doi.org/10.1038/s41467-019-09365-w>
- Batten ST. 2013. Terminology of metal–organic frameworks and coordination polymers (IUPAC Recommendations 2013). *Pure and Applied Chemistry*, 85(8):1715–1724. Choe JH. 2021. MOF–74 type variants for CO₂ capture. *Materials Chemistry Frontiers*, 5:5172–5185. <https://doi.org/10.1039/D1QM00205H>
- Ding M. 2019. Carbon capture and conversion using metal–organic frameworks and MOF–based materials. *Chemical Society Review*, 48:2783–2830. Gu Q. 2020. Metal–Organic Frameworks (MOFs)–boosted filtration membrane technology for water sustainability. *APL Materials*, 8:04092–040115. <https://doi.org/10.1039/C8CS00829A>
- Heo DY. 2020. Metal–Organic Framework Materials for Perovskite Solar Cells. *Polymers*, 12:2061–2193. <https://doi.org/10.3390/polym12092061>
<https://profmof.com/>
<https://novomof.com/>
<https://www.sigmaaldrich.com/PL/pl/technical-documents/technical-article/materials-science-and-engineering/photovoltaics-and-solar-cells/metal-organic-frameworks>
- Kahdom M. 2018. Metal–organic frameworks (MOFs) in water filtration membranes for desalination and other applications. *Applied Materials Today*, 11:219–230. <https://doi.org/10.1016/j.apmt.2018.02.008>
- Lee SJ. 2020. Seawater Desalination Using MOF–Incorporated Cu–Based Alginate Beads without Energy Consumption. *ASC Applied Materials Interfaces*, 12:1631916326. <https://doi.org/10.1021/acsami.9b22843>
- Lin RB. 2019. Exploration of porous metal–organic frameworks for gas separation and purification. *Coordination Chemistry Reviews*, 378:87–103. <https://doi.org/10.1016/j.ccr.2017.09.027>
- Moosavi SH. 2020. Understanding the diversity of the metal–organic framework ecosystem. *Nature Communications*, 11:4068–4077. <https://doi.org/10.1038/s41467-020-17755-8>

- Pettinari C. 2017. Application of metal-organic frameworks. *Polymer International*, 66:731–744. <https://doi.org/10.1002/pi.5315>
- Ren J. 2015. A more efficient way to shape metal-organic framework (MOF) powder materials for hydrogen storage applications. *Int. J. Hydrogen Energy*, 40(13), 4617–4622. <https://doi.org/10.1016/j.ijhydene.2015.02.011>
- Safaei M. 2019. A review on metal-organic frameworks: Synthesis and applications. *Trends in Analytical Chemistry*, 118:401–425. <https://doi.org/10.1016/j.trac.2019.06.007>
- Sharmine E. 2016. Introductory Chapter in Metal-Organic Frameworks (MOFS). *Metal-Organic Frameworks* published by INTECH. <https://doi.org/10.5772/64797>
- Silva P. 2015. Multifunctional metal-organic frameworks: from academia to industrial applications. *Chem. Soc. Rev.*, 44: 6774–6803. <https://doi.org/10.1039/C5CS00307E>
- Starosta W. ed. 2020. PET-MOF-CLEANWATER PROJECT. Monography published by the Institute of Nuclear Chemistry and Technology ISBN 978-83-946412-3-8
- Yaghi OM. 1996. T-Shaped Molecular Building Units in the Porous Structure of $\text{Ag}(4,4'\text{-bpy})\cdot\text{NO}_3$. *J. Am. Chem. Soc.*, 118:295–296. <https://doi.org/10.1021/ja953438l>
- Yap MH. 2017. Synthesis and applications of MOF-derived porous nanostructures. *Green Energy and Environment*, 2:218–245. <https://doi.org/10.1016/j.gee.2017.05.003>
- Zhang X. 2020. A historical overview of the activation and porosity of metal-organic frameworks. *Chem. Soc. Rev.*, 49:7406–7427. <https://doi.org/10.1039/D0CS00997K>



Chapter 2

Synthesis of zirconium porous sorbents from waste PET flakes

Wojciech Starosta ^{a*}, Jianwei Ren ^b,
Philiswa Nosizo Nomngongo ^{c,d}

^a*Institute of Nuclear Chemistry and Technology, 03-195
Warsaw, Dorodna 16, Poland*

^b*University of Johannesburg, Johannesburg, Kingsway and University Road,
Auckland Park, 2092, P.O. Box 524, Auckland Park, 2006,
Johannesburg, South Africa*

^c*Department of Chemical Sciences, University of Johannesburg,
Doornfontein Campus, P.O. Box 17011, Johannesburg, 2028,
South Africa, 2028, South Africa*

^d*Department of Science and Innovation–National Research Foundation
South African Research Chair Initiative (DSI-NRF SARChI), Nanotechnology for
Water, University of Johannesburg, Doornfontein 2028, South Africa*

**Corresponding author. Email: w.starosta@iuchtj.waw.pl*

1. Introduction

Polyethylene terephthalate (PET) is a thermoplastic polymer synthesised by polycondensation of terephthalic acid and ethylene glycol monomers. Developed in 1942, it found its way into fiber production. The advances in polymer processing in the 1970s, in particular the development of injection stretch blow molding process, made the mass production of beverage bottles possible. Since then, PET polyester has been an excellent choice as a material in many industries. Factors such as its chemical resistance, strength-to-weight ratio, shatterproof properties, and low cost to product, make it an accessible solution for consumable product packaging [1].

The widespread use and high consumption of PET plastics, low biodegradability, and low recycling rates resulted in rapid increase in the volume of PET waste. Existing PET recycling technologies (chemical, mechanical, and incineration) have not been sufficiently applied in practice. Chemical PET depolymerisation to terephthalic acid for reuse

in PET production faces a price barrier due to the difficulty of delivering a product with the desired purity at a competitive price. The mechanical reprocessing of waste PET to pellets is limited to the low number of cycles due to the degradation of mechanical properties in subsequent cycles of recycling. The incineration of PET requires the removal of toxic gaseous pollutants and doesn't match the requirements of a circular economy. For these reasons, landfilling is at present a common practice for the PET waste management. This poses a serious threat to the environment in the long term due to the slow release of microplastic particles and toxic chemicals [3–5].

The development of new economically efficient ways to recycle PET waste is of paramount importance. Such a proposal is the concept of using waste PET as a linker source for the synthesis of porous metal-organic sorbents. It is worth noting that PET polymer contains a significant amount of terephthalic acid (86 wt %). This ligand is frequently used for the synthesis of valuable porous metal-organic framework materials (MOF), for example, UiO-66, MIL-53, MIL-101. MOFs are considered as materials with a broad spectrum of applications, for example, in the field of gas storage, gaseous mixture separations, heavy metal removal from solutions etc. The possibility of synthesis of selected MOFs using direct PET flakes or terephthalic ligand recycled from PET has already been demonstrated [6,7]. The review on the concept of PET recovery from PET bottles for reuse in MOFs synthesis has been recently published [8].

The aim of the PET-MOF-CLEANWATER project is to investigate the possibility of using PET waste for the synthesis of organometallic compounds of MOF type and to demonstrate the usefulness of such obtained sorbents for the removal of toxic elements from water. Two possibilities are explored in the course of the project. The first consists of recovering terephthalic acid using chemical methods of PET depolymerisation. The recovered terephthalic acid would then be used to synthesise MOF type sorbents. The zirconium terephthalate UiO-66 is mainly considered here due to its high chemical stability over a wide pH range and a high tolerance to structural defects that can be of the missing ligand or missing cluster type. The tolerance to defects is an important property as it ensures the stability of the structure during the process of its functionalisation. The functionalisation process is aimed at incorporating into the structure a functional group showing a chemical affinity for the metal to be adsorbed. The functionalisation process can be carried out at the synthesis stage or after its completion [9–11]. In the first case, a ligand containing a single coordinating group and a side functional group not participating in the coordination is added to the reaction mixture. In the second case, the structure building ligands are exchanged with another

ligand containing coordinating groups and the desired side functional group. Ligand exchange is carried out in solution after the completion of the primary synthesis.

The second possibility explored in the project is to synthesise sorbents directly from PET flakes using environmentally friendly solvents. The development of such a process would enable the simplification of the synthesis, saving of chemicals and, as a result, increase the economic efficiency of sorbents synthesis. An additional benefit would be the opportunity to reduce problematic PET waste and use the products made from it for environmental purposes.

The paper presents results of work carried out on:

- different PET depolymerisation methods and application of the recovered terephthalic acid for the synthesis of UiO-66 sorbents,
- synthesis of zirconium sorbents and zirconium sorbent precursors in acetic acid and acetone solutions directly from PET flakes,
- synthesis of UiO-66 sorbent in gamma-valerolactone solvent,
- functionalisation of sorbents applying modulated synthesis and post-synthetic ligand exchange methods, and
- evaluation of the suitability of the produced materials for mercury sorption from aqueous solutions.

2. Synthesis of UiO-66 sorbents using terephthalic acid recovered by PET chemical depolymerisation

The general synthesis scheme is shown in Figure 1. In the first step, PET flakes cut out from light-blue coloured water bottles were depolymerised using alkaline or neutral hydrolysis methods. Four different variants of depolymerisation were used:

1. depolymerisation under reflux at 190 °C in a mixture of water and ethylene glycol. In typical synthesis 22 g PET, 8.7 g NaOH, 100 ml H₂O, 87 ml ethylene glycol were used (sample s1),
2. alkaline hydrolysis under reflux at 120 °C in 8M water solution of sodium hydroxide (sample s2),
3. alkaline depolymerisation in hydrothermal reactor at 170°C, 180 °C, and 190 °C. In typical synthesis 6 g PET, 8 g NaOH and 150 ml of water were used (sample s3), and
4. neutral hydrolysis in hydrothermal reactor in water at 200°C, typically 16 g PET were used (sample s4).

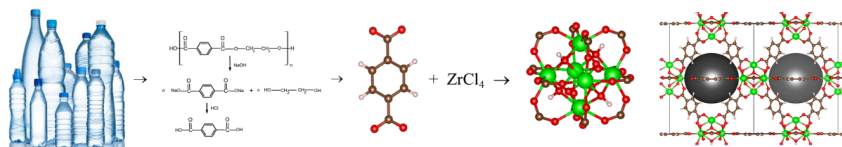


Figure 1: The scheme of the synthesis of UiO-66 sorbent using waste PET-derived terephthalic acid.

After the completion of the alkaline depolymerisation reaction, the resulting solution was diluted with water and subjected to filtration. Terephthalic acid was recovered from the filtrate by precipitation with sulfuric acid. The high efficiency around 95% was obtained except in the case of alkaline hydrolysis under reflux at 120°C. The NMR and X-ray diffraction spectra measured for the obtained materials confirmed their compliance with terephthalic acid offered commercially by Sigma-Aldrich.

In order to confirm the practical usefulness of the obtained depolymerisation products, UiO-66 sorbents were synthesised using recycled terephthalic acid. The synthesis of UiO-66 was carried out according to the procedures described in the literature. DMF was used as solvent and zirconium chloride as metal source. Synthesis was carried out at 120 °C on oil bath in Pyrex bottle. The diffraction spectra of the resulting products shown in Figure 2 confirmed an excellent agreement with that of the UiO-66 structure. The porous nature of synthesis products was confirmed by BET measurements. Values in the range of 1200 – 1300 m²/g were obtained for the specific surface area.

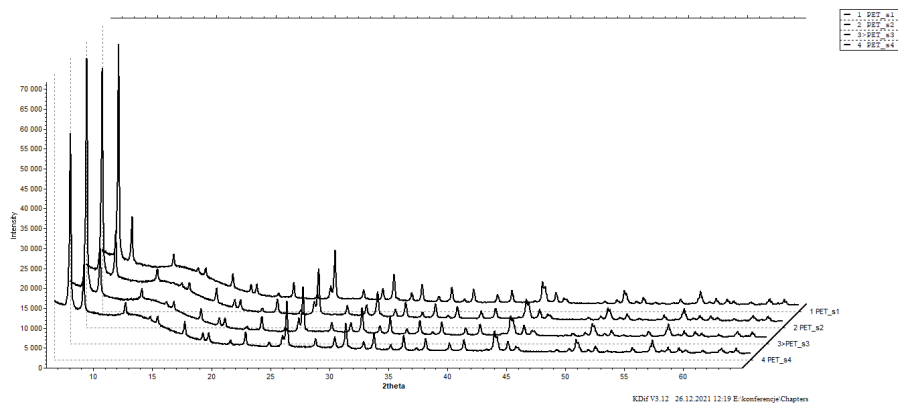


Figure 2: XRD diffraction spectra of the UiO-66 structure synthesised with terephthalic linker obtained by waste PET depolymerisation using different variants of this process (sample s1, s2, s3, s4).

The sorbents obtained were functionalised with mercaptoacetic acid. The functionalisation was carried out by soaking the sorbent in 0.1 M mercaptoacetic acid solution in DMF or ethanol at 80°C for a few hours with continuous stirring. The sorption capacity tests were carried out in batch mode contacting 15 mg of sorbent with 10 ml of water mercury chloride solution with a concentration of 0.01M for 2 hours. The sorbent was then recovered by filtration on a track-etched membrane and used for structural and elemental content studies. The morphology of the sorbent was retained after functionalisation and after mercury sorption as shown in SEM image in Figure 3. The elemental content analysis by EDS method confirmed the successful mercaptoacetic acid ligand embedding in the sorbent and adsorption of the mercury on the sorbent. The average value of the molar ratio of sulphur to zirconium content after functionalisation was equal to 1.06 and mercury to zirconium molar ratio after sorption was 0.51.

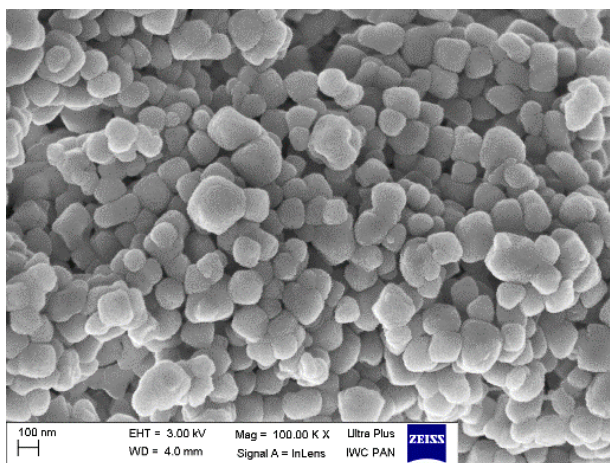


Figure 3: SEM image of sorbent (sample1) after functionalization with mercaptoacetic acid and mercury sorption.

For the quick determination of mercury accumulated on sorbent, we used the X-ray fluorescence spectroscopy. Fluorescence studies were performed on a home-made instrument equipped with a low-power rhodium X-ray tube operating at 40 kV. The ratio of areas under the $L\alpha$ line of mercury line and $K\alpha$ line of zirconium allows the determination of the relative content of mercury to zirconium. For the determination of absolute value of mercury to zirconium ratio calibration standards were prepared.

The X-ray fluorescence spectra of sorbent (sample s1) after mercury sorption is shown in Figure 4.

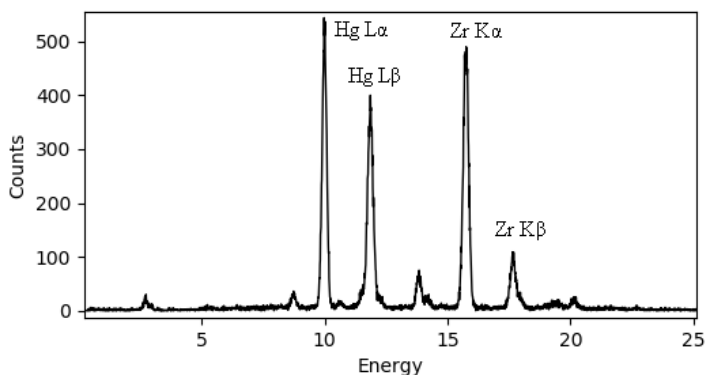


Figure 4: X-ray fluorescence spectrum of sorbent (sample s1) after mercury sorption. The intensities ratio of mercury L_{β} line to zirconium K_{α} line is equal to 0.906 (estimated molar ratio Hg/Zr = 1.17)

3. **Synthesis of zirconium sorbents directly from PET flakes**

Dimethylformamide (DMF), commonly used solvent for MOF synthesis, is considered toxic and harmful for the environment. Developing a method of synthesis using a different solvent is paramount for larger than laboratory-scale applications. The synthesis of zirconium MOF with hexagonal structure using direct waste PET in formic acid and acetone mixture has been reported in [12]. Our research indicates the possibility of solvothermal synthesis of porous zirconium structure directly from PET flakes in a pressure reactor in acetic acid and acetone mixture at temperatures in the range 160 – 190°C. In typical synthesis 1 g of PET (5 mM) flakes, 1.15 g of $ZrCl_4$ (5 mM), 75 ml of acetic acid and 75 ml of acetone were used. The X-ray diffraction spectrum of material obtained, measured on PETRA III/P02.1 line of DESY (Hamburg) synchrotron at $\lambda = 0.20735 \text{ \AA}$ is shown in Figure 5. The spectrum obtained agrees well with the X-ray diffraction spectrum of zirconium complex with terephthalic acid, possessing hexagonal close-packed structure with parameters $a=b=14.71731 \text{ \AA}$, $c=36.9794 \text{ \AA}$, $\gamma=120^\circ$ already reported in the literature. The structural building unit for this structure containing 12 zirconium atom clusters which can be interpreted as fused two octahedral clusters known from UiO-66 structure, is presented in Figure 6. The obtained structure was porous and BET measurements gave the value of $524.30 \text{ m}^2/\text{g}$ for the specific surface area. We also found that the structure has sorption properties for ruthenium from water solution and after functionalisation with mercaptoacetic acid or mercaptosuccinic acid also for mercury (see Table I)

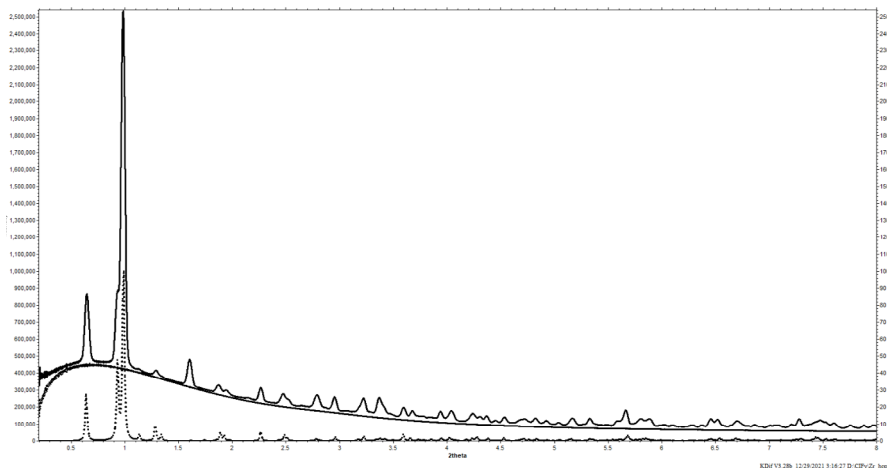


Figure 5: XRD diffraction spectra of Zr hcp structure measured at PETRAIII/ P02.1 synchrotron line in Hamburg at $\lambda = 0.20735 \text{ \AA}$ (upper), empty capillary (middle) and XRD spectrum calculated for Zr_hcp structure (dotted line)

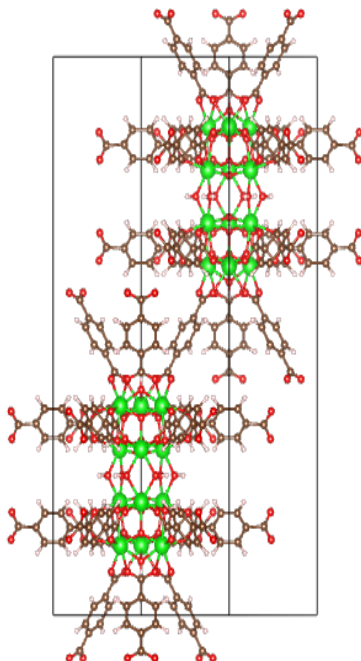


Figure 6: A view of the unit cell of zirconium hcp structure, (zirconium – green, oxygen – red, carbon – gray).

Continuing the research on the search for new synthesis methods, we found that it is possible to convert PET to fine powder at a low temperature of 120°C in acetic acid/ acetone solution and also in acetic acid solution alone in the presence of zirconium ions. In typical synthesis 1g of PET flakes, 1,61 g of $ZrOCl_2 \cdot 8H_2O$, 40 ml of acetic acid or 20 ml of acetic acid and 20 ml of acetone were used. The synthesis was done on an oil bath in Pyrex 100 ml bottles. The crystalline nature of the material obtained was confirmed by X-ray diffraction studies (Figure 7) and SEM microscopic examinations (Figure 8).

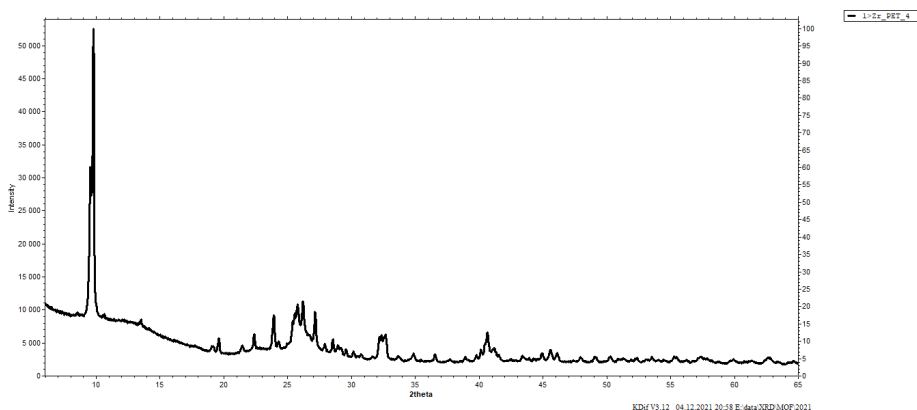


Figure.7: XRD spectrum of material synthesized directly from PET flakes at 120°C in acetic acid/acetone mixture.

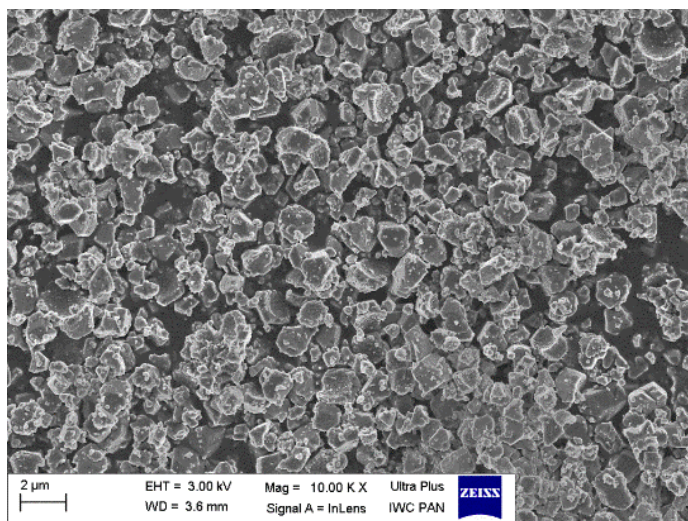


Figure 8: SEM image of material obtained from PET flakes in acetic acid/acetone mixture at 120°C.

The crystal structure of the material obtained is currently being investigated. It is worth noting that in the observed spectrum, the reflections belonging to PET or terephthalic acid are not visible. We suppose that the resulting material can be zirconium complex with mixed, terephthalic acid, and acetic acid ligands. Such complexes synthesised from zirconium chloride and terephthalic acid in acetic acid have been reported recently [13–14]. We have also found that the material synthesised may serve as a precursor for the synthesis of mercury sorbent. We performed functionalisation of this material using five different ligands (mercaptosuccinic acid, mercaptoacetic acid, L-cysteine, EDTA and thiosalicylic acid) in ethanol or DMF at 60°C. The relative intensities of mercury to zirconium measured by X-ray fluorescence method are presented in Table I.

Table 1: The results of an evaluation of the sorption capacity of the materials synthesised at different temperatures and after functionalisation.

Ligand	$I_{\text{Hg}}/I_{\text{Zr}}$
Synthesised in acetic acid/acetone mixture at different temperatures	
170°C, mercaptoacetic acid	0.336
180°C, mercaptoacetic acid	0.294
Synthesised at temperature 120°C and functionalised with	
Mercaptosuccinic acid	0.103
Mercaptoacetic acid	0.136
L-cysteine	0.481
EDTA	0.086
Thiosalicylic acid	0.224

The functionalised sorbent shows fast kinetics. The results of the sorption kinetics study for sorbent synthesised at 120°C and functionalised with mercaptosuccinic acid are shown in Figure 9. The data of activity remaining in the solution were obtained by the radiotracer method using mercury ^{107}Hg isotope. A good approximation to experimental data was achieved using the second-order kinetics model.

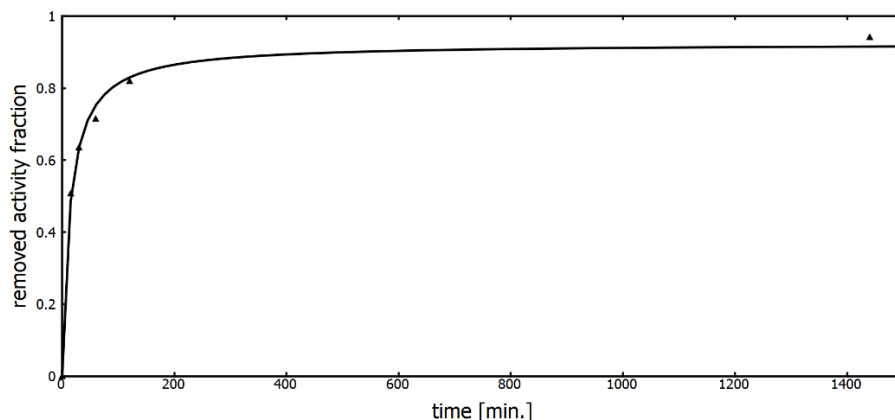


Figure 9: The time dependence of mercury activity removal from water solution for sorbent synthesised at 120°C using waste PET flakes and functionalised with mercaptosuccinic acid.

4. Synthesis of UiO-66 sorbent in GVL (gamma-valerolactone)

Gamma-valerolactone is a colourless liquid boiling at 230°C. It is obtained from levulinic acid and is considered an environmentally friendly solvent. Structural scheme of gamma-valerolactone is shown in Figure 10.

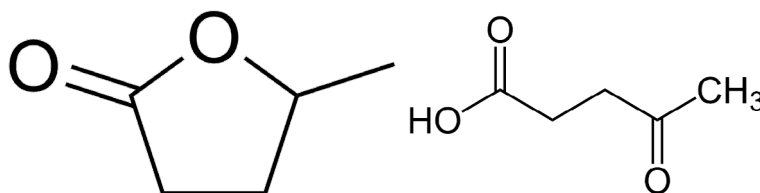


Figure 10: Structural scheme of gamma-valerolactone (left) and levulinic acid (right)

The synthesis of UiO-66 structure was performed in a Pyrex bottle at 120°C in 25 ml GVL using 5.4 mM $ZrOCl_2 \cdot 8H_2O$, 5.4 mM of terephthalic acid and 6 ml of formic acid used as modulator. The mass of the obtained product was equal to 0.81 g (0.54 efficiency). The SEM picture of the product showing regular crystals is presented in Figure 11.

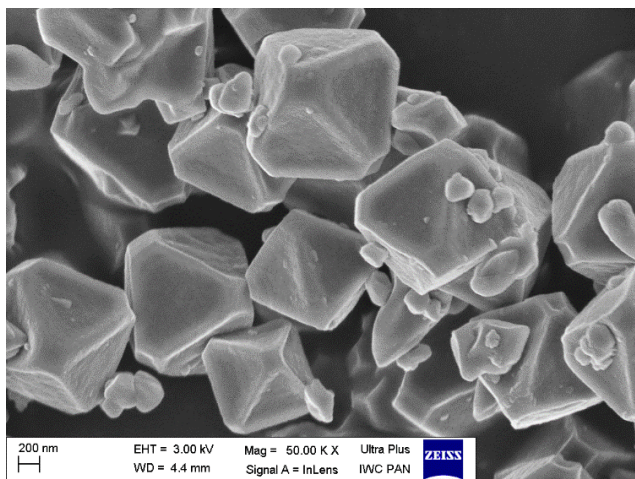


Figure 11: SEM picture of UiO-66 synthesised in gamma-valerolactone.

The sorbent was functionalised in a post-synthetic process with mercaptosuccinic acid and sorption kinetic of modified sorbent was studied using the radiotracer method. 10 ml of 0.01M water solution of mercury chloride was contacted with 15 mg of sorbents and activities remaining in the solution were measured at different times. The results showing the amount of mercury activity accumulated on sorbent are presented in Figure 12. The best fitting was obtained using the Elovich kinetics model, which assumes that the rate of adsorption of solute decreases exponentially as the amount of adsorbed solute increases.

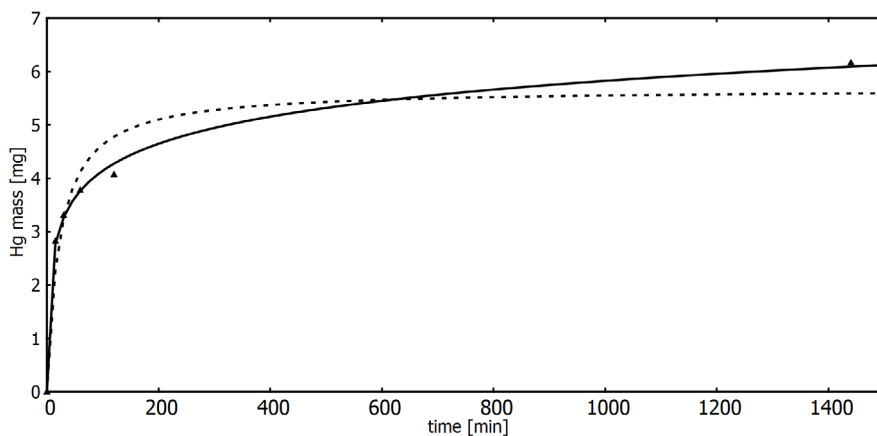


Figure 12: Time dependence of mercury activity accumulated on sorbent. Solid line – Elovich model, dashed line – second order kinetic model.

5. Conclusions

A synthesis of valuable UiO-66 type sorbents for toxic elements removal from water using waste PET as a linker source is possible. In the course of the project, different methods of PET waste utilisation for the synthesis of UiO-66 -based sorbents and their functionalisation were tested. The two routes seem to be possible for large-scale environmentally friendly synthesis. The first, one is based on depolymerisation of waste PET using chemical methods and on the usage of recovered terephthalic acid for UiO-66 synthesis using the environmentally friendly solvent, for example, GVL. The second one is based on the direct synthesis of sorbents from PET waste flakes. The acetic acid/acetone mixture at different ratios can be used for that purpose in the presence of zirconium salt. It has been shown that the decomposition of PET flakes to fine powder is possible in pure acetic acid at temperature as low as 120°C in the presence of zirconium salts. The resulting powder can serve as the precursor which can be converted to a usable sorbent after functionalisation. However, additional research studies are necessary to find optimal reaction parameters and determine phase purity of resulting material and efficiency of the process.

The understanding of the sorption mechanisms, especially their dependence on structural and morphological parameters of the sorbent is important for the development of practical applications.

Synchrotron- based methods for the study of nanomaterials like total scattering and pair distribution function (PDF) determination and high-resolution powder diffraction (HRPD) may be helpful to explore these possibilities.

6. Acknowledgements

We acknowledge:

- DESY (Hamburg, Germany), a member of the Helmholtz Association HGF, for the provision of experimental facilities. Parts of this research were carried out at PETRA III, beamline P02.1 within the rapid access program 2021A under proposal ID RA1-200010270.
- The financial support from The Polish National Centre for Research and Development under the PET-MOF-CLEANWATER Project. The studies on waste PET-derived metal-organic framework (MOFs) as cost-effective adsorbents for removal of hazardous elements from polluted water has been gratefully acknowledged.



References

1. Geyer, B et al., Recycling of poly (ethylene terephthalate) – A review focusing on chemical methods, *eXPRESS Polymer Letters* 10, 7 (2016) 559–586. <https://doi.org/10.3144/expresspolymlett.2016.53>
2. Damayanti et al., Strategic Possibility Routes of Recycled PET, *Polymers* 2021, 13, 1475. <https://doi.org/10.3390/polym13091475>
3. Takada, H. and Bell, L. Plastic Waste Management Hazards. International Pollutants Elimination Network (IPEN), 2021.
4. Barnard, E, Arias, R and Thielemans, W. Chemolytic depolymerisation of PET: A Review, *Green Chemistry*, 23,11(2021) 3765–3789. <https://doi.org/10.1039/D1GC00887K>
5. Vollmer, I et al., Beyond Mechanical Recycling: Giving New Life to Plastic Waste, *Angew. Chem. Int. Ed.*, 59, 36 (2020) 15402–15423. <https://doi.org/10.1002/anie.201915651>
6. Dyosiba, X et al., Feasibility of Varied Polyethylene Terephthalate Wastes as a Linker Source in metal-organic Framework UiO-66(Zr) Synthesis, *Ind. Eng. Chem. Res.*, 58, 36 (2021) 17010 –17017. <https://doi.org/10.1021/acs.iecr.9b02205>
7. Ren, J et al., Green synthesis of chromium-based metal-organic framework (Cr-MOF) from waste polyethylene terephthalate (PET) bottles for hydrogen storage applications, *International Journal of Hydrogen Energy*, 41, 40 (2016) 18141–18146. <https://doi.org/10.1016/j.ijhydene.2016.08.040>
8. El-Sayed, M, et al., Waste to MOFs: Sustainable Linker, Metal and Solvent Source for Value-added MOF Synthesis and Applications, *Green Chemistry*, 22, 2 (2020) 4082–4104. <https://doi.org/10.1039/D0GC00353K>
9. Schaate, A et al., Modulated Synthesis of Zr-Based Metal–Organic Frameworks: From Nano to Single Crystals, *Chem. Eur. J.* 17 (2011) 6643–6651. <https://doi.org/10.1002/chem.201003211>
10. Forgan, R, Modulated Self-assembly of Metal–organic Frameworks, *Chem. Sci.*, 11, (2020) 4546. <https://doi.org/10.1039/D0SC01356K>
11. Cohen, S, Postsynthetic Methods for the Functionalization of Metal–Organic Frameworks, *Chem, Rev.*, 112, 2 (2012) 970–1000. <https://doi.org/10.1021/cr200179u>
12. Zhou, L et al., Direct synthesis of robust hcp UiO-66(Zr) MOF Using poly (ethylene terephthalate) Waste as Ligand Source, *Microporous and Mesoporous Materials*, 290 (2019) 109674. <https://doi.org/10.1016/j.micromeso.2019.109674>

13. Leubner, L et al. Expanding the Variety of Zirconium-based Inorganic Building Units for Metal Organic Frameworks, *Angew. Chem. Int. Ed.*, 58 (2019) 10995–11000. <https://doi.org/10.1002/anie.201905456>
14. Leubner et al., Design and Precursor-based Solid State Synthesis of Mixed Linker Zr-MIL-140A, *Journal of Materials Chemistry*, 59, 20 (2020) 15250–15261. <https://doi.org/10.1021/acs.inorgchem.0c02221>

Chapter 3

Batch, fixed-bed column and hybrid microfiltration process studies of radiocesium removal from contaminated water by nanocomposite SiEA-KNiFe sorbent

Dagmara Chmielewska-Śmietanko ^a, Agnieszka Miśkiewicz ^a

^a *Institute of Nuclear Chemistry and Technology,
Dorodna 16, 03-195 Warsaw, Poland*

1. Introduction

Currently, there are more than 440 nuclear fission reactors in 30 countries generating about 12% of the world's supply of electricity [1, 2]. Most of the commercial nuclear power reactors are light water reactors (LWRs). One of the three types of LWRs is the pressurised water reactor (PWR), which is the most common construction of nuclear reactors and constitutes about 60% of the world's nuclear power plants [3]. In a PWR, light water serves as a coolant which removes the heat produced inside the reactor core by the nuclear fission reaction. Moreover, in PWR, water is also a moderator which slows down neutrons that are released during the nuclear fission process [4].

In fuel material (uranium oxide), due to fission reaction, new chemical species which influence the mechanical properties of the fuel ceramics and fuel clads are formed. The concentration of caesium in spent fuel from LWR can exceed 5 g kg^{-1} [5]. Many radionuclides form aqueous complexes that are soluble in cooling water. Moreover, water favours the dissolution of the rod/fuel matrix, which leads to the release of radionuclides trapped in the fuel matrix [6]. Furthermore, iodine may also induce stress corrosion cracking in zirconium alloys, which can lead to clad failure and fission products (^{137}Cs , ^{134}Cs) release into the primary water-cooling circuit [7].

Water is also the most common medium used to store spent fuel after being removed from the reactor core. Fuel rods are stored in a

pond for over 20 years and if stored, spent fuel assemblies have defects fission products (^{137}Cs , ^{134}Cs , ^{90}Sr and ^{131}I) represent the main part of water activity [8, 9].

Caesium radioisotopes present in cooling water in the primary water circuit of the nuclear reactor and in the water in spent fuel storage pools are responsible for the main part of activity of water in the cooling loop of PWRs as well as in the spent fuel storage pools. Radiocaesium is the main threat to humans and the environment, because of the highest contribution in low-level radioactive waste (LLRW), long half-life, relatively high energy gamma radiation, and high mobility [10]. The important isotopes are ^{134}Cs (half-life 2.1 years) and ^{137}Cs (half-life 30.0 years). ^{134}Cs and ^{137}Cs contribute strongly to LLRW activity during the first decades or centuries after fuel discharge [11].

Caesium is a metal from the alkali metal group with chemical similarity to sodium and potassium [11]. Caesium is present in a solution as a free hydrated cation Cs^+ with little or no tendency to create soluble complexes [12]. Soil with a large surface area composed of small porous mineral and organic particles has more potential for radionuclides to react chemically. Caesium is strongly bound by material with ion-exchange properties like clays or zeolites [11].

Caesium may remain dissolved or be adsorbed on sediments. Next, it can be taken up by fish or animals. Caesium is easily bound by plant roots from the solution and can be translocated to the shoots. Plants usually concentrate caesium in their tissues compared to the outer source of the element. Moreover, caesium deposited on leaves may partially be absorbed through the pores and transferred to the plant tissue. In the next step, caesium can incorporate into edible animal tissue and concentrate in milk. Animals provide a food source of caesium for humans. It concentrates mainly in muscles. Bioaccumulation of radiocaesium in the body increases the cancer risk because of the tissues' exposure to the beta particles as well as high-energy gamma radiation.

Liquid radioactive waste (LRW) must meet very strict standards before its safe discharge into the environment. Elements such as the level of radioactivity, concentration of heavy metals, and organic compounds in LRW are precisely regulated by national standards, therefore, to reach them, the LRW has to be treated to reduce their volume and decrease the radioactivity level and harmful substances [13]. There are many methods applied for LRW treatment. These are: chemical precipitation, ion exchange/sorption, thermal evaporation, foam separation, solvent extraction, and membrane processes [14, 15]. Low or very low radionuclides concentration in the LRW limits the application of most

above-mentioned processes used in radionuclides separation. Therefore, the most common method still used for LRW treatment is ion exchange, which is a form of the sorption process. The ion exchange process offers several advantages over others. It requires simple and compact equipment and is very effective in converting low concentrations of the radioactive species dispersed in a large volume of liquid into a small volume of solid material which can be easily disposed of. One should remember that the major difficulty in low-level radioactive waste (LLRW) treatment is its very low radiocaesium concentration compared to the level of competitive ions present in seawater.

For a complete description of radiocaesium sorption onto SiEA-KNiFe sorbent mechanism and performance, this work presents the results of batch, fixed-bed column, and hybrid membrane process studies. Batch studies were carried out to establish the optimum conditions of sorption to obtain equilibrium sorption isotherms and to evaluate the sorption capacity of SiEA-KNiFe sorbent for radiocaesium present in the aqueous phase.

2. Materials and methods

2.1. Method for SiEA-KNiFe sorbent synthesis

All steps of the SiEA-KNiFe sorbent synthesis method have been described in detail previously [16]. Briefly, the SiEA-KNiFe sorbent synthesis method is based on the modification of silica with nickel-potassium hexacyanoferrate and ethanolamine, followed by an appropriate drying and grinding procedure (Figure 1). Then, the size fraction of sorbent particles suitable for application in a chosen process configuration is separated by sieving.

2.2. Methods of SiEA-KNiFe sorbent characterisation

Scanning Electron Microscopy (SEM) images of the composite ion exchanger were obtained using a Zeiss Ultra Plus scanning electron microscope located in the Institute of High-Pressure Physics of Polish Academy of Sciences. This microscope is dedicated to ultra-high-resolution imaging. Patented column Gemini is a part of the microscope. The microscope enables the study of samples in a very wide range of voltage (from 20 eV to 30 kV) and even when low voltage is applied, a high resolution of the image is retained. Samples of the SiEA-KNiFe sorbent were studied with a low accelerating voltage of 2 kV. Samples for the SEM examination were prepared according to a standard procedure, fixed with conductive glue, and coated with a thin layer of carbon. The samples were examined at a magnification of $\times 1000$ and $\times 100000$.

The energy dispersive X-ray spectroscopy, using a Bruker Quantax 400 was employed to check the composition of the sorbent before and after caesium and cobalt sorption from a non-active solution of caesium and cobalt salts. The Bruker Quantax 400 analyser is located in the Institute of High-Pressure Physics of Polish Academy of Sciences. It is equipped with ultra-high throughput (up to 300 kcounts/s) detector with an energy resolution of 127 eV and active area of 30 mm². The Bruker Quantax 400 enables the detection of compounds starting from boron. The elemental composition of each sample was determined in two different regions of the sample to confirm its homogeneity and to obtain the most representative result concerning the structural properties of the synthesised material.

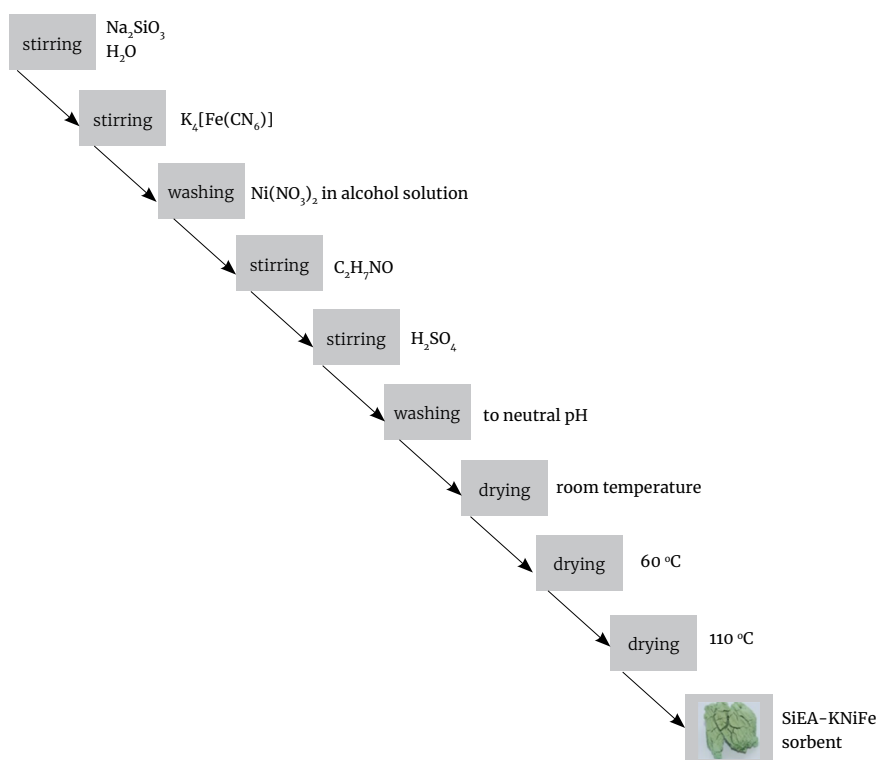


Figure 1: Flow-chart of the SiEA-KNiFe sorbent synthesis procedure.

2.3. Experimental procedures

Radioactive ¹³⁴Cs was obtained using the thermal neutron irradiation of 1 mg of CsCl for 30 min in the MARIA nuclear reactor (Otwock-Świerk, Poland) using a neutron flux of approximately $7 \times 10^{13} \text{ n cm}^{-2} \text{ s}^{-1}$. Then samples were cooled down for 12 h. Next, radioactive CsCl was dissolved

in 100 mL of deionised water to obtain a radioactive solution. A small amount of this solution was added to each sample of non-active CsCl as the radiotracer.

The activity of the samples was measured using a system of high purity Ge detector, model GS 6020 Canberra-Packard. The activity of ^{134}Cs was calculated from the 604.7 keV and 795.9 keV peaks using a computer program (GIENE 2000).

2.4. Process configuration applied in radiocaesium removal from the aqueous solutions

Sorption experiments were performed in batch mode by shaking up the 5 mL of CsCl solution (labelled with ^{134}Cs radiotracer solution) with 3 mg of the SiEA-KNiFe sorbent in an orbital shaker at a speed of 300 rpm. For the solutions preparation, either deionised water or seawater from Gdansk Bay, Poland (Baltic Sea) was used. Before the sorbent was added, 2.5 mL of labelled sample was collected, and its activity was determined using the gamma spectrometry method. After the phases had been stirred for the assumed contact time, the liquids were separated from the solids first by use of a centrifuge (15 min at 4000 rpm) and next by filtration through a cellulose membrane (round filters ROTILABO® Type 112A, retention range: 8–12 μm , thickness: 0.16 mm). 2.5 mL of the filtrate was sampled for its activity measurements, using gamma spectrometry. All the experimental data were of duplicate determinations.

The sorption of the radionuclide was expressed in terms of the distribution coefficient (K_d) according to the following equation:

$$K_d = \frac{A_0 - A_e}{A_e} \times \frac{V}{m}$$

where A_0 is the initial activity of the radionuclide in the solution, A_e is the activity of the radionuclide at equilibrium, V is the solution volume (mL), and m is the mass of the sorbent (g).

Laboratory-scale glass columns were used in the fixed-bed column sorption studies. The beds in the columns were composed of 0.3 g of the SiEA-KNiFe sorbent and three different fractions of the particles of the SiEA-KNiFe sorbent were examined. The inside diameter of the column was 1 cm, and the length bed available for the adsorption was 1.4 cm. 40 mL of caesium solutions with a concentration $10^{-2} \text{ mol dm}^{-3}$ were prepared in deionised water and in seawater labelled with ^{134}Cs radiotracer. One millilitre of each labelled solution was collected, and its activity was determined using the gamma spectrometry method. In the next step,

the caesium solution was pumped using a peristaltic pump through the columns at a flow rate 0.9 mL min^{-1} . The samples of output solution were collected at the exit of the column in the predetermined time intervals correlating with effluent volume until sorbent saturation had been reached and the activity of every mL of collected effluent was measured using gamma spectrometry.

An AMICON 8050 stirred membrane cell (Merck Millipore, Merck Sp. z o.o., Poland) equipped with a polyethersulfone (PES) microfiltration membrane with a nominal pore size of 0.03 mm and an effective area of $4.18 \times 10^{-3} \text{ m}^2$ provided by Microdyn-Nadir GmbH was used in the combined adsorption-membrane filtration process. 350 mL of the caesium stock solutions with a concentration of $5 \times 10^{-5} \text{ mol dm}^{-3}$ labelled with ^{134}Cs radiotracer in deionised water and seawater were prepared. Before the SiEA-KNiFe sorbent was added, 1 mL of labelled sample was collected, and its activity was determined using the gamma spectrometry method. Next, 0.21 g of the SiEA-KNiFe sorbent with a particle size in the range $90\text{--}150 \text{ mm}$ was added to each caesium stock solution labelled with ^{134}Cs radiotracer and the integrated adsorption-membrane filtration process started. The permeate flux was under 0.1 MPa feed pressure and the filtrated solution was stirred at a speed of 500 rpm . The samples of permeate with a volume of 1 mL each were collected at predetermined time intervals and analysed using gamma spectrometry.

3. Results

3.1. SiEA-KNiFe sorbent properties

SEM images of the synthesised SiEA-KNiFe sorbent are shown in Figure 2. The SiEA-KNiFe consists of irregular particles that differ in size from 20 to 260 nm (Figure 2a). The higher magnification allowed the observation of the porous surface of sorbent particles composed of a large amount of tiny, $\sim 20 \text{ nm}$ nanoparticles (Figure 2b).

The EDX spectrum analysis enabled the determination of the amount of caesium bound onto the SiEA-KNiFe sorbent. The EDX spectrum obtained for SiEA-KNiFe sorbent after radiocaesium sorption confirmed caesium bonding. The average amount of caesium bound onto the SiEA-KNiFe after caesium sorption was determined to be about $7.5 \text{ wt.}\%$, which corresponds with the amount of caesium calculated from the results of the gamma spectrometry experiments.

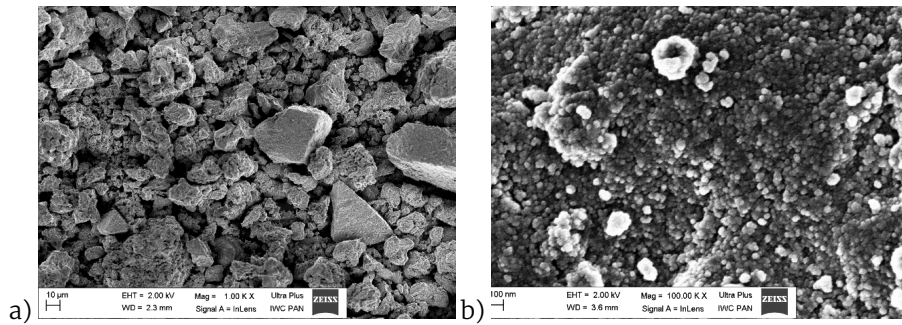


Figure 2: SEM images of SiEA-KNiFe sorbent particles in magnification: $\times 1000$ (a), $\times 100000$ (b).

3.2. Sorption experiments

The effect of contact time on ^{134}Cs uptake was studied for CsCl deionised water or seawater solution with a concentration of $5 \times 10^{-5} \text{ mol dm}^{-3}$. The pH of the CsCl solutions was 6 and the temperature 25°C . The time dependence of ^{134}Cs sorption onto the SiEA-KNiFe sorbent in deionised water solutions and in seawater is shown in Figure 3. The sorption of caesium onto the SiEA-KNiFe sorbent is a fast process. After 15 min of shaking, 95% caesium ions are removed from the caesium deionised water solution and the caesium seawater solution. However, the adsorption rate in the second step of the process is relatively slow because the external surface of micropores is approximately saturated with the adsorbed ion, and the exchange reaction took place mainly on the internal surface of micropores. The presence of other ions strongly competing with caesium ions for adsorption sites in seawater solutions results in a longer contact time needed for equilibrium to be reached. For CsCl, solutions in seawater takes longer for equilibrium to be reached (18 hours) and it relates to the presence of other ions strongly competing with ^{134}Cs for adsorption sites. Thus, two hours of equilibration time was selected in the following experiments for CsCl solutions in deionised water, and the time of 18 hours was selected for CsCl solutions in seawater.

Further experiments confirmed that caesium adsorption is constant in a pH range of 2–12 and sorption effectiveness is observed with the increase in temperature. The reason for this decrease in sorption performance could originate from thermal destabilisation, which causes an increase in the mobility of Cs^+ ions on the surface of the solid with increasing temperature, thus enhancing the desorption steps [17, 18]. Therefore, the sorption of caesium should be carried out at room temperature.

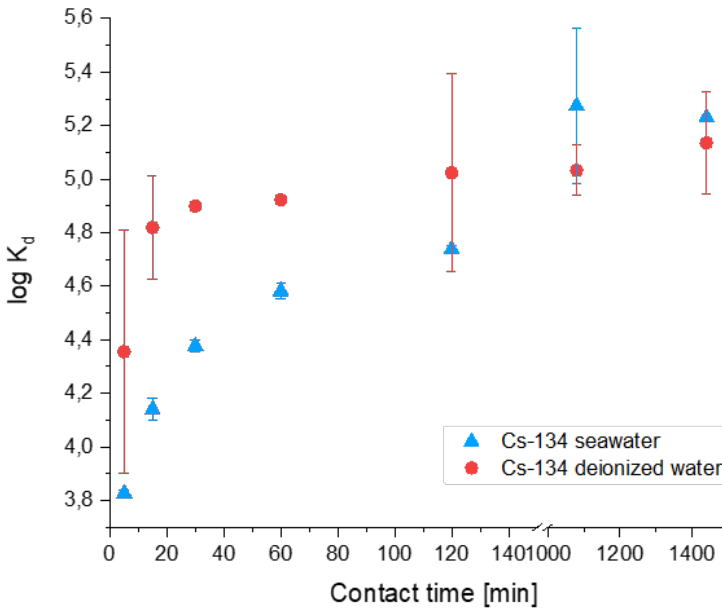


Figure 3: The effect of contact time on the sorption of ^{134}Cs onto the SiEA-KNiFe sorbent from deionized water and seawater solution of CsCl.

Fixed-bed column experiments is a good source of data for scaling-up the sorption process to industrial applications. Results of radiocaesium sorption onto SiEA-KNiFe sorbent in column experiments are presented as breakthrough curves (Figure 4). The breakthrough point indicates the instance at which the caesium ion is effectively discharged on the eluate. The breakthrough point is arbitrarily inferred for C_t/C_0 at 0.05. The presence of competitive ions, such as Na^+ , K^+ , Mg^{2+} and Ca^{2+} in seawater, which compete with radiocaesium for active sites negatively reflects on adsorption capacity. The influence of the sorbent particle size on the sorption effectiveness was studied for four different size fractions of the SiEA-KNiFe sorbent particles: 150–180 mm, 180–250 mm, 250–355 mm and all particles with sizes below 250 mm (< 250 mm), including particles with nanometric sizes. It can be also observed that the larger the particles of the sorbent, the more effective the radiocaesium uptake. This effect suggests that the intra-particle diffusion is the slowest stage of the radiocaesium diffusion process. This can be caused by the too narrow internal channels in the framework in the smaller sorbent particles, which can be a result of the intensive sorbent grinding.

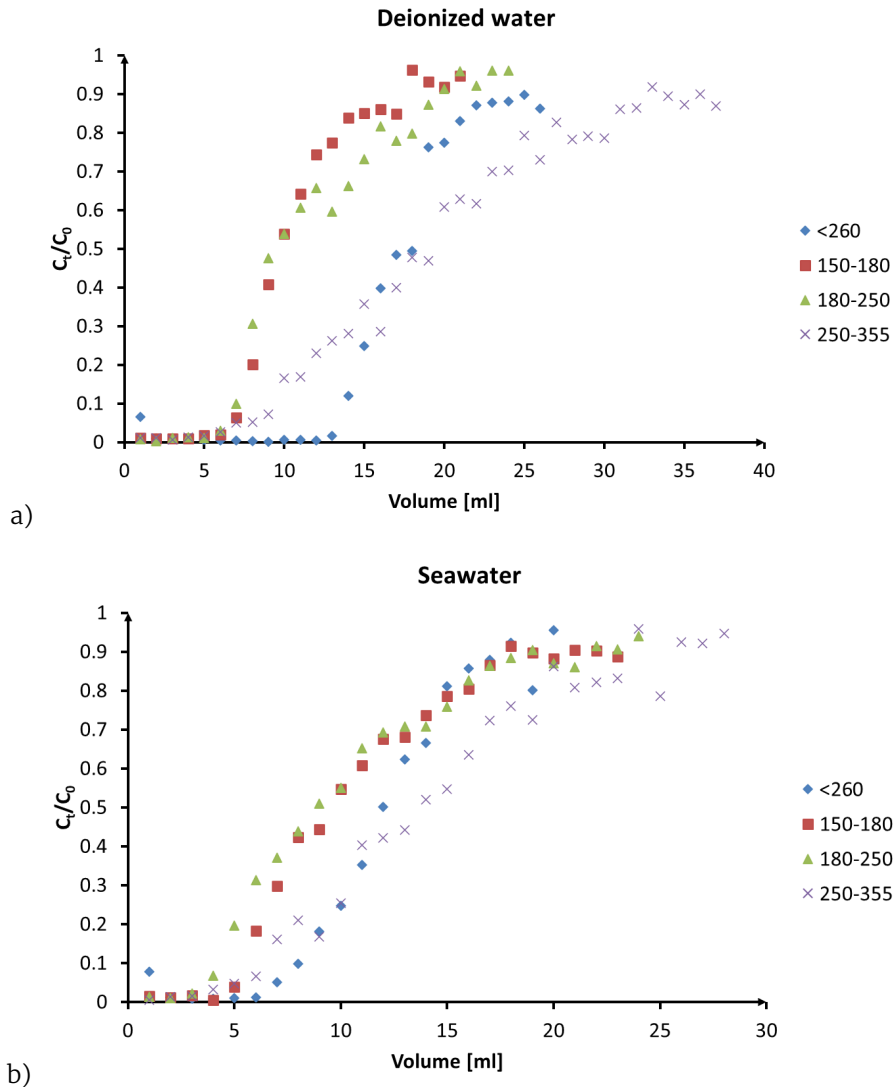


Figure 4: The breakthrough curves for the radiocaesium sorption in the fixed-bed process on the SiEA-NiFe sorbent particles with different size fractions: (a) ^{134}Cs solutions in deionised water, (b) ^{134}Cs solutions in seawater.

Radiocaesium removal for deionised water and seawater solutions is shown in Figure 5. The equilibrium was reached after 17 minutes of the process duration and 96 % and 94 % of ^{134}Cs from the deionised water solution and seawater solution were removed, respectively. The equilibrium in the hybrid membrane process was reached much faster than in the batch process. Moreover, the application of simultaneous sorption on the SiEA-

KNiFe sorbent and filtration using the microfiltration (MF) membrane allows the separation of sorbent particles after radiocaesium removal more effectively.

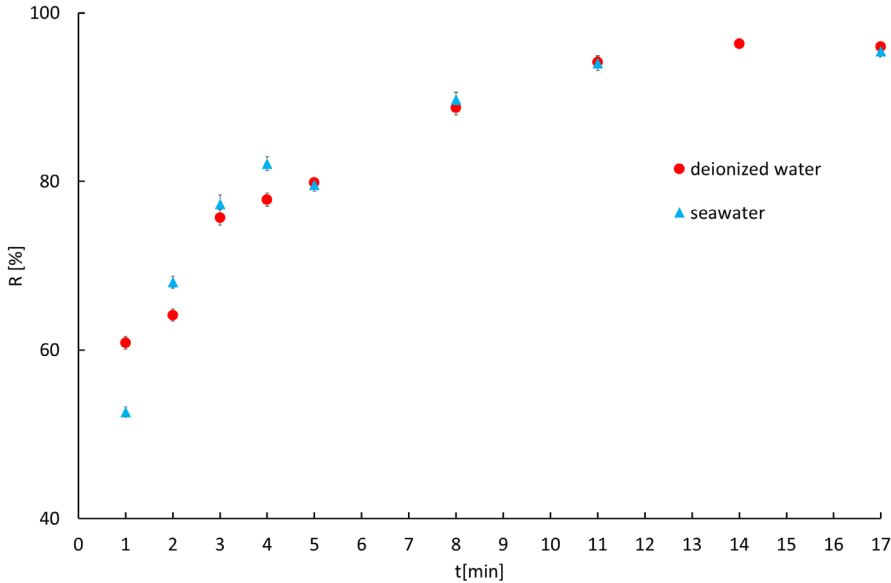


Figure 5: Radiocaesium removal for deionised water and seawater solutions.

4. Conclusions

The form of “cake” in which the SiEA-KNiFe sorbent is obtained allows to grind it and choose the size fraction appropriate for application in different process configurations. The experiment carried out in this work confirmed that the SiEA-KNiFe sorbent can be effectively used for radiocaesium removal in batch, fixed-bed column, and hybrid membrane processes. The batch process was helpful in sorption parameters optimisation. Conducted experiments enabled the determination of the suitable contact time for the radiocaesium removal from deionised water and seawater solutions as 2 hours and 18 hours, respectively. Moreover, room temperature is recommended to obtain higher effectiveness of ^{134}Cs removal, while pH doesn't influence radiocaesium uptake. In case of the fixed-bed column process, larger particles of SiEA-KNiFe sorbent are recommended to apply as bed in order to avoid problems with the caesium ions transport caused by the too narrow internal channels in the framework in the smaller sorbent particles which result in lower effectiveness of the sorbent in this process configuration. The hybrid membrane process combining sorption

on the SiEA-KNiFe sorbent and MF allows reaching equilibrium within 17 minutes, so much faster than in the case of the batch process. This mode also provides high effectiveness of radiocaesium uptake from deionised water and seawater solutions. Moreover, this configuration also enables a much easier sorbent particle separation after ^{134}Cs removal.




References

1. World Nuclear Association. 2016. *2016/2017 WNA Pocket Guide on Reactors. Nuclear Power Reactor Characteristics*. [Retrieved 20 December 2021] www.world-nuclear.org.
2. Cattant F, Crusset D & Féron D. 2008. Corrosion Issues in Nuclear Industry Today. *Materials today*, 11(10):32–37. [https://doi.org/10.1016/S1369-7021\(08\)70205-0](https://doi.org/10.1016/S1369-7021(08)70205-0)
3. Hesketh KW. 1996. Power Reactors. In PD Wilson (eds). *The Nuclear Fuel Cycle. From Ore to Waste*, New York: Oxford University Press. 78–101.
4. AREVA S.A. 2009. *The Path of Greatest Certainty*. [Retrieved 20 December 2021] www.epr-reactor.co.uk/
5. Neeb KH. 1997. *The Radiochemistry of Nuclear Power Plants with Light Water Reactors*. Berlin: de Gruyter. 750. <https://doi.org/10.1515/9783110812015>
6. Burns PC, Ewing RC & Navrotsky A. 2012. Nuclear Fuel in a Reactor Accident. *Science*, 335:1184–1188. <https://doi.org/10.1126/science.1211285>
7. Feron D. 2012. Overview of Nuclear Materials and Nuclear Corrosion Science and Engineering. In D Feron (eds). *Nuclear Corrosion Science and Engineering*. UK: Woodhead Publishing. 31–56. <https://doi.org/10.1533/9780857095343.1.31>
8. Haslett DE. 1996. Transport and Storage of Irradiated Fuel. In PD Wilson (eds). *The Nuclear Fuel Cycle. From Ore to Waste*. New York: Oxford University Press. 102–115.
9. International Atomic Energy Agency. 1997. *Further Analysis of Extended Storage of Spent Fuel*. Vienna.
10. Nagy P, Vajda N, Pinter T & Fel K. 2016. Activities of ^{134}Cs , ^{135}Cs and ^{137}Cs in the Primary Coolant of VVER-440 Reactors. *Journal of Radioanalytical and Nuclear Chemistry*, 307:1045–1053. <https://doi.org/10.1007/s10967-015-4311-2>
11. Wilson PD. 1996. Environmental Radioactivity. In PD Wilson (eds). *The Nuclear Fuel Cycle. From ore to Waste*. New York: Oxford University Press. 207–228.

12. Zhu YG & Smolders E. 2000. Plant uptake of radiocaesium: a review of mechanisms, regulation and application. *Journal of Experimental Botany*, 51(351):1635–1645. <https://doi.org/10.1093/jexbot/51.351.1635>
13. Zakrzewska-Trznadel G, Harasimowicz M & Chmielewski AG. 2001. Membrane Processes in Nuclear Technology–application for Liquid Radioactive Waste Treatment. *Separation and Purification Technology*, 22(Supplement C):617–625. [https://doi.org/10.1016/S1383-5866\(00\)00167-2](https://doi.org/10.1016/S1383-5866(00)00167-2)
14. Rahman ROA, Ibrahim HA & Hung YT. 2011. Liquid Radioactive Wastes Treatment: A Review. *Water*, 3(2):551. <https://doi.org/10.3390/w3020551>
15. Anderson DR, Plant AM & Girardi F.1981. Radioactive Waste: Advanced Management Methods for Medium Active Liquid Waste. Radioactive Waste Management. Vol. 1. Brussels and Luxemburg: Harwood Academic Publishers. 143.
16. Chmielewska D, Siwek M, Wawszczak D, Henczka M, Sartowska M, Starosta W & Dudek J. 2018. Nanocomposite SiEA-KNiFe sorbent – Complete Solution from Synthesis Through Radiocesium Sorption to Vitrification using the sol–gel Method. *Journal of Industrial and Engineering Chemistry*, 67:407–416. <https://doi.org/10.1016/j.jiec.2018.07.015>
17. Abdel-Karim AAM, Zaki AA, Elwan W, El-Naggar MR & Gouda MM. 2016. Experimental and Modeling Investigations of Cesium and Strontium Adsorption onto Clay of Radioactive Waste Disposal. *Applied Clay Science*, 132–133:391–401. <https://doi.org/10.1016/j.clay.2016.07.005>
18. Khandaker S, Toyohara Y, Kamida S & Kuba T. 2018. Adsorptive Removal of Cesium from Aqueous Solution Using Oxidized Bamboo Charcoal. *Water Resources and Industry*, 19:35–46. <https://doi.org/10.1016/j.wri.2018.01.001>

Chapter 4

MOF-assisted membrane process for removal of radionuclides and other hazardous elements from aqueous solutions

Agnieszka Miśkiewicz , Grażyna Zakrzewska-Kołtuniewicz ,
Wojciech Starosta 

*Institute of Nuclear Chemistry and Technology,
Dorodna 16, 03-195 Warsaw, Poland
e-mail: g.zakrzewska@ichtj.waw.pl*

Abstract

This paper presents research on the application of the sorption-assisted membrane process for the removal of hazardous elements from aqueous solutions. As adsorbent in this process, metal-organic-framework compounds (MOFs) have been tested. The hybrid process was carried out in the Amicon-stirred cell and in the Couette-Taylor helical flow membrane contactor equipped with a metallic tubular membrane.

1. Introduction

Membrane processes are widely used in environmental protection technologies, especially in the treatment of industrial wastewater and treatment of surface and groundwater (Konieczny, Wszelaka-Rylik & Macherzyński 2019:20–29; Racar, Dolar, Špehar & Košutić 2017:386–392). They have also been successfully employed for liquid radioactive waste treatment (Zakrzewska-Trznadel 2013:119–130; IAEA Technical Report 2004). The main advantages that make membrane processes more widely used include, the variety of membrane techniques, low energy consumption, no need to add chemical additives, (i.e. waste reduction), easy scale-up (by the modular system), and continuous separation. Moreover, membrane systems are flexible, and it is simple to combine them with other treatment methods to perform hybrid processes, which are efficient and selective for particular components that we want to

recover. One of the possibilities of creating such an effective hybrid unit is to combine pressure membrane techniques, i.e. microfiltration (MF), ultrafiltration (UF), or nanofiltration (NF) with the sorption process in sorption-assisted membrane filtration. Such a hybrid arrangement is very attractive because of its high removal efficiency while consuming low energy. A sorption-assisted UF process has been studied as a potential method for water purification and the treatment of wastewaters of different types (Hilbrandt, Shemer, Ruhl, Semiat & Jekel 2019:23–28; Vaziri, Ghomsheh, Azimi & Mirzaei 2021:1–7; Maimoun, Djafer, Djafer, Marin-Ayral & Ayral 2020:001–011; Cojocar, Zakrzewska-Trznadel & Jaworska 2009:599–609; Cojocar, Zakrzewska-Trznadel & Miskiewicz 2009:610–620). Recently, such a hybrid process has been used to treat liquid radioactive waste (Miśkiewicz & Zakrzewska-Kołtuniewicz 2021). The paper presents research on the application of a biosorption-assisted ultrafiltration process using alginic acid and sodium alginate for the removal of selected radionuclides (^{60}Co , ^{85}Sr and ^{137}Cs from radioactive liquid waste). Various types of sorbents can be used in the assisted filtration processes. Low-cost abundantly available compounds, for example, agricultural and household wastes, industrial by-products, sludge, soil, and ore materials are of great interest in wastewater treatment processes (De Gisi, Lofrano, Grassi & Notarnicola 2016:10–40). The current research, presented in this work, includes the use of MOF sorbent in the sorption-assisted microfiltration to remove hazardous compounds from aqueous solutions such as mercury in the form of Hg^{2+} ions.

In the current experiments, we focused on the separation of mercury, a toxic element whose emissions harm ecosystems and threaten human health. Global mercury pollution is caused by human activities like mining and the combustion of fossil fuels. When mercury gets into air and water, it is transformed by micro-organisms into methylmercury, especially the toxic form, which accumulates in fish, shellfish, and other animals that feed on fish. Due to its toxicity, mercury should be controlled and removed from the environment.

2. Methodology

2.1. Sorption-assisted microfiltration

Sorption-assisted microfiltration (SMF) is a combination of classical MF with sorption of ions (including metallic element and radionuclide ions) on sorbent dispersed in solution, as it is shown schematically on Figure.

4.1. Such a hybrid process causes a more effective separation of small ions, which are bound with sorbent forming bigger particles.

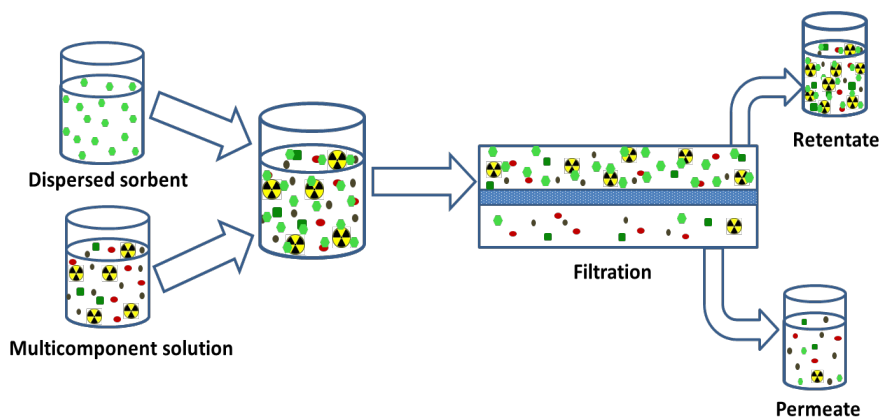


Figure 1: A scheme of sorption-assisted microfiltration process.

The MOFs can be used in the SMF process, and proper functionalisation of the sorbents can ensure high partition coefficients for elements present in the solution. The extensive literature on the subject, including the experience of the team from the Council for Scientific and Industrial Research (CSIR), Republic of South Africa, as well as research conducted at the Institute of Nuclear Chemistry and Technology (INCT) have shown that it is possible.

2.2. Metal-organic-framework (MOF) sorbent

For the sorption of Hg^{2+} from water UiO-66, metal-organic-framework sorbent functionalised with mercaptoacetic acid (thioglycolic acid, $\text{C}_2\text{H}_4\text{O}_2\text{S}$) was synthesised. The synthesis was performed in dimethylformamide using terephthalic acid, zirconium chloride, and mercaptoacetic acid under reflux at 120°C . The mercaptoacetic acid was chosen for its $-\text{SH}$ group and its affinity for mercury. The content of mercaptoacetic acid in the reaction mixture was fixed at 50 equivalents of zirconium. The SEM picture of synthesised sorbent I showing aggregates of small nanocrystals is presented in Figure. 4.2.

On the basis of analysis by Energy-dispersive X-ray spectroscopy (EDS) made by the MOF's manufacturer, the atomic ratio of $-\text{SH}$ group to zirconium was estimated at 0.32. The estimated size of the produced MOF's crystals was about 50 nm, but they formed larger agglomerates, which could be retained by the MF or UF membrane.

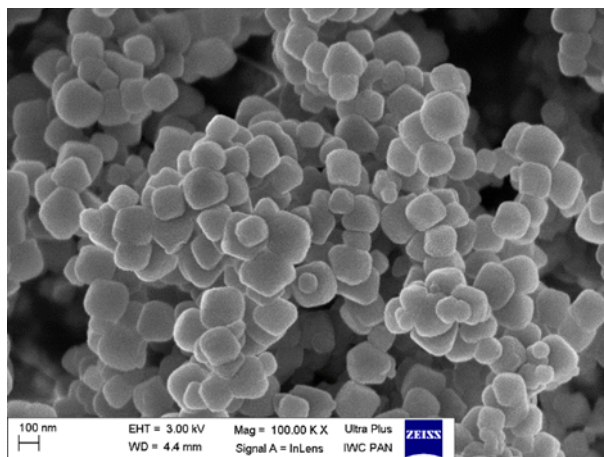


Figure2: SEM image of sorbent made using the Scanning Electron Microscope Zeiss Ultra Plus.

2.3. Membrane fouling

Membranes used in sorption-assisted filtration processes are susceptible to fouling due to deposition of the dispersed sorbent on the membrane. This is followed by continuous permeate flux decline, therefore, the efficiency of the entire separation process diminishes over time. It is important to suppress all negative phenomena that occur in the vicinity of the membrane by adjusting process parameters that avoid the sorbent layer development. An alternative method is to promote the turbulence in the membrane module by introducing movable parts, special baffles which improve mass exchange conditions or by application of pulse flow. In present studies, a Couette-Taylor flow (CTF) creating the vortices by use of a movable part inside the module that results in a self-cleaning effect of the membrane surface was applied. CTF is a combination of the axial Poiseuille flow and the rotating Couette flow with axisymmetric Taylor vortices. Such a combination results in limited axial dispersion coefficients in relation with dispersion coefficients in other directions, independence of mixing intensity on residence time of medium in the apparatus, and good transport parameters (Zakrzewska-Trznadel, Harasimowicz, Miskiewicz, Jaworska, Dłuska & Wroński 2009:108–116).

2.4. Radiotracers method

In this work, the use of the radiotracer method to assess the efficiency of Hg^{2+} sorption on MOF and the efficiency of retention of these ions on the membrane was proposed. Radiotracers provide a convenient tool to study

the behaviour of metal ions in aqueous solutions (Petroni, Pires, & Munita 2004:239–243; Badillo-Almaraz, Solache-Ríos, Badillo-Almaraz, Zarate-Morales & Flores-Moreno 2017:113–118). An important advantage of the radiotracer method is that it is often possible to add carrier-free isotopes to the sample without disturbing the concentration of the ion of interest. Radioisotope tracers can be used at very low concentrations as radiation detectors are extremely sensitive. In general, measurements of radiation of gamma/beta emitting nuclides of high precision and sensitivity can be made relatively rapidly with minimal sample processing.

3. Experimental

3.1 Materials

Mercury nitrate ($\text{Hg}(\text{NO}_3)_2 \cdot \text{H}_2\text{O}$), Sigma-Aldrich, was used as a metal ions source. The radiolabelled compound $^{197}\text{Hg}(\text{NO}_3)_2$ was used as a radiotracer in all experiments. To obtain the ^{197}Hg radioisotope, a sample of nonradioactive $\text{Hg}(\text{NO}_3)_2$ with a mass of 1.2 mg was irradiated for one hour in a stream of $5 \cdot 10^{14}$ neutrons/ cm^2 in the Research Nuclear Reactor (MARIA) (National Centre for Nuclear Research, Świerk, Poland). The obtained radiotracer with an initial activity of approx. 25 MBq was dissolved in 0.6 cm^3 of 2% HNO_3 and then used as a radiolabeling solution. The MOF sorbent type MAA3(4) was applied in the SMF filtration experiments. Sodium hydroxide obtained from CHEMPUR, Poland was used for adjusting the pH of the reaction mixture. Distilled water was used in all experiments.

3.2. Membrane apparatuses

For the preliminary investigation of MOF-assisted filtration for removal of Hg^{2+} ions from water solutions, a stirred membrane cell was used. The experimental system consisted of an AMICON 8400 stirred membrane cell (Merck Millipore, Merck Sp. z o.o., Poland) with a polyethersulfone (PES) flat-sheet membrane (molecular weight cut-off = 10 kDa; diameter = 0.067 m) provided by Merck Millipore (Merck Sp. z o.o., Poland) and compressed nitrogen as a pressure source.

In further experiments, the Couette-Taylor Flow (CTF) membrane contactor was used. The membrane installation is schematically presented in Figure. 4.3. The tubular metal membrane used in the installation was made by sintering of metals such as 16–18% Cr, 10–14% Ni, 2–3% Mo, and 65–72% Fe. For experiments with MOF sorbents, a membrane with pore size of 0.1 μm , was selected.

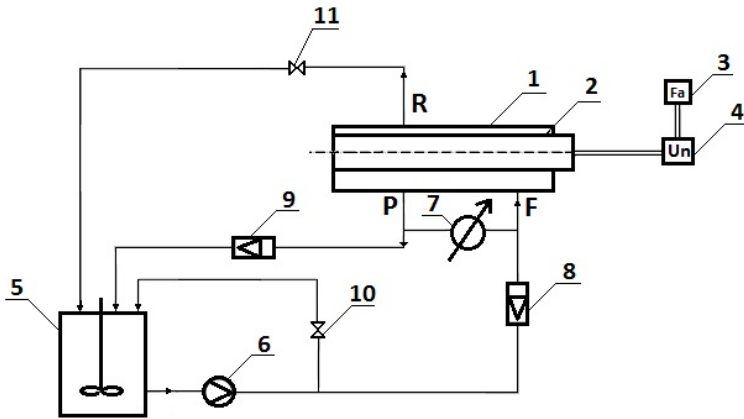


Figure 3: Experimental set-up: 1- membrane contactor, 2 – rotation shaft, 3 – power inverter, 4 – motor, 5 – feed tank with mechanical a stirrer, 6 – pump, 7 – manometer, 8, 9 – flowmeters, 10, 11 – valves.

This set-up worked in a closed system, meaning that the permeate and concentrate streams were returned to the feed tank (5) after exiting the membrane contactor. Feed solutions for filtration experiments were prepared by mixing the appropriate amount of 0.01 M Hg^{2+} stock solution with a certain amount of MOF sorbent to receive its concentration of 0.5-2 g/L in the feed solution and a small amount (10-30 μL) of tracer solution. Prior to the filtration experiment, the pH was adjusted with NaOH and the feed solution was stirred for one hour (experimentally determined to be sufficient time for Hg^{2+} ions adsorption on MOF particles). During the tests performed in the Amicon filtration cell, a transmembrane pressure was maintained at 0.5 to 2 bar. In the case of the CTF membrane module process parameters were as follows:

- transmembrane pressure, p : in the range of 0.3 – 0.5 bar,
- feed flow rate, Q_s : in the range of 1.2 – 2.2 L/min, and
- rotation frequency of the inner shaft, Ω : 2100 rpm.

The parameters of filtration were selected using the experiment design technique and after the optimisation procedure, which enables full observation of the effects of mutual interactions of the variables characterising the system.

During the filtration, permeate samples were collected periodically and analysed in relation to the Hg^{2+} content. The Hg^{2+} contents in the feed solution and the permeate were determined by measuring the radioactivity

of $^{197}\text{Hg}^{2+}$ radiotracer using the gamma counter LG-1b (INCT, Poland). The Hg^{2+} retention coefficient was then calculated according to the formula (1):

$$R = 1 - \frac{A_P}{A_F} \quad (1)$$

where A_P and A_F represent the activity of radiotracer in the permeate and feed, respectively.

4. Results and discussion

4.1 Preliminary investigation on sorption-assisted filtration for Hg^{2+} removal from aqueous solutions

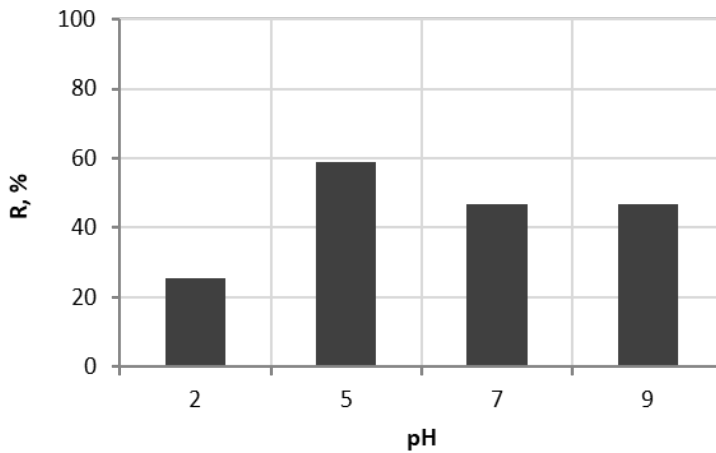
Tests with flat microfiltration membranes were performed to determine the parameters of the SMF process and to initially assess the effectiveness of the method and the obtained retention coefficients. These experiments also allowed the rate of deposition of the sorbent on the membrane to be observed and the prediction of membrane fouling that could interfere with the process performed later in the target flow system. Prior to key investigations, the influence of pH and reagents ratio on the retention coefficient (R) of Hg^{2+} ions were determined. The reagents were mixed for one hour and then placed in the Amicon filtration cell with a PES flat membrane with an MW cut-off of 10 kDa. The obtained permeate was analysed for the content of Hg^{2+} and then the retention coefficients (R) of these ions were calculated. Results of these investigations are presented in Table 4.1 and in Fig. 4.4 and 4.5.

As it turned out, the highest retention coefficients were obtained for the ratio of the reagents equal to 1/1 ($R = 86\%$). On the other hand, when the lower concentration of sorbent was used, that is, the ratio of 2/1 and 4/1, R was lower and amounted to 51% and 45%, respectively. Bearing in mind the possibility of significant membrane fouling in the case of using a high concentration of sorbent (2 g/L), it was decided to carry out further research at its average concentration, 1 g/L, which gives the reagent ratio (Hg/MOF) equal to 2/1.

As for the influence of pH, studies have shown that it is most advantageous to conduct the process at a pH of approx. 5 (Figure.4.4). Further experiments were carried out at pH 5.5.

Table 1: The results of the study of the influence of the reagent ratio on the retention coefficient (R) of Hg^{2+} ions.

Hg^{2+} concentration, mol/L	Sorbent concentration, g/L	Reagents mass ratio (Hg/MOF), g/g	R, %
0.01	0.5	4/1	45.67
0.01	1	2/1	51.38
0.01	2	1/1	86.23

**Figure 4:** The pH influence on the retention coefficient (R) of Hg^{2+} ions; reagent ratio: 2/1.

An example of the MOF-assisted filtration process run carried out in the Amicon cell is shown in Figure 4.5. As evident, at the beginning of the process, the retention coefficient of Hg^{2+} increases and then, after ca 20 minutes, it stabilises at the level of about 51%.

Maintaining the parameters of the Hg^{2+} sorption on the MOF sorbent, established in the above-described experiments (pH = 5.5, Hg/MOF = 2/1), the process was transferred to a continuous membrane installation, namely to a system with a CTF flow module (Figure. 4.3).

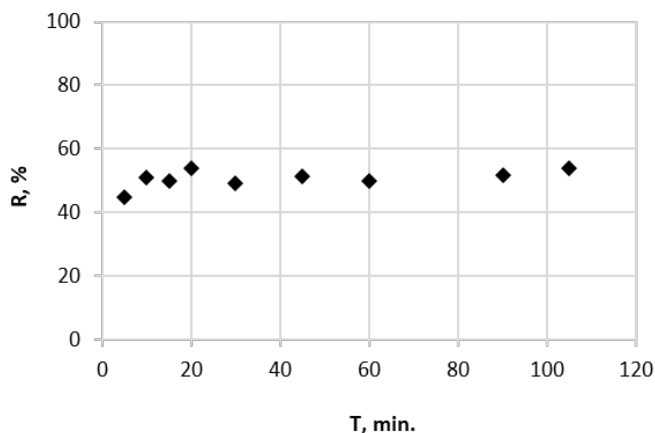


Figure 5: The change in the retention coefficient (R) of Hg ions during the MOF-assisted filtration process, carried out in the Amicon filtration cell; pH: 5.5, reagent ratio: 2/1.

4.2 MOF-assisted MF for Hg²⁺ removal from water solution in CTF membrane contactor

The MOF-assisted microfiltration carried out in the membrane installation with CTF membrane contactor was performed with the various process parameters, namely feed flow rate (Q_s : 1.2, 1.5 and 2.2 L/min) and transmembrane pressure (p : 0.3 and 0.5 bar). The influence of the feed flow rate on the retention factor of Hg²⁺ is illustrated in Figure. 4.6. As can be seen, when the feed flow increases, the retention ratio increases slightly. Regardless of the feed flow rates used, there is a noticeable increase in the retention coefficient during the process. After two hours, R reached high values: 93–99%.

When considering the influence of transmembrane pressure (Figure. 4.7), it should be stated that the higher the pressure, the higher the retention coefficient of Hg²⁺ ions have been achieved.

Waste PET-MOF-Cleanwater

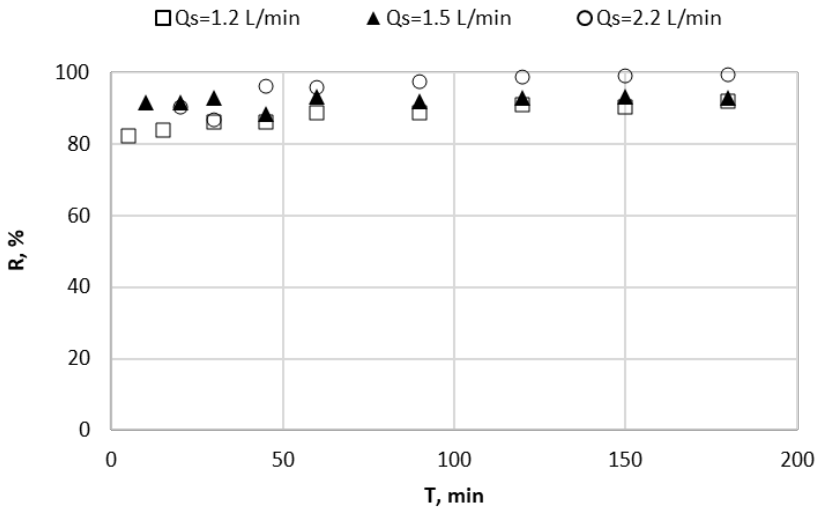


Figure 6: The influence of the feed flow rate (Q_s) on the retention factor of Hg^{2+} .

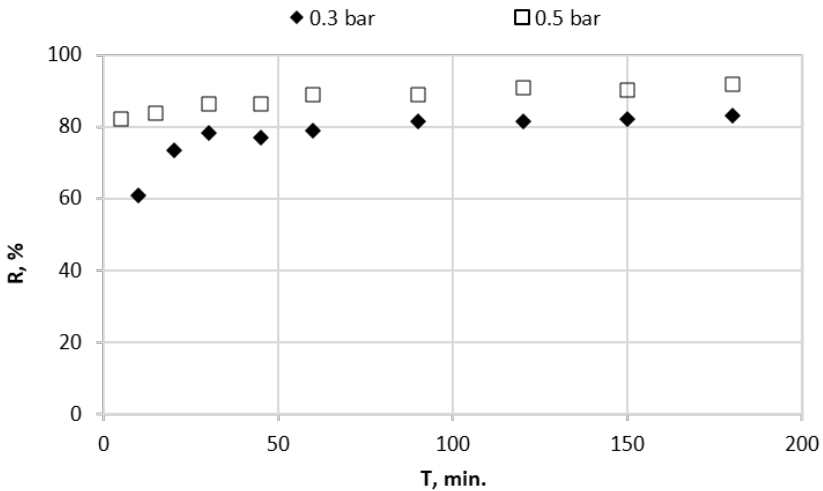


Figure 7: The influence of the transmembrane pressure (p) on the retention factor of Hg^{2+} .

Summarising the results obtained during sorption-assisted microfiltration carried out in the membrane module (CTF) with helical flow, it should be stated that Hg^{2+} ions can be effectively removed by the SMF method. Depending on the applied process parameters, R changed in the range of

83–99%. These results are much better than those obtained when running the process in the dead-end membrane cell (see section 4.1).

5. Conclusions

The process of separation of Hg^{2+} from water solutions can be effectively performed in the MF system with the membrane contactor with helical flow. The use of MOF sorbent results in sufficient separation of Hg^{2+} ions with over 80 % efficiency at 2:1 (Hg/MOF) ratio. The process parameters such as transmembrane pressure and the feed flow rate, affect the efficiency of Hg^{2+} ions separation. The process of Hg^{2+} ions sorption on MOF is significantly influenced by the pH and the reagent concentration ratio.

6. Acknowledgement

The financial support from the Polish National Centre for Research and Development under the PET-MOF-CLEANWATER project. The studies on waste PET-derived metal-organic framework (MOFs) as cost-effective adsorbents for removal of hazardous elements from polluted water” have been gratefully acknowledged.

References

1. Badillo-Almaraz VE, Solache-Ríos MJ, Badillo-Almaraz V, Zarate-Morales A, Flores-Moreno A. 2017. Radiotracer techniques (^{18}F) and modeling of fluoride sorption on alumina. *Journal of Fluorine Chemistry*, 199: 113–118. <https://doi.org/10.1016/j.jfluchem.2017.04.001>
2. Cojocar C, Zakrzewska-Trznadel G, Jaworska A. 2009. Removal of cobalt ions from aqueous solutions by polymer-assisted ultrafiltration using experimental design approach. Part 1: Optimization of complexation conditions. *Journal of Hazardous Material*, 169: 599–609. <https://doi.org/10.1016/j.jhazmat.2009.03.145>
3. Cojocar C, Zakrzewska-Trznadel G, Miskiewicz A. 2009. Removal of cobalt ions from aqueous solutions by polymer-assisted ultrafiltration using experimental design approach. Part 2: Optimization of hydrodynamic conditions for a cross-flow ultrafiltration module with rotating part. *Journal of Hazardous Material*, 169: 610–620. <https://doi.org/10.1016/j.jhazmat.2009.03.148>
4. De Gisi S, Lofrano G, Grassi M, Notarnicola M. 2016. Characteristics and adsorption capacities of low-cost sorbents for wastewater treatment: A review. *Sustainable Materials and Technologies*, 9:10–40. <https://doi.org/10.1016/j.susmat.2016.06.002>

5. Hilbrandt I, Shemer H, Ruhl AS, Semiat R, Jekel M. 2019. Comparing fine particulate iron hydroxide adsorbents for the removal of phosphate in a hybrid adsorption/ultrafiltration system. *Separation and Purification Technology*, 221: 23–28. <https://doi.org/10.1016/j.seppur.2019.03.044>
6. International Atomic Energy Agency. 2004. Application of membrane technologies for liquid radioactive waste processing. Technical Report Series No.431.
7. Konieczny KH, Wszelaka-Rylik M, Macherzyński B. 2019. Membrane processes innovation in environmental protection: review. *Archives of Environmental Protection*, 45(4):20–29.
8. Maimoun B, Djafer A, Djafer L, Marin-Ayral RM, Ayral A. 2020. Wastewater treatment using a hybrid process coupling adsorption on marl and microfiltration. *Membrane Water Treatment*, 11(4): 001–011.
9. Miśkiewicz A, Zakrzewska-Kołtuniewicz G. 2021. Application of biosorbents in hybrid ultrafiltration/sorption processes to remove radionuclides from low-level radioactive waste. *Desalination and Water Treatment*, 1–9, DOI: 10.5004/dwt.2021.27870, (In press). <https://doi.org/10.5004/dwt.2021.27870>
10. Petroni SLG, Pires MAF, Munita CS. 2004. Use of radiotracer in adsorption studies of copper on Peat. *Journal of Radioanalytical and Nuclear Chemistry*, 259(2): 239–243. <https://doi.org/10.1023/B:JRNC.0000017295.68663.6b>
11. Racar M, Dolar D, Špehar A, Košutić K. 2017. Application of UF/NF/RO membranes for treatment and reuse of rendering plant wastewater. *Process Safety and Environmental Protection*, 105(C):386–392. <https://doi.org/10.1016/j.psep.2016.11.015>
12. Vaziri M, Ghomsheh SMT, Azimi A, Mirzaei M. 2021. Hybrid of Adsorption and Nanofiltration Processes as a Capable Removal Method for HANs Removal. *South African Journal Chemical Engineering*, 36: 1–7. <https://doi.org/10.1016/j.sajce.2020.12.002>
13. Zakrzewska-Trznadel G, Harasimowicz M, Miskiewicz A, Jaworska A, Dłuska E, Wroński S. 2009. Reducing fouling and boundary-layer by application of helical flow in ultrafiltration module employed for radioactive wastes processing. *Desalination*, 240: 108–116. <https://doi.org/10.1016/j.desal.2007.10.091>
14. Zakrzewska-Trznadel G. 2013. Advances in membrane technologies for the treatment of liquid radioactive waste. *Desalination*, 321: 119–130. DOI: 10.1016/j.desal.2013.02.022. <https://doi.org/10.1016/j.desal.2013.02.022>

Chapter 5

The production of prototypical MOFs from waste-PET provides a stepping-stone towards MOFs-based water-harvesting applications

Jianwei Ren ^{a,*}, Tien-Chien Jen ^a, Wojciech Starosta ^b,
Bożena Sartowska ^b, Philiswa Nosizo Nomngongo ^c

^aUniversity of Johannesburg, Johannesburg, Kingsway, and University Road,
Auckland Park, 2092, P.O. Box 524, Auckland Park, 2006,
Johannesburg, South Africa

^bLaboratory of Materials Research, Institute of Nuclear Chemistry and
Technology, Dorodna 16, 03-195 Warsaw, Poland

^cDepartment of Chemical Sciences, University of Johannesburg,
Doornfontein Campus, P.O. Box 17011, Johannesburg, 2028, South Africa

*Corresponding author. Tel: +27 11 559 2103. Email: jren@uj.ac.za (J. Ren)

Abstract

Metal-organic frameworks (MOFs)-based atmospheric water harvesting (AWH) has become an interesting research topic to address water scarcity in the arid regions. However, the availability of the cost-effective prototypical MOFs materials poses an actual challenge for their wide applications. In this work, the production of prototypical MOFs from waste PET is recognised as an important stepping-stone towards MOFs-based AWH applications.

Keywords: Metal-organic frameworks, Atmospheric water harvesting, Prototypical MOFs, Waste PET

1. Global warming affects the water scarcity

A popular quote by Leonardo da Vinci acknowledges that water is a driving force of nature, and people use water for almost everything. It is a precious commodity. Water scarcity has been a global systemic risk that is developing over time. As a result, six billion people will face different levels of water scarcity during a certain number of months per year by

2050 [1,2]. Some intensive discussions and strong evidence have linked the specific events or an increase in their numbers to the human influence on climate changes, such as non-stopping CO₂ emission in a short time [3]. As shown in Figure 1, the research conducted by Kummu *et al.* [4] found that the population facing water scarcity has increased by nearly 16-fold since the 1900s although the population increased only 4-fold. In particular, the improved living standards and the pursuit for economic growth have been attributed to the water scarcity. Global warming essentially has a negative impact on the water cycles.

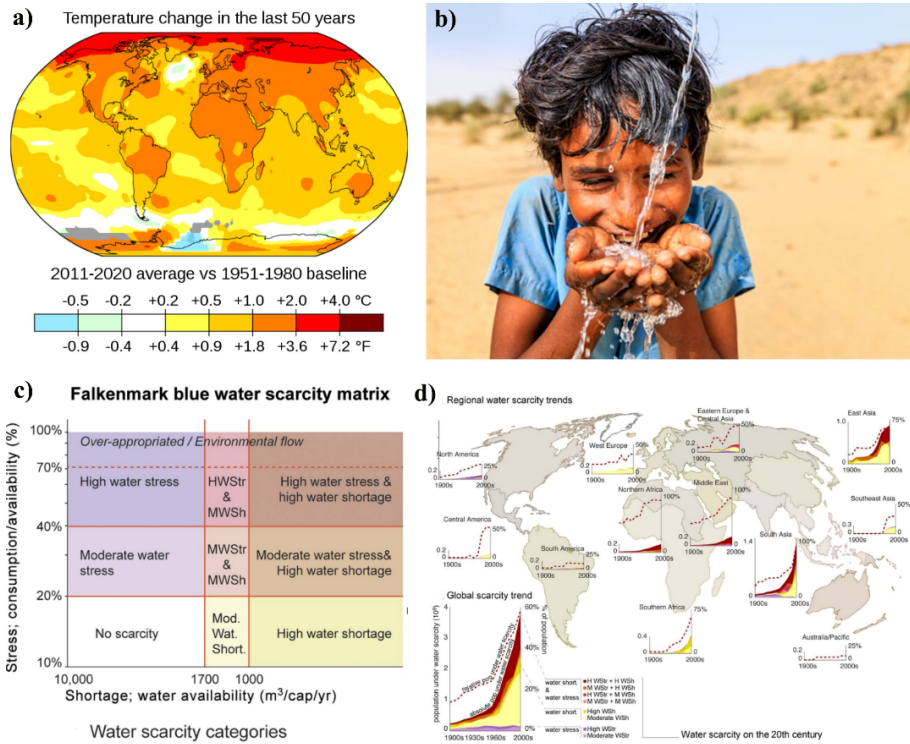


Figure 1: a) Temperature changes in the last 50 years. b) Global warming essentially is a water story. c) Adopted water scarcity matrix, d) Regional and global water scarcity trajectories. Reproduced with permission from ref 1. Copyright ©2016 Springer Nature Limited.

Clearly, water is an ultimately finite resource, so its scarcity has posed a more serious threat than is currently acknowledged. Scientific, technological, and philosophical advances will certainly alleviate future freshwater scarcity. Regardless of these factors, global warming and associated changes to the water cycle vastly complicate the challenge of

sustaining freshwater supplies for the foreseeable future. Although global warming has so far not been fully reflected, it is responsible for the visible sea-ice loss. Extreme events such as heatwaves, drying soil, and a change in climate are evidence of global warming, and the climate models have consistently projected temperature increases in tropical countries over the coming decades. More specifically, it was projected that poor countries that have contributed minimally to climate change will experience more increase in variability, and this would amplify the inequality associated with the impact of a changing climate. As a matter of climate justice, it is essential for the relatively wealthy to bear the expenses for digging deeper wells, paying for the electricity consumption, and treating lower-quality freshwater [5,6]. Similar to the oil war, the freshwater scarcity threat will eventually turn into comprehensive debates and political conflicts in many countries in the arid regions of the globe, and the more critical local patterns than global patterns will make the problem more difficult to solve. From the literature point of view, one local-focus rather than a global-focus remedial measure can be proposed to support a more sustainable population and economic growth: using the atmospheric water as a freshwater resource in arid regions globally.

2. The atmospheric water as freshwater resource in different forms

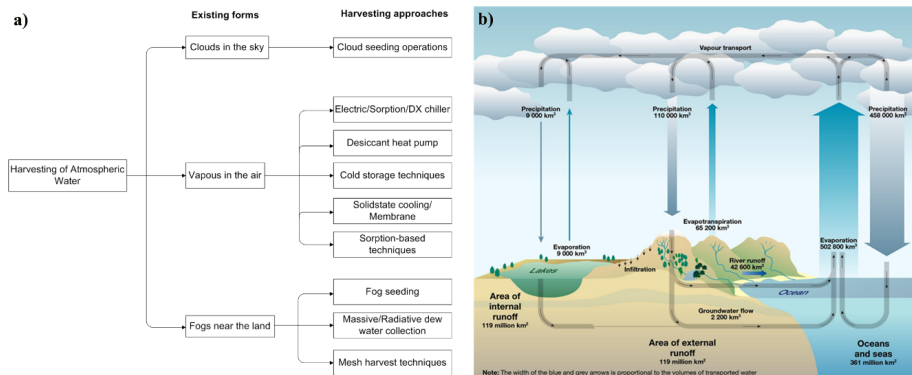


Figure 2: a) Atmospheric water exists in three main forms. b) The isotopic composition of atmospheric water vapour.

As shown in Figure 2, about 10^{21} litres of water exist in the atmosphere at any given time in three basic forms – clouds floating in the sky, fog close to the land, and water vapour in the air.

More liquid water likely tends to become atmospheric water under global warming conditions. Theoretically, this portion of water has the

potential to water the arid regions of the world. Unlike the desalination process, minimum influence may disrupt the hydrological cycle when water is taken out of the air [7]. Besides, the source of the atmospheric water is normally clean, and the water quality is high enough to make the water suitable for drinking and other domestic or agricultural purposes [8]. In other words, atmospheric water harvesting seems to be a geographically and climatically independent water production method for disaster relief needs and decentralised water supply. The demonstrations on atmospheric water harvesting have been made in several traditional ways, such as artificial rain or cloud seeding for cloud water harvesting, fog seeding or mesh techniques for fog water harvesting, and dew water harvesting using water bamboo tower. Traditionally, the harvesting of fog water and dew water was achieved with clear economic feasibility in areas with high humidity, fog gathering, or cloud cover [9].

In humid regions, water vapour can be condensed and harvested in the form of dew water by cooling it on a surface below its dew point temperature. Usually, the cooling technologies are classified as passive cooling, solar-regenerated desiccant, and active cooling. Ideally, when the water is taken out of the air, there is minimum influence to disrupt the hydrological cycle or steal water away from important critical sources nearby. In fact, the fog is a cloud but with physical contact with the surface of the earth, and the harvesting of water occurs when the fog droplets impact and intercept the harvesting surfaces. In other words, although fog water harvesting promises to be a low-cost approach for drinking water, crop irrigation, livestock watering, and forest restoration in dryland mountains, it is highly dependent on the geographical factors and conditions for fog occurrence. Typically, the combination of an ocean with a near-coast mountainous region is favourable for such fog harvesting. Clearly, the setting-up of such a system for fog water harvesting is subject to limited rain at least for a significant time period of a year [10].

By referring to the project demonstrations of fog harvesters in Figure 3a, the mesh types design (Figure 3b) play a critical role in determining the system efficiency, and the appropriate tuning of the wetting characteristics of the surfaces, reducing the wire radii and optimising the wire spacing, all lead to more efficient fog harvesting [12]. Figure 3c illustrates the project demonstrations for fog water harvesting in arid or seasonally arid regions. In this regard, Jarimi and co-workers [13] have done comprehensive work by reviewing the critical aspects of the fog harvesters, including design, efficiency and feasibility studies, mesh topology, surface wettability, as well as biomimicry-inspired fog water harvesters. With the prerequisite of temperature below its saturation point, only a limited number of places where fog can be naturally formed from moist air provided that. In fact, the fog was

reported as an alternative freshwater source less accessible than seawater. Besides, although dew water can be extracted from the air by cooling to a temperature lower than the air dew point, several stepping-stone works reported that the energy consumption is high, especially when solar energy is used due to low convention efficiency, low specific yields (SY), and low daytime relative humidity (RH). However, a target with average daily drinking water of five litres per day per person can be achieved experimentally in the demonstration of materials-based atmospheric water harvesting [14]. Apparently, a local-focus rather than global-focus remedial measure can be proposed to support more sustainable population and economic growths, that is, using materials-based techniques to collect the atmospheric water as a freshwater resource in arid regions globally.

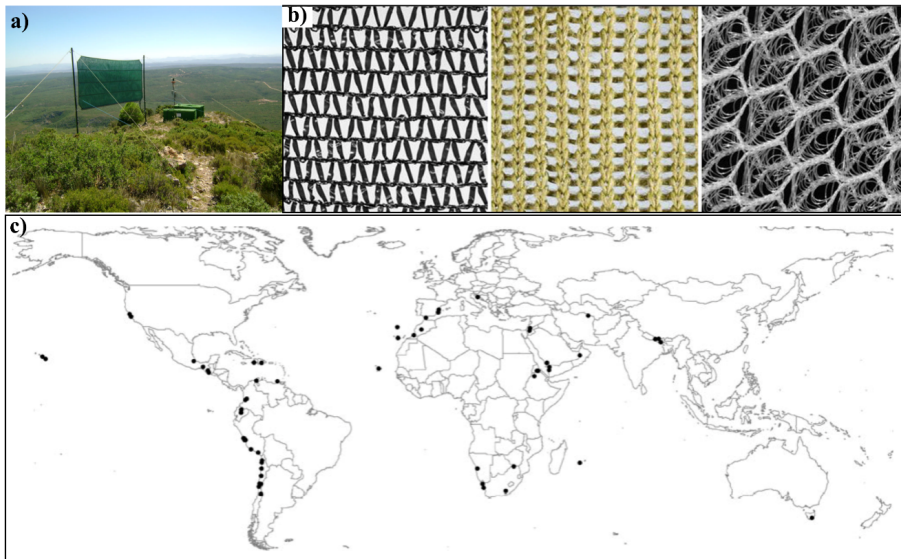


Figure 3: a) The project demonstration of the fog harvester. b) The used mesh for the fog water collection. c) Project demonstrations for fog water harvesting in arid or seasonally arid regions. Re-organised from ref [10, 11].

The relative humidity (ϕ) represents the ratio of the partial pressure of water vapour (P_w) to the saturation pressure (P_s), while the absolute humidity (ω) represents the maximum amount of water that can be extracted from the air [15].

$$\phi = \frac{P_w}{P_s(T)} \quad (1)$$

The relation between relative humidity, absolute humidity, temperature, and total air pressure can be described using equation (2).

$$\phi = \frac{\omega P}{(0.622 + \omega) P_s(T)} \quad (2)$$

3. Materials-based atmospheric water harvesting (AWH)

3.1. Working principle of materials-based AWH

The traditional AWH in humid regions can be realised by using fog harvest or by condensation. However, in regions with low RH below 30%, it is mandatory to bring down the air temperature below the freezing point, and such direct cooling of air to condense water turns out to be energy-consuming and impractical. It requires untenable amounts of electrical power to operate the refrigeration units. Apparently, this requires an effective way to concentrate the water vapour at acceptable energy consumption. As illustrated in Figure 4a, for the AWH in the arid regions with RH around 20% (*point a*), it must be cooled to the dew point (*point b*) to allow the water saturation. In contrast, for the AWH in the humidity regions with RH around 90% (*point c*), the cooling is minimal towards (*point d*). The employment of materials will essentially lift the desert air with low RH (*point a*) up to the high RH (*point c*) and then reaches the water saturation more efficiently than direct cooling. Generally, the direct cooling approach is applicable in the green region, and the materials-based can work in the pink region to turn the desert air into tropical air for further AWH purposes. Thus far, almost all the technology explorations have been focusing on the humid conditions in the green region with the principles of direct air cooling by using the condensation cycle. In other words, the direct cooling approach is only applicable in limited regions globally as shown in Figure 4b. In contrast, the materials-based AWH is capable of facilitating water harvesting from the air and delivering clean water. Accordingly, some materials, including inorganic salts, zeolites, porous silica, and composite matrices were tested to solve the dew point issue that has posed challenges for them to be implemented at lower RH conditions [16,17]. However, the literature revealed that all these materials pose different challenges in reality. These include slow-onset start, slow adsorption/desorption kinetics, low AWH capacity at low RH, and require extensive desorption energy.

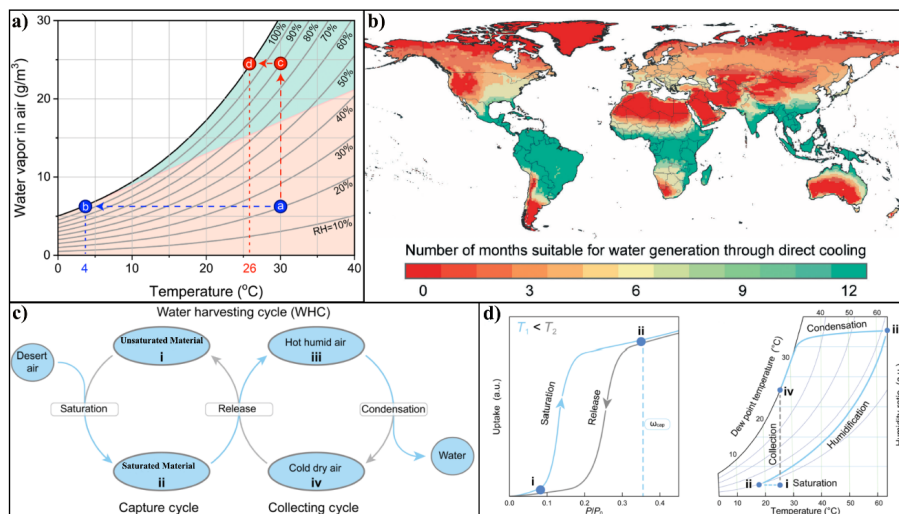


Figure 4: a) The modified psychrometric chart and b) The applicable regions for direct cooling. c) Materials-based AWH consists of the capture and collecting cycles. d) The capture cycle is defined by the sorption isotherm of the applied sorbent material, and the collecting cycle is defined by the psychrometric chart. Modified from Ref. [18–20] with permissions.

The materials-based AWH provides the possible capacity for water vapour concentration by materials beds from the air, which can later be recovered in a thermal-driven step. As shown in Figure 4c, a materials-based AWH cycle consists of a capture cycle and a collecting cycle. The unsaturated adsorbent materials will get saturation when exposed to air at night, and the water is released from the saturated sorbent materials when exposed to sunlight at daytime. The collection cycle takes place when the released water vapour humidifies the air in the vicinity of the materials at daytime, and liquefied water can be collected on the condenser under the function of condensation. This means, the materials-based AWH systems have the potential to be operated in arid regions by using a low-grade thermal energy source and achieving a low specific energy consumption per unit mass water production [21]. Being an efficient AWH system, firstly, it shall accommodate the general global scenario of being able to harvest atmospheric water at low humidity. Secondly, the adsorption-desorption kinetics of the water cycle shall be sufficient to allow the production of sufficient water. Thirdly, the working capacity should be high enough for the sake of energy saving for cycling. Currently, the most popular materials are represented by inorganic salts, zeolites, and porous polymers. Besides, many efforts had focused on the development strategies of superior

adsorbent materials and system designs with sustainable considerations. Clearly, in Figure 4d, the capture cycle is determined by the sorption isotherm of the sorbent materials, and the collection cycle is defined by the psychrometric chart. It is worth noting that the collection cycle can continue until the humidity ratio is too low to reach the dew point.

3.2. Criteria for materials-based AWH applications

The discussions above show that there are prerequisites for a high-performance AWH system such as a type IV or type V water adsorption isotherm with minimal or no hysteresis, a steep uptake below 25% with a high adsorption capacity below 35%, and ideally a significant shift of the inflection point for isotherms recorded at different temperature. The specialised materials play a key role in those processes. The key here is not just the amount of water absorbed, but also the amount that can be released via low-grade heat sources.

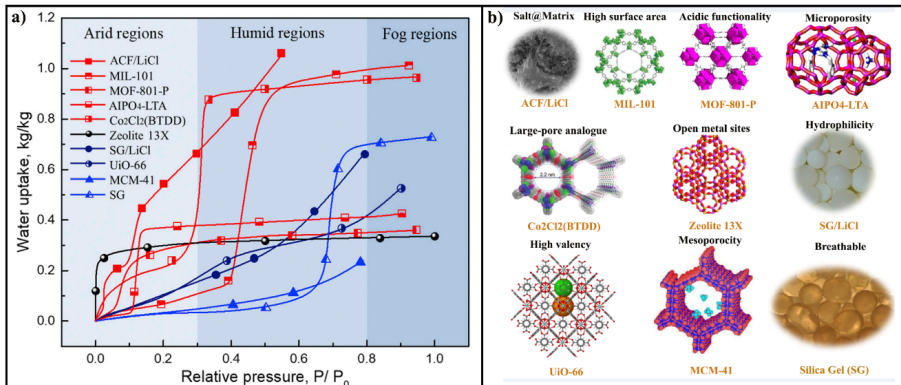


Figure 5: a) The promising materials reported in the literature for AWH. b) Different functionalities for materials design. Reproduced from Ref. [22] with permission.

As atmospheric water harvesting depends mainly on ambient relative humidity (RH), three applicable regions are usually discussed in the literature: fog regions with RH >80%, humid regions with 30% < RH < 80%, and arid regions with RH < 30%. As illustrated in Figure 5 [22], examples of materials like UiO-66 MOF with high valency perform well in the fog regions, MIL-101 MOF with high surface area performs well in the humid regions and the activated carbon fiber (ACF)/LiCl type of salt@matrix composite can perform well in both humid and arid regions. As summarised by De Lange *et al.* [23] and Burtch *et al.* [24], the criteria for the materials development to be used for water adsorption/desorption applications are: (i) S-shape of the water adsorption isotherm at 298 K. (ii) High

water sorption capacity at low humidity <30% RH. (iii) Low regeneration temperature <100 °C. (iv) High pore volume. This is desirable for improved performance, and the consistent microstructures will ensure a stepped absorption performance within a narrow RH range. (v) Adsorption steps should be located in the pressure range $0.1 < p/p_0 < 0.3$, which not only increases the temperature lift but also decreases the desorption temperature. (vi) Hysteresis between adsorption and desorption branches should be avoided if possible. (vii) The materials should show a stable adsorption/desorption performance over thousands of cycles.

The sudden water uptakes in S-shape isotherm mean that the adsorbent can be regenerated by lower temperature heat sources. The narrow RH interval is well in accordance with the fixed working conditions of the adsorptive chiller. However, an open system usually experiences a very wide range of weather conditions during one day or through a whole year, and in such a case, an S-shape isotherm with a lower RH at the onset of the isotherm is necessary to equip the ability to collect sufficient water under any climate conditions. To maximise the capacity, a linear isotherm is expected for dehumidification, whose uptake will increase along with the rising RH.

Based on the above analysis, the ideal adsorbent material for water vapour harvesting applications should have features as follows: (i) in the adsorption process (<25 °C), their water sorption capacity should increase linearly with RH and (ii) in the desorption process (>35 °C), their water sorption capacity should drop steeply with increased temperature (S-type isotherms). From the literature point of view, the current commercial and laboratory available materials are difficult to fully satisfy these features, which are either temperature-insensitive or RH-sensitive. Some composite materials have been reported as a useful approach to designing high-performance, temperature-sensitive materials for water vapour harvesting [25-27]. Through open adsorbing metal sites and binding water prior to pore filling, the pore diameter can be effectively reduced to the critical diameter. In the review work conducted by Zhou *et al* [28], the materials-based AWH mechanism, fundamental requirements, and structural design principles were summarised into the general four aspects that include high water uptake, face capture/release, low energy demand, and cycling stability.

3.2. Selection of prototypical MOFs for AWH applications

For the selection of the optimal sorbent materials, several critical properties such as hydrophilicity, pore diameter, and stability must be taken into consideration [29]. In choosing a sorbent material, a balance

between the high affinity for water vapour and desorption energy must be struck. In this regard, metal-organic frameworks (MOFs) as a new generation of porous materials are able to accommodate all these required flexibilities and tune the water uptake step by varying factors such as pore size and hydrophilicity for water vapour harvesting applications in arid regions. Typically, the pore hydrophilicity of the selected MOFs shall be sufficient to allow the water nucleation and the pore-filling under the arid condition (<30% RH). Canivet *et al* [30] suggested disclosing the underlying mechanism by using three parameters including (i) the Henry constant (K_H) related to the slope of the adsorption isotherm at very low water partial pressures, (ii) the relative pressure at which half of the total water capacity is reached, and the maximum water adsorption capacity (Q_m). Typically, the Henry constant K_H mainly describes the surface adsorption properties, and pore-filling pressure mostly reflects the pore size. Clearly, both of them are correlated to reflect the hydrophobicity-hydrophilicity of the MOF material, which can be modified by the linker functionalisation. The total water uptake is correlated with the porous volume at the exception of MOFs with gate-opening properties and superhydrophobicity such as ZIF-8. For the water adsorption under a given temperature, the pore diameter shall be smaller than the critical diameter of 20 Å of the water molecule to avoid the undesirable hysteresis upon water desorption, which can be estimated from the equation:

$$D_c = 4\sigma T_c / (T_c - T) \quad (3)$$

where D_c refers to the size of the water molecule, T is the temperature, and $T_c = 647$ K is the bulk critical temperature for water.

In other words, given a case of water vapour adsorption at room temperature, the critical apparent pore diameter determining the mechanism of adsorption is expected to be around 20 Å. Beyond this value, the pore-filling will occur through irreversible capillary condensation accompanied by capillary hysteresis loops, and below this critical diameter, pore-filling is continuous and reversible unless the MOF material exhibits some adsorption-induced flexibility. Fundamentally, this implies that an adsorbent with a pore diameter around 20 Å will result in the water pre-adsorption on the open metal sites prior to pore-filling. The sequential pore-filling starts from the smallest pore and progresses to the middle and largest pores. Thereafter, the internal available volume can be maximised for filling with water while avoiding irreversible capillary condensation. This serves as a general strategy in designing superior sorbents to proceed with a reversible pore filling [31]. An observed step water uptake

behaviour on MOF-801 and MOF-841 at 10% RH implied a spectacular binding of water at desert air condition. Further investigations showed the initial formation of pore shape-dependent water aggregates in the MOF pores, and these aggregates later served as the seeds to attract the additional water molecules into the pores [32]. Overall, the formation of those water seeds drove the isotherm into a step profile by contributing to the enhancement of water binding. Attributing by the polar secondary building units (SBUs) and nonpolar organic linkers, the release of water was enabled under mild conditions by following a cooperative mechanism as indicated by the step isotherm behaviour.

Unlike other materials and technologies, MOFs are the only materials known to work anytime and anywhere. The main challenge for MOF industrialisation is the negative view on large-scale MOF production in a cost-effective manner. There seems to be a general tendency and misconception that all MOFs are unstable to water, polar solvents, too expensive, and low yielding to scale up. Cost reduction will be possible if a mass production process can be developed.

4. Prototypical MOFs production from waster-PET provides an important stepping-stone

Costs are crucial to determine the business case and viability of any commercial application. MOFs are really compelling in terms of performance, but right now the scalability to larger volumes is limited for certain types and the cost is also high. In traditional forms of MOF synthesis such as solvothermal methods, a very wide space is required to tune the reaction parameters such as reaction temperature, time, stoichiometry, and so on. Generally, the availability of cost-effective MOFs remains a real challenge in the wide implementation of MOFs-based AWH systems (Figure 6).

So far, a library of MOFs has been reported to display a broad variety of behaviour for water adsorption applications, and these earlier works provided the main guidelines for the design of MOFs with specific hydrophilicity-hydrophobicity properties. Table 1 lists the water affinities of MOF samples from the hydrophilic HKUST-1 MOF to the very hydrophobic MOF ZIF-8. The mesoporous MIL-101 showed an exceptional water capacity of 1 g g^{-1} [33]. The large water capacity of MIL-101 exhibited an adsorption isotherm of combined type I and type V. Such isotherms consist of two steps starting from the water adsorption at the inorganic clusters (type I) and followed by the filling of the mesoporous cavities (type V) [34,35].



Figure 6: Pilot-scale production of cost-effective MOFs remains a knowledge gap

Some of the earlier work focused on the green synthesis of the target MOFs. Chen *et al.* [37] reported an aqueous solution-based synthesis of prototypical UiO-66-NH₂ at room temperature, which offered the advantages such as reduction of toxic byproducts, reduction of operation costs, and increased safety in the MOF production. Zhao and co-workers [38] used HNO₃ as an additive to produce prototypical MIL-101(Cr) in >100 g quantities with yields near 70% and BET-surface areas around 4000 m² g⁻¹. Recently, research has been focused on the chemical engineering aspects of MOF production.

Table 1: MOFs studied in literature for AWH applications

MOFs	SA ^a (m ² g ⁻¹)	V _p ^b (cm ³ g ⁻¹)	Uptake capacity ^c (g kg ⁻¹)	Working capacity ^d (g kg ⁻¹)	Water desorbed (%)
MIL-125(Ti)	1153	0.47	323	313	97
MIL-125(Ti)-NH ₂	1358	0.55	413	409	99
UiO-66(Zr)	959	0.40	347	338	97
UiO-66(Zr)-NH ₂	1109	0.46	364	355	98
MOF-808(Zr)	1880	0.69	744	714	96
MIL-101(Cr)	2579	1.63	1263	1246	98

MOFs	SA ^a (m ² g ⁻¹)	V _p ^b (cm ³ g ⁻¹)	Uptake capacity ^c (g kg ⁻¹)	Working capacity ^d (g kg ⁻¹)	Water desorbed (%)
HKUST-1(Cu)	1512	0.41	218	105	48
MIL-53(Al)	814	0.41	13	2	15
ZIF-8(Zn)	1835	0.69	15	6	40

^aSurface area calculated from Brunauer-Emmett-Teller (BET) model analysis of N₂ gas adsorption-desorption isotherm at 77 K. ^bPre volume calculated at p/p₀=0.4 of N₂ adsorption isotherm (77 K). ^cWater vapor uptake capacity was determined gravimetrically, and the value is taken from the first cycle adsorption at 70% RH and 22 °C at ambient pressure. ^dWorking capacity was determined gravimetrically by the difference in the amount of water desorbed and adsorbed during water cycle stability and recovery studies. Modified from Ref. [36].

4.1. Proof-of-concept of prototypical MOFs production from waste PET

The terephthalic acid (BDC) after being retrieved from plastic bottles was tested by gas chromatography (GC) which showed that the concentration was more than 99%, which is comparable to that of commercial BDC. This recycled BDC was used as the organic ligand in the synthesis of MIL-53 (Fe). After the initial proof-of-concept was approved by producing MOFs from the clear PET [39–40], experimental trials were conducted on the coloured waste PET and food trays. The results are shown in Figure 7.

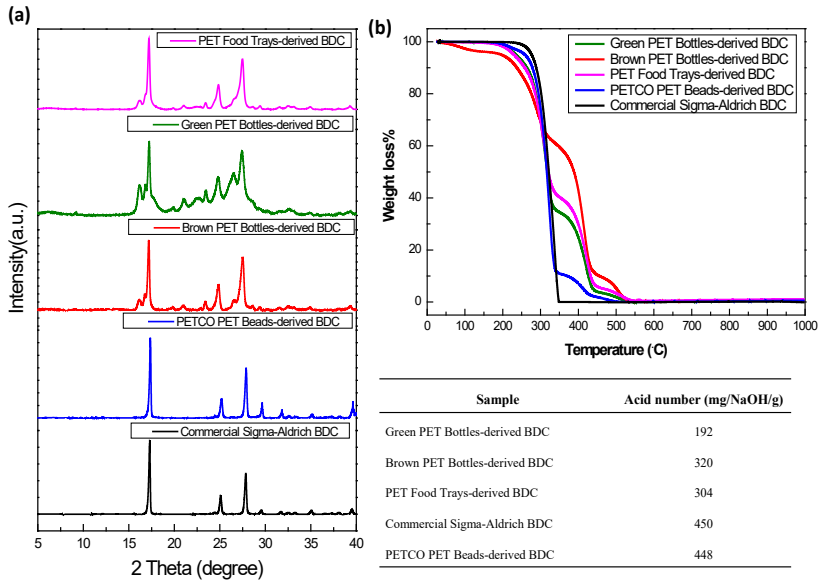


Figure 7: (a) PXRD patterns, and (b) TGA curves of the BDC samples derived from different PET sources. Right bottom Table: the titration results of the acid numbers from different BDC samples

Figure 7 shows the X-ray diffraction (XRD) patterns and the thermogravimetric analysis (TGA) curves of the BDC products from different PET sources. As compared to the commercial Sigma-Aldrich BDC sample with a purity of 98%, the crystallinity of PETCO PET Beads-derived BDC is very close to that of the commercial BDC, as evidenced by the similar acid number of 448 mg NaOH/g against 450 mg NaOH/g. As indicated by the XRD patterns, the crystallinity of the Brown PET Bottles-derived-BDC sample is close to that of the PET Food Trays-derived BDC sample. Meanwhile, the containing acid numbers are also nearly the same. In contrast, the crystallinity of the Green PET Bottles-derived BDC is the lowest with an acid number of only 192 mg NaOH/g. It can be seen from Figure 7b that the purity of different BDC samples are slightly different.

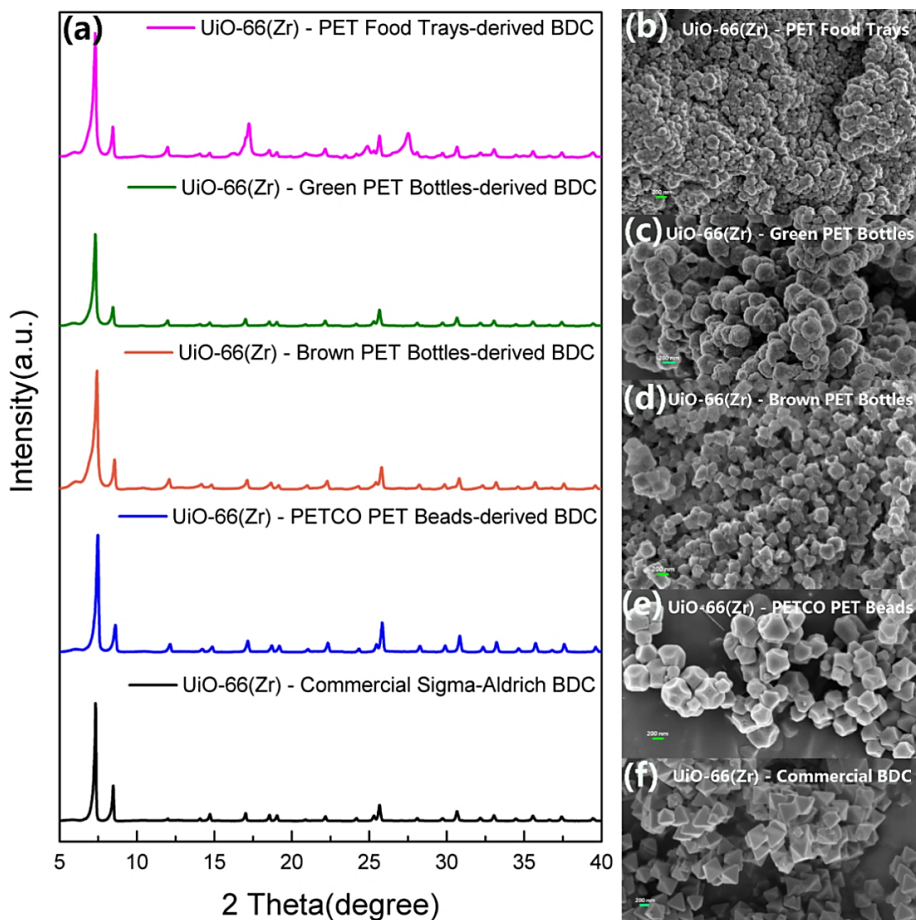


Figure 8: (a) XRD patterns, and (b-f) SEM images of the Zr-MOF samples prepared from different BDC sources

Several characteristic reflection signals in Figure 8a confirmed the successful synthesis of MOF UiO-66(Zr) from different PET-derived BDC when compared to the simulated XRD pattern. The relative crystallinities of the obtained MOF UiO-66(Zr) samples are comparable to that from commercial BDC feedstock from Sigma-Aldrich. However, as shown in Figure 8b, the Zr-MOF sample synthesised from Green PET Bottles-derived BDC shows the lowest relative crystallinity. The scanning electron microscope (SEM) images in Figure 8b-f show the quite differed morphologies of the obtained MOF UiO-66(Zr) samples.

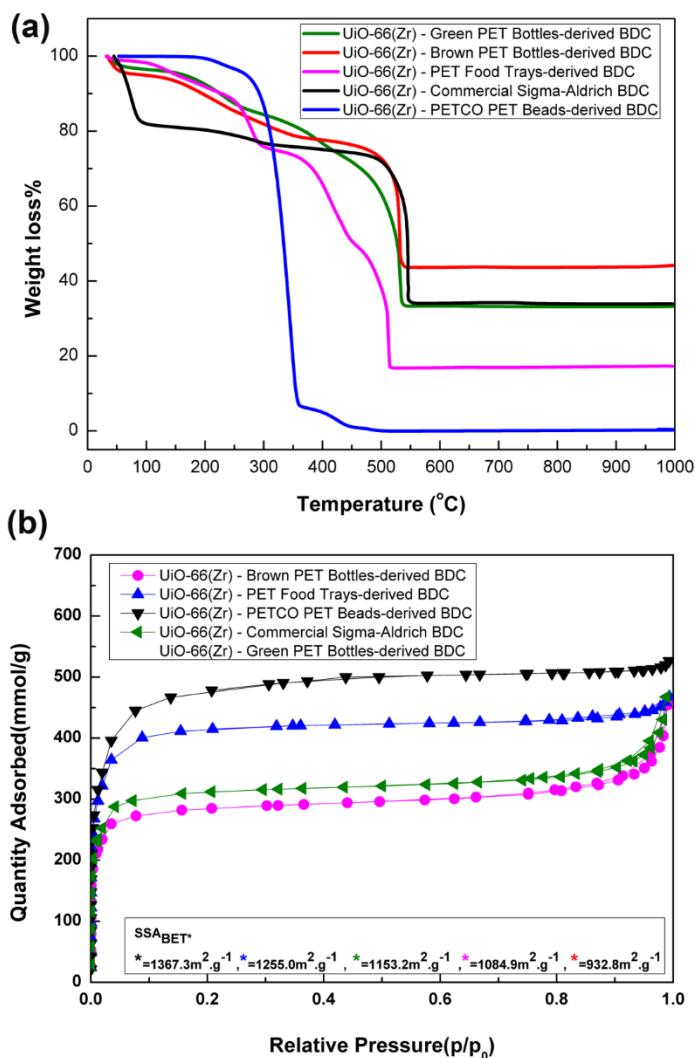


Figure 9: (a) TGA curves and (b) N₂ sorption of the MOF UiO-66(Zr) samples prepared from different BDC sources.

Figure 9a shows the TGA properties of the obtained MOF UiO-66(Zr) prepared from different BDC sources. The N₂ and H₂ sorption isotherms presented in Figure 9b indicate that all the PET-derived MOF UiO-66(Zr) materials have relatively lower N₂ and H₂ adsorption levels, but the obtained values are comparable to that from the commercial feedstock as well as other previously developed MOF UiO-66(Zr) materials. MOF UiO-66(Zr) samples were also synthesised from the coloured PET bottles-derived BDC, where the effects of additives and colorants should be considered on the textural properties of the prepared MOF UiO-66(Zr). The experiment

results suggested that the MOF UiO-66(Zr) samples from the clear PET food trays-derived BDC have lower textural properties than those from the clear PET beads-derived BDC. The reason could be the effects of additives and colorants from the green and brown coloured bottles.

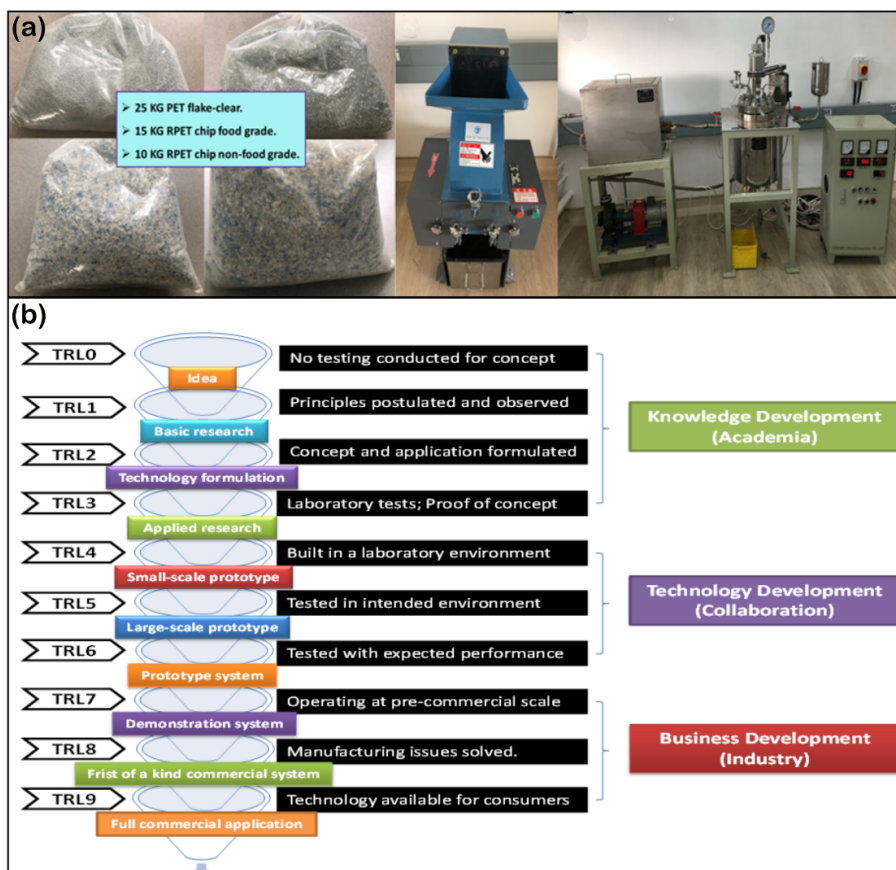


Figure 10: (a) Upscaled production of the target MOFs from waste-PET. (b) The technology readiness level (TRL).

With that knowledge in hand, the prototypical MOFs production was scaled-up to 1 kg/batch in our laboratory, as illustrated in Figure 10a, and the technology readiness level (TRL) referring to Figure 10b can be defined between 6–7.

5. Conclusion

In summary, this work experimentally demonstrated the production of prototypical MOFs materials from various waste PET streams including the PET food trays, green and brown PET bottles. The results provided

a stepping-stone towards the implementation of MOFs-based AWH systems.

References

1. Mekonnen, M.M.; Hoekstra, A.Y. Four billion people facing severe water scarcity. *Sci Adv* **2016**, *2*, e1500323. <https://doi.org/10.1126/sciadv.1500323>
2. Boretti, A.; Rosa, L. Reassessing the projections of the world water development report. *npj Clean Water* **2019**, *2*, 15. <https://doi.org/10.1038/s41545-019-0039-9>
3. D. Coumou, S. Rahmstorf. A decade of weather extremes. *Nat Clim Change* **2012**, *2*, 491–496. <https://doi.org/10.1038/nclimate1452>
4. Kummu, M.; Guillaume, J.H.A.; de Moel, H.; Eisner, S.; Flörke, M.; Porkka, M.; Siebert, S.; Veldkamp, T.I.E.; Ward, P.J. The world's road to water scarcity: shortage and stress in the 20th century and pathways towards sustainability. *Sci Rep* **2016**, *6*, 38495. <https://doi.org/10.1038/srep38495>
5. Bathiany, S.; Dakos, V.; Scheffer, M.; Lenton, T.M. Climate models predict increasing temperature variability in poor countries. *Sci Adv* **2018**, *4*, eaar5809. <https://doi.org/10.1126/sciadv.aar5809>
6. Wada, Y.; de Graff, I.E.M.; van Beek, L.P.H. High-resolution modelling of human and climate impacts on global water resources. *J Adv Model Earth Syst* **2016**, *8*, 735–763. <https://doi.org/10.1002/2015MS000618>
7. Nikolayev, V.S.; Beysens, D.; Gioda, A.; Milimouka, I.; Katiushin, E.; Morel, J.P. Water recovery from dew. *J Hydrol.* **1996**, *182*, 19–35. [https://doi.org/10.1016/0022-1694\(95\)02939-7](https://doi.org/10.1016/0022-1694(95)02939-7)
8. Khalil, B.; Adamowski, J.; Shabbir, A.; Jang, C.; Rojas, M.; Reilly, K.; Ozga-Zielinski, B. A review: dew water harvesting from radiative passive collectors to recent developments of active collectors. *Sustain Water Resour. Manag.* **2016**, *2*, 71–86. <https://doi.org/10.1007/s40899-015-0038-z>
9. Habeebullah, B.A. Potential use of evaporator coils for water extraction in hot and humid areas. *Desalination* **2009**, *237*, 330–345. <https://doi.org/10.1016/j.desal.2008.01.025>
10. Klemm, O.; Schemenauer, R.S.; Lummerich, A.; Cereceda, P.; Marzol, V.; Corell, D.; van Heerden, J.; Reinhard, D.; Gherezghiher, T.; Olivier, J.; Osses, P.; Sarsour, J.; Frost, E.; Estrela, M.J.; Valiente, J.A.; Fessehaye, G.M. Fog as a fresh-water resource: overview and perspectives. *AMBIO* **2012**, *41*, 221–234. <https://doi.org/10.1007/s13280-012-0247-8>

11. Choiniere-Shields, E (2013). The cloud harvester catches and stores fresh water from fog. From <http://inhabitat.com/httpinhabitat-comwadminpost-phppost519497actioneditmessage1/>
12. Park, K.-C.; Chhatre, S.S.; Srinivasan, S.; Cohen, R.E.; McKinley, G.H. Optimal design of permeable fiber network structures for fog harvesting. *Langmuir* **2013**, *29*, 13269–13277. <https://doi.org/10.1021/la402409f>
13. Jarimi, H.; Powell, R.; Riffat, S. Review of sustainable methods for atmospheric water harvesting. *Int J Low-Carbon Technol* **2020**, *15*, 253–276. <https://doi.org/10.1093/ijlct/ctz072>
14. Lord, J.; Thomas, A.; Treat, N.; Forkin, M.; Bain, R.; Dulac, P.; Behroozi, C.H.; Mamutov, T.; Fongherser, J.; Kobilansky, N.; Washburn, S.; Truesdell, C.; Lee, C.; Schmaelzle, P.H. Global potential for harvesting drinking water from air using solar energy. *Nature* **2021**, *598*, 611–617. <https://doi.org/10.1038/s41586-021-03900-w>
15. Gengel, Y.A.; Boles, M.A. Thermodynamics: an engineering approach 6th edition (SI units). The McGraw-Hill Companies, Inc., New York, 2007.
16. Yu, N.; Wang, R.; Lu, Z.; Wang, L. Development and characterization of silica gel-LiCl composite sorbents for thermal energy storage. *Chem Eng Sci* **2014**, *111*, 73–84. <https://doi.org/10.1016/j.ces.2014.02.012>
17. Ng, E.-P.; Mintova, S. Nanoporous materials with enhanced hydrophilicity and high water sorption capacity. *Microporous Mesoporous Mater* **2008**, *114*, 1–26. <https://doi.org/10.1016/j.micromeso.2007.12.022>
18. Liu, C.-H.; Nguyen, H.L.; Yaghi, O. Reticular chemistry and harvesting water from desert air. *AsiaChem* **2020**, *1*, 18–25. <https://doi.org/10.51167/acm00007>
19. Xu, W.T.; Yaghi, O.M. Metal-organic frameworks for water harvesting from air, anywhere, anytime. *ACS Cent Sci* **2020**, *6*, 1348–1354. <https://doi.org/10.1021/acscentsci.0c00678>
20. Fathieh, F.; Kalmutzki, M.J.; Kapustin, E.A.; Waller, P.J.; Yang, J.; Yaghi, O.M. Practical water production from desert air. *Sci Adv* **2018**, *4*, No. eaat3198. <https://doi.org/10.1126/sciadv.aat3198>
21. William, G.E.; Mohamed, M.H.; Fatouh, M. Desiccant system for water production from humid air using solar energy. *Energy* **2015**, *90*, 1707–1720. <https://doi.org/10.1016/j.energy.2015.06.125>
22. Tu Y.D.; Wang, R.Z.; Zhang, Y.N.; Wang, J.Y. Progress and expectation of atmospheric water harvesting. *Joule* **2018**, *2*, 1452–1475. <https://doi.org/10.1016/j.joule.2018.07.015>

23. de Lange, M.F.; Verouden, K.J.F.M.; Vlugt, T.J.H.; Gascon, J.; Kapteijin, F. Adsorption-driven heat pumps: the potential of metal-organic frameworks. *Chem Rev* **2015**, *115*, 1220–12250. <https://doi.org/10.1021/acs.chemrev.5b00059>
24. Burtch, N.C.; Jasuja, H.; Walton, K.S. Water stability and adsorption in metal-organic frameworks. *Chem Rev* **2014**, *114*, 10575–10612. <https://doi.org/10.1021/cr5002589>
25. Alayli, Y.; Hadji, N.E.; Leblond, J. A new process for the extraction of water from air. *Desalination* **1987**, *67*, 227–229. [https://doi.org/10.1016/0011-9164\(87\)90246-3](https://doi.org/10.1016/0011-9164(87)90246-3)
26. Kallenberger, P.A.; Fröba, M. Water harvesting from air with a hygroscopic salt in a hydrogel-derived matrix. *Commun Chem* **2018**, *1*, 28. <https://doi.org/10.1038/s42004-018-0028-9>
27. Fathieh, F.; Kalmutzki, M.J.; Kapustin, E.A.; Waller, P.J.; Yang, J.; Yaghi, O.M. Practical water production from desert air. *Sci Adv* **2018**, *4*, No. eaat3198. <https://doi.org/10.1126/sciadv.aat3198>
28. Zhou, X.Y.; Lu, H.Y.; Zhao, F.; Yu, G.H. Atmospheric water harvesting: a review of material and structural designs. *ACS materials Lett* **2020**, *2*, 671–684. <https://doi.org/10.1021/acsmaterialslett.oc00130>
29. Rieth, A.J.; Yang, S.; Wang, E.N.; Dincă, M. Record atmospheric fresh water capture and heat transfer with a material operating at the water uptake reversibility limit. *ACS Cent Sci* **2017**, *3*, 668–672. <https://doi.org/10.1021/acscentsci.7b00186>
30. Canivet, J.; Bonnefoy, J.; Daniel, C.; Legrand, A.; Coasne, B.; Farrusseng, D. Structure-property relationships of water adsorption in metal-organic frameworks. *New J Chem* **2014**, *38*, 3102–3111. <https://doi.org/10.1039/C4NJ00076E>
31. Bon, V.; Senkovska, I.; Evans, J.D.; Wöllner, M.; Hölzel, M.; Kaskel, S. Insights into the water adsorption mechanism in the chemically stable zirconium-based MOF DUT-67 – a prospective material for adsorption-driven heat transformations. *J Mater Chem A* **2019**, *7*, 12681–12690. <https://doi.org/10.1039/C9TA00825J>
32. Furukawa, H.; Gandara, F.; Zhang, Y.B.; Jiang, J.; Queen, W.L.; Hudson, M.R.; Yaghi, O.M. Water adsorption in porous metal-organic frameworks and related materials. *J Am Chem Soc* **2014**, *136*, 4369–4381. <https://doi.org/10.1021/ja500330a>
33. Küsgens, P.; Rose, M.; Senkovska, I.; Fröde, H.; Henschel, A.; Siegle, S.; Kaskel, S. Characterization of metal-organic frameworks by water adsorption. *Microporous Mesoporous Mater* **2009**, *120*, 325–330. <https://doi.org/10.1016/j.micromeso.2008.11.020>

34. Düren, T.; Bae, Y.-S.; Snurr, R.Q. Using molecular simulation to characterise metal-organic frameworks for adsorption applications. *Chem Soc Rev* **2009**, *38*, 1237–1247. <https://doi.org/10.1039/b803498m>
35. Canivet, J.; Fateeva, A.; Guo, Y.M.; Coasne, B.; Farrusseng, D. Water adsorption in MOFs: fundamentals and applications. *Chem Soc Rev* **2014**, *43*, 5594–5617. <https://doi.org/10.1039/C4CS00078A>
36. Logan, M.W.; Langevin, S.; Xia, Z.Y. Reversible atmospheric water harvesting using metal-organic frameworks. *Sci Rep* **2020**, *10*, 1492. <https://doi.org/10.1038/s41598-020-58405-9>
37. Chen, Z.J.; Wang, X.J.; Islamoglu, T.; Farha, O.K. Green synthesis of a functionalized zirconium-based metal-organic framework for water, and ethanol adsorption. *Inorganics* **2019**, *7*, 56. <https://doi.org/10.3390/inorganics7050056>
38. Zhao, T.; Jeremias, F.; Boldog, I.; Nguyen B.; Henninger, S.K.; Janiak C. High-yield, fluoride-free and large-scale synthesis of MIL-101(Cr). *Dalton Trans* **2015**, *44*, 16791–16801. <https://doi.org/10.1039/C5DT02625C>
39. Ren, J.; Dyosiba, X.; Musyoka, N.M.; Langmi, H.W.; North, B.C.; Mathe, M. Green synthesis of chromium-based metal-organic framework (Cr-MOF) from waste polyethylene terephthalate (PET) bottles for hydrogen storage applications. *Inter J Hydrogen Energy* **2016**, *41*, 18141–18146. <https://doi.org/10.1016/j.ijhydene.2016.08.040>
40. Ren, J.; Dyosiba, X.; Musyoka, N.M.; Langmi, H.W.; Mathe, M.; Liao, S. Review on the current practices and efforts towards pilot-scale production of metal-organic frameworks (MOFs). *Coord Chem Rev* **2017**, *352*, 187–219. <https://doi.org/10.1016/j.ccr.2017.09.005>

Chapter 6

Nanocomposite membranes for the removal of dyes

Azile Nqombolo ^{a,b}, Anele Mpupa ^{a,b}, Jianwei Ren ^c,
Philliswa Nosizo Nomngongo ^{a,b}

^a*Department of Chemical Sciences, University of Johannesburg, Doornfontein Campus, P.O. Box 17011, Doornfontein, 2028, South Africa*

^b*DSI/NRF SARCHI Chair: Nanotechnology for Water, University of Johannesburg, Doornfontein, 2028, South Africa*

^c*Department of Mechanical Engineering Science University of Johannesburg, Cnr Kingsway and University Road, Auckland Park, Johannesburg 2092, South Africa*

Abstract

The scarcity of affordable, sustainable, safe, and clean water is one of the major challenges faced by the world. The use of polymeric membranes in wastewater treatment has become a major solution in fighting water scarcity. Some of these membranes (microfiltration, ultrafiltration, and nanofiltration) operate at low pressure when compared to reverse osmosis. However, permeability, selectivity, and fouling limit the application of these polymeric membranes. The incorporation of nanomaterials into the polymeric matrix has resolved such problems in membrane technology. Recent studies show that nanomaterials such as metal organic frameworks (MOFs), graphene oxide (GO), multi-walled carbon nanotubes (MWCNTs), and iron-based nanoparticles are promising nanomaterials for membrane technology with high permeability, selectivity, and antifouling performance. This chapter represents the application of MOF-based nanocomposite membranes for the rejection of anionic and cationic dyes. This chapter reviews various nanocomposite membranes in dye rejection. Conclusions and future perspectives have been drawn and discussed.

Keywords: Membrane technology, Ultrafiltration, Nanomaterials, Cationic dyes, Membrane fouling

1. Introduction

Fast urbanisation and industrialisation cause water contamination and result in a shortage of drinking water (Vila-Traver *et al.*, 2020). Therefore, it is essential to protect the existing water sources by cleaning wastewater contaminated with different pollutants. The removal of dyes and heavy metals has become vital due to their toxicity and irreversibility at wide concentration ranges (Varghese, Paul and Latha, 2019) (Nqombolo *et al.*, 2019). Textile and paper industries generate large amounts of effluent. The discharged effluents contain water pollutants such as salt, suspended organics, toxic ions, coloured organics, and pH (Ahmed *et al.*, 2020). Dyes can be categorised as basic, reactive, acidic, direct or as metal complexes (Minitha *et al.*, 2017) (Chaari *et al.*, 2019). Acidic dyes are negatively charged while basic dyes are positively charged. Synthetic dyes are toxic due to their accumulation in organisms, mutagenic properties, biodegradable and carcinogenic (Almeida and Corso, 2019) (Suzuki *et al.*, 2020). Hence, it is essential to remove dyes before discharging them to the environment (Deng *et al.*, 2019). Membrane technology has attracted more researchers due to its efficiency in water purification (Mansor *et al.*, 2020).

Methylene blue (MB) is considered as one of the hazardous dyes as it is used in industrial applications such as chemicals and textile (Mouni *et al.*, 2018). However, the accumulation of MB is toxic and dangerous to humans. MB is water soluble and is normally used in dyeing leather, colouring paper and as an antiseptic (Fadillah *et al.*, 2019). Researchers have developed various technologies for dye rejection, such as precipitation (Pandey, Singh and Hitkari, 2018), chemical oxidation (Zhu *et al.*, 2020), ultrafiltration (Bouazizi *et al.*, 2017), adsorption (Bhatti *et al.*, 2020), photo-catalysis (Nguyen and Juang, 2019), and coagulation (Beluci *et al.*, 2019). However, post-treatment is required for these methods, hence membranes have been widely used and they have shown great performance in dye rejection.

Membranes can selectively remove targeted pollutants as they have different sizes (Judd, 2017). Membrane filtration processes require pressure and these pressure-driven membranes include microfiltration (Cheng and Hong, 2017), ultrafiltration (UF) (Xu *et al.*, 2018), nanofiltration (NF) (Oatley-Radcliffe *et al.*, 2017), reverse osmosis (RO) (Jiang, Li and Ladewig, 2017), and forward osmosis (M. Zhang *et al.*, 2020). Microfiltration is normally used in removal of yeasts, prokaryotes, fungi, and suspended solids. UF is used in the removal of macromolecules, colloids, and viruses, while NF removes organic matters and heavy metals. RO is used in the production of ultrapure water, water reuse, and salt rejection (desalination). NF and UF have been explored in nanocomposite

membranes for dye rejection. These filtration methods are considered to be environmentally friendly, energy-efficient, and low-cost when compared to the reverse osmosis membranes that require high pressure.

Apart from the widespread application of membranes and their efficiency, they are prone to fouling, which becomes a huge setback in their application (Goh *et al.*, 2018). Fouling occurs when hydrophobic polymers interact with the pollutant to form a cake layer. These hydrophobic polymers include polyethersulfone (PES), polysulfone (PSF), and polyvinylidene difluoride (PVDF). These polymers have high mechanical and thermal resistance, firmness and are simple to process. The membrane roughness and hydrophilicity can affect the fouling, which results in decreased water permeation due to pore blocking or formation of cake layer (Yin *et al.*, 2020) (Zheng *et al.*, 2018). Membrane fouling results in a short lifespan of the membrane and low selectivity. Most pollutants are hydrophobic bovine serum albumin (BSA), therefore, increasing the hydrophilicity of the membrane is crucial (Wang *et al.*, 2019). Various methods such as blending of fillers with polymer, blending (Kausar, 2017), and grafting (S. Zhang, Manasa, *et al.*, 2020) have shown great improvement in membrane hydrophilicity.

Blending of different polymers has shown enhanced performance of the polymeric membranes. Also, grafting has demonstrated high protein resistance during rejection. Moreover, composite membrane is one of the trends in improving the performance of the blended polymers with nanofillers. Such nanofillers include metal organic frameworks (S. Zhang, Liu, *et al.*, 2020), TiO_2 (Li *et al.*, 2017), graphene oxide (GO) (Nawaz *et al.*, 2020) and Al_2O_3 (Uzal *et al.*, 2017). This chapter highlights MOF-based nanocomposite membranes for rejection of both anionic dyes and cationic dyes.

2. Application of nanocomposite membranes for dye rejection

Nano-enabled PSF/PVA membranes have been used for the rejection of Congo red. The 0.5 wt% showed high rejection when SiO_2 was used instead of ZnO (Khumalo *et al.*, 2019). The increase in the content loadings of the nanoparticles increased the rejection of Congo red (CR) This is attributed to the electrostatic interaction between the dye (CR) and the membrane surface. Moreover, the size exclusion from the membrane pores also played a role in the rejection process (Khumalo *et al.*, 2019). PVA/PEI nanocomposite membranes used in rejection of three dyes (Congo red, bromomethylmol blue, and direct yellow) exhibited high rejection of 99.7% (Soyekwo *et al.*, 2020). Another study that was carried out by Mehdi

and co-workers showed high rejection of reactive red 120; they used PVDF nanofiltration membranes. The increase in contact angle and water permeation was due to the modification of the bare PVDF membranes with HDTMA clinoptilolite nanoparticles (Hosseinifard, Aroon and Dahrazma, 2020).

The study reported by Hebbar showed the rejection of methylene blue and rhodamine B with rejection percentages of 97% and 94%, respectively. This was done at pH 7, using halloysite nanotubes nanocomposite membranes (Hebbar *et al.*, 2018). Clay-hyperbranched epoxy/PPSU composite membranes exhibited high rejection of both dyes when compared to the pristine polymer membrane. Methyl orange (MO) showed higher rejection than methylene blue (MB), which is attributed to electrostatic interaction between the negatively charged MO and clay-hyperbranched epoxy (Mahmoudian and Balkanloo, 2017). The study showed the rejection of CR and MB using PDA/RGO/HKUST-1 yielding a 89.2 % and 99.8 % rejection for CR and MB, respectively (Liu *et al.*, 2019). Also, tannic acid coated boehmite (TA-BM)/PES membranes for the rejection of Direct Red 16 (96%) compared to the PES membrane. The 0.5 wt.% of TA-BM/PES membrane showed high antifouling performance (96% Flux recovery ratio (FRR)) and 3.604 irreversible fouling resistance (R_{ir}) (Oulad *et al.*, 2020). A study reported by Alam and colleagues showed the use of PVDF/ Biopolymer k-carrageenan (kCg) membrane for methyl orange (MO) rejection. The optimum condition (1 wt %) of kCg gave a percentage rejection of 71 % (Alam *et al.*, 2019). Another anionic dye RR198 has been rejected using NCD-blended membranes. The high rejection observed (99,2 %) was due to the electrostatic repulsion between the negatively charged membrane and the anionic dye (Koulivand *et al.*, 2020). $\text{SiO}_2/\text{Fe}_3\text{O}_4/\text{PES}$ membranes (Sc-MNP-COOH)/PES for Reactive Green 19, Direct Black 38 and Rhodamine B rejection of more than 90 % due to the electrostatic interaction between the surface of the membrane and the dyes. The bare PES membrane showed low percentage rejection due to the absence of these electrostatic interactions (Vatanpour *et al.*, 2019). Studies showing rejection of anionic and cationic dyes using nanocomposite membranes are shown in Table 1 & 2, the incorporation of nanocomposites in the membranes enhanced the rejection performance of the bare polymer membranes.

Table 1: Nanocomposite membranes for anionic dye rejection

Material	Analytes	Performance (%)	References
DNDs/PES	Reactive Orange 29 and Reactive Green 19	86.9 and 89.4	(Vatanpour et al., 2018)
Fe ₃ O ₄ -MDA	Reactive green 19	Above 98	(Koulivand, Shahbazi and Vatanpour, 2019)
Silver loaded chitosan nanoparticles	Reactive Orange 16 Reactive Black 5	86.13 and 81.21	(Kolangare et al., 2019)
Layered GO (Borate GO)	Methyl orange	74.02	(Yan et al., 2020)
PANI nanofibers	Reactive red 120	99.25	(Kajekar et al., 2015)
(TA-BM)/PES membrane	Licorice and Direct Red	96	(Oulad et al., 2020)
Graphene quantum dots (GQDs)/PVC	Reactive blue	96	(Vatanpour et al., 2020)
PANI-GO/PVDF	Methyl orange	95	(Nawaz et al., 2020)
PES-Fe ₃ O ₄ -APTES	Reactive green 19	96 & 98	(Koulivand, Shahbazi and Vatanpour, 2019)
TOC/PVDF	Eriochrome black T	83.5	(Van Tran, Kumar and Lue, 2019)
H-PAN-ETA	Acid fuchsin	94	(Yun et al., 2020)

Table 2: Nanocomposite membranes for rejection of cationic dyes

Membrane material	Analytes	Performance (%)	References
Layered GO (Borate GO)	Methylene blue	88.56	(Yan et al., 2020)
Ag+ -PEI@HPAN	Crystal violet	99.2	(Liu et al., 2018)
TETA-MWCNT/PES	Crystal violet and Rhodamine B	98.43 and 99.23	(Peydayesh, Mohammadi and Bakhtiari, 2018)
MIL-53/PVDF UF membrane	Rhodamine B	99.7	Zhao Siyu 2020
PEBAX/CWCTs	Malachite green	98.7	(Mousavi, Asghari and Mahmoodi, 2020)
Nanoparticle/PES	Rhodamine B	91.96–96.92	(Otitoju et al., 2020)
Pd nanoparticles/PSF	Crystal violet	99	(Goswami et al., 2018)
GO/PES	Methylene blue	71	(Marjani et al., 2020)
UiO-66/PGPTFC	Methylene blue & Rhodamine B	94	Fang Si-Yuan 2020
Zr-MOF-PUF	Methylene blue & Rhodamine B	97.57 and 98.80	(Li et al., 2018)

3. Conclusion

Ever since membrane technology emerged in water treatment application, much research has been done to modify these membranes to improve their fouling resistance, mechanical or thermal properties. Various nanomaterials have been used to develop hydrophilic polymeric membranes with enhanced properties and performance. MOFs and GO are widely used as fillers in nanocomposite membranes for the removal of both organic and inorganic pollutants from water. In rejection of anionic and cationic dyes, UF and NF membranes have been used with different fillers. Water molecules are transported through these hydrophilic fillers,

while rejection occurs due to the electrostatic interactions between the dyes and the filler in the composite membranes. Nanocomposite membranes are potential candidates in water treatment application due to the exceptional properties from the incorporated nanomaterials. The use of nanocomposite membranes in dye rejection has stirred tremendous interest as promising future membranes to treat wastewater treatment.

4. Acknowledgements

The authors want to acknowledge the University of Johannesburg, Department of Chemical Sciences. They also wish to acknowledge Global Excellence Stature (GES 4.0) for financial support (Azile Nqombolo).

References

1. Ahmed, S. *et al.* (2020) 'Use of natural bio-sorbent in removing dye, heavy metal and antibiotic-resistant bacteria from industrial wastewater', *Applied Water Science*. Springer, 10(5), pp. 1–10. <https://doi.org/10.1007/s13201-020-01200-8>
2. Alam, J. *et al.* (2019) 'k-Carrageenan–A versatile biopolymer for the preparation of a hydrophilic PVDF composite membrane', *European Polymer Journal*. Elsevier, 120, p. 109219. <https://doi.org/10.1016/j.eurpolymj.2019.109219>
3. Almeida, E. J. R. and Corso, C. R. (2019) 'Decolorization and removal of toxicity of textile azo dyes using fungal biomass pelletized', *International journal of environmental science and technology*. Springer, 16(3), pp. 1319–1328. <https://doi.org/10.1007/s13762-018-1728-5>
4. Beluci, N. de C. L. *et al.* (2019) 'Hybrid treatment of coagulation/flocculation process followed by ultrafiltration in TiO₂-modified membranes to improve the removal of reactive black 5 dye', *Science of the Total Environment*. Elsevier, 664, pp. 222–229. <https://doi.org/10.1016/j.scitotenv.2019.01.199>
5. Bhatti, H. N. *et al.* (2020) 'Efficient removal of dyes using carboxymethyl cellulose/alginate/polyvinyl alcohol/rice husk composite: Adsorption/desorption, kinetics and recycling studies', *International Journal of Biological Macromolecules*. Elsevier, 150, pp. 861–870. <https://doi.org/10.1016/j.ijbiomac.2020.02.093>
6. Bouazizi, A. *et al.* (2017) 'Removal of dyes by a new nano-TiO₂ ultrafiltration membrane deposited on low-cost support prepared from natural Moroccan bentonite', *Applied clay science*. Elsevier, 149, pp. 127–135. <https://doi.org/10.1016/j.clay.2017.08.019>

7. Chaari, I. *et al.* (2019) 'Comparative study on adsorption of cationic and anionic dyes by smectite rich natural clays', *Journal of Molecular Structure*. Elsevier, 1179, pp. 672–677. <https://doi.org/10.1016/j.molstruc.2018.11.039>
8. Cheng, H. and Hong, P.-Y. (2017) 'Removal of antibiotic-resistant bacteria and antibiotic resistance genes affected by varying degrees of fouling on anaerobic microfiltration membranes', *Environmental science & technology*. ACS Publications, 51(21), pp. 12200–12209. <https://doi.org/10.1021/acs.est.7b03798>
9. Deng, S.-Q. *et al.* (2019) 'Hydrolytically stable nanotubular cationic metal-organic framework for rapid and efficient removal of toxic oxo-anions and dyes from water', *Inorganic Chemistry*. ACS Publications, 58(4), pp. 2899–2909. <https://doi.org/10.1021/acs.inorgchem.9b00104>
10. Fadillah, G. *et al.* (2019) 'Electrochemical removal of methylene blue using alginate-modified graphene adsorbents', *Chemical Engineering Journal*. Elsevier, 378, p. 122140. <https://doi.org/10.1016/j.cej.2019.122140>
11. Goh, P. S. *et al.* (2018) 'Membrane fouling in desalination and its mitigation strategies', *Desalination*. Elsevier, 425, pp. 130–155. <https://doi.org/10.1016/j.desal.2017.10.018>
12. Goswami, R. *et al.* (2018) 'Biogenic synthesized Pd-nanoparticle incorporated antifouling polymeric membrane for removal of crystal violet dye', *Journal of environmental chemical engineering*. Elsevier, 6(5), pp. 6139–6146. <https://doi.org/10.1016/j.jece.2018.09.046>
13. Hebbar, R. S. *et al.* (2018) 'Fabrication of polyetherimide nanocomposite membrane with amine functionalised halloysite nanotubes for effective removal of cationic dye effluents', *Journal of the Taiwan Institute of Chemical Engineers*. Elsevier, 93, pp. 42–53. <https://doi.org/10.1016/j.jtice.2018.07.032>
14. Hosseinifard, S. M., Aroon, M. A. and Dahrazma, B. (2020) 'Application of PVDF/HDTMA-modified clinoptilolite nanocomposite membranes in removal of reactive dye from aqueous solution', *Separation and Purification Technology*. Elsevier, 251, p. 117294. <https://doi.org/10.1016/j.seppur.2020.117294>
15. Jiang, S., Li, Y. and Ladewig, B. P. (2017) 'A review of reverse osmosis membrane fouling and control strategies', *Science of the Total Environment*. Elsevier, 595, pp. 567–583. <https://doi.org/10.1016/j.scitotenv.2017.03.235>
16. Judd, S. J. (2017) 'Membrane technology costs and me', *Water Research*. Elsevier Ltd, 122, pp. 1–9. doi: 10.1016/j.watres.2017.05.027. <https://doi.org/10.1016/j.watres.2017.05.027>

17. Kajekar, A. J. *et al.* (2015) 'Preparation and characterization of novel PSf/PVP/PANI-nanofiber nanocomposite hollow fiber ultrafiltration membranes and their possible applications for hazardous dye rejection', *Desalination*. Elsevier, 365, pp. 117–125. <https://doi.org/10.1016/j.desal.2015.02.028>
18. Kausar, A. (2017) 'Scientific potential of chitosan blending with different polymeric materials: A review', *Journal of Plastic Film & Sheetting*. Sage Publications Sage UK: London, England, 33(4), pp. 384–412. <https://doi.org/10.1177/8756087916679691>
19. Khumalo, N. P. *et al.* (2019) 'Dual-functional ultrafiltration nano-enabled PSf/PVA membrane for the removal of Congo red dye', *Journal of Water Process Engineering*. Elsevier, 31, p. 100878. <https://doi.org/10.1016/j.jwpe.2019.100878>
20. Kolangare, I. M. *et al.* (2019) 'Antibiofouling hollow-fiber membranes for dye rejection by embedding chitosan and silver-loaded chitosan nanoparticles', *Environmental Chemistry Letters*. Springer, 17(1), pp. 581–587. <https://doi.org/10.1007/s10311-018-0799-3>
21. Koulivand, H. *et al.* (2020) 'Novel antifouling and antibacterial polyethersulfone membrane prepared by embedding nitrogen-doped carbon dots for efficient salt and dye rejection', *Materials Science and Engineering*: Elsevier, p. 110787. <https://doi.org/10.1016/j.msec.2020.110787>
22. Koulivand, H., Shahbazi, A. and Vatanpour, V. (2019) 'Fabrication and characterization of a high-flux and antifouling polyethersulfone membrane for dye removal by embedding Fe₃O₄-MDA nanoparticles', *Chemical Engineering Research and Design*. Elsevier, 145, pp. 64–75. <https://doi.org/10.1016/j.cherd.2019.03.003>
23. Li, J. *et al.* (2018) 'Zirconium-based metal organic frameworks loaded on polyurethane foam membrane for simultaneous removal of dyes with different charges', *Journal of colloid and interface science*. Elsevier, 527, pp. 267–279. <https://doi.org/10.1016/j.jcis.2018.05.028>
24. Li, N. *et al.* (2017) 'Precisely-controlled modification of PVDF membranes with 3D TiO₂/ZnO nanolayer: enhanced anti-fouling performance by changing hydrophilicity and photocatalysis under visible light irradiation', *Journal of Membrane Science*. Elsevier, 528, pp. 359–368. <https://doi.org/10.1016/j.memsci.2017.01.048>
25. Liu, S. *et al.* (2018) 'Chelation-assisted in situ self-assembly route to prepare the loose PAN-based nanocomposite membrane for dye desalination', *Journal of Membrane Science*. Elsevier, 566, pp. 168–180. <https://doi.org/10.1016/j.memsci.2018.09.002>

26. Liu, Y. *et al.* (2019) 'A polydopamine-modified reduced graphene oxide (RGO)/MOFs nanocomposite with fast rejection capacity for organic dye', *Chemical Engineering Journal*. Elsevier, 359, pp. 47–57. <https://doi.org/10.1016/j.cej.2018.11.105>
27. Mahmoudian, M. and Balkanloo, P. G. (2017) 'Clay-hyperbranched epoxy/polyphenylsulfone nanocomposite membranes', *Iranian Polymer Journal*. Springer, 26(9), pp. 711–720. <https://doi.org/10.1007/s13726-017-0556-7>
28. Mansor, E. S. *et al.* (2020) 'Advanced eco-friendly and adsorptive membranes based on Sargassum dentifolium for heavy metals removal, recovery and reuse', *Journal of Water Process Engineering*. Elsevier, 37, p. 101424. <https://doi.org/10.1016/j.jwpe.2020.101424>
29. Marjani, A. *et al.* (2020) 'Effect of graphene oxide on modifying polyethersulfone membrane performance and its application in wastewater treatment', *Scientific Reports*. Nature Publishing Group, 10(1), pp. 1–11. <https://doi.org/10.1038/s41598-020-58472-y>
30. Minitha, C. R. *et al.* (2017) 'Adsorption behaviour of reduced graphene oxide towards cationic and anionic dyes: Co-action of electrostatic and π - π interactions', *Materials Chemistry and Physics*. Elsevier, 194, pp. 243–252. <https://doi.org/10.1016/j.matchemphys.2017.03.048>
31. Modi, A. and Bellare, J. (2019) 'Efficient removal of dyes from water by high flux and superior antifouling polyethersulfone hollow fiber membranes modified with ZnO/cGO nanohybrid', *Journal of Water Process Engineering*. Elsevier, 29, p. 100783. <https://doi.org/10.1016/j.jwpe.2019.100783>
32. Mouni, L. *et al.* (2018) 'Removal of Methylene Blue from aqueous solutions by adsorption on Kaolin: Kinetic and equilibrium studies', *Applied Clay Science*. Elsevier, 153, pp. 38–45. <https://doi.org/10.1016/j.clay.2017.11.034>
33. Mousavi, S. R., Asghari, M. and Mahmoodi, N. M. (2020) 'Chitosan-wrapped multiwalled carbon nanotube as filler within PEBA thin film nanocomposite (TFN) membrane to improve dye removal', *Carbohydrate Polymers*. Elsevier, p. 116128. <https://doi.org/10.1016/j.carbpol.2020.116128>
34. Nawaz, H. *et al.* (2020) 'Polyvinylidene fluoride nanocomposite super hydrophilic membrane integrated with Polyaniline-Graphene oxide nano fillers for treatment of textile effluents', *Journal of Hazardous Materials*. Elsevier, 403, p. 123587. <https://doi.org/10.1016/j.jhazmat.2020.123587>

35. Nguyen, C. H. and Juang, R.-S. (2019) 'Efficient removal of methylene blue dye by a hybrid adsorption–photocatalysis process using reduced graphene oxide/titanate nanotube composites for water reuse', *Journal of Industrial and Engineering Chemistry*. Elsevier, 76, pp. 296–309. <https://doi.org/10.1016/j.jiec.2019.03.054>
36. Nqombolo, A. *et al.* (2019) 'Adsorptive removal of lead from acid mine drainage using cobalt-methylimidazolate framework as an adsorbent: kinetics, isotherm, and regeneration', *Environmental Science and Pollution Research*. Environmental Science and Pollution Research, 26(4), pp. 3330–3339. <https://doi.org/10.1007/s11356-018-3868-z>
37. Oatley-Radcliffe, D. L. *et al.* (2017) 'Nanofiltration membranes and processes: A review of research trends over the past decade', *Journal of Water Process Engineering*. Elsevier, 19, pp. 164–171. <https://doi.org/10.1016/j.jwpe.2017.07.026>
38. Otitoju, T. A. *et al.* (2020) 'Influence of nanoparticle type on the performance of nanocomposite membranes for wastewater treatment', *Journal of Water Process Engineering*. Elsevier, 36, p. 101356. <https://doi.org/10.1016/j.jwpe.2020.101356>
39. Oulad, F. *et al.* (2020) 'Fabrication and characterization of a novel tannic acid coated boehmite/PES high performance antifouling NF membrane and application for licorice dye removal', *Chemical Engineering Journal*. Elsevier, 397, p. 125105. <https://doi.org/10.1016/j.cej.2020.125105>
40. Pandey, G., Singh, S. and Hitkari, G. (2018) 'Synthesis and characterization of polyvinyl pyrrolidone (PVP)-coated Fe₃O₄ nanoparticles by chemical co-precipitation method and removal of Congo red dye by adsorption process', *International Nano Letters*. Springer, 8(2), pp. 111–121. <https://doi.org/10.1007/s40089-018-0234-6>
41. Peydayesh, M., Mohammadi, T. and Bakhtiari, O. (2018) 'Effective treatment of dye wastewater via positively charged TETA-MWCNT/PES hybrid nanofiltration membranes', *Separation and Purification Technology*. Elsevier, 194, pp. 488–502. <https://doi.org/10.1016/j.seppur.2017.11.070>
42. Soyekwo, F. *et al.* (2020) 'Construction of an electroneutral zinc incorporated polymer network nanocomposite membrane with enhanced selectivity for salt/dye separation', *Chemical Engineering Journal*. Elsevier, 380, p. 122560. <https://doi.org/10.1016/j.cej.2019.122560>
43. Suzuki, M. *et al.* (2020) 'Biological treatment of non-biodegradable azo-dye enhanced by zero-valent iron (ZVI) pre-treatment', *Chemosphere*. Elsevier, 259, p. 127470. <https://doi.org/10.1016/j.chemosphere.2020.127470>

44. Van Tran, T. T., Kumar, S. R. and Lue, S. J. (2019) 'Separation mechanisms of binary dye mixtures using a PVDF ultrafiltration membrane: Donnan effect and intermolecular interaction', *Journal of Membrane Science*. Elsevier, 575, pp. 38–49. <https://doi.org/10.1016/j.memsci.2018.12.070>
45. Uzal, N. *et al.* (2017) 'Enhanced hydrophilicity and mechanical robustness of polysulfone nanofiber membranes by addition of polyethyleneimine and Al₂O₃ nanoparticles', *Separation and Purification Technology*. Elsevier, 187, pp. 118–126. <https://doi.org/10.1016/j.seppur.2017.06.047>
46. Varghese, A. G., Paul, S. A. and Latha, M. S. (2019) 'Remediation of heavy metals and dyes from wastewater using cellulose-based adsorbents', *Environmental Chemistry Letters*. Springer, 17(2), pp. 867–877. <https://doi.org/10.1007/s10311-018-00843-z>
47. Vatanpour, V. *et al.* (2018) 'Effect of detonation nanodiamond on the properties and performance of polyethersulfone nanocomposite membrane', *Diamond and Related Materials*. Elsevier, 90, pp. 244–255. <https://doi.org/10.1016/j.diamond.2018.10.027>
48. Vatanpour, V. *et al.* (2019) 'A novel antifouling ultrafiltration membranes prepared from percarboxylic acid functionalized SiO₂ bound Fe₃O₄ nanoparticle (SCMNP-COOH)/polyethersulfone nanocomposite for BSA separation and dye removal', *Journal of Chemical Technology & Biotechnology*. Wiley Online Library, 94(4), pp. 1341–1353. <https://doi.org/10.1002/jctb.5894>
49. Vatanpour, V. *et al.* (2020) 'Anti-fouling and permeable polyvinyl chloride nanofiltration membranes embedded by hydrophilic graphene quantum dots for dye wastewater treatment', *Journal of Water Process Engineering*. Elsevier, 38, p. 101652. <https://doi.org/10.1016/j.jwpe.2020.101652>
50. Vila-Traver, J. *et al.* (2020) 'Climate change and industrialization as the main drivers of Spanish agriculture water stress', *Science of The Total Environment*. Elsevier, p. 143399. <https://doi.org/10.1016/j.scitotenv.2020.143399>
51. Wang, Y. *et al.* (2019) 'Preparation of super-hydrophilic polyphenylsulfone nanofiber membranes for water treatment', *RSC Advances*, 9(1), pp. 278–286. <https://doi.org/10.1039/C8RA06493H>
52. Xu, Z. *et al.* (2018) 'Antifouling polysulfone ultra filtration membranes with pendent sulfonamide groups', *Journal of Membrane Science*. Elsevier B.V., 548(August 2017), pp. 481–489. <https://doi.org/10.1016/j.memsci.2017.11.064>

53. Yan, X. *et al.* (2020) 'Layer-by-layer assembly of bio-inspired borate/graphene oxide membranes for dye removal', *Chemosphere*. Elsevier, p. 127118. <https://doi.org/10.1016/j.chemosphere.2020.127118>
54. Yin, X. *et al.* (2020) 'The growth process of the cake layer and membrane fouling alleviation mechanism in a MBR assisted with the self-generated electric field', *Water Research*. Elsevier, 171, p. 115452. <https://doi.org/10.1016/j.watres.2019.115452>
55. Yun, J. *et al.* (2020) 'High efficient dye removal with hydrolyzed ethanolamine-Polyacrylonitrile UF membrane: Rejection of anionic dye and selective adsorption of cationic dye', *Chemosphere*. Elsevier, 259, p. 127390. <https://doi.org/10.1016/j.chemosphere.2020.127390>
56. Zhang, M. *et al.* (2020) 'Engineering a nanocomposite interlayer for a novel ceramic-based forward osmosis membrane with enhanced performance', *Environmental science & technology*. ACS Publications, 54(12), pp. 7715–7724. <https://doi.org/10.1021/acs.est.0c02809>
57. Zhang, S., Manasa, P., *et al.* (2020) 'Grafting copolymer of thermo-responsive and polysaccharide chains for surface modification of high performance membrane', *Separation and Purification Technology*. Elsevier, 240, p. 116585. <https://doi.org/10.1016/j.seppur.2020.116585>
58. Zhang, S., Liu, Y., *et al.* (2020) 'Water-soluble MOF nanoparticles modified polyethersulfone membrane for improving flux and molecular retention', *Applied Surface Science*. Elsevier, 505, p. 144553. <https://doi.org/10.1016/j.apsusc.2019.144553>
59. Zheng, Y. *et al.* (2018) 'Membrane fouling mechanism of biofilm-membrane bioreactor (BF-MBR): Pore blocking model and membrane cleaning', *Bioresour. Technol.* Elsevier, 250, pp. 398–405. <https://doi.org/10.1016/j.biortech.2017.11.036>
60. Zhu, M. *et al.* (2020) 'Ultra-high flux of graphene oxide membrane modified with orientated growth of MOFs for rejection of dyes and oil-water separation', *Chinese Chemical Letters*. Chinese Chemical Society, (2019). doi: 10.1016/j.ccllet.2020.04.011. <https://doi.org/10.1016/j.ccllet.2020.04.011>

Chapter 7

Application of various metal-organic frameworks in analytical methods: recent trends and future perspectives

Philiswa Nosizo Nomngongo ^{a,b*}, Azile Nqombolo ^{a,b},
Jianwei Ren ^c, Tien-Chien Jen ^c, Wojciech Starosta ^d,
Bożena Sartowska ^d

^aDepartment of Chemical Sciences, University of Johannesburg, Doornfontein Campus, P.O. Box 17011, Johannesburg, 2028, South Africa

^bDepartment of Science and Innovation–National Research Foundation South African Research Chair Initiative (DSI–NRF SARChI), Nanotechnology for Water, University of Johannesburg, Doornfontein 2028, South Africa

^cUniversity of Johannesburg, Johannesburg, Kingsway and University Road, Auckland Park, 2092, P.O. Box 524, Auckland Park, 2006, Johannesburg, South Africa

^dLaboratory of Materials Research, Institute of Nuclear Chemistry and Technology, Dorodna 16, 03–195 Warsaw, Poland

*Corresponding author. Tel: +27 11 559 6571.
Email: pnnomngongo@uj.ac.za (P.N. Nomngongo)

Abstract

Water scarcity and pollution are serious environmental problems and global concerns that affect millions of people. For this reason, there is increasing demand for frequent water quality monitoring. Therefore, there is a need for the development of efficient analytical platforms and methodologies that combine high accuracy, affinity, sensitivity, and selectivity towards various pollutants. Metal-organic frameworks (MOFs) have emerged as promising adsorbents, stationary phases, supports, and active coating for pollutant detection, extraction, sample clean-up, and separation. This chapter summarises the recent advances and trends in the application of MOFs in various analytical methodologies such as solid-phase extraction, solid-phase microextraction, and electrochemical sensors. A brief discussion of the synthesis strategies and their incorporation into various nanomaterials to increase the affinity of the resultant adsorbent towards

various analytes is made. The application of MOF-based adsorbents for extraction, preconcentration, separation, and detection of pollutants in water systems is reported.

Keywords: Metal-organic frameworks, Solid phase extraction, Solid phase microextraction, Electrochemical sensors, Environmental pollutants

1. Introduction

Water pollution is considered one of the severe problems faced worldwide, and it needs to be solved urgently [1]. Several pollutants resulting from different activities and diffuse pollution are continually detected in the aquatic environment. These pollutants enter the aquatic environment and have a great potential to have various adverse ecological and human health effects [2]. These chemicals are classified as highly hazardous compounds because most of them are known to be endocrine disruptors, and the rate at which they are released cannot be effectively controlled since a number of these are used all over the world [3]. A significant number of pollutants have been detected in different aquatic environments due to the advanced analytical detection levels. These chemicals include dyes, heavy metals, and pharmaceuticals which are used as medicine for both animals and humans as well as in farming industries [4]. Their presence in the environment has drawn much attention [5], because most of these contaminants are pharmacologically active, non-degradable, persistent in the environment, and they also have potentially negative effects on ecology and human health [4]. Attention continues to grow in finding analytical methodologies for the detection and monitoring of these substances in the environmental water systems. Their presence in water systems causes several negative health effects such as hormonal, nervous, and reproductive system disorders. Other related health effects include obesity, cardiovascular as well as cancer [6]. In the past few years, the discovery of various pollutants in different environmental matrices has increased and these pollutants are found at concentrations that are capable of causing harmful effects on humans and other living organisms [7].

Given the above, analytical chemistry played a significant role in the development of methodologies for the detection, control, and monitoring of numerous environmental pollutants in a selective, sensitive, accurate, precise, and reliable way. Due to the complexity of environmental samples and low analyte concentrations, the analysis process undergoes various steps that affect analytical performance [8]. These steps include sampling, sample preparation, detection, and data processing. It is worth mentioning that even during a chromatographic separation or electrochemical detection or spectroscopic/spectrometric analysis, the

presence of interferences is the major challenge in environmental analysis where organic, inorganic, and biological components co-exist and interact [9]. As a result, sample preparation plays a vital role in the sample matrix elimination, sample clean-up, and preconcentration of target analytes before the detection process [8,9]. Additionally, the improvement of stationary phases in chromatography applications and the use of functional materials in the modification of electrodes in electrochemical detection have recently received more attention [10,11].

Advancements in functional materials have received great interest in modern analytical chemistry due to their potential applications in numerous analytical methodologies [11–13]. Owing to their captivating features, metal-organic frameworks (MOFs) have been used in a wide range of applications (Figure 1). As seen in Figure 1, MOFs have been designed to meet the analytical challenges in sampling, sample preparation (that is, extraction, preconcentration, and sample clean-up), sensing, and chromatographic separation to improve analytical instrumentations' selectivity, sensitivity, and detection limit [11,13].

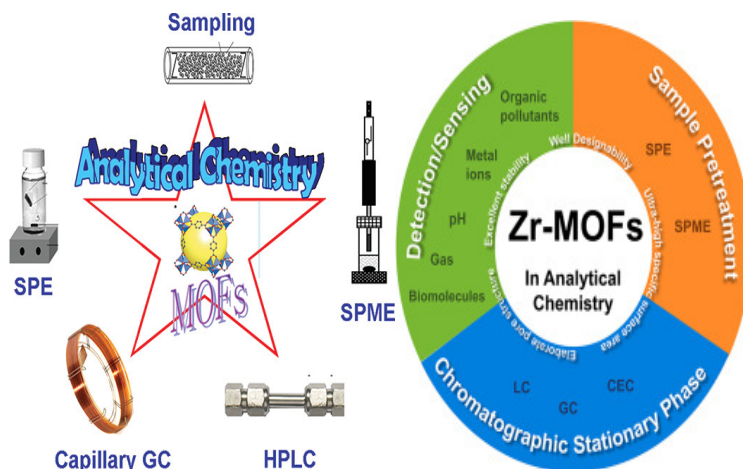


Figure 1: Application of metal-organic frameworks in various areas of analytical chemistry. Adapted and reproduced with permission from refs [11,13].

Considering the rapid developments in the application of MOFs in the analytical chemistry field, this chapter reviews the recent trends in the utilisation of analytical MOF-based methods. This chapter places particular emphasis on trends in the utilisation of MOFs in sample preparation (sorbent-based extraction methods) and electrochemical sensing. The overview will be limited to articles published between 2019

and 2022. This chapter also highlights a brief introduction of MOFs and MOFs-nanocomposites.

2. Metal-organic frameworks

Metal-organic frameworks (MOFs) are a group of porous materials that have attracted significant attention in different fields of research [14]. They are crystalline clusters or metal centres linked with organic ligands through coordination bonds creating stretched, arranged networks [15]. The richness of the geometry and connectivity of metal nodes and ligands can lead to the preparation of MOFs with specific structures and topology, which can be tailored for a specific application [16]. Furthermore, MOFs pose high surface area, thermal and chemical stability, versatile architectures, tunable pore size, simple metal nodes, and ligands modification as well as mild synthetic conditions [17]. Several metal ions and organic ligands with different functional groups have been used in the preparation of MOFs. As a result, most MOFs have been prepared using transition metals such as Cr, Cu, Fe, Mn, Co, Ni, , Zr, and Zn [18][19] and organic linkers containing various functional groups [20]. Sundriya *et al.*, [21] reported the synthesis of manganese MOF using a one-step solvothermal method. In their study, 1,4-benzenedicarboxylate was used as an organic linker. The resultant MOF displayed a high specific surface area, chemical, and thermal stability. Some of the ligands used in the synthesis of metal-organic frameworks are shown in Table 1, where they are used in different applications and have shown high performance.

The MOFs formed from carboxylate ligands and N-donor ligands are said to be water-stable [28-30]. The ligands used in the synthesis of MOFs should be water stable because the water molecules may easily replace the ligand leading to the collapse of MOFs or this can block the active sites [31]. The strength of the ligand-metal bond plays an important role in the MOF water stability. MOF instability is caused by (i) ligand displacement, when a water molecule is inserted into the ligand-metal bond causing ligand escape and formation of cation hydrate. Also, (ii) hydrolysis, where the ligand-metal bond is broken by water and a hydrated cation is formed as well as a protonated ligand [32]. MOFs that are formed by mixed linkers (ligands) like carboxylates and nitrogen donors have been studied [33]. Abazari and co-workers have synthesised MOF from N-donor piperazine and imidazole-4,5-dicarboxylate for the degradation of cloxacillin, ampicillin, and amoxicillin antibiotics with 89, 88, and 92.5%, respectively. The ligands assist in MOF stability and reusability in adsorption studies and photodegradation [34].

Table 1: Various ligands used in MOF preparation and their application

Metal ions	Ligand	Application	Performance	References
Cd(II) and Co(II)	bis-pyridyl-tris-amide ligand benzene-1,3-diacrylic acid (BDA) 4,4'-oxybisbenzoic acid (OBA)	Gas adsorption	High adsorption capacity	[22]
Ho(III)	H ₂ dtp = 4'-(3,5-dicarboxyphenyl)- 4,2':6'4"-terpyridine	Th(IV) separation from rare earth metals (REEs)	Separation factor Th/La (19.2); Th/Eu (7.5); Th/Y (21.6); Th/Lu (6.2); Th/Ce (18.9)	[23]
Cd(II)	1,4-bis(benzimidazol-1-yl)-2- butylene	Sensing Cr ₂ O ₇ ²⁻ and acetylacetone	N/A	[24]
Ni(II) and Cd(II)	[Cd(5-BrIP)(TIB)] _n (1) [Ni ₂ (5-BrIP) ₂ (TIB) ₂] _n (2) 1,3,5-tris(imidazol-1-ylmethyl) benzene (TIB)	Sensing of picric acid [2,4,6-trinitrophenol, TNP]	paper strip at 365 nm radiation by Cd(II) LMOF (1)-coated paper strip	[25]
Zr(IV)	2-Aminoterephthalic acid	Photo degradation	94% Cr(VI) reduction	[26]
Zr(IV)	2-(thiophene-2-carboxamido) benzene-1,4-dicarboxylic acid	Catalysis	94% and 95% yields	[27]

Carboxylates are considered as hard ligands and they can form strong bonds when bonded to strong metal ions such as Zr, Zn, and Cu among others [35]. In addition, carboxylate can easily coordinate with metals in the first row of transition metals under hydrothermal and solvothermal conditions. For instance, Jasuja and co-workers synthesised new water-stable MOFs using the first-row transition such as nickel, cobalt, copper, and zinc. The MOFs were obtained by incorporating structural factors such as catenation and ligand steric [36]. Li *et al.* synthesised uranium-based MOF that was found to be stable with large pores [37]. The MOF was prepared by combining the negatively charged uranyl carboxylates $[\text{UO}_2(\text{RCOO})_3]^-$ metal node with a square-like tetracarboxylate organic ligand. According to the BET results obtained, the prepared MOF gave a high surface area of about $2100 \text{ m}^2 \text{ g}^{-1}$. In addition, the carboxylate-based MOF was water stable and was selectively absorbing positively charged species [37]. When N-donor ligands were compared to amines, they showed better donor ability towards metal ions forming a more stable compound [30]. The metal N-coordination bond is labile when compared to the metal-carboxylate bond. This reduces the porosity of networks even though it makes it easy to rearrange during self-assemble. It is said that the use of mixed linkers, for example, N-donor and carboxylates leads to a framework that is doubly interpenetrated reducing its pore size [38].

Gao and others used a solvothermal method to prepare a series of Cu, Zn, Co, and Mn-based MOFs with mixed N-donor ligands and carboxylates [39]. Transition metals are the choice of metals to be used with these carboxylates as they form variations of coordination geometries to obtain different networks, also the use of two carboxylates to form high porous MOFs [40]. Several researchers have modified MOFs to enhance their removal performance and photocatalytic degradation; herein we combine the properties of MOFs with other nanomaterials to achieve/obtain high removal efficiency. Such nanomaterials include chitosan, magnetic nanoparticles, graphene oxide, and multi-walled carbon nanotubes.

2.1 Synthesis of MOFs

The synthesis of nanoscale MOFs has gained much attention. This is done to assist in accomplishing the application of MOFs than bulk MOFs. Top-down and bottom-up methods have been used in the MOF synthesis. The top-down method includes solvent-induced delamination exfoliation (SIDE), sonication-assisted liquid exfoliation (SALE), and micromechanical exfoliation (ME) (Du *et al.*, 2019; Xie *et al.*, 2020) [42]. The bottom-up method includes interface-mediated synthesis (ImS), hydrosolvothermal synthesis (HsS) [43] 44], and Langmuir-blodgen Hm

(LBm). These methods are widely used in the synthesis of single-crystal MOF and ultrathin MOFs which are in the range of 2–10 nm [45]. In the interface-mediated method, ultrathin materials such as MOFs grow through liquid/air /solid interface. Various materials can be modified to provide specific functional groups responsible for different applications; MOFs can be modified by the addition of pyridyl or amine moieties. Post-synthetic modification to prepare MOFs with high mechanical and physical properties, an organic ligand, can be altered to accommodate functional groups introduced [46].

3. Application of metal-organic frameworks in analytical methods

3.1 MOFs in sample preparation

In most environmental water analyses, direct identification and quantification of analytes are not suitable due to the complexity of the sample matrix (which may contain a mixture of the analytes with different chemical properties and co-existing substances) [47]. Therefore, a suitable sample preparation that could be converting any environmental sample type into a format that is ideal for precise and accurate quantification of the analytes is required. Sample preparation plays a remarkable influence on total analysis time and the quality of the analytical data obtained after instrumental analysis [8,47,48]. Therefore, the selection of a suitable sample preparation method depends on the chemical properties of the analytes, sample matrix, and the analytical detection method to be used [49]; [50]. Sample preparation methods such as solid phase extraction (SPE), dispersive solid-phase extraction (DSPE), magnetic solid-phase extraction (MSPE), and different modes of solid-phase microextraction (SPME) (in-tube, stir-bar, fabric, fibre, and thin-film) have been developed as seen in Figure 2 [48]. The success of these analytical methods depends on the selection of suitable adsorbent or coating material [48,51]. As a result, a substantial number of adsorbent materials with attractive characteristics have been used in the above-mentioned analytical sample preparation methods. These include molecularly imprinted polymers [52,53], porous organic polymers [54], covalent organic frameworks [55,56], zeolites [57], layered double hydroxide [58], carbon nanomaterials [59,60], and MOFs [11,48,61,62], among others. The application of MOFs as adsorbents in various solid phase-based extraction methods has recently emerged due to their remarkable properties.

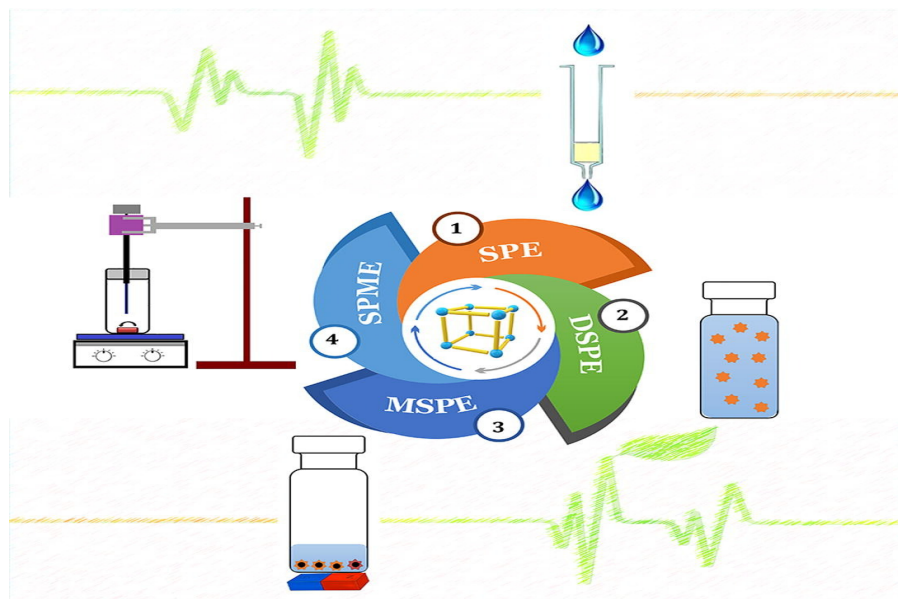


Figure 2: Application of metal-organic frameworks in different sample preparation methodologies. Adapted and reproduced with permission from Ref [48]

3.2.1 Solid phase extraction

Solid-phase extraction (SPE) is one of the extensively used sample preparation techniques that utilise an adsorbent to extract, isolate, and preconcentrate the target analytes from a specific sample [63,64]. Various types of adsorbents [65–67] and formats [51,63,65] have been reported in the literature and they cover all potential interactions with the analytes [63,64]. This study will briefly review the application of MOFs in traditional SPE, DSPE, micro SPE (μ -SPE), pipette tip SPE (PT-SPE) and MSPE for environmental analysis.

Traditional SPE can be performed as an offline or online preconcentration procedure. Both these modes enhance the detection sensitivity of the analytical instrument [68]. In a study reported by Amini and co-workers [69], an online micro solid-phase extraction (online- μ SPE) used electrospun polyacrylonitrile/ Zn-metal organic framework 74 @graphene oxide (PAN/Zn-MOF-74@GO) nanocomposite as an adsorbent [69]. The method was used for extraction and preconcentration of chlorobenzenes complex environmental samples before a high-performanceliquid chromatography analysis. The incorporation of MOF-74 in the nanocomposite enhances the affinity, surface area, and performance of the adsorbent material [69]. As a result, acceptable linearities in

the range of 0.25–700 ng mL⁻¹ with the coefficient of determination ≥ 0.9991 were obtained under optimum conditions. Furthermore, limits of detection (LODs), intra-day, and inter-day precisions were 0.08–1.10 ng mL⁻¹, 4.1%–9.5% and 5.8%–12.1%, respectively.

Martínez-Pérez-Cejuela *et al.* [70] developed on-line solid-phase extraction capillary electrophoresis with ultraviolet detection (SPE-CE-UV). The online SPE method used a hybrid material composed of nano-metal organic framework (HKUST-1) @organic polymer (nano-MOF@polymer) as illustrated in Figure 3. The developed SPE was investigated for extraction and preconcentration of fluoroquinolones (FQs) in several real complex samples, including river water. The developed SPE-CE-UV method showed low LODs and acceptable accuracy as well as very high preconcentration factors (up to 500,000 times). The high sensitivity of the developed method was accredited to the porous structures and nanostructures of the hybrid MOF nanocomposite. The use of hybrid MOF nanocomposite also enabled good separation between the investigated analytes (see typical chromatogram in Figure 3).

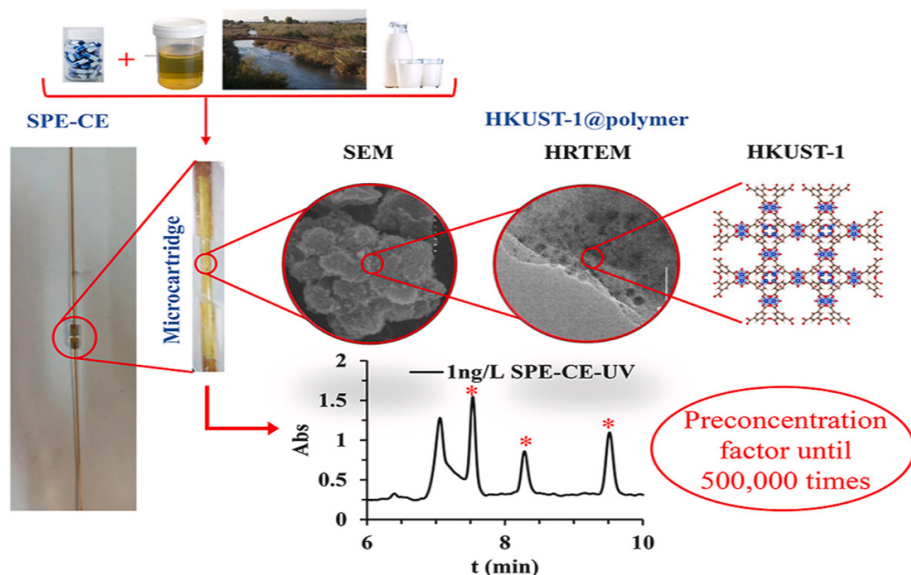


Figure 3: Schematic diagram illustrating the development of an online solid-phase extraction capillary electrophoresis. Adapted and reproduced with permission from Ref [70].

In traditional SPE, an adsorbent is often prepared or packed in a cartridge and the interaction between the solid phase material and target analyte is driven by the sample flow rate [64]. This feature becomes a critical challenge when nanomaterials are used as adsorbents because the small

particles block the frits, thus generating backpressure, which makes it difficult for the sample to pass through [64]. Therefore, alternative approaches to conventional SPE have been developed. These include DSPE, MSPE, and D- μ SPE, among others. In these SPE approaches, the adsorbent is dispersed into the sample matrix using a mechanical shaker, ultrasonication, or vortex. These methods allow close contact and effective interaction between the adsorbent and the analyte, thus increasing the overall extraction efficiency. The advantage of these methods is that the conditioning of sorbent is eliminated. Additionally, the extraction process is achieved by using low amounts of adsorbents (low milligram range).

Ghaemi *et al.* [71], developed a D- μ SPE utilising a microcrystalline cellulose/metal-organic framework 199 hybrid (MCC/MOF-199) as a solid material. The developed D- μ SPE method was used for preconcentration of chlorophenols in water before high-performance liquid chromatography-ultraviolet detection (HPLC-UV) determination. The combination of MCC on MOF-199 led to enhanced extraction capabilities. Under optimum conditions, the LODs, linearity, and %RSD were 0.1-200 ng mL⁻¹, 0.03-0.05 ng mL⁻¹ and 6.8%, respectively. Moreover, the applicability of the D- μ SPE-HPLC-UV method was investigated by analysing chlorophenols in different real water samples (mineral, river, and wastewater samples) and acceptable recoveries ranging from 95.8-99.5% were obtained. Duo and co-workers [72] designed a novel fusiform-like magnetic metal-organic framework material (Fe₃O₄-NH₂@MOF-235) as an adsorbent in MSPE of benzoylurea insecticides in tap water samples before HPLC. Acceptable linearity (1.0-300.0 μ g L⁻¹), LOD (0.25-0.5 μ g L⁻¹) and extraction recoveries (84.0-99.6%) were obtained. The adsorption mechanism was dominated by the hydrophobic and π - π stacking interactions between Fe₃O₄-NH₂@MOF-235 and benzoylurea insecticides. The remarkable properties of the MOF-based adsorbents allowed the use of very little adsorbent at a very short analysis time (<10 min).

In response to Green Analytical Chemistry (GAC), miniaturised SPE methods such as pipette tip solid-phase extraction (PT-SPE) employing MOFs as adsorbents have been reported [73-78]. For example, Su *et al.* [78] developed PT-SPE based on amino functionalised MOF@COF hybrid adsorbent combined with HPLC-UV for the analysis of sulfonamides in environmental water. Some researchers synthesised cotton@UiO-66 by growing UiO-66 on the surface of cotton fibre at room temperature. The resultant cotton@UiO-66 adsorbent was found to be effective for PT-SPE of herbicides in tap water samples. The combination of MOF-based PT-SPE with HPLC resulted in a facile and efficient analytical method with remarkable analytical characteristics. These include a wide linear range (1.4-280 μ g/L), low LOD (0.1-0.3 μ g/L), acceptable recoveries (83.3-

107%), and precision (<6.7%). Table 2 indicates that SPE approaches are powerful sample preparation strategies and with a suitable adsorbent, they allow a wide variety of analytes to be analysed. As shown in Table 2, the use of MOFs shows that these methods are effective enough to improve the performance of a wide range of analytical instruments. Furthermore, it can be seen from this table that a series of water-stable MOF materials have been used.

In most cases, the adsorption mechanism of ionic pollutants is driven by the surface charge of the MOF material, and this limits their applications for the extraction of nonionic organic pollutants. Such challenges are usually solved by the incorporation of other nanomaterials or functional groups. For example, Gao *et al.* [79] introduced amino groups on the surface of MIL-101(Cr) which promoted the increase of Lewis base sites (LBSs) density in surface modification of nanosized material thus allowing better interactions between the dyes and adsorbent. Functionalisation or modification of MOF materials proved to be beneficial to adsorption capacity and increases selectivity and affinity of the adsorbent. Environmental matrices are very complex, therefore, used hybrid materials to increase porosity and crystallinity have been explored (Table 2). For instance, hybrid MOF-based nanocomposite materials in Table 2 proved to be effective adsorbents for the MSPE, DPE, and online SPE, among others.

3.2.2 Solid phase microextraction

The basic principle of SPME methods is based on two steps, that is, extraction and desorption of target analytes from sample matrix [89,90]. The extraction step encompasses the partitioning of target analytes to the coating material (adsorbent). These methods are known as non-exhaustive and rely on the equilibrium between the sample matrix and the solid phase material [89,90]. The desorption step is performed after equilibrium and is achieved by placing the coated fibre into a vial containing elution solvent or the injection port of a GC [89,90]. MOFs and MOF-nanocomposite have been used as active materials in various SPME methods. For instance, Wang *et al.*, [60] developed a novel spiral-SPME fibre coated with zeolitic imidazolate framework-67 (ZIF-67) derived hollow multi-shelled structures Co_3O_4 /carbon nanomaterials. The coating was used to capture trace concentrations of polycyclic aromatic hydrocarbons (PAHs) in environmental water samples. The use of MOFs-based adsorbent composition in the spiral fibre demonstrated higher selectivity for extraction of PAHs compared with brominated flame retardants and endocrine chemicals. The high affinity of the fibre coating towards PAHs was attributed to strong π - π stacking force, hydrophobic

Table 2: Application of MOFs and nanocomposite in various solid phase extraction methods for environmental water analysis

Analytes	Analytical methods	Adsorbent	Linearity	LOD	%RSD	Refs
Sulfonamides	MSPE/HPLC-DAD	Magnetic MOF@COF hybrid nanosphere	10–2000 ng/mL	0.1–0.5 ng/mL	3-9	[80]
Malathion	DSPME/UHPLC-MS/MS	Cu-BTC-MOF	-	4.0 µg/L	<10	[81]
Non-steroidal anti-inflammatory drugs (NSAIDs)	MSPE/UPLC-MS/MS	Core-shell magnetic Fe ₃ O ₄ @MIL-100(Fe)	0.1–30 µg L ⁻¹	0.02–0.09 µg L ⁻¹	<9.6	[82]
Phthalic acid esters	DSPE/LC-MS	Basolite® F300 MOF	5–500 µg L ⁻¹	6.6–21 ng/L	<20%	[83]
Organophosphorus pesticides	DSPE-GC-FID	Zinc-based MOF	0.1–100 ng mL ⁻¹	0.03–0.21 ng mL ⁻¹	5.4–8.5	[84]
Polar estrogens	µ-SPE/UHPLC-MS/MS	MIL-101(Cr)	0.005–100 µg L ⁻¹	0.95–23 ng L ⁻¹	<9.9	[85]
Cr ³⁺ , Pb ²⁺	DSPE/FAAS	ZIF-8/ZIF-67 core-shell	0.5–200 µg L ⁻¹	0.10–0.15 µg L ⁻¹	1.9–2.7	[65]
Cu ²⁺	MSPE/UV-Vis	Fe ₃ O ₄ @MOF@COF	0.05–1.2 µM	37.6 nM	4.14	[86]
Silver	MSPE/FAAS	MIL-101(Cr)/Fe ₃ O ₄ @SiO ₂ @2-ATP	0.2–200 ng mL ⁻¹	0.05 ng mL ⁻¹	4.5–9.3	[87]

Analytes	Analytical methods	Adsorbent	Linearity	LOD	%RSD	Refs
Allergenic disperse dyes	DSPE/UHPLC-MS/MS	NH ₂ -MIL 101 (Cr)	0.010–10 µg L ⁻¹	0.36–16.9 ng/L	2.1–7.8	[79]
Polycyclic aromatic hydrocarbons	D-µSPE/UHPLC-FD	Silica@MOF CIM-80(Al)	0.02–1.0 µg L ⁻¹	0.005–0.1 µg L ⁻¹	<14	[88]
Malachite green, rhodamine B, methyl orange and acid red 18 dyes	PT-SPE/HPLC	Co-MOF	0.5–200.0 µg/L	0.09–0.38 µg/L	<6.4	[74]
Fluoroquinolones	PT-SPE/HPLC-FLD	Zeolitic imidazole framework-8/cellulose aerogel	1.0–512 ng L ⁻¹	0.34–1.7 ng L ⁻¹	<6.0	[76]
Nitrazepam, oxazepam	PT-SPE/HPLC	Polyacrylonitrile/MIL-53(Fe) electrospun nanofiber	5.0–1000 ng mL ⁻¹	1.5–2.5 ng mL ⁻¹	≤7.6	[73]
Parabens	PT-µSPE/HPLC-UV	Cr-MOF adsorbent	1.0–200.0 µg/L	0.24–0.25 µg/L	5.78	[75]

interactions. In addition, the spiral fibre was reported to have the potential of increasing the contact area between adsorbent and PAHs. The developed S-SPME method exhibited wide linearity ($0.005\text{--}1000\ \mu\text{g L}^{-1}$), low LOD ($0.002\text{--}2.7\ \mu\text{g L}^{-1}$) and acceptable precision ($0.7\text{--}10.7\%$). The performance of the developed S-SPME fibre proved to have excellent extraction efficiencies and enrichment abilities for the analysis of PAHs compared with commercially available SPME fibres.

In another study, Amini *et al.*, [91] reported the application of novel electrospun polyacrylonitrile/nickel-based metal-organic framework nanocomposite (PAN/Ni-MOF) nanosorbent as the coating on a stainless-steel wire. The PAN/Ni-MOF coated stainless-steel wire was employed for headspace solid-phase microextraction (HS-SPME) of organophosphorus pesticides in water samples and food samples. The analytes of interest were quantified using corona discharge ion mobility spectrometry (CD-IMS). The developed HS-SPME exhibited remarkable analytical performance such as linearity ($0.5\text{--}300\ \text{ng mL}^{-1}$), LODs ($0.2\text{--}0.3\ \text{ng mL}^{-1}$), and intra-day precision ($\leq 5.2\%$). The application of MOFs and MOF-based nanocomposites in various modes of SPME proves to be receiving great attention in environmental analysis. Table 3 shows that MOFs and MOF-based nanocomposites are suitable candidates for extraction of pharmaceuticals and personal care products, polycyclic aromatic hydrocarbon, per- and polyfluoroalkyl substances (PFASs), organic dyes, heavy metals in complex environmental waters samples.

3.4 Electrochemical sensors

An electrochemical sensor is an analytical device that has a sensitive component that undergoes chemical changes upon interactions with an analyte and a transducer that converts the chemical changes into measurable signals [12,98]. Electrochemical sensors are one of the promising analytical methods for the detection and identification of various analytes that can be easily oxidised or reduced in environmental water matrices [12,98]. The electrochemical oxidation or reduction reactions occur on the surface of the electrode. Therefore, for better sensitivity and selectivity, the surface of the electrode is usually modified by immobilising the active materials as shown in Figure 4 [12]. The modified electrode provides more active sites for the electrochemical redox reaction with the target analyte [12], thus resulting in a rapid reaction rate and enhanced sensitivity toward the target analytes (Figure 4).

Table 3: Application of MOFs and nanocomposite in various SPME modes for environmental water analysis

Analytes	Analytical method	Sorbent	Linearity	LOD	%RSD	Refs
Nonsteroidal anti-inflammatory drugs (NSAIDs)	SPME/GC	Zr-MOF@GO	0.01–500 $\mu\text{g L}^{-1}$	0.001–0.030 $\mu\text{g L}^{-1}$	-	[92]
Fluoroquinolones	In tube SPME/HPLC-FLD	ZIF-8@monolith composite	0.001–5.0 $\mu\text{g/L}$	0.14–0.61 ng/L	<10	[93]
Odorants	SPME/	MOF-74	0.005–100 $\mu\text{g/L}$	0.01–0.9 ng L^{-1}	<8.7–9.4	[62]
Polycyclic aromatic hydrocarbons	HS-SPME/GC	Metal azolate frameworks (MAF-66)	0.01–100 $\mu\text{g L}^{-1}$	0.1–7.5 ng L^{-1}	0.23–4.2	[94]
Perfluorooctanoic acid (PFOA)	SPME/MS	Water-resistant MOFs: ZIF-8, UiO-66, MIL88-A, and Tb ₂ (BDC) ₃	-	11 ng L^{-1}	-	[95]
Polycyclic aromatic hydrocarbons	SPME/GC-MS	HKUST-1 membrane	0.01–10 $\mu\text{g L}^{-1}$	0.12–9.9 ng L^{-1}	2.6–14	[96]
Polycyclic aromatic hydrocarbons (PAHs), personal care products (PCPs)	DI-SPME-GC-FID	ZIF-8	2.0–100 $\mu\text{g L}^{-1}$	0.6–2.0 $\mu\text{g L}^{-1}$		[97]

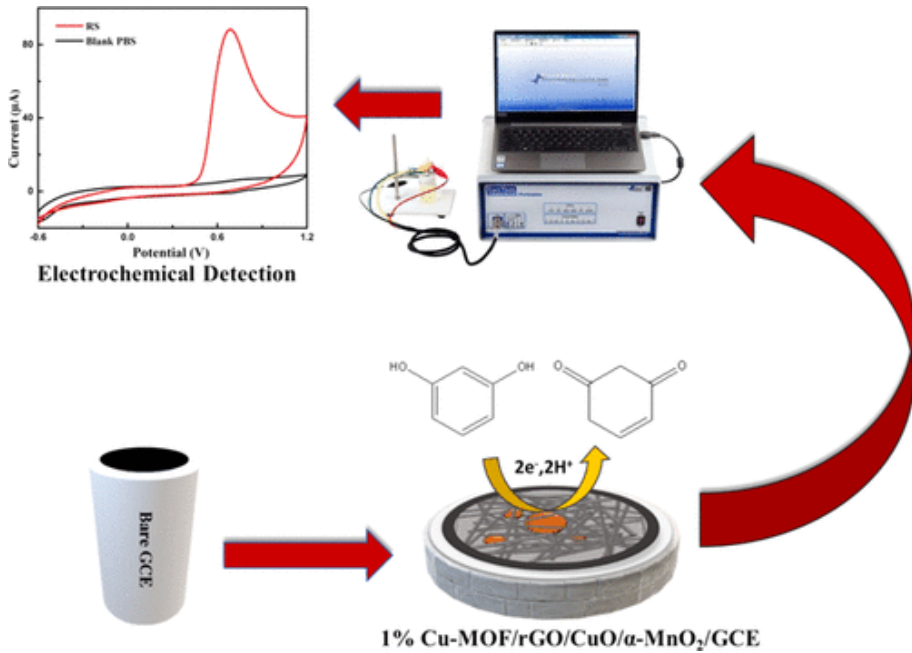


Figure 4: Schematic illustrating the fabrication of an electrochemical sensor. Adapted and reproduced with permission from ref [99].

Metal-organic frameworks have proven to be promising electrochemical sensing platforms due to their remarkable characteristics [98,100,101], namely:

- Unique structural characteristics (tunable porosity, large surface areas, and cavities) and unsaturated metal coordination sites (See Figure 5). The unique features give MOFs and MOF-based nanocomposites superior catalytic capabilities, which warrants them to be useful candidates as effective coating materials for electrochemical electrodes.
- The large surface area and high porosity MOF materials become beneficial in the preconcentration and mass transfer of the analytes from the sample to the surface of the electrode, thus effectively amplifying the analytical signal response and enhancing the sensitivity of the electrochemical sensor.
- The unique particle size and shape of the MOF cavities and channels (Figure 5) allow enhanced selectivity towards the target analytes via a process called size exclusion effects.

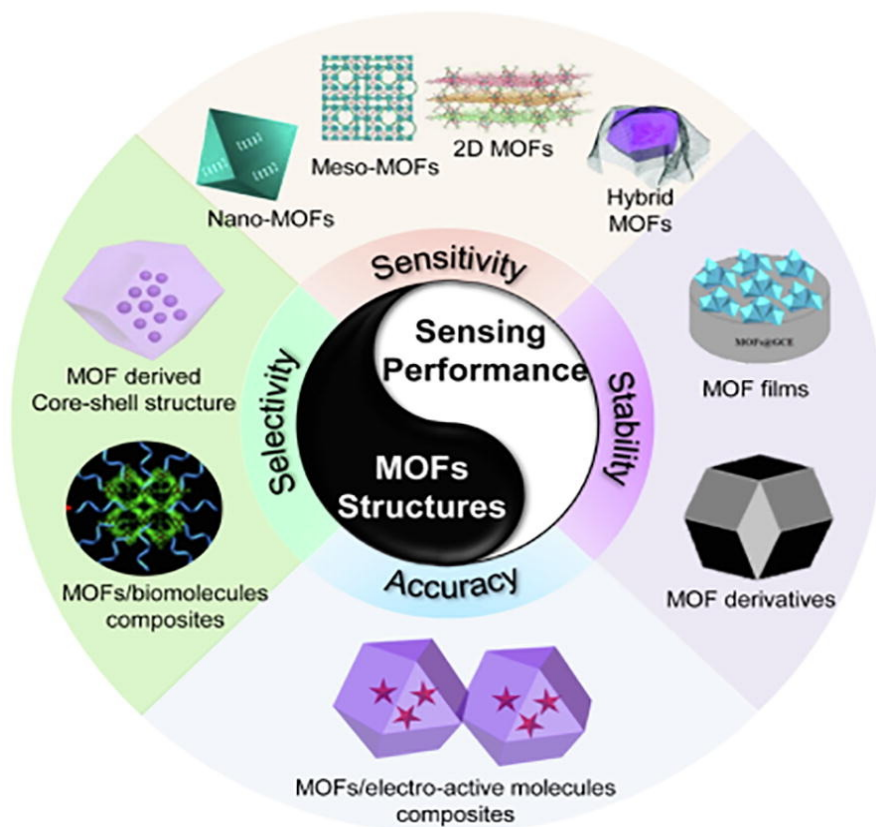


Figure 5: Structure–performance relationship of MOF-based materials for advanced electrochemical sensing applications. Adapted and reproduced with permission from ref [101].

Inspired by the above-mentioned attractive features, a wide range of MOFs and nanocomposites with improved and superior electroactivities have been used as electrochemical sensing platforms of inorganic and organic pollutants in water systems (Table 4). Kokkinos *et al.*, [102], reposted the combination of 3D–printing technology and a highly efficient calcium-based metal–organic framework (Ca–MOF) as a glassy carbon electrode (GCE) sensing platform for determination Hg(II). The Ca–MOF was prepared using N,N′-bis(2,4-dicarboxyphenyl)-oxalamide and N,N-dimethylacetamide), which proved to increase the selectivity of the electrochemical sensor towards Hg(II). In another study, Wan *et al.*, [66] constructed an electrochemical sensor for the simultaneous detection of Cd²⁺, Pb²⁺, and Cu²⁺. The electrochemical sensing platform was fabricated using ferrocenecarboxylic acid-functionalised UiO-66 (Fc-NH₂-UiO-66)

and thermally reduced graphene oxide (trGNO) to give an overall final material termed trGNO/Fc-NH₂-UiO-66 nanocomposite. The porous structure and large specific surface area of NH₂-UiO-66 were beneficial to the effective extraction, adsorption, and preconcentration of the target analytes. Additionally, the incorporation of trGNO and Fc improves the electrochemical activity and electron conductivity of the trGNO/Fc-NH₂-UiO-66/GCE sensing platform.

The MOF-based electrochemical sensors have also received more attention in the determination of fast and efficient tracking of emerging contaminants. For instance, Chen *et al.*, [103] developed an electrochemical sensor based on nitrogen-doped Cu MOFs modified electrode (N-Cu-MOF/GCE). The designed N-Cu-MOFs had an average particle size of 450 nm, unique octahedral shapes, and a large surface area of 1184 m² g⁻¹. These extraordinary properties demonstrated excellent electroanalytical capability for the detection of dopamine and sulfonamides. The designed N-Cu-MOF/GCE exhibited wide linear ranges (0.50 nM–1.8 mM), low LOQ (0.15 nM–0.003 μM). Song *et al.*, [104], designed a novel electrochemical aptasensor based on NH₂-MIL-101(Fe)/CNF@AuNPs electrode for the detection of tetracycline antibiotics in environmental water samples. The authors mentioned that the analytical signals generated from the interaction between tetracycline antibiotics and the electrode were amplified by the NH₂-MIL-101(Fe)/CNF@AuNPs, which resulted in the lowest detection limits and good selectivity. Additionally, the NH₂-MIL-101(Fe)/CNF@AuNPs electrode exhibited high stability.

4. Conclusion and future perspectives

Recent developments and applications of MOF and MOF-based nanocomposites on sample preparation and electrochemical sensor have been reviewed and discussed. To date, the reported findings indicate that the application of MOF and MOF-based nanocomposites in analytical methods is gaining popularity. Depending on the nature of the analytes, literature findings showed that the MOFs and MOF-based nanocomposites have different selectivity and adsorption mechanisms. Other than a large surface area, unique cavities, thermal stability and porosity, π–π stacking, electrostatic and hydrophobic interactions drive the adsorption mechanism. These properties of MOF materials gain more attention as electrochemical sensing platforms for both inorganic and organic pollutants.

In this review, a concise report on the recent applications of MOF materials as efficient adsorbents for the extraction and pre-concentration of different target organic and inorganic pollutants (pharmaceutical and

Table 4: Summary of the applications of MOFs materials as an electrochemical sensing platform for the detection of environmental pollutants

Analytes	Electrochemical sensing platform	Linearity	LOD	%RSD	Refs
Cd ²⁺ , Cu ²⁺ , Hg ²⁺ , Pb ²⁺	UiO-66-NH ₂ /GaOOH/GCE	0.10–2.50 μM	0.006–0.028 μM	3.4–5.8	[10]
Cu ²⁺ , Pb ²⁺ , Cd ²⁺	Fc-NH ₂ -Ni-MOF/GCE	0.001–2.0 μM	0.2–7.1 nM	4.1–7.4	[66]
Cd ²⁺	Fe ³⁺ @MOF-867@PPy/GCE	0–130 μg L ⁻¹	0.29 μg L ⁻¹	-	[105]
Pb(II), Cu(II), Hg(II)	MIL-47(as)/CPE	1–10 μM	29.01–87.80 nM	-	[106]
As	GO/Zn-MOF-GCE	0.2–25 μg L ⁻¹	0.06 μg L ⁻¹	2.1	[107]
Resorcinol	Cu-MOF/rGO/CuO/α-MnO ₂ /GCE	0.2 to 22 μM	0.2 μM	-	[99]
paraoxon and chlorpyrifos.	TiO ₂ functionalized graphene oxide@UiO-66 (TGO@UiO-66)/GCE	1.0–300.0 nM	0.2–1.0 nM	<4.6	[108]
Nitrites	Cu-MOF/Au/GCE	0.1–4000 and 4000–10000 μM	82 nM	4.3	[109]
Dichlorophen	RGO@Ce-MOF/GCE	0.02–10 μM	0.007 μM	3.6	[110]
Mercury (II)	Thioether-Zr-MOF/ screen-printed carbon electrodes	0.01 nM–3 μM	7.3 fM	2.2–4.0	[111]
Ciprofloxacin	NH ₂ -UiO-66/RGO sensor	0.02 to 1 μM	6.67 nM	-	[112]
Pb ²⁺ and Cd ²⁺	MWCNTs-COOH/UiO-66-NH ₂ /MWCNTs-COOH/GCE	1–511 μg L ⁻¹	0.071–0.090 μg L ⁻¹	5.9–6.8	[113]
Nitro-aromatic compounds	Cu-MOF(JUC-62)@pOMC-3/GCE	0.05–4.20 μM	18 μM	-	[114]

personal care products, dyes, phenols, polycyclic aromatic hydrocarbons, and heavy metals) from environmental water samples. Additionally, the porous nature of MOF materials proved to be a candidate to replace conventional adsorbents used in SPE and SPME. Furthermore, MOF materials are promising adsorbent materials in the analysis of challenging contaminants such as emerging micropollutants and organic dyes. The future applications of MOFs as adsorbents in analytical chemistry still need a lot of research in terms of green synthesis of new MOFs (prepared from waste materials) with impressive properties such as good selectivity, higher chemical stability, and super adsorption capacity as well as better reusability and separability. Furthermore, combining MOFs with other novel nanomaterials has proven to further enhance the adsorption and conductivity properties of MOFs. The resultant adsorbent materials could be used in various extraction methods (SPME, DSPE, SPME, and SPE) and electrochemical sensing techniques to assist the researchers to improve the performance of their analytical techniques for the analysis of a wide range of pollutants present in complicated environmental matrixes. Finally, this chapter has proven that the opportunity and future of using MOF-based materials in the field of analytical science look highly promising.

5. Acknowledgements

This study received financial support from the Department of Science and Innovation-National Research Foundation South African Research Chairs Initiative (DSI-NRF SARChI) grant no. 91230.

References

1. A.R. Ribeiro, O.C. Nunes, M.F.R. Pereira, A.M.T. Silva, An overview on the advanced oxidation processes applied for the treatment of water pollutants defined in the recently launched Directive 2013/39/EU, *Environment International*. 75 (2015) 33–51. <https://doi.org/10.1016/j.envint.2014.10.027>
2. V. Geissen, H. Mol, E. Klumpp, G. Umlauf, M. Nadal, M. van der Ploeg, S.E.A.T.M. van de Zee, C.J. Ritsema, Emerging pollutants in the environment: A challenge for water resource management, *International Soil and Water Conservation Research*. 3 (2015) 57–65. <https://doi.org/10.1016/j.iswcr.2015.03.002>
3. M. Tobajas, C. Belver, J.J. Rodriguez, Degradation of emerging pollutants in water under solar irradiation using novel TiO₂-ZnO/clay nanoarchitectures, *Chemical Engineering Journal*. 309 (2017) 596–606. <https://doi.org/10.1016/j.cej.2016.10.002>

4. M.C. Campos-Mañas, P. Plaza-Bolaños, J.A. Sánchez-Pérez, S. Malato, A. Agüera, Fast determination of pesticides and other contaminants of emerging concern in treated wastewater using direct injection coupled to highly sensitive ultra-high performance liquid chromatography-tandem mass spectrometry, *Journal of Chromatography A*. 1507 (2017) 84–94. <https://doi.org/10.1016/j.chroma.2017.05.053>
5. K. Grabicova, R. Grabic, M. Blaha, V. Kumar, D. Cervený, G. Fedorova, T. Randak, Presence of pharmaceuticals in benthic fauna living in a small stream affected by effluent from a municipal sewage treatment plant, *Water Research*. 72 (2015) 145–153. <https://doi.org/10.1016/j.watres.2014.09.018>
6. M. Bilal, M. Adeel, T. Rasheed, Y. Zhao, H.M.N. Iqbal, Emerging contaminants of high concern and their enzyme-assisted biodegradation – A review, *Environment International*. 124 (2019) 336–353. <https://doi.org/10.1016/j.envint.2019.01.011>
7. A.J. Ebele, M. Abou-Elwafa Abdallah, S. Harrad, Pharmaceuticals and personal care products (PPCPs) in the freshwater aquatic environment, *Emerging Contaminants*. 3 (2017) 1–16. <https://doi.org/10.1016/j.emcon.2016.12.004>
8. M.C. Moreno-Bondi, M.D. Marazuela, S. Herranz, E. Rodriguez, An overview of sample preparation procedures for LC-MS multiclass antibiotic determination in environmental and food samples, *Analytical and Bioanalytical Chemistry*. 395 (2009) 921–946. <https://doi.org/10.1007/s00216-009-2920-8>
9. M. Llaver, M.N. Oviedo, E.F. Fiorentini, P.Y. Quintas, R.G. Wuilloud, Analytical developments and applications of ionic liquids for environmental studies, *Trends in Environmental Analytical Chemistry*. 1 (2021) e00131. <https://doi.org/10.1016/j.teac.2021.e00131>
10. J. Ru, X. Wang, X. Cui, F. Wang, H. Ji, X. Du, X. Lu, GaOOH-modified metal-organic frameworks UiO-66-NH₂: Selective and sensitive sensing four heavy-metal ions in real wastewater by electrochemical method, *Talanta*. 234 (2021) 122679. <https://doi.org/10.1016/j.talanta.2021.122679>
11. H. Zhang, P. Xiong, G. Li, C. Liao, G. Jiang, Applications of multifunctional zirconium-based metal-organic frameworks in analytical chemistry: Overview and perspectives, *TrAC Trends in Analytical Chemistry*. 121 (2020) 116015. <https://doi.org/10.1016/j.trac.2020.116015>
12. C. Chuang, C. Kung, Metal-organic frameworks toward electrochemical sensors: challenges and opportunities, *Electroanalysis*. 32 (2020) 1885–1895. <https://doi.org/10.1002/elan.202060111>

13. Z.-Y. Gu, C.-X. Yang, N.A. Chang, X.-P. Yan, Metal-organic frameworks for analytical chemistry: from sample collection to chromatographic separation, *Accounts of Chemical Research*. 45 (2012) 734–745. <https://doi.org/10.1021/ar2002599>
14. G. Maurin, C. Serre, A. Cooper, G. Férey, The new age of MOFs and of their porous-related solids, *Chemical Society Reviews*. 46 (2017) 3104–3107.
15. Y. Sun, H.C. Zhou, Recent progress in the synthesis of metal-organic frameworks, *Science and Technology of Advanced Materials*. 16 (2015). <https://doi.org/10.1088/1468-6996/16/5/054202>.
16. J.D. Evans, B. Garai, H. Reinsch, W. Li, S. Dissegna, V. Bon, I. Senkovska, R.A. Fischer, S. Kaskel, C. Janiak, N. Stock, D. Volkmer, Metal-organic frameworks in Germany: From synthesis to function, *Coordination Chemistry Reviews*. 380 (2019) 378–418. <https://doi.org/10.1016/j.ccr.2018.10.002>.
17. F. Maya, C.P. Cabello, R.M. Frizzarin, J.M. Estela, Magnetic solid-phase extraction using metal-organic frameworks (MOFs) and their derived carbons, *Trends in Analytical Chemistry*. 90 (2017) 142–152. <https://doi.org/10.1016/j.trac.2017.03.004>.
18. W. Ruan, C. Mu, B. Wang, A. Nie, C. Zhang, X. Du, J. Xiang, F. Wen, Z. Liu, Metal-organic framework derived cobalt phosphosulfide with ultrahigh microwave absorption properties, *Nanotechnology*. 29 (2018) 405703. <https://doi.org/10.1088/1361-6528/aad39b>
19. P. Karthik, A.R.M. Shaheer, A. Vinu, B. Neppolian, Amine Functionalized Metal-Organic Framework Coordinated with Transition Metal Ions: d-d Transition Enhanced Optical Absorption and Role of Transition Metal Sites on Solar Light Driven H₂ Production, *Small*. 16 (2020) 1902990. <https://doi.org/10.1002/sml.201902990>
20. P.-C. Shi, X. Lin, J. Liang, X.-X. Li, Y.-B. Huang, R. Cao, A flexible porous copper-based metal-organic cage for carbon dioxide adsorption, *Inorganic Chemistry Communications*. 78 (2017) 28–31. <https://doi.org/10.1016/j.inoche.2017.02.015>
21. S. Sundriyal, S. Mishra, A. Deep, Study of manganese-1, 4-benzenedicarboxylate metal organic framework electrodes based solid state symmetrical supercapacitor, *Energy Procedia*. 158 (2019) 5817–5824. <https://doi.org/10.1016/j.egypro.2019.01.546>
22. Y. Li, H. Liu, H. Wang, J. Qiu, X. Zhang, GO-guided direct growth of highly oriented metal-organic framework nanosheet membranes for H₂/CO₂ separation, *Chemical Science*. 9 (2018) 4132–4141. <https://doi.org/10.1039/c7sc04815g>

23. Y. Xiong, Y. Gao, X. Guo, Y. Wang, X. Su, X. Sun, Water-stable metal-organic framework material with uncoordinated terpyridine site for selective Th (IV)/Ln (III) separation. *ACS Sustainable Chemistry & Engineering*. 7(3) (2018), 3120–3126. <https://doi.org/10.1021/acssuschemeng.8b04875>
24. Y.-J. Yang, Y.-H. Li, D. Liu, G.-H. Cui, A dual-responsive luminescent sensor based on a water-stable Cd (ii)-MOF for the highly selective and sensitive detection of acetylacetone and Cr 2 O 7 2- in aqueous solutions, *Cryst Eng Comm*. 22 (2020) 1166–1175. <https://doi.org/10.1039/C9CE01546A>
25. Y. Rachuri, B. Parmar, K.K. Bisht, E. Suresh, Mixed ligand two-dimensional Cd (II)/Ni (II) metal organic frameworks containing dicarboxylate and tripodal N-donor ligands: Cd (II) MOF is an efficient luminescent sensor for detection of picric acid in aqueous media, *Dalton Transactions*. 45 (2016) 7881–7892. <https://doi.org/10.1039/C6DT00753H>
26. X. Du, X. Yi, P. Wang, J. Deng, C.C. Wang, Enhanced photocatalytic Cr(VI) reduction and diclofenac sodium degradation under simulated sunlight irradiation over MIL-100(Fe)/g-C 3 N 4 heterojunctions, *Cuihua Xuebao/Chinese Journal of Catalysis*. 40 (2019) 70–79. [https://doi.org/10.1016/S1872-2067\(18\)63160-2](https://doi.org/10.1016/S1872-2067(18)63160-2).
27. S.P. Tripathy, S. Subudhi, R. Acharya, R. Acharya, M. Das, K. Parida, Adsorptive removal of Cr(VI) onto UiO-66-NH₂ and its determination by radioanalytical techniques, *Journal of Radioanalytical and Nuclear Chemistry*. 322 (2019) 983–992. <https://doi.org/10.1007/s10967-019-06761-w>.
28. F. Su, J. Yu, C. Zhou, S. Li, P. Ma, X. Zhang, Z. Wang, Two ZnII-based MOFs constructed with biphenyl-2, 2', 5, 5'-tetracarboxylic acid and flexible N-donor ligands: syntheses, structures and properties, *Acta Crystallographica Section C: Structural Chemistry*. 76 (2020) 547–556. <https://doi.org/10.1107/S205322962000604X>
29. V. Gupta, S. Tyagi, A.K. Paul, Development of biocompatible iron-carboxylate metal organic frameworks for pH-responsive drug delivery application, *Journal of Nanoscience and Nanotechnology*. 19 (2019) 646–654. <https://doi.org/10.1166/jnn.2019.15402>
30. R. Ye, J. Yang, X. Zhang, L. Zhang, Y. Yao, Diverse Zn (II) MOFs assembled from V-shaped asymmetric multicarboxylate and N-donor ligands, *Journal of Molecular Structure*. 1106 (2016) 192–199. <https://doi.org/10.1016/j.molstruc.2015.10.086>.

31. F. Bigdeli, H. Ghasempour, A. Azhdari Tehrani, A. Morsali, H. Hosseini-Monfared, Ultrasound-assisted synthesis of nano-structured Zinc(II)-based metal-organic frameworks as precursors for the synthesis of ZnO nano-structures, *Ultrasonics Sonochemistry*. 37 (2017) 29–36. <https://doi.org/10.1016/j.ultsonch.2016.12.031>.
32. A. Ayati, M.N. Shahrak, B. Tanhaei, M. Sillanpää, Emerging adsorptive removal of azo dye by metal-organic frameworks, *Chemosphere*. 160 (2016) 30–44. <https://doi.org/10.1016/j.chemosphere.2016.06.065>.
33. K. Sun, L. Li, X.L. Yu, L. Liu, Q. Meng, F. Wang, R. Zhang, Functionalization of mixed ligand metal-organic frameworks as the transport vehicles for drugs, *Journal of Colloid and Interface Science*. 486 (2017) 128–135. <https://doi.org/10.1016/j.jcis.2016.09.068>.
34. R. Abazari, A.R. Mahjoub, G. Salehi, Preparation of amine functionalized g-C₃N₄@H/SMOF NCs with visible light photocatalytic characteristic for 4-nitrophenol degradation from aqueous solution, *Journal of Hazardous Materials*. 365 (2019) 921–931. <https://doi.org/10.1016/j.jhazmat.2018.11.087>.
35. H.L. Nguyen, F. Gándara, H. Furukawa, T.L.H. Doan, K.E. Cordova, O.M. Yaghi, A Titanium-Organic Framework as an Exemplar of Combining the Chemistry of Metal- and Covalent-Organic Frameworks, *Journal of the American Chemical Society*. 138 (2016) 4330–4333. <https://doi.org/10.1021/jacs.6b01233>.
36. H. Jasuja, Y. Jiao, N.C. Burtch, Y.G. Huang, K.S. Walton, Synthesis of cobalt-, nickel-, copper-, and zinc-based, water-stable, pillared metal-organic frameworks, *Langmuir*. 30 (2014) 14300–14307. <https://doi.org/10.1021/la503269f>.
37. Y. Li, K. Zhou, M. He, J. Yao, Synthesis of ZIF-8 and ZIF-67 using mixed-base and their dye adsorption, *Microporous and Mesoporous Materials*. 234 (2016) 287–292. <https://doi.org/10.1016/j.micromeso.2016.07.039>.
38. M. Eddaoudi, J. Kim, N. Rosi, D. Vodak, J. Wachter, M.O. Keffe, O.M. Yaghi, J. Kimrn, O.M. Yaghi, Systematic Design of Pore Size and Functionality in Isoreticular MOFs and Their Application in Methane Storage All use subject to JSTOR Terms and Conditions Systematic Design and Functionality MOFs and Size Isoreticular in Application Storage, *Science*. 295 (2013) 469–472. <https://doi.org/10.1126/science.1067208>
39. Y.P. Gao, L. Guo, Y.H. Lv, W. Dong, M. Jia, F. Chang, A series of 1-D, 2-D and 3-D coordination polymers self-assembled from a flexible dicarboxylate and mixed N-donor ligands: syntheses, structural diversity, and luminescent properties, *Journal of Coordination Chemistry*. 69 (2016) 3745–3761. <https://doi.org/10.1080/00958972.2016.1239087>.

40. K. Zhu, C. Chen, H. Xu, Y. Gao, X. Tan, A. Alsaedi, T. Hayat, Cr(VI) Reduction and Immobilization by Core–Double–Shell Structured Magnetic Polydopamine@Zeolitic Idazolate Frameworks–8 Microspheres, *ACS Sustainable Chemistry and Engineering*. 5 (2017) 6795–6802. <https://doi.org/10.1021/acssuschemeng.7b01036>.
41. H. Xie, Y. Wei, J. Li, S. Wang, H. Li, Y. Zhao, M. Zhao, X. Chen, In-situ exfoliation of graphitic carbon nitride with metal–organic framework via a sonication–assisted approach for dispersive solid–phase extraction of perfluorinated compounds in drinking water samples, *Journal of Chromatography A*. (2020) 461337. <https://doi.org/10.1016/j.chroma.2020.461337>
42. P. Zhao, M. Jian, Q. Zhang, R. Xu, R. Liu, X. Zhang, H. Liu, A new paradigm of ultrathin 2D nanomaterial adsorbents in aqueous media: graphene and GO, MoS₂, MXenes, and 2D MOFs, *Journal of Materials Chemistry A*. 7 (2019) 16598–16621.
43. J. Qiu, X. Li, R. Gref, A. Vargas–Berenguel, *Carbohydrates in metal organic frameworks: Supramolecular assembly and surface modification for biomedical applications*, in: *Metal–Organic Frameworks for Biomedical Applications*, Elsevier, 2020: pp. 445–465.
44. B. Mandal, J.S. Chung, S.G. Kang, Exploring the geometric, magnetic and electronic properties of Hofmann MOFs for drug delivery, *Physical Chemistry Chemical Physics*. 19 (2017) 31316–31324.
45. Y.Z. Chen, R. Zhang, L. Jiao, H.L. Jiang, Metal–organic framework–derived porous materials for catalysis, *Coordination Chemistry Reviews*. 362 (2018) 1–23. <https://doi.org/10.1016/j.ccr.2018.02.008>.
46. J. Li, H. Wang, X. Yuan, J. Zhang, J.W. Chew, Metal–organic framework membranes for wastewater treatment and water regeneration, *Coordination Chemistry Reviews*. 404 (2020) 213116. <https://doi.org/10.1016/j.ccr.2019.213116>.
47. A.B. Kanu, Recent developments in sample preparation techniques combined with high–performance liquid chromatography: A critical review, *Journal of Chromatography A*. 1654 (2021) 462444.
48. M. Bazargan, F. Ghaemi, A. Amiri, M. Mirzaei, Metal–organic framework–based sorbents in analytical sample preparation, *Coordination Chemistry Reviews*. 445 (2021) 214107.
49. M. Pérez–Rodríguez, R.G. Pellerano, L. Pezza, H.R. Pezza, An overview of the main foodstuff sample preparation technologies for tetracycline residue determination, *Talanta*. 182 (2018) 1–21.

50. N. Manousi, G.A. Zachariadis, E.A. Deliyanni, V.F. Samanidou, Applications of metal-organic frameworks in food sample preparation, *Molecules*. 23 (2018) 2896.
51. F. Maya, C.P. Cabello, R.M. Frizzarin, J.M. Estela, G.T. Palomino, V. Cerda, Magnetic solid-phase extraction using metal-organic frameworks (MOFs) and their derived carbons, *TrAC Trends in Analytical Chemistry*. 90 (2017) 142–152.
52. S. Jakavula, N.R. Biata, K.M. Dimpe, V.E. Pakade, P.N. Nomngongo, A critical review on the synthesis and application of ion-imprinted polymers for selective preconcentration, speciation, removal and determination of trace and essential metals from different matrices, *Critical Reviews in Analytical Chemistry*. (2020) 1–13.
53. N. Mpayipheli, A. Mpupa, P.N. Nomngongo, Vortex-Assisted Dispersive Molecularly Imprinted Polymer-Based Solid Phase Extraction of Acetaminophen from Water Samples Prior to HPLC-DAD Determination, *Separations*. 8 (2021) 194.
54. S.K. Selahle, N.J. Waleng, A. Mpupa, P.N. Nomngongo, Magnetic solid phase extraction based on nanostructured magnetic porous porphyrin organic polymer for simultaneous extraction and preconcentration of neonicotinoid insecticides from surface water, *Frontiers in Chemistry*. 8 (2020) 852.
55. Z.-H. Deng, X. Wang, X.-L. Wang, C.-L. Gao, L. Dong, M.-L. Wang, R.-S. Zhao, A core-shell structured magnetic covalent organic framework (type Fe₃O₄@ COF) as a sorbent for solid-phase extraction of endocrine-disrupting phenols prior to their quantitation by HPLC, *Microchimica Acta*. 186 (2019) 108.
56. X. Yang, J. Wang, W. Wang, S. Zhang, C. Wang, J. Zhou, Z. Wang, Solid phase microextraction of polycyclic aromatic hydrocarbons by using an etched stainless-steel fiber coated with a covalent organic framework, *Microchimica Acta*. 186 (2019) 145.
57. P. Baile, J. Medina, L. Vidal, A. Canals, Determination of four bisphenols in water and urine samples by magnetic dispersive solid-phase extraction using a modified zeolite/iron oxide composite prior to liquid chromatography diode array detection, *Journal of Separation Science*. 43 (2020) 1808–1816.
58. L. Nyaba, T.S. Munonde, A. Mpupa, P.N. Nomngongo, Magnetic Fe₃O₄@ Mg/Al-layered double hydroxide adsorbent for preconcentration of trace metals in water matrices, *Scientific Reports*. 11 (2021) 1–15.

59. Q. Zhang, Y. Zhi, L. Bao, Y. Zheng, X. Wang, L. Jiang, Y. Wu, Determination of six parabens in biological samples by magnetic solid-phase extraction with magnetic mesoporous carbon adsorbent and UHPLC-MS/MS, *Journal of Chromatography B*. 1179 (2021) 122817.
60. F. Wang, X. Wang, X. Cui, H. Ji, Y. Liu, X. Du, X. Lu, Development of ZIF-67 derived hollow multishelled structures Co₃O₄/carbon nanomaterials as spiral solid-phase microextraction fiber for superior capture of fifteen PAHs, *Separation and Purification Technology*. 276 (2021) 119367.
61. A. Gutiérrez-Serpa, I. Pacheco-Fernández, J. Pasán, V. Pino, Metal-organic frameworks as key materials for solid-phase microextraction devices—a review, *Separations*. 6 (2019) 47.
62. F. Wei, Y. He, X. Qu, Z. Xu, S. Zheng, D. Zhu, H. Fu, In situ fabricated porous carbon coating derived from metal-organic frameworks for highly selective solid-phase microextraction, *Analytica Chimica Acta*. 1078 (2019) 70–77.
63. C. Calderilla, F. Maya, L.O. Leal, V. Cerdà, Recent advances in flow-based automated solid-phase extraction, *TrAC Trends in Analytical Chemistry*. 108 (2018) 370–380.
64. A. Chisvert, S. Cárdenas, R. Lucena, Dispersive micro-solid phase extraction, *TrAC Trends in Analytical Chemistry*. 112 (2019) 226–233.
65. Y.A. Ghorbani, S.M. Ghoreishi, M. Ghani, Derived N-doped carbon through core-shell structured metal-organic frameworks as a novel sorbent for dispersive solid phase extraction of Cr (III) and Pb (II) from water samples followed by quantitation through flame atomic absorption spectrometry, *Microchemical Journal*. 155 (2020) 104786.
66. J. Wan, Y. Shen, L. Xu, R. Xu, J. Zhang, H. Sun, C. Zhang, C. Yin, X. Wang, Ferrocene-functionalized Ni (II)-based metal-organic framework as electrochemical sensing interface for ratiometric analysis of Cu²⁺, Pb²⁺ and Cd²⁺, *Journal of Electroanalytical Chemistry*. 895 (2021) 115374.
67. S. Hamidi, A. Taghvimi, N. Mazouchi, Micro solid phase extraction using novel adsorbents, *Critical Reviews in Analytical Chemistry*. 51 (2021) 103–114.
68. Y. Wang, A. Zhu, Y. Fang, C. Fan, Y. Guo, Z. Tan, Y. Yin, Y. Cai, G. Jiang, Dithizone-functionalized C₁₈ online solid-phase extraction-HPLC-ICP-MS for speciation of ultra-trace organic and inorganic mercury in cereals and environmental samples, *Journal of Environmental Sciences*. 115 (2022) 403–410.

69. S. Amini, H. Ebrahimzadeh, S. Seidi, N. Jalilian, Application of electrospun polyacrylonitrile/Zn-MOF-74@ GO nanocomposite as the sorbent for online micro solid-phase extraction of chlorobenzenes in water, soil, and food samples prior to liquid chromatography analysis, *Food Chemistry*. (2021) 130330.
70. H. Martínez-Pérez-Cejuela, F. Benavente, E.F. Simó-Alfonso, J.M. Herrero-Martínez, A hybrid nano-MOF/polymer material for trace analysis of fluoroquinolones in complex matrices at microscale by on-line solid-phase extraction capillary electrophoresis, *Talanta*. 233 (2021) 122529.
71. F. Ghaemi, A. Amiri, Microcrystalline cellulose/metal-organic framework hybrid as a sorbent for dispersive micro-solid phase extraction of chlorophenols in water samples, *Journal of Chromatography A*. 1626 (2020) 461386.
72. H. Duo, X. Lu, S. Wang, L. Wang, Y. Guo, X. Liang, Synthesis of magnetic metal-organic framework composites, Fe₃O₄-NH₂@ MOF-235, for the magnetic solid-phase extraction of benzoylurea insecticides from honey, fruit juice and tap water samples, *New Journal of Chemistry*. 43 (2019) 12563-12569.
73. S. Amini, H. Ebrahimzadeh, S. Seidi, N. Jalilian, Polyacrylonitrile/MIL-53 (Fe) electrospun nanofiber for pipette-tip micro solid phase extraction of nitrazepam and oxazepam followed by HPLC analysis, *Microchimica Acta*. 187 (2020) 1-10.
74. S.H. Hashemi, M. Kaykhaii, A.J. Keikha, E. Mirmoradzehi, G. Sargazi, Application of response surface methodology for optimization of metal-organic framework based pipette-tip solid phase extraction of organic dyes from seawater and their determination with HPLC, *BMC Chemistry*. 13 (2019) 1-10.
75. M. Kaykhaii, S.H. Hashemi, F. Andarz, A. Piri, G. Sargazi, G. Boczkaj, Chromium-based metal organic framework for pipette tip micro-solid phase extraction: an effective approach for determination of methyl and propyl parabens in wastewater and shampoo samples, *BMC Chemistry*. 15 (2021) 1-12.
76. L. Li, H. Zhang, Q. Zhang, T. Wang, X. Hou, Macro-microporous zeolitic imidazole framework-8/cellulose aerogel for semi-automated pipette tip solid phase extraction of fluoroquinolones in water, *Analytica Chimica Acta*. 1184 (2021) 338984.

77. Y. Su, S. Wang, N. Zhang, P. Cui, Y. Gao, T. Bao, Zr-MOF modified cotton fiber for pipette tip solid-phase extraction of four phenoxy herbicides in complex samples, *Ecotoxicology and Environmental Safety*. 201 (2020) 110764.
78. Z. Chen, C. Yu, J. Xi, S. Tang, T. Bao, J. Zhang, A hybrid material prepared by controlled growth of a covalent organic framework on amino-modified MIL-68 for pipette tip solid-phase extraction of sulfonamides prior to their determination by HPLC, *Microchimica Acta*. 186 (2019) 1–11.
79. S. Gao, X. Li, X. Bao, K. Chen, X. Liu, F. Qian, X. Shen, Preconcentration of allergenic disperse dyes in environmental water samples based on amino functionalized metal-organic framework, *Microchemical Journal*. 157 (2020) 105059.
80. Z. Chen, Z. He, X. Luo, F. Wu, S. Tang, J. Zhang, Synthesis of MOF@COF hybrid magnetic adsorbent for microextraction of sulfonamides in food and environmental samples, *Food Analytical Methods*. 13 (2020) 1346–1356.
81. M. Habila, B. Alhenaki, A. El-Marghany, M. Sheikh, A. Ghfar, Z. ALOthman, M. Soylak, Metal organic frameworks enhanced dispersive solid phase microextraction of malathion before detection by UHPLC-MS/MS, *Journal of Separation Science*. 43 (2020) 3103–3109.
82. S. Liu, S. Li, W. Yang, F. Gu, H. Xu, T. Wang, D. Sun, X. Hou, Magnetic nanoparticle of metal-organic framework with core-shell structure as an adsorbent for magnetic solid phase extraction of non-steroidal anti-inflammatory drugs, *Talanta*. 194 (2019) 514–521.
83. J. González-Sálamo, M.Á. González-Curbelo, J. Hernández-Borges, M.Á. Rodríguez-Delgado, Use of Basolite® F300 metal-organic framework for the dispersive solid-phase extraction of phthalic acid esters from water samples prior to LC-MS determination, *Talanta*. 195 (2019) 236–244.
84. A. Amiri, R. Tayebee, A. Abdar, F.N. Sani, Synthesis of a zinc-based metal-organic framework with histamine as an organic linker for the dispersive solid-phase extraction of organophosphorus pesticides in water and fruit juice samples, *Journal of Chromatography A*. 1597 (2019) 39–45.
85. S.C. Tan, H.K. Lee, A metal-organic framework of type MIL-101 (Cr) for emulsification-assisted micro-solid-phase extraction prior to UHPLC-MS/MS analysis of polar estrogens, *Microchimica Acta*. 186 (2019) 1–9.
86. W.-T. Li, W. Shi, Z.-J. Hu, T. Yang, M.-L. Chen, B. Zhao, J.-H. Wang, Fabrication of magnetic Fe₃O₄@ metal organic framework@ covalent organic framework composite and its selective separation of trace copper, *Applied Surface Science*. 530 (2020) 147254.

87. S.H. Mousavi, M. Manoochehri, F.A. Taromi, Fabrication of a novel magnetic metal-organic framework functionalized with 2-aminothiophenol for preconcentration of trace silver amounts in water and wastewater, *RSC Advances*. 11 (2021) 13867–13875.
88. A. Gutiérrez-Serpa, A.I. Jiménez-Abizanda, F. Jiménez-Moreno, J. Pasán, V. Pino, Core-shell microparticles formed by the metal-organic framework CIM-80 (Al)(Silica@ CIM-80 (Al)) as sorbent material in miniaturized dispersive solid-phase extraction, *Talanta*. 211 (2020) 120723.
89. V. Jalili, A. Barkhordari, A. Ghiasvand, A comprehensive look at solid-phase microextraction technique: A review of reviews, *Microchemical Journal*. 152 (2020) 104319.
90. M.M. Khataei, Y. Yamini, M. Shamsayei, Applications of porous frameworks in solid-phase microextraction, *Journal of Separation Science*. 44 (2021) 1231–1263.
91. S. Amini, H. Ebrahimzadeh, S. Seidi, N. Jalilian, Preparation of Polyacrylonitrile/Ni-MOF electrospun nanofiber as an efficient fiber coating material for headspace solid-phase microextraction of diazinon and chlorpyrifos followed by CD-IMS analysis, *Food Chemistry*. 350 (2021) 129242.
92. H. Liu, H. Fan, S. Dang, M. Li, A. Gu, H. Yu, A Zr-MOF@ GO-Coated Fiber with High Specific Surface Areas for Efficient, Green, Long-Life Solid-Phase Microextraction of Nonsteroidal Anti-inflammatory Drugs in Water, *Chromatographia*. 83 (2020) 1065–1073.
93. J. Pang, Y. Liao, X. Huang, Z. Ye, D. Yuan, Metal-organic framework-monolith composite-based in-tube solid phase microextraction on-line coupled to high-performance liquid chromatography-fluorescence detection for the highly sensitive monitoring of fluoroquinolones in water and food samples, *Talanta*. 199 (2019) 499–506.
94. M. Liu, J. Liu, C. Guo, Y. Li, Metal azolate framework-66-coated fiber for headspace solid-phase microextraction of polycyclic aromatic hydrocarbons, *Journal of Chromatography A*. 1584 (2019) 57–63.
95. P. Suwannakot, F. Lisi, E. Ahmed, K. Liang, R. Babarao, J.J. Gooding, W.A. Donald, Metal-organic framework-enhanced solid-phase microextraction mass spectrometry for the direct and rapid detection of perfluorooctanoic acid in environmental water samples, *Analytical Chemistry*. 92 (2020) 6900–6908.


96. S. Sun, L. Huang, H. Xiao, Q. Shuai, S. Hu, In situ self–transformation metal into metal–organic framework membrane for solid–phase microextraction of polycyclic aromatic hydrocarbons, *Talanta*. 202 (2019) 145–151.
97. P. Rocío–Bautista, A. Gutiérrez–Serpa, A.J. Cruz, R. Ameloot, J.H. Ayala, A.M. Afonso, J. Pasán, S. Rodríguez–Hermida, V. Pino, Solid–phase microextraction coatings based on the metal–organic framework ZIF–8: Ensuring stable and reusable fibers, *Talanta*. 215 (2020) 120910.
98. T. Ma, H. Li, J.–G. Ma, P. Cheng, Application of MOF–based materials in electrochemical sensing, *Dalton Transactions*. 49 (2020) 17121–17129.
99. T. Iftikhar, Y. Xu, A. Aziz, G. Ashraf, G. Li, M. Asif, F. Xiao, H. Liu, Tuning electrocatalytic aptitude by incorporating α -MnO₂ nanorods in Cu–MOF/rGO/CuO hybrids: electrochemical sensing of resorcinol for practical applications, *ACS Applied Materials & Interfaces*. 13 (2021) 31462–31473.
100. Y. Xu, Q. Li, H. Xue, H. Pang, Metal–organic frameworks for direct electrochemical applications, *Coordination Chemistry Reviews*. 376 (2018) 292–318.
101. C.–S. Liu, J. Li, H. Pang, Metal–organic framework–based materials as an emerging platform for advanced electrochemical sensing, *Coordination Chemistry Reviews*. 410 (2020) 213222.
102. C. Kokkinos, A. Economou, A. Pournara, M. Manos, I. Spanopoulos, M. Kanatzidis, T. Tziotzi, V. Petkov, A. Margariti, P. Oikonomopoulos, 3D–printed lab–in–a–syringe voltammetric cell based on a working electrode modified with a highly efficient Ca–MOF sorbent for the determination of Hg (II), *Sensors and Actuators B: Chemical*. 321 (2020) 128508.
103. S. Chen, C. Wang, M. Zhang, W. Zhang, J. Qi, X. Sun, L. Wang, J. Li, N–doped Cu–MOFs for efficient electrochemical determination of dopamine and sulfanilamide, *Journal of Hazardous Materials*. 390 (2020) 122157.
104. J. Song, M. Huang, X. Lin, S.F.Y. Li, N. Jiang, Y. Liu, H. Guo, Y. Li, Novel Fe–based metal–organic framework (MOF) modified carbon nanofiber as a highly selective and sensitive electrochemical sensor for tetracycline detection, *Chemical Engineering Journal*. 427 (2022) 130913.
105. Y. Li, Y. Cai, K. Shao, Y. Chen, D. Wang, A free–standing poly–MOF film fabricated by post–modification and interfacial polymerization: A novel platform for Cd²⁺ electrochemical sensors, *Microporous and Mesoporous Materials*. (2021) 111200.

106. B. Niu, B. Yao, M. Zhu, H. Guo, S. Ying, Z. Chen, Carbon paste electrode modified with fern leave-like MIL-47 (as) for electrochemical simultaneous detection of Pb (II), Cu (II) and Hg (II), *Journal of Electroanalytical Chemistry*. 886 (2021) 115121.
107. M. Baghayeri, M. Ghanei-Motlagh, R. Tayebee, M. Fayazi, F. Narenji, Application of graphene/zinc-based metal-organic framework nanocomposite for electrochemical sensing of As (III) in water resources, *Analytica Chimica Acta*. 1099 (2020) 60–67.
108. N. Karimian, H. Fakhri, S. Amidi, A. Hajian, F. Arduini, H. Bagheri, A novel sensing layer based on metal-organic framework UiO-66 modified with TiO₂-graphene oxide: application to rapid, sensitive and simultaneous determination of paraoxon and chlorpyrifos, *New Journal of Chemistry*. 43 (2019) 2600–2609.
109. H. Chen, T. Yang, F. Liu, W. Li, Electrodeposition of gold nanoparticles on Cu-based metal-organic framework for the electrochemical detection of nitrite, *Sensors and Actuators B: Chemical*. 286 (2019) 401–407.
110. X. Tu, Y. Xie, X. Ma, F. Gao, L. Gong, D. Wang, L. Lu, G. Liu, Y. Yu, X. Huang, Highly stable reduced graphene oxide-encapsulated Ce-MOF composite as sensing material for electrochemically detecting dichlorophen, *Journal of Electroanalytical Chemistry*. 848 (2019) 113268.
111. L. Fu, K. Xie, A. Wang, F. Lyu, J. Ge, L. Zhang, H. Zhang, W. Su, Y.-L. Hou, C. Zhou, High selective detection of mercury (II) ions by thioether side groups on metal-organic frameworks, *Analytica Chimica Acta*. 1081 (2019) 51–58.
112. X. Fang, X. Chen, Y. Liu, Q. Li, Z. Zeng, T. Maiyalagan, S. Mao, Nanocomposites of Zr (IV)-based metal-organic frameworks and reduced graphene oxide for electrochemically sensing ciprofloxacin in water, *ACS Applied Nano Materials*. 2 (2019) 2367–2376.
113. Z. Lu, W. Zhao, L. Wu, J. He, W. Dai, C. Zhou, H. Du, J. Ye, Tunable electrochemical of electrosynthesized layer-by-layer multilayer films based on multi-walled carbon nanotubes and metal-organic framework as high-performance electrochemical sensor for simultaneous determination cadmium and lead, *Sensors and Actuators B: Chemical*. 326 (2021) 128957.
114. C. Liu, X. Bo, L. Guo, A novel electrochemical sensing platform of JUC-62 metal-organic framework/platelet ordered mesoporous carbon for high selective detection of nitro-aromatic compounds, *Sensors and Actuators B: Chemical*. 297 (2019) 126741.



Chapter 8

Post-synthetic modification of zirconium terephthalate sorbents and their application for sorption of selected toxic elements from water

Rafał Walczak ^a, Iga Zuba ^a, Wojciech Starosta ^{a*},
Jianwei Ren ^b

^a*Institute of Nuclear Chemistry and Technology, 03-195 Warsaw,
Dorodna 16, Poland*

^b*University of Johannesburg, Johannesburg, Kingsway and University Road,
Auckland Park, 2092, P.O. Box 524, Auckland Park, 2006,
Johannesburg, South Africa*

Corresponding author email: w.starosta@ichtj.waw.pl

1. Introduction

Metal-organic Framework (MOF) porous materials have been a subject of interest for about two decades. The discovered recipe for their synthesis consisting of a combination of highly tunable metal nodes and ditopic or multitopic ligands resulted in the exponential growth of new structures. At present, a wealth of material on synthesis, structural, and functional properties have been accumulated. It shows a potentially wide range of applications in the field of gas storage, separation of gaseous mixtures, catalysis, drug delivery, energy, and environment protection. The unique features of MOFs, such as large specific surface area, diversity of possible structures, and theoretical possibility of a design structure for specific applications make them suitable for industrial applications [1]. However, extensive application research is required before a potentially beneficial solution can be put into practice. The issue of economic efficiency and technical suitability should be resolved first.

In the framework of the PET-MOF-CLEANWATER project, the possibility of application of waste PET- derived terephthalic ligand for the synthesis of MOFs suitable for toxic elements removal from water are being explored. The aim of the project is to contribute to the resolution of



two issues. The first is to reduce the environmental impact of the growing amount of PET wastes. It aims to recover terephthalic acid from waste PET and reuse it for synthesis of mechanically and thermally stable porous MOF-type sorbents. The second one is to demonstrate the usefulness of the sorbents obtained in this way for the removal of toxic pollutants from water, for example, radionuclides and heavy metals.

Nuclear power is a mature technology that can make a vital contribution toward global low-carbon energy needs. The sustainable growth of nuclear energy to meet the needs of the future generations is heavily dependent on the practices followed currently in the management of nuclear waste. Recently, there has been growing interest in observing MOF applications for radionuclide waste immobilisation and storage. The high porosity, modularity, and synthetic diversity of metal-organic frameworks (MOFs) make them attractive candidate materials for selective sensing and sequestration of the radionuclides present in the nuclear wastes [2,3]. The results of these studies provide a promising alternative to sequestering nuclear wastes and open new ways for more efficient waste management to make nuclear power more feasible. In the present report, the results of our studies on the removal of technetium, ruthenium, and uranium radionuclides from water solution are presented. Additionally, we provide the data for the removal of mercury, classified by the World Health Organization (WHO) among the ten highly toxic heavy metal contaminants of water.

2. Material synthesis

In our study, we focused on structures built with terephthalic acid and zirconium. The reason for this choice is the chemical resistance in aqueous environments of MOFs constructed with metals of high valence. Moreover, the zirconium terephthalate UiO-66 structure is known for its tolerance for the structural defects of missing linker or missing site types. This makes it possible to functionalise the structure by incorporating a ligand possessing a functional group showing affinity to the metal to be adsorbed. Functionalisation may be carried out directly in the synthesis step or in the post-synthetic process.

Three different types of zirconium terephthalate UiO-66 type sorbents have been synthesised:

1. UiO-66_FA - synthesised according to literature procedure [4]. Briefly, 4 mM of zirconium chloride and 4 mM of terephthalic acid were dissolved in 100 ml of DMF. 50 eq of formic acid (FA) was added as a modulator to create the structure containing structural defects. The solution was refluxed at 120°C for 24 hours. Thereafter,

- powdered material was recovered by filtration, washed in DMF and acetone, and dried at 120°C under vacuum. The XRD studies confirmed a synthesis of UiO-66 structure.
2. Zr_hcp – synthesised directly from PET flakes in acetic acid/acetone mixture at temperature in the range of 160 –190°C. In each synthesis, 2.625 g of zirconium chloride and 1.875 g of PET flakes were added to 75 ml of acetone and 75 ml of formic acid solution. The mixture was processed in Berghof-300 pressurised reactor for 24 hours. The obtained material was porous (the specific surface area was 524.30 cm²/g) and identified as zirconium complex with hexagonal close packed structure ($a=b = 14.71309 \text{ \AA}$, $c = 36.979496 \text{ \AA}$)
 3. Zr_PET – synthesised directly from PET flakes in acetic acid/acetone mixed solvent at temperature as low as 120 °C. In typical synthesis 1g of PET and 1.611 g of zirconium oxychloride octahydrate were added to the solution of 20 ml acetone and 20 ml acetic acid. The resulting mixture was heated in sealed Pyrex bottle for five days on oil bath at temperature of 120°C. The obtained powder material was crystalline, but its structure is not known at present. We suppose that it is a zirconium complex with acetate and terephthalate ligands similar to zirconium complexes with terephthalate and acetic acid ligands described already [5,6]. It was also found that resulting material can be functionalised in a post-synthetic process in a solution containing monocarboxylic acid possessing an amino group. After functionalisation, this material acquires sorption capacity for pertechnetate anion. The thermogravimetric data for UiO-66_FA and Zr_hcp presented in Figure 1 confirm high temperature stability of these structures up to temperatures of around 500°C and their defective character. The number of lacking terephthalate linkers for UiO-66_FA structure was estimated as equal to 2.6.

For the functionalisation of the structures, different monocarboxylic (or dicarboxylic) acids possessing amino group or mercapto (-SH) group were applied.

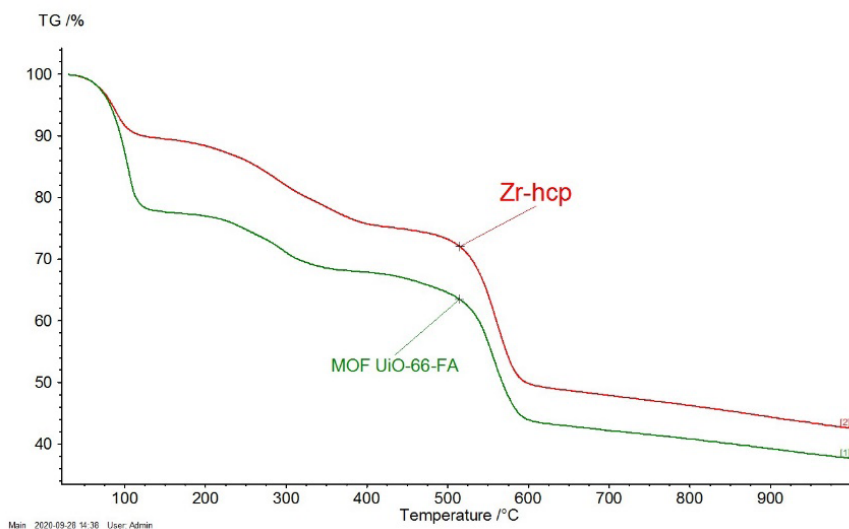


Figure 1: TGA data for defective Zr_hcp structure synthesised from PET waste flakes in acetone/acetic acid mixture and for defective UiO-66_FA sorbent synthesized with formic acid as modulator

3. Sorption of pertechnetate anion from water solution

^{99}Tc is long-lived isotope ($t_{1/2} = 213000$ years) created in a reactor as a fission product of ^{235}U (6.18 % yield) and ^{239}Pu (6.21% yield). Ground state ^{99}Tc decays by beta emission ($E_{\text{max}} = 292$ keV), while the metastable isomer $^{99\text{m}}\text{Tc}$ ($t_{1/2} = 6.0$ h) decays rapidly by emitting a gamma photon. Large quantities of technetium have been produced in the course of nuclear weapons research and are stored in underground tanks containing mixed radioactive waste awaiting reprocessing and subsequent disposal. Technetium (^{99}Tc) is an abundant fission product of particular concern in nuclear reprocessing and waste solidification technologies because of the high solubility and mobility of Tc (VII) pertechnetate (TcO_4^-), and the stable form of technetium in aerobic environments. Tc is volatile during waste vitrification. It can leach from vitrified glass, and greatly interfere with the separation of uranium and plutonium during the PUREX solvent extraction process, making it one of the most problematic radionuclides in the nuclear fuel cycle. Therefore, direct removal of pertechnetate anion from the solutions of used nuclear fuel is considered beneficial to make progress in the recovery of uranium and plutonium from nuclear wastes and as a means of eliminating ^{99}Tc discharge into the environment. It is possible to capture and remove TcO_4^- using a number of processes such as ion exchange, extraction, and precipitation [7,8]. Each of these processes

has its own advantages and disadvantages, but pertechnetate removal by ion exchange has received the most attention to date because of its ease of implementation, cost efficiency, and high ^{99}Tc recovery rate. MOF-type sorbents have an advantage over sorbents of other types due to their construction, which gives the possibility to shape the structure and size of pores and their physicochemical properties in a wide range. But relatively few materials have been tested directly for TcO_4^- ion exchange [9,10]. It is also worth mentioning that protonated zirconium complex with 2-amino-1,4-benzene dicarboxylic UiO-66- NH_2 has been found as an effective adsorbent for the removal from water perrhenate anion ReO_4^- , non-radioactive surrogate of pertechnetate, even in the presence of other competing anions [11].

We recently conducted a study on pertechnetate anion sorption from water for a number of sorbents synthesised using terephthalic acid linker derived from waste PET. The four different types of sorbents were synthesised. One of them is well-known MIL-101(Cr) synthesised according to the literature procedure [12]. The others were UiO-66-FA, Zr hcp and Zr-PET types described in the material synthesis section.

All the sorbents were functionalised in the post-synthetic process in order to introduce the amino group to the structure. For the MIL-101 structure, ethylenediamine was grafted to uncoordinated chromium sites created by dehydration at 150°C for 12 hours. For the three others, functionalisation with 2-aminobenzoic acid, glycine, and 3,5-diaminobenzoic acid was carried out in the post-synthetic ligand exchange process. The last step in the functionalisation consisted of protonating the incorporated amino group of the sorbent in the 4N HCl solution. As a result, cationic MOFs were obtained for which weakly bound chlorine anion can be exchanged in water solution for pertechnetate anion.

The sorption kinetics studies of the sorbents have been performed using the radiotracer method. The $^{99\text{m}}\text{Tc}$ isotope in the chemical form of pertechnetate anion has been used as a tracer. $^{99\text{m}}\text{TcO}_4^-$ was eluted from $^{99\text{Mo}}/^{99\text{m}}\text{Tc}$ generator (POLATOM production) with 8 mL 0.9% NaCl water solution. The activity of $^{99\text{m}}\text{TcO}_4^-$ was at the level of 1 GBq. To each sample of 15 mg MOF in 10 mL of water 50 μL of $^{99\text{m}}\text{TcO}_4^-$ was added (around 6 MBq). The control samples without MOF sorbent were also prepared. All the samples were mixed for a predetermined time. After mixing, samples were centrifuged and 1 mL of supernatant was taken and its activity was measured with a gamma counter. By comparing the measured values with the activity of the control sample, the percentage of activity remaining in the solution was determined.

A high pertechnetate anion removal rate was found for the sorbents being studied. The results of the MIL-101(Cr) case are shown in Figure 2 and for modified UiO-66_FA in Figure 3. In the case of MIL-101(Cr), 92.1% removal efficiency, near saturation value (96.5%) has been achieved after 1 hour.

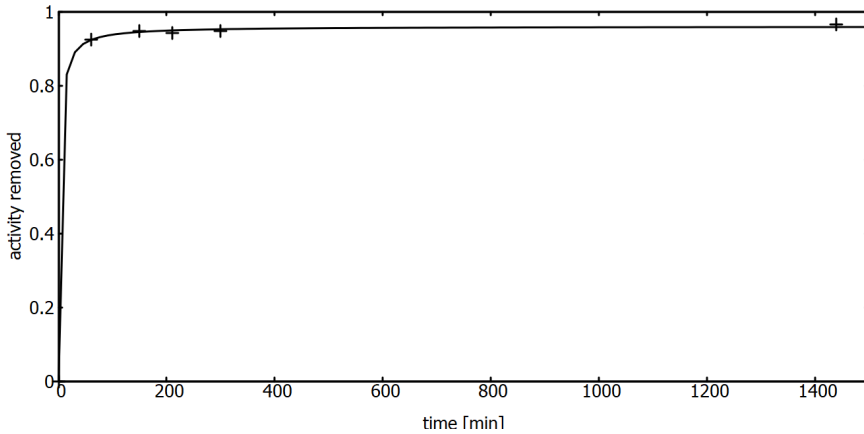


Figure 2: Kinetics of pertechnetate anion removal for MIL-101(Cr) type sorbent grafted with ethylenediamine and protonated in 4N HCl.

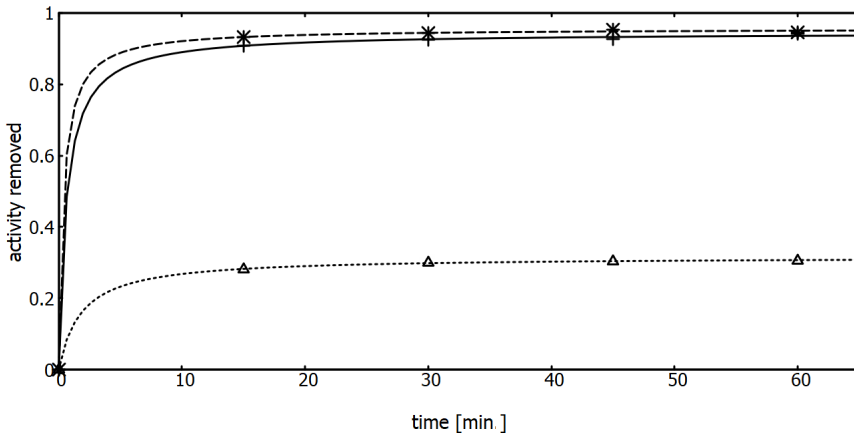


Figure 3: Kinetics of technetium anion removal from water for UiO-66_FA type sorbent modified in post-synthetic ligand exchange process with 2-aminobenzoic acid (solid line), glycine (dashed line) and 3,5-diaminobenzoic acid (dotted line).

The dependence of sorption capacity on solution pH was also investigated. The results showing the pH dependence of distribution coefficient for zirconium complex with 2-aminoterephthalic acid UiO-66_NH₂

and zirconium complex Zr_hcp, modified by post-synthetic ligand exchange process with 2-aminobenzoic acid are presented in Figure 4. The graph shows similar dependence on pH in the range of 2-9 pH for both sorbents. The values of the distribution coefficient for modified Zr_hcp solvent synthesised by a procedure developed during the project exceed those obtained for UiO-66_NH₂ synthesised from a commercial 2-aminoterephthalic ligand.

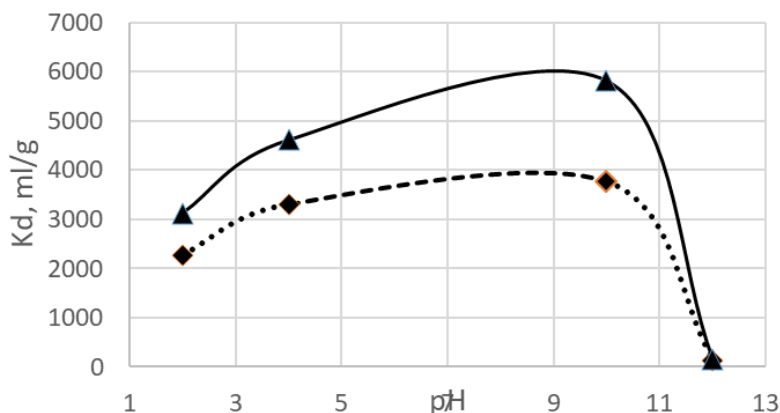


Figure 4: pH dependence of distribution coefficient for Zr_hcp (solid line) and UiO-66_NH₂ sorbents (dotted line).

4. Sorption of uranyl ion from water solution

Uranium is a fissile material required for nuclear energy production. Hence, it is considered as a strategic material, and there is a strong interest in securing stable sources of uranium supply. Due to the limited natural resources of uranium, the possibility of obtaining uranium from seawater is often explored. Nuclear weapons research has resulted in the accumulation of large quantities of nuclear waste requiring reprocessing. The inadvertent release of radioactive materials into the environment poses potential severe threats to human health. Hence, the separation of uranium from water is becoming a topic of great interest from the point of view of both reasonable utilisation of uranium resources and environmental protection. The subject has been recently reviewed [13].

In our search for applications of MOFs built around terephthalate linker, we performed studies on the possibility of application of robust UiO-66 structure for sorption of uranyl ion from water. For this purpose, the functionalisation of the UiO-66 structure will be necessary. It will be aimed to incorporate within their structure a functional group sensitive to the uranium species to be adsorbed. To check this possibility, we

synthesised UiO-66 type structures using the modulation synthesis method and applied different modulators based on benzene and pyridine carboxylic acids having the amine group in different positions. The amino group free benzene acid was also included in the study. The ligands applied as modulators are shown in the Figure 5.

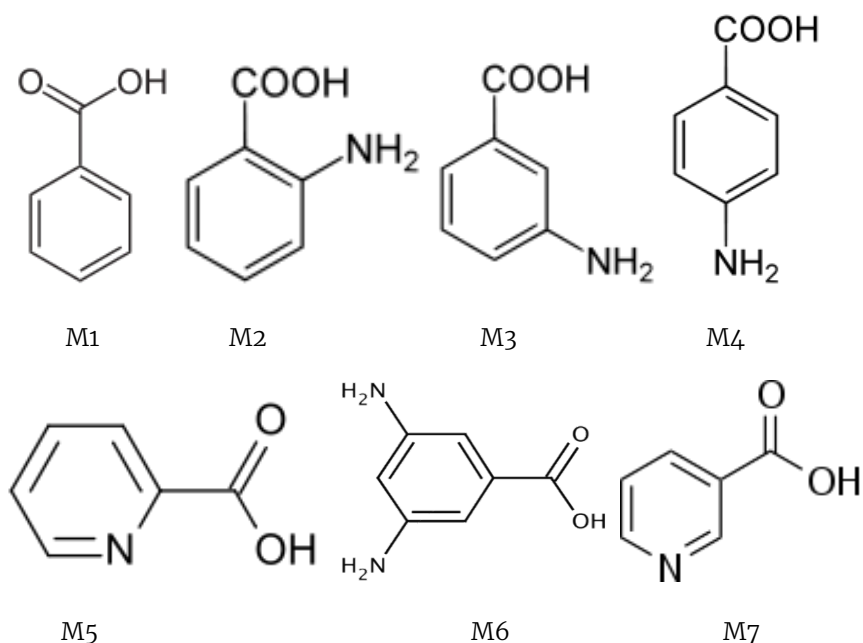


Figure 5: Structural schemes of modulators used in the study: M1 – benzoic acid, M-2 – 2-aminobenzoic acid, M3 – 3-aminobenzoic acid, M4 – 4-aminobenzoic acid, M5 – 3,5-diaminobenzoic acid, M6 – 2-pyridinecarboxylic acid, M7 – 3-pyridinecarboxylic acid.

For the synthesis, zirconium chloride, terephthalic acid and modulators in molar ratios of 1:1:10 were used. The synthesis was performed in eight-dram glass vials on an oil bath at a temperature of 120°C for 24 hours. Synthesised material was recovered by filtration, purified by washing in DMF and methanol, and finally dried in a dry box. For the screening of the best sorbents, 50 mg of each material was contacted with 10 mL of uranyl nitrate water solution with concentration of 200 mg U/L in plastic vials and shaken overnight. After that the sorbents were recovered by filtration using a track-etched membrane with a 0.4 μm pore diameter. The uranium to zirconium molar ratios on sorbent were determined by inductively coupled plasma mass spectrometry (ICP-MS) and are given in Table I.

The highest value was obtained for the case of a 3,5-diaminobenzoic acid modulator possessing two amino group on third and fifth positions in benzene ring. It is interesting to note that some adsorption of uranyl ion has been obtained also for UiO-66 structure not having amino group (modulator M1). Such effect has been reported already and was interpreted as the result of structural defects [14].

Table 1: The results of U/Zr molar ratio for different modulators.

Modulator	M1	M2	M3	M4	M5	M6	M7
U/Zr	0.089	0.000	0.195	0.207	0.327	0.132	0.024

The sorption isotherm for UiO-66 functionalised with 3,5-diaminobenzoic acid is shown in Figure 6. The best approximation has been obtained by applying the Langmuir model. The saturation value of sorption capacity has been determined as 240 mg U/g.

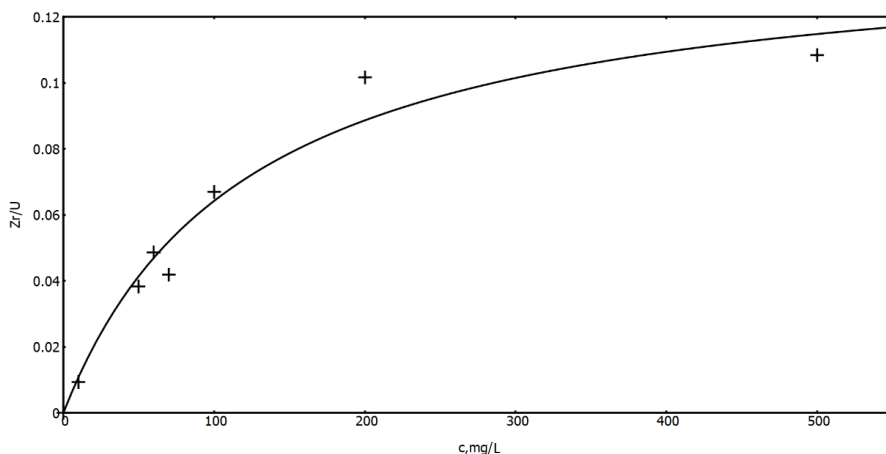


Figure 6: Sorption isotherm for the UiO-66 structure modified by modulated synthesis with 10 eq. of 3,5-diaminobenzoic acid modulator

5. Sorption of mercury from water solution

The World Health Organization (WHO) has listed mercury (Hg) as one of the ten pollutants of particular concern for public health. Mercury can be released from several sources such as electronics, paints, pharmaceuticals, paper and pulp, chloralkali, oil refinement, plastics, rubber processing, and manufacturing industries. Other significant (>10%) sources of Hg emission include coal and fossil fuel combustion (25%) and non-

ferrous metal production. Moreover, mercury compounds can persist and accumulate in the environment, causing severe toxicity to humans and animals, especially methyl-mercury. The fate of inorganic mercury ions in nature is its turning into methyl mercury due to the aerobic action of micro-organisms.

There are various methods of removing heavy metals from aqueous environment, which include reverse osmosis, chemical precipitation, ion exchange, coagulation, and adsorption. Adsorption is best suited for this purpose due to its simplicity and cost efficiency.

The high affinity of Hg-compounds to sulfhydryl ($-SH$) groups has been reported in numerous studies [15]. In the present report, we present the results of our studies on incorporating this group into zirconium UiO-66 MOF for converting them to effective mercury sorbent. Both known strategies for MOF functionalisation, modulated synthesis method and post-synthetic ligand exchange were utilised. For the modulated synthesis, mercaptoacetic acid (MAA) and mercaptosuccinic acid (MSA) were applied as modulators. Synthesis was conducted by refluxing the synthesis mixture containing zirconium chloride, terephthalic acid, and modulator dissolved in DMF solvent at 120°C for 24 hours. In the case of mercaptoacetic acid, five modulator concentrations equal to 10, 20, 50, 70, 90 and 100 eq of zirconium, respectively, were applied. The SEM images and XRD diffraction patterns confirmed crystallinity of synthesised materials (Figure 7, Figure 8). The successful incorporation of $-SH$ group into UiO-66 structure has been confirmed by EDS analysis. The ratio of molar S/Zr content was determined as equal to 0.21 for the case of 10 eq MAA modulator content, 0.32 for the 50 eq and 0.32 for the case of 100 eq.

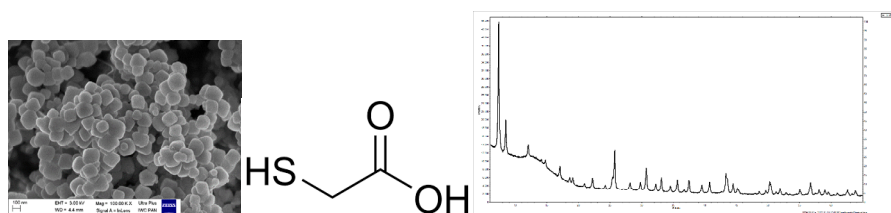


Figure 7: SEM image and diffraction pattern of UiO-66 modified with 50 eq. mercaptoacetic acid

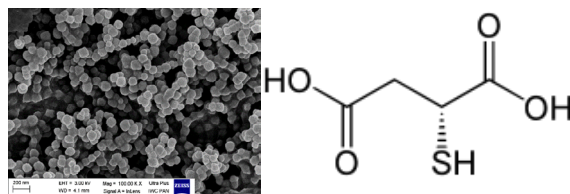


Figure 8: SEM image of UiO-66 type sorbent synthesized by modulation synthesis method at terephthalic acid/mercaptosuccinic acid ratio equal to 3:1

The sorption capacity of the sorbents has been determined using radiotracer methods. The mercury ^{197}Hg isotope obtained by neutron flux activation of mercury nitrate of natural composition in the MARIA reactor in Świerk, Poland, has been used as radiotracer. The sorption studies were carried out on samples containing 15 mg of sorbent suspended in 10 mL of mercury chloride solution with varying concentrations of mercury of 0.5 to 10 mM and labelled with radioactive mercury isotope. The results of the study showing mass of mercury (in mg) accumulated on 15 mg of sorbent after two hours of contact are presented in Figure 9. The experimental data were approximated with Langmuir isotherm.

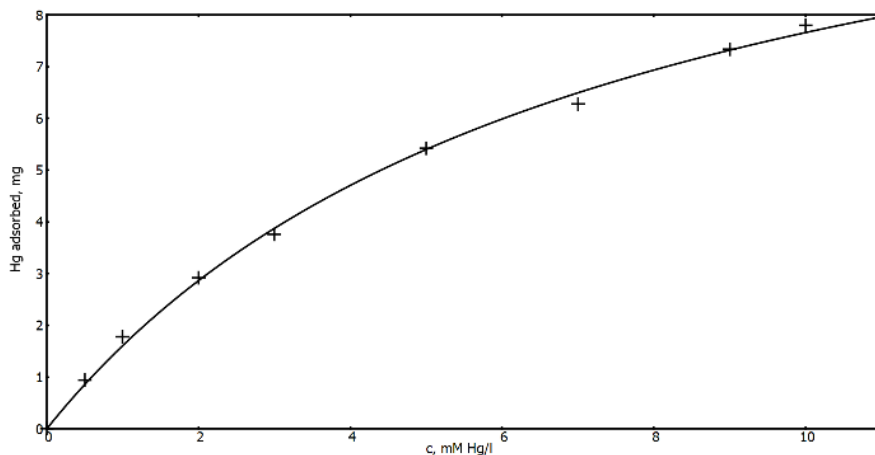


Figure 9: Sorption isotherm for UiO-66_FA synthesised by modulation synthesis method with 50 eq. MAA approximated with Langmuir model.

The functionalisation of zirconium structures in post-synthetic ligand exchange with mercaptosuccinic acid in DMF solvent has been found efficient for making them sensitive to mercury. Post-synthetic exchange has been carried out for UiO-66_FA and for Zr_PET structures. The kinetics properties of both sorbents have been determined using the

radiotracer method. The results are shown in Figure 10. The experimental data were approximated using the kinetic Elovitch model.

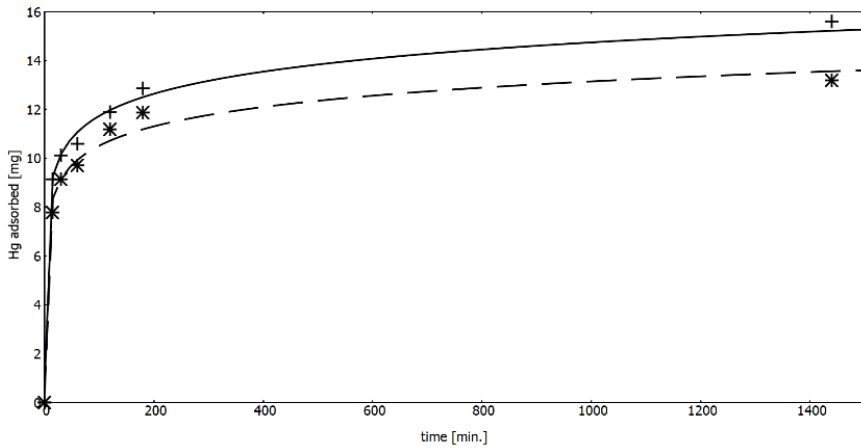


Figure 10: Kinetics of mercury adsorption on UiO-66_FA (solid line) and Zr_PET (dashed line) modified with mercaptosuccinic acid approximated with Elovich model.

6. Sorption of ruthenium

Ruthenium isotopes ^{101}Ru (5.17%), ^{103}Ru (3.03%), and ^{106}Ru (0.4%) are produced in a reactor as a fission product of ^{235}U . During the process of uranium and plutonium recovery by extraction, (PUREX) high-level liquid waste is produced (HLLW). HLLW contains a significant amount of platinum group metals (PGM) such as palladium, ruthenium, and rhodium. It was estimated that one ton of HLLW of spent nuclear fuel from a light water reactor (LWR) contains around 4 kg of PGMs. The estimated content of fission-generated PGMs varies depending on the nature of fuel, burn up, cooling time etc, but significantly covers the amount obtained naturally [16]. It has been suggested that PUREX raffinate can be used as a source of the ruthenium and palladium capable of meeting growing industrial demands.

Ruthenium is one of extremely troublesome radionuclide in reprocessing process of the spent nuclear fuel and most difficult to remove because of a large fission yield, relatively long half-live ($\text{Ru-106 } T_{1/2} = 369\text{d.}$) and complex chemistry (oxidations states from 0 to +8 and tendency to formation of large number of complexes). The volatility of the ruthenium oxide RuO_4 presents a technical problem for the vitrification of nuclear wastes [17]. Due to the volatile nature of ruthenium tetroxide, it gets deposited in the process pipelines and stacks. Moreover, ruthenium

(along with other platinum group metals) tends to form a separate phase in the vitrification process and hence, deteriorate the stability of a vitrified product. Attempts have been made over the years to separate radio-ruthenium from radioactive feeds, including the acidic high-level liquid waste (HLLW) as well as the alkaline low-level liquid waste (LLW) or intermediate level liquid wastes (ILLW). Solvent extraction, precipitation, ion-exchange, etc. are some of the commonly employed techniques for the separation of radio-ruthenium from radioactive feeds.

In the present report, the preliminary results on MOF application for ruthenium removal from water using Zr_hcp sorbent synthesised in the course of this work are presented. The pH dependence of distribution coefficient on pH water solution of ruthenium chloride is shown in Figure 11. In the studies 50 mg of sorbent were administered to 10 mL of ruthenium chloride solution with a concentration of ruthenium 5 $\mu\text{g/g}$.

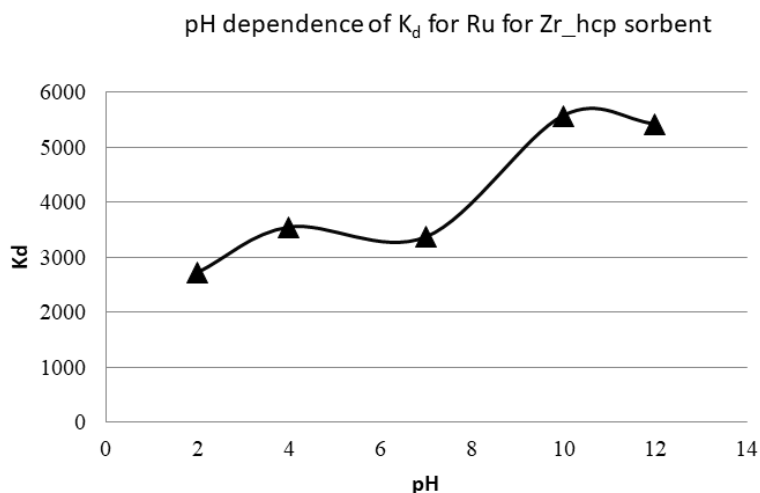


Figure 11: pH dependence of distribution coefficient for ruthenium ion sorption from water solution.

7. Conclusions

UiO-66 type MOF is a chemically resistant porous structure that can serve as a starting material for sorbents synthesis for selected radionuclides and heavy metals removal from water. For this purpose, it is necessary to carry out the functionalisation of relatively chemically inert UiO-66 to introduce into their structure a ligand containing a side functional group showing affinity to the metal which is to be adsorbed. PET waste material

can be used for the UiO-66 sorbent synthesis using a two-steps or one-step procedure. In the two-steps procedure, PET should be depolymerised to recover terephthalic acid, which will then be used to synthesise the final product. In a one-step synthesis, zirconium terephthalate sorbents can be synthesised directly from PET flakes. The examples of application of zirconium terephthalate structures synthesised by one pot method for sorption of radionuclides relevant to nuclear technologies as well for sorption of mercury were presented.

However, further research is needed to optimise the synthesis and functionalisation process of UiO-66 sorbents and to adapt their rheological properties to industrial requirements.

8. Acknowledgments

The financial support from The Polish National Centre for Research and Development under the PET-MOF-CLEANWATER project. The studies on waste PET-derived metal-organic framework (MOFs) as cost-effective adsorbents for removal of hazardous elements from polluted water has been gratefully acknowledged.

References

1. J. Ren et al., Review on the current practices and efforts towards pilot-scale production of metal-organic frameworks (MOFs), *Coord. Chem. Rev.* 352,2017, 187. <https://doi.org/10.1016/j.ccr.2017.09.005>
2. A.A. Bersenneva et al., “Boarding-Up”: Radiation Damage and Radionuclide Leaching Kinetics in Linker-Capped Metal-Organic Frameworks, *Inorg. Chem.* 2020, 59, 1, 179–183. <https://doi.org/10.1021/acs.inorgchem.9b01310>
3. K. Jin et al., Metal-organic frameworks as a versatile platform for radionuclide management, *Coord. Chem. Rev.*, 2021, 427, 213473. <https://doi.org/10.1016/j.ccr.2020.213473>
4. M. Taddei et al., Band gap modulation in zirconium-based metal-organic frameworks by defect engineering, *J. Mat. Chem. A*, 2019, 17, 23781. <https://doi.org/10.26434/chemrxiv.8143319>
5. S. Leubner et al. Expanding the Variety of Zirconium-based Inorganic Building Units for Metal Organic Frameworks, *Angew. Chem. Int. Ed.* 2019, 58, 10995–11000. <https://doi.org/10.1002/anie.201905456>
6. S. Leubner et al., Design and Precursor-based Solid State Synthesis of Mixed Linker Zr-MIL-140A, *Inorg. Chem.* 2020, 59, 15250–15261. <https://doi.org/10.1021/acs.inorgchem.0c02221>

7. C.I. Pearce et al., Technetium immobilization by materials through sorption and redox-driven processes: A literature review, *Science of The Total Environment*, 2020, 716, 132849. <https://doi.org/10.1016/j.scitotenv.2019.06.195>
8. D. Banerjee, et al., Removal of TcO_4^- ions from solution: materials and future outlook, *Chem. Soc. Rev.* 2016,45, 2724. <https://doi.org/10.1039/C5CS00330J>
9. D. Banerjee et al., Removal of Pertechnetate-Related Oxyanions from Solution Using Functionalized Hierarchical Porous Frameworks, *Chem. Eur.J.* 2016,22,17581–1758. <https://doi.org/10.1002/chem.201603908>
10. Lin Zhu, et al., Identifying the Recognition Site for Selective Trapping of $^{99}\text{TcO}_4^-$ in a Hydrolytically Stable and Radiation Resistant Cationic Metal-Organic Framework, *J.Am. Chem. Soc.* 2017, 139,14,873
11. D. Banerjee et al., Zirconium-Based Metal-Organic Framework for Removal of Perrhenate from Water, *Inorg. Chem*, 2016, 55, 8241. <https://doi.org/10.1021/acs.inorgchem.6b01004>
12. J. Zhang et al., Adsorption of Uranyl ions on Amine-functionalization of MIL-101(Cr) Nanoparticles by a Facile Coordination-based Post-synthetic strategy and X-ray Absorption Spectroscopy Studies, *Scientific Reports* 5:13514, 2015. <https://doi.org/10.1038/srep13514>
13. Weiting Yang et al., Metal-organic framework-based materials for the recovery of uranium from aqueous solutions, *Inorg. Chem. Front.*, 2019,6, 1924. <https://doi.org/10.1039/C9QI00386J>
14. L. Yuan et al., Defect engineering in metal-organic frameworks: a new strategy to develop applicable actinide sorbents, *Chem. Commun.* 2018, 54, 370. <https://doi.org/10.1039/C7CC07527H>
15. O. P. Ajsuvakova et al., Sulfhydryl groups as targets of mercury toxicity, *Coord. Chem. Rev.* 2020, 417, 213343X. Yan et al., Recent progress in the removal of mercury ions from water-based MOFs materials, *Coord. Chem. Rev.*, 2021, 443, 214034. <https://doi.org/10.1016/j.ccr.2021.214034>
16. F. Li, Y. Shnag, Z.Ding, H.Weng, J.Xiao, M.Lin, Efficient extraction and separation of palladium (Pd) and ruthenium (Ru) from simulated HLLW by photoreduction, *Separation and Purification Technology*, 2017, 182, 9–18. <https://doi.org/10.1016/j.seppur.2017.03.029>
17. C.Krause, B.Luckscheiter, Properties and behaviour of the platinum group metals in the glass resulting from the vitrification of simulated nuclear fuel reprocessing waste, *Journal of Materials Research*, 1991, 6, 12, 2535–2546. <https://doi.org/10.1557/JMR.1991.2535>

Chapter 9

Reuse of waste PET bottles through the production of activated carbon, an adsorbent to remove radionuclides from aqueous solutions

L. Fuks , I. Herdzik-Koniecko , M. Rogowski 

*Institute of Nuclear Chemistry and Technology, Dorodna 16, 03-195
Warsaw, Poland*

E-mail: leon.ichtj@gmail.com

Abstract

End-of-life polyethylene terephthalate (PET) bottles were used to prepare activated carbon by thermal carbonisation at 850 °C for 0.5 hours followed by chemical activation with a boiling aqueous solution of zinc chloride (ZnCl₂). The batch adsorption of mono-, di- and trivalent cationic radionuclides was then examined at ambient temperature.

The main physicochemical properties of the obtained material that may determine its adsorption properties have also been studied.

1. Introduction

A statistical Pole throws away almost one hundred polyethylene terephthalate (PET) bottles annually, which form tens of thousands of tons of these packaging per year [1]. The main problems with the waste bottles include that, when collected, they take up a lot of space and each piece decomposes in up to 500 years. In addition, in Poland, only 40% of PET bottles are fully recycled. The rest, if it does not go to landfills, is thrown directly to the environment [2]. For this reason, both public education and recycling of used PET packaging are so important in protecting the environment. In most other European Union countries, recycling rates of plastic bottles is higher, with Lithuania, Czech, and Netherlands leading the list [3]. In 2018, only six European countries processed less used PET packaging than Poland (see, Figure 1).



Figure 1: Recycling rate of plastic waste in Europe, 2018 [3]

Recycled PET bottles are not only used as a raw material in the production of packaging. Obtained granules from grinded plastic bottles can be used to produce fleece, which maintains good thermal properties. It has been estimated that about 35 bottles are needed to produce one blouse from this material. Other products in the clothing industry, such as ski clothes, tents, and backpacks, are also made of polyester fibers [1].

Recycling of PET bottles is a process conducted not only for ecological reasons. Apart from reducing the ever-increasing amount of waste, recycling also allows for obtaining materials that are potentially useful in other areas of life. In the process of pyrolysis of packages from PET, we can produce the activated carbons (ACs) that are specific materials widely used in industry [4-7]. ACs are materials that have a large chemical resistance, great specific surface area and high porosity, and are non-toxic [8,9]. ACs are used, among other things, to remove impurities (either in the gas phase or in liquids). The superiority of the ACs over other purifying materials lies not only in the high purity of the purified solvent but also in cheapness of the purifying material. In addition, designing and operating the purification processes is simple and does not require highly specialised staff. Thus, the use of solid extraction (sorption) of metals on the ACs in the wastewater management seems to be a potential method of treating the liquid radioactive waste (RLW) [10,11].

The aim of the presented work was to check whether an extremely simple recycling method of the PET bottles may be used for producing a material suitable for decontamination of water containing the radionuclides.

2. Experimental

2.1. Preparation of the carbon powder

Powdered carbon has been formulated by adapting a method proposed by Bratek *et al.* [12]. Used mineral water bottles made of PET were cut into small pieces (approx. 1 cm², each) and about 5g of sample were placed in quartz crucibles and high temperature carbonised (1098 K) in a nitrogen atmosphere (flux of about 10 dm³·h⁻¹). A vacuum furnace (Nabertherm, VHT series) was used. The temperature of the process was raised from room temperature at a rate of 1 K/min, then kept constant for 30 minutes. The resulting carbon material was cooled at the same rate (full pattern of the temperature changes vs. time is shown in Figure 2). Yield of the process was assigned to about 20 %. The obtained material was grinded and analysed for the total organic carbon (TOC) (Analytic Jena Multi N/C 3100 with autosampler and high-temperature combustion chamber HT 1300). It was found that the material consisted of 99.32±1.03 % carbon.

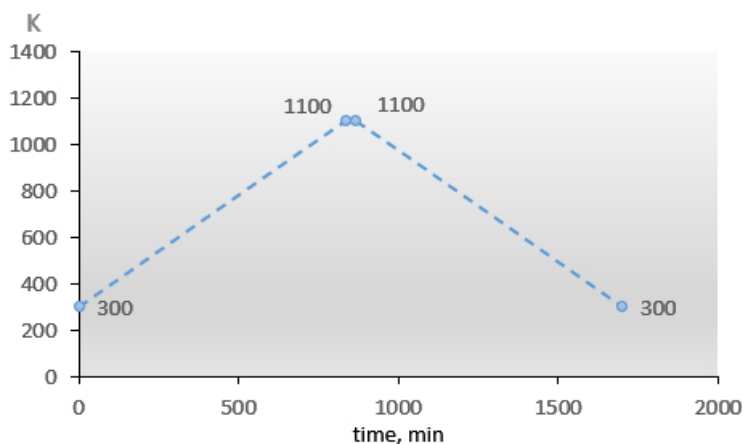


Figure 2: Time dependent temperature of the carbonisation process.

2.2. Activation of the carbon powder

During carbonisation, a certain porous structure is already formed, but its parameters are insufficient for practical application. Therefore, the product should be subjected to activation, aimed at ‘developing’ the pores. During the chemical charcoal activation in an industrial scale, the raw material is subjected to treatment with certain chemical activation agents. The most often used are phosphoric acid, natrium hydroxide, or zinc chloride. Then, the material is heated to 720–950 °C in an activation furnace. The resulting material is then washed with water until the

activating agent is removed. The obtained activated carbon is dried and often sieved to get particles of the desired specific size range.

In this work, the crude carbon samples were chemically activated to obtain activated carbon (AC) in not so radical conditions. In these studies, the following activators were used: ZnCl_2 , CaCl_2 , H_3PO_4 , KOH , HNO_3 , HCl or H_2O_2 , separately. A one-step process was carried out, according to Caturl *et al.* [13]. An aqueous solution containing one of the above-mentioned agents was mechanically mixed for eight hours. (Usually overnight) with a sample of carbon suspended in. A temperature of mixing was kept at 85°C . Then, the samples were filtered, accurately washed with deionised water until an excess of the activating agent was removed and dried at 80°C to a constant mass. After grinding, the material was exposed for one day to the ambient atmosphere and stored for further experiments.

In the case of using hydrogen peroxide for activation, about 30 g of the raw carbon was suspended in 200 ml of 10% H_2O_2 solution and stirred for 2 hours at room temperature [14]. The obtained AC solid was then rinsed with water, dried at 80°C to a constant mass and after the 24 hours exposition to an air stored for the experiments.

The obtained material has been characterised by several methods, which are listed in Table 1. A more detailed description of the results obtained is presented in sections 3.1-3.5.

2.3. Chemicals and radionuclides

Chemicals used in this work were delivered from Merck-Sigma-Aldrich or Avantor Performance Materials (Polish branches) as the materials of pure p.a. grade. Throughout the work, deionised water was used.

The commercial charcoal adsorbent *Norit CNR116* was chosen to be a reference material in these studies. The commercially available product was treated with 10 % HCl for removal inorganic impurities.

Carrier-free radionuclides (i.e., free from any stable isotopes and radiochemically monoisotopic) of caesium-137 ($t_{1/2}=30.07$ y; $E_\gamma=661.7$ keV), strontium-85 ($t_{1/2}=64.8$ d; $E_\gamma=514$ keV), cobalt-60 ($t_{1/2}=5.3$ y; $E_\gamma= 1.173$ and 1.332 MeV) and americium-241 ($t_{1/2}=432.2$ y; $E_\gamma=59.5$ keV) were bought from POLATOM Świerk (Poland). Radionuclides Sr-85 and Tc-99m were used instead of Sr-90 and Tc-99 because of their easier radiometric detection.

$\text{NaTcO}_4(\text{Tc-99m})$ was eluted from a Mo-99/Tc-99m commercial generator (GE Healthcare, supplied by Biker, Warszawa, Poland) as the 0.9% saline solution of ca 100 MBq·cm⁻³ specific radioactivity.

2.4. Studies on sorption of the radionuclides

Batch sorption experiments, also called static sorption, were performed by adding a known quantity of the AC sorbent to a solution containing impurities (in our case, radioactively contaminated) of known concentration. These suspensions were strongly shaken or vortexed throughout the desired time. Concentrations of the radionuclides in the initial solution, as well as in the final one, were detected radiometrically and their difference was treated as the amount of the radionuclide (q_e) be separated by a solid sorbent and used in Eq. 1.

$$q_e = (C_0 - C_e) \cdot \frac{V}{m} \quad (1)$$

where C_0 and C_e are the initial and equilibrium concentrations of the radionuclides (any units of the radiation activity concentration), m and V stand as the mass of AC (g) and volume of the solution (mL) used in the experiments, respectively.

2.5. Details of methods used for characterisation of the AC materials and the devices used

See Table 1.

3. Results and discussion

3.1. Vibrational (FTIR) spectra: no chemical changes after activation of the raw carbon

Transmission spectra in the mid infrared region, both PET carbon and the activated PET carbon with the $ZnCl_2$ solution are presented in Figure 3.

A comparison of the spectrum registered for the crude PET carbon with this of the material treated with $ZnCl_2$ shows that both spectra, even though they have rather poorly developed peaks, resemble each other. A reliable method for the numerical comparison of two spectra requires calculating the Pearson's correlation coefficient (P.c.c.), which must be between -1 and $+1$. A zero value describes spectra that do not correlate at all, that is, are completely different. On the contrary, values not far from ± 1 suggest that both spectra are of great similarity, and therefore, that both compared substances are identical [15]. The computed value of the P.c.c., for the PET- and the $ZnCl_2$ activated carbon is 0.998. Therefore, it may

Table 1: Methods of characterisation of the AC and the devices used

Characteristic	Methods	Devices
Confirmation of synthesis result	Recording of the FT-IR spectra of the dried materials	Nicolet iS10 (Thermo Fisher Scientific Instrument, USA)
Amorphous vs. crystalline structure	Powder X-ray diffraction	HZG-4 diffractometer (Seifert GmbH, Germany)
Specific surface area and pore volumes	N ₂ adsorption-desorption isotherms measured at 77.3 K	ASAP 2024 automatic sorption analyzer (Micromeritics, USA)
Charge of the surface	Determination of the zeta potential (PZ, ζ n)	Zetasizer Nano ZS instrument (Malvern, UK)
Decomposition temperatures	Thermogravimetric (TGA) and derivative thermogravimetric (DTG) analyses	Linseis Stapt 1600 (Linseis Corporation, Selb, Germany)
Topography and elemental composition of the surface	Scanning Electron Microscopy	DSM 942 Scanning Electron Microscope (Zeiss - Leo, Germany)
	Energy-dispersive X-ray spectroscopic (EDS) microanalysis	Quantax 400 (Bruker, Germany)
Adsorption properties	Batch adsorption with radiometric analyses	Heidolph Multi Reax test-tube shaker and MPW-251 centrifuge
		Perkin Elmer 2480 Wizard2© Automatic Gamma Counter
		Thermo Scientific Dionex ICS-5000 DC chromatographic set

be postulated that chemical activation does not result with the significant change in chemical structure of the material.

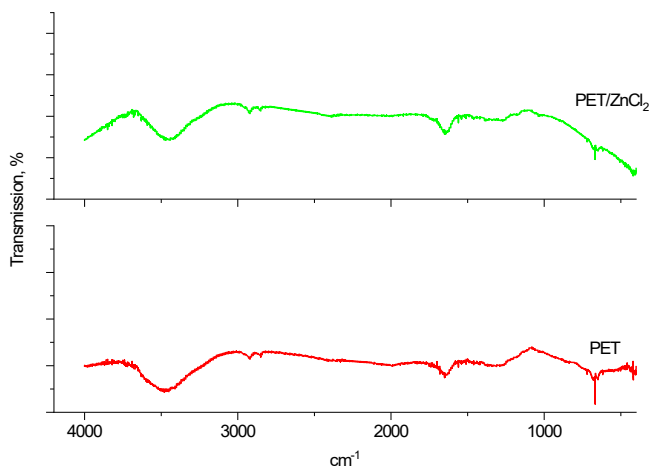


Figure 3: Mid infrared transmission spectra of the PET carbon and the ZnCl₂ activated PET carbon sorbents.

In both spectra, the only wide bands can be observed in the region of about 3500–3600 cm⁻¹, and are accompanied by weak peaks in the regions of about 1650 cm⁻¹ and about 670 cm⁻¹. As a rule, in the carbon spectra, the bands in the area of about 3500 cm⁻¹ are characteristic for stretching vibrations of the -OH hydroxyl groups. Weak peaks at about 1650 cm⁻¹ were attributed as stretching C=C of the aromatic rings [16]. Angular deformations of CH groups of aromatic rings outside the planes of the rings are usually related to low frequency bands (about 700 cm⁻¹) [17].

3.2. Crystallographic studies

Carbonic materials can occur in various structural forms: some of them are the amorphous materials, others are crystalline (for example, graphite). Plots of the X-ray powder diffraction obtained for the ZnCl₂ activated PET carbon and Norit CNR116 materials are shown in Figure 4.

Diffraction of the ZnCl₂ activated PET carbon reveals the existence of two distinct, but broad bands found at $2\theta = 23.2$ and 43.7° . It may be found in the literature that they are characteristic for a graphitic structure [18] and are commonly described as the (0 0 2) and (1 0 0) reflections of the graphitic carbon [19]. The corresponding diffraction of Norit CNR116, in turn, is characteristic for the amorphous materials.

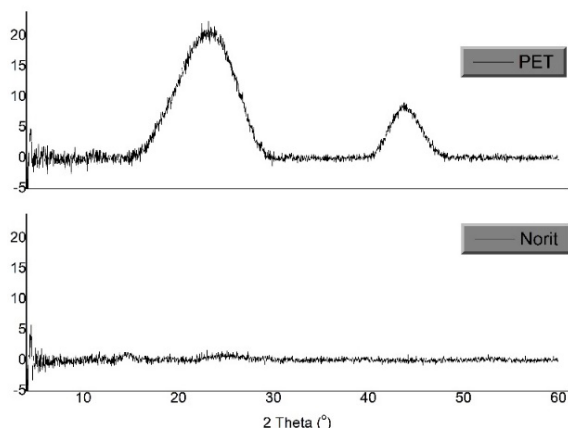


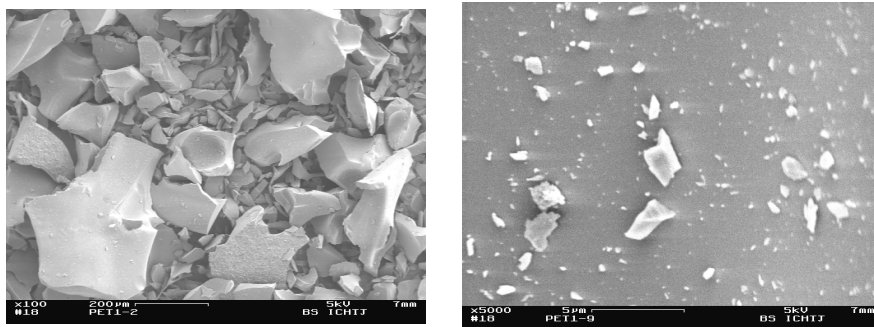
Figure 4: X-ray powder diffraction of the ZnCl_2 activated PET carbon and Norit CNR116.

3.3. Scanning electron microscopy (SEM)

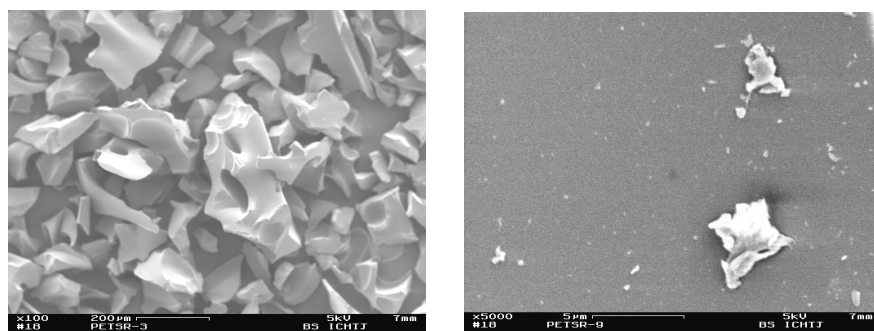
Scanning electron microscopy (SEM) equally to the transmission microscopy performed in the visible light and to the confocal laser scanning microscopy, gives us numerous interesting information on the surface topography of the studied material. This technique, however, allows for both a higher magnification and a deeper penetration of the surface. In turn, the SEM method with energy dispersive X-ray spectroscopy (EDX) provides information on the elemental composition of the sample surface. Both SEM and EDX are simple and non-destructive methods which permit for prompt measurements of different matrices.

Images shown in Figure 5 present the surface of the waste PET carbon particles, of the chemically activated with the ZnCl_2 solution, and of the Norit CNR116 reference material. Photographs made in the 100x magnification reveal that the surface of the PET carbon particles has crevices, gaps, and crystals of various sizes (Figures 5a and 5b). In addition, some crystals have large holes. The surface of the Norit material is more compact than that of the other materials. This observation corresponds well with the results of the XRD studies presented in part 3.2. Surfaces of the samples observed under the magnification of 5000x reveal, however, more distinct differences. That of the activated PET carbon is more uniform as compared with the Norit one and some micro agglomerates can be seen on the PET carbon surface. On the surface of the Norit material, one can observe the micropores leading to the interior of the particle.

(a)



(b)



(c)

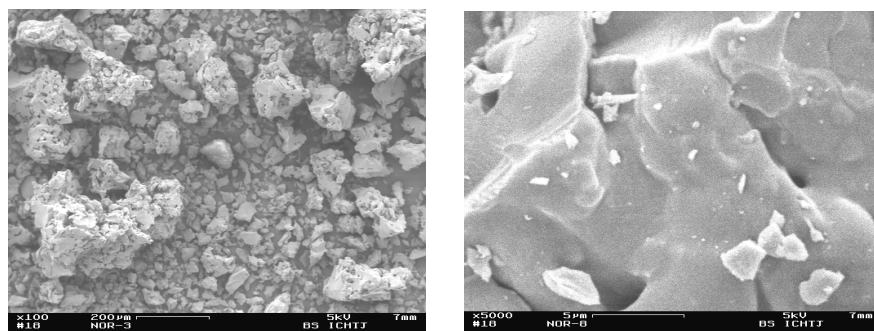


Figure 5: SEM images (100x magnification - left, and 5000x - right pictures) of the PET carbon: raw material (a), sorbent saturated with SrCl₂ (b); Norit CNR116 reference material (c)

3.4. Point of zero charge (PZC) of the sorbent surface

Among the main properties of the sorbent that contribute to adsorption of the ionic species is its point of zero charge (PZC). The PZC parameter

describes the pH, for which the surface of the adsorbent is not charged (meaning, is neutral). It means that the surface contains the equal number of the positively and negatively charged binding groups. Below the pH described as the PZC, the surface is positively charged and over this pH, it is negatively charged. So, comparing the PZC with the pH of the solution to be purified informs if a metal cation ion can be sorbed by a sorbent: cations interact preferably with a negatively charged surface.

Values of the PZC for the crude PET carbon and the $ZnCl_2$ activated were determined to be: 1.1 ± 0.1 , 0.7 ± 0.1 , and 3.3 ± 0.3 for the raw material, $ZnCl_2$ activated, and Norit, respectively. When comparing the above values with the pH dependent speciation of the radionuclides studied (Figure 6) it can be seen, that for pH of the solutions greater than one (the PZC), either the AC or the raw carbonic sorbent or Norit are mainly positively charged. Therefore, for pH values greater than 1, they are capable of sorbing the radionuclides.

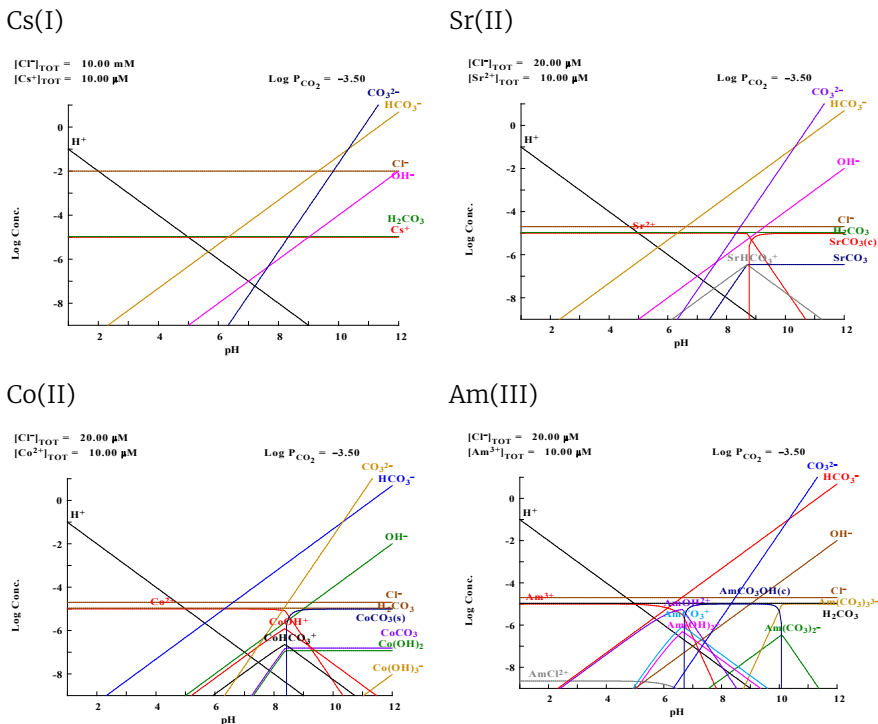


Figure 6: Speciation of Cs(I), Sr(II), Co(II) and Am(III) complexes in aqueous solutions of different pH. Simulation computed using the Medusa program [20].

3.5. Surface potential and adsorption of metals

One of the most important properties of the material that determines its sorption properties is the charge of the surface. To describe the magnitude of this charge, we often use—a quantity called the zeta potential (ZP), which tells us about the potential difference on both sides of the boundary between the solids and liquids. In this work, we have determined the ZP for a broad range of the solution pH, namely for 3.5, 4.2, 6.9 and 10.4. For the raw carbonic materials, we have found that the values are 18.1 mV, -29.3 mV, -49.6 mV, and -47.2 mV, respectively. The corresponding values for the ZnCl₂ activated carbon, being correspondingly -10.6, -31.3, -50.1, and -44.4 mV, are presented in the upper part of Figure 7. It can be seen that the data do not differ each other and the most negative values are in the region of the neutral solutions (pH around 7). It has also been found that even in the strongly acidic solutions reach in protons, both examined materials preserve their negatively charged groups. These negative charges come most of all from the presence of the carboxyl groups, which are reported to occur on the surface of the activated carbon [21]. It can be seen that with decreasing acidity of the solutions, i.e. with decreasing number of protons, in accordance with the law of mass action, dissociation of these carboxyl groups is favoured. So, a charge of the surface (ZP) becomes more negative.

Detailed data on the dependence of sorption of the radioactive metals determined in this work will be presented in section 3.7. However, already now, in order to compare them with the changes of ZP along the pH series in the lower part of Figure 7, selected data for strontium (II) are presented. It can be seen that both patterns are reversed. When the ZPs of the activated carbon surface become more negative, the electrostatic attraction with the positively charged cations increases and vice versa.

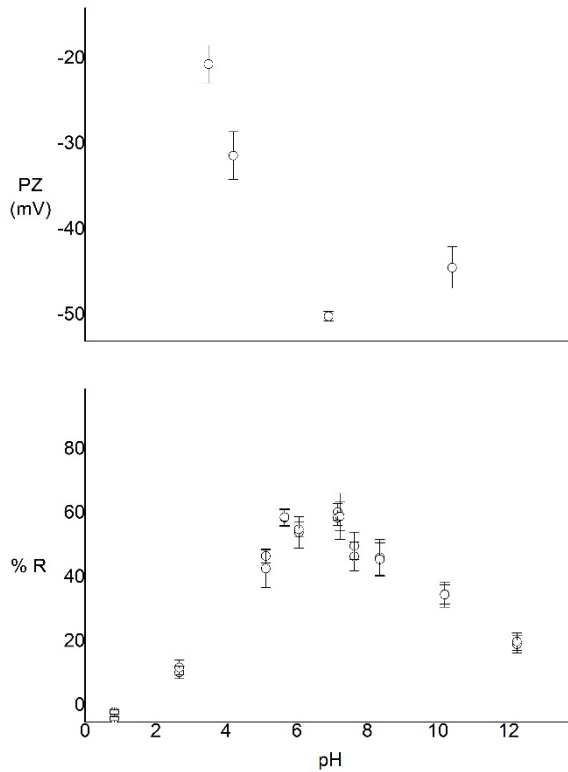


Figure 7: Changes of zeta potential (ZP) of the ZnCl_2 activated carbon with pH (upper part) and the adsorption properties of strontium (II) by this material (bottom).

3.6. Sorption properties of the carbonaceous material: chemical activation.

Carbon materials are used as popular sorbents effective in the removal of metal ions from aqueous solutions because of their valuable properties, for example, their relatively great porosity and big surface area, high adsorption capacity, low price and, most importantly, high chemical inertness [22-24].

There are cases where carbon materials do not adsorb fully metals that exist in aqueous solutions in trace or ultra-trace concentrations. So, many times, authors have proposed some preliminary methods for their surface modification (often, activation) in order to enhance their adsorption properties [25-29].

Besides some physical methods (e.g. high-temperature heating), this goal may be reached by chemical methods that apply certain chemical

agents. Typically, the latter provides better results than the former [30]. Nevertheless, the chemical activation method also has some limitations. Among the most important, one should mention the need of removal an excess of the activation agents by washing the carbon with a large volume of water, which may result in the adverse environmental problems.

The result of the action of different activating chemicals was checked by comparing the adsorption property of each AC sample with this of raw material. The cumulative graph of such comparison is presented in Figure 8, where the raw material is named PET. One may see that using the $ZnCl_2$ containing aqueous solution results in the best results. The adsorption properties are comparable to those of the commercial Norit CNR116 AC adsorbent.

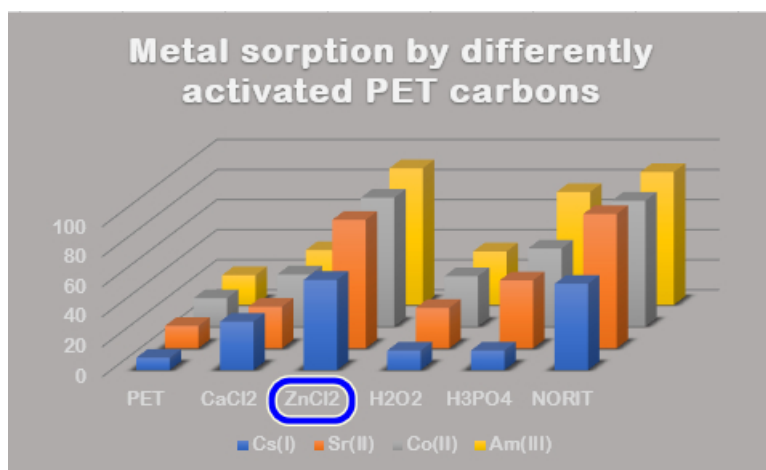


Figure 8: Sorption of the radioactive metal ions by carbon samples activated with different chemicals. Sorption by Norit CNR116 reference material is also shown.

3.7. Sorption properties of the carbonaceous material: the pH and sorbent dosage dependence.

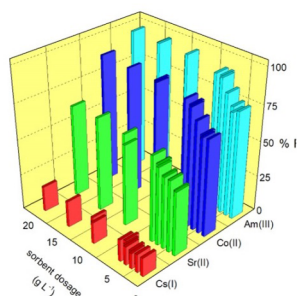
When designing a sorption process on an industrial scale, it is important to know the dose of the sorbent that ensures the efficient removal of metals. In the present work, eight different doses of the chemically activated carbon sorbent were examined. They ranged from 1 to 20 $g \cdot L^{-1}$.

The obtained results are shown in Figure 9. It has been found that up to the adsorbent dose of about 5 $g \cdot L^{-1}$, the removal efficiency improves for each metal. Then, the removal effectiveness reaches a plateau value. Such an increasing trend may be explained in terms of the growing number of

sorption centres, for the homogenous surface sorbents being related to the mass of these materials. Above the dose of $5 \text{ g}\cdot\text{L}^{-1}$, the number of the sorption centres exceeds this of the sorbate metal ions, especially if they are in the nca1 concentration.

In conclusion, a dose of $5 \text{ g}\cdot\text{L}^{-1}$ of the sorbent seems to be the suitable amount for the proposed procedure.

(a)



(b)

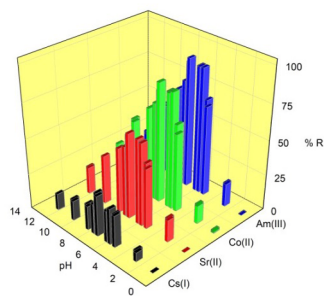


Figure 9: (a) Dependence of the adsorption efficiency, %R, of the radioactive metals on the adsorbent dose; (b) Relation between the acidity of the solution and the efficacy of mono-, di-, and trivalent radioactive metals removal by the PET carbon.

Another factor of the greatest importance in determining the metal sorption is the acidity of the solution. It affects both the charge of the adsorbent surface and the speciation of metals. In this work, the effect of the pH was studied within the pH range of about 11 units. Results presented in Figure 9 show that the %R values for each radioactive metal arise its maximum value placed in the range from pH 5 to pH 8. These features have been found already for sorption by different activated carbon materials, e.g. in [28, 29].

3.8. Sorption properties of the carbonaceous material: metal sorption capacity of the PET carbon

A specific amount of metal that may be adsorbed (called as adsorption capacity, CEC), was determined in the present work using non-radioactive

1 No Carrier Added (nca) radionuclide solution means that no carrier atoms have been added and that during its preparation special actions have been undertaken to minimise contamination with stable isotopes of the element in question. However, it does not mean the monoisotopic radioactive substance [Glossary: Definitions and Terminology; <https://link.springer.com/content/pdf/bbm%3A978-81-322-2607-9%2F1.pdf>].

caesium(I), strontium (II) or cobalt (II) chlorides, respectively. Aqueous solutions containing any metal salt in the concentration of $10 \text{ g}\cdot\text{L}^{-1}$ were agitated for six hours with a weighed amount of sorbent. Then, the phases were separated, and the initial and equilibrium solutions were subjected to the metal content analysis using a method of ion chromatography.

It has been found that the adsorption capacity of strontium (II) sorbed at pH 6 was $2.1 \text{ mg}\cdot\text{g}^{-1}$ for the raw carbon and $2.7 \text{ mg}\cdot\text{g}^{-1}$ for the ZnCl_2 activated carbon. The reference value for the Norit CNR116 is two times larger ($5.2 \text{ mg}\cdot\text{g}^{-1}$). However, one should remember that the procedure for the carbonisation of the PET material and further activation may be not optimum. Data found in the relevant literature on the different activated carbon materials produced in the optimum conditions show that the CEC varies from only $2 \text{ mg}\cdot\text{g}^{-1}$ to about $180 \text{ mg}\cdot\text{g}^{-1}$ [31].

In turn, adsorption capacity values for caesium(I) and cobalt (II) have been determined to be $4.4 \text{ mg}\cdot\text{g}^{-1}$ and $4.1 \text{ mg}\cdot\text{g}^{-1}$, respectively. The lack of correlation between the adsorption capacity, metal ionic radii, and the ionic charges suggests that the total sorption capacity depends on the adsorption of different hydration forms of these metals present in the mother solution.

4. Conclusion

- About 80 % carbon content of the produced sample indicates that better pyrolysis conditions should be found so that the result in more carbon-containing (less impurities) materials.
- The structure of the material does not change upon activation and differs from the commercial charcoals.
- The obtained material meets the requirements necessary for use in the purification of radioactively contaminated water.

5. Additional information

- This study was supported by the Institute of Nuclear Chemistry and Technology through the financial support of the Polish Ministry of Climate and Environment for the statutory activity of the INCT.
- Author contributions: L. F. conceptualisation, physicochemical and sorption studies, writing - original draft preparation; I. H.-K.: physicochemical and sorption studies, writing - review and editing; M. R.: synthesis of the carbonic material.
- All authors have read and agreed to the published version of the manuscript.
- The authors declare no competing interests.

References


1. <https://esbud.pl/na-czym-polega-recykling-butelek-pet/>; accessed on 08.12.2021
2. https://next.gazeta.pl/next/7,161716,27839289,woda-gazowana-bez-jednorazowej-butelki-czy-to-mozliwe.html#do_w=52&do_v=221&do_st=RS&do_sid=294&do_a=294&s=BoxBizImg1/; accessed on 10.12.2021 (in Polish)
3. <https://www.europarl.europa.eu/news/en/headlines/society/20181212STO21610/plastic-waste-and-recycling-in-the-eu-facts-and-figure>; accessed on 08.12.2021
4. M. Dias, M.C.M. Alvim-Ferraz, M.F. Almeida, J. Rivera-Utrilla, M. Sanchez-Polo, *Waste materials for activated carbon preparation and its use in aqueous-phase treatment: a review*, Journal of Environmental Management 85 (2007) 833–846. <https://doi.org/10.1016/j.jenvman.2007.07.031>
5. N.T. Kartel¹, N.V. Gerasimenko, N.N. Tsyba, A.D. Nikolaichuk, G.A. Kovtun, *Synthesis and study of carbon sorbent prepared from polyethylene terephthalate*, Russian Journal of Applied Chemistry 74 (2001) 1765–1767. <https://doi.org/10.1023/A:1014894211046>
6. N.V. Sych, N.T. Kartel, N.N. Tsyba, V.V. Strelko, *Effect of combined activation on the preparation of high porous active carbons from granulated post-consumer polyethyleneterephthalate*, Applied Surface Science 252 (2006) 8062–8066. <https://doi.org/10.1016/j.apsusc.2005.10.009>
7. W. Bratek, A. Swiatkowski, M. Pak, S. Biniak, M. Bystrzejewski, R. Szmigielski, *Characteristics of activated carbon prepared from waste PET by carbon dioxide activation*, Journal of Analytical and Applied Pyrolysis 100 (2013) 1–198. <https://doi.org/10.1016/j.jaap.2012.12.021>
8. B. Viswanathan. P. Indra Neel, T. K. Varadarajan, *Methods of Activation and Specific Applications of Carbon Materials*, e-book: National Centre for Catalysis Research, Indian Institute of Technology Madras (2009), 164 pp. <https://doi.org/10.1007/s10563-009-9074-8>
9. X. Chen, S. Jeyaseelan, N. Graham, *Physical and chemical properties study of the activated carbon made from sewage sludge*, Waste Management 22 (2002) 755–760. [https://doi.org/10.1016/S0956-053X\(02\)00057-0](https://doi.org/10.1016/S0956-053X(02)00057-0)
10. N.B. Singh, Garima Nagpal, Sonal Agrawal, Rachna, *Water purification by using Adsorbents: A Review*, Environmental Technology & Innovation, 11 (2018) 187–240. <https://doi.org/10.1016/j.eti.2018.05.006>

11. Z.K. George, E.A. Deliyanni, K.A. Matis, *Activated carbons produced by pyrolysis of waste potato peels: cobalt ions removal by adsorption*, *Colloids Surf. A Physicochem. Eng. Asp.*, 490 (2016), 74–83. <https://doi.org/10.1016/j.colsurfa.2015.11.038>
12. W. Bratek, A. Swiatkowski, M. Pak, S. Biniak, M. Bystrzejewski, R. Szmigielski, *Characteristics of activated carbon prepared from waste PET by carbon dioxide activation*, *J. Anal. Appl. Pyrolysis*. 100 (2013) 192–198. <https://doi.org/10.1016/j.jaap.2012.12.021>
13. F. Caturla, M. Molina-Sabio, F. Rodríguez-Reinoso, *Preparation of activated carbon by chemical activation with ZnCl₂*, *Carbon*. 29 (1991) 999–1007. [https://doi.org/10.1016/0008-6223\(91\)90179-M](https://doi.org/10.1016/0008-6223(91)90179-M)
14. Y. Xue, B. Gao, Y. Yao, M. Inyang, M. Zhang, A.R. Zimmerman, K.S. Ro, *Hydrogen peroxide modification enhances the ability of biochar (hydrochar) produced from hydrothermal carbonization of peanut hull to remove aqueous heavy metals: Batch and column tests*, *Chem. Eng. Journal*. 200–202 (2012) 673–680. <https://doi.org/10.1016/j.cej.2012.06.116>
15. N. Sadlej-Sosnowska, A. Ocios, L. Fuks, *Selectivity of similar compounds' identification using IR spectrometry: β -lactam antibiotics*, *J. Mol. Struct.*, 792–793, (2006) 110–114. <https://doi.org/10.1016/j.molstruc.2005.12.054>
16. S. Mopoung, P. Moonsri, W. Palas, S. Khumpai, S., *Characterization and Properties of Activated Carbon Prepared from Tamarind Seeds by KOH Activation for Fe(III) Adsorption from Aqueous Solution*, *Sci. World Journal*. ID 415961 (2015) 1–9. <https://doi.org/10.1155/2015/415961>
17. N. Labbeä, D. Harper, T. Rials, *Chemical Structure of Wood Carbon by Infrared Spectroscopy and Multivariate Analysis*, *J. Agric. Food Chem.* 54 (2006) 3492–3497. <https://doi.org/10.1021/jf053062n>
18. B.S. Girgis, Y.M. Temerk, M.M. Gadelrab, I.D. Abdullah, *X-ray Diffraction Patterns of Activated Carbons Prepared under Various Conditions*, *Carbon Sci.* 8 (2007) 95–100. <https://doi.org/10.5714/CL.2007.8.2.095>
19. N. Zhao, S. Wu, C. He, C. Shi, E. Liu, X. Du, J. Li, *Hierarchical porous carbon with graphitic structure synthesized by a water soluble template method*, *Materials Letters*. 87 (2012) 77–79. <https://doi.org/10.1016/j.matlet.2012.07.085>
20. KTH Royal Institute of Technology, *Medusa KTH Programme*. Stockholm, Sweden: Royal Institute of Technology (2020). <https://www.kth.se/che/medusa/downloads-1.386254> (last accessed: 20.12.2020)
21. A.M. Anielak, M. Grzegorzczuk-Nowacka, *Significance of zeta potential in the adsorption of fulvic acid on aluminum oxide and activated carbon*, *Pol. J. Environ. Stud.* 20 (2011) 1381–1386.

22. A. Seco, P. Marzal, C. Gabaidon, J. Ferrer, *Adsorption of heavy metals from aqueous solution to activated carbon in single Cu and Ni system and in binary Cu-Ni, Cu-Cd and Cu-Zn system*, J. Chem. Technol. Biotechnol. 68 (1997) 23–30. [https://doi.org/10.1002/\(SICI\)1097-4660\(199701\)68:1<23::AID-JCTB595>3.0.CO;2-N](https://doi.org/10.1002/(SICI)1097-4660(199701)68:1<23::AID-JCTB595>3.0.CO;2-N)
23. M. Sanchez-Polo, J. Rivera-Utrilla, *Adsorbent-Adsorbate Interactions in the adsorption of Cd(II) and Hg(II) on ozonized activated carbons*, Environ. Sci. Technol. 36 (2002) 3850–3854. <https://doi.org/10.1021/es0255610>
24. R. Qadeer, J. Hanif, M. Saleem, M. Afzal, *Adsorption of samarium on activated charcoal from aqueous solution*, J. Chem. Soc. Pakistan. 14 (1992) 91–96.
25. A.F. Taiwo, N.J. Chinyere, *Sorption Characteristics for Multiple Adsorption of Heavy Metal Ions Using Activated Carbon from Nigerian Bamboo*, J. Materials Sci. Chem. Eng. 4 (2016) 39–48. <https://doi.org/10.4236/msce.2016.44005>
26. I. Uzhun, F. Guzel, *Adsorption of Some Heavy Metal Ions from Aqueous Solution by Activated Carbon and Comparison of Percent Adsorption Results of Activated Carbon with those of Some Other Adsorbents*, Turk. J. Chem. 24 (2000) 291–297.
27. M. Cox, A.A. Pichugin, E.I. El-Shafey, Q. Appleton, *Sorption of precious metals onto chemically prepared carbon from flax shive*, Hydrometallurgy. 78 (2005) 137–144. <https://doi.org/10.1016/j.hydromet.2004.12.006>
28. T. Mitkov, G. Gicheva, *Heavy metal ions sorption onto activated carbon*, Annual of the University of Mining and Geology “St. Ivan Rilski”, Mining and Mineral processing, Part VI. 55 (2012) 214–216.
29. B. Xiao, K.M. Thomas, *Competitive Adsorption of Aqueous Metal Ions on an Oxidized Nanoporous Activated Carbon*, Langmuir. 20 (2004) 4566–4578. <https://doi.org/10.1021/la049712j>
30. B. Viswanathan, P. Indra Neel, T.K. Varadarajan, *Methods of Activation and Specific Applications of Carbon Materials*, e-book by National Centre for Catalysis Research, Indian Institute of Technology Madras, 164 (2009) https://www.researchgate.net/publication/299393936_Methods_of_Activation_and_Specific_Applications_of_Carbon_Materials#fullTextFileContent; accessed on 26.12.2021.
31. S. Rangabhashiyam, N. Anu, M.S. Giri Nandagopal, N. Selvaraju, *Relevance of isotherm models in biosorption of pollutants by agricultural byproducts*, J. Environm. Chem. Eng. 2 (2014) 398–414. <https://doi.org/10.1016/j.jece.2014.01.014>

Chapter 10

Nanoporous carbon adsorbents derived from PET waste for the adsorption of environmental contaminants in aqueous matrices

Tshimangadzo S. Munonde ^{a,b,*},
Philiswa Nosizo Nomngongo ^{a,b,c*}

^aDepartment of Chemical Sciences, University of Johannesburg, Doornfontein Campus, P.O. Box 17011, Doornfontein, 2028, South Africa

^bDST/NRF SARChI Chair: Nanotechnology for Water, University of Johannesburg, Doornfontein, 2028, South Africa

^cDST/Mintek Nanotechnology Innovation Centre, University of Johannesburg, Doornfontein, 2028, South Africa

*Corresponding authors: 215077511@student.uj.ac.za and pnnomngongo@uj.ac.za

Abstract

This chapter discusses the valorisation of polyethylene terephthalate (PET) waste converted into nanoporous carbon for the removal of environmental contaminants in aqueous matrices. The structural, physical, and chemical properties that are key to the performance of PET waste-derived nanoporous carbon are briefly discussed. The synthetic routes uncovering all the interesting properties of nanoporous properties were deliberated. Some key studies sourced from the literature are identified and discussed to evaluate the viability and sustainability of nanoporous carbon as effective adsorbents for the removal of pollutants within the environmental water matrices. Future prospects are deliberated to visualise some key areas requiring attention within the general PET waste beneficiation research.

Keywords: PET waste, Nanoporous carbon, Adsorption, Environmental, Valorisation

1. Introduction

The global production of polyethylene terephthalate (PET) bottles reached 13.1 million tons in 2020 [1], aiding for the recycling and repurposing of PET waste as a crucial global responsibility. Subsequently, polyethylene terephthalate is now recognised as the third most widely used polymer in the production of packaging materials after polyethylene (PE) and polypropylene (PP) [2,3]. Considering that only one PET bottle is recycled for every four PET bottles traded, landfills are overflowing with million tons of discarded PET bottles [4]. Moreover, PET bottles do not biodegrade, instead they photodegrade, taking up to 1000 years for each bottle to decompose [4,5]. Conventionally used plastic recycling methods, such as incineration and mechanical recycling are not economically viable and also raise some environmental concerns [1]. To avoid a global PET waste bottle catastrophe, the production of high value-added products from PET waste bottles has been recognised [6–8]. Since PET was identified as a condensation polymer made by the reaction of terephthalic acid (BDC) and ethylene glycol (EG), PET waste has been repurposed and used for the production of various synthetic materials such as metal-organic frameworks (MOFs) [6,7] and polybutylene terephthalate (PBT) [9], as well as products such as cleaner asphalt pavement materials [8,10] and textile materials [11], among others. Interestingly, due to their high carbon content, the absence of mineral matter and impurities, PET waste has been used in the preparation of nanoporous carbon (NPC) [12]. Owing to their adjustable pore structures and functional groups such as the OH group, nanoporous carbons have attracted attention in energy storage [13], catalysis [14], adsorption [15–17], among other applications. As an example, Ubaidullah, et al. [18] fabricated a high surface area nitrogen doped mesoporous carbon (N-MC) through an economically feasible approach using waste PET plastic bottles through MOF-5 construction. The synthesised N-MC displayed a high specific surface area of $\sim 2243 \text{ m}^2 \text{ g}^{-1}$ with mesopores ($\sim 14 \text{ nm}$), and an excellent electrochemical energy storage performance. The authors concluded that the fabrication of N-MC using PET waste makes it an appealing process for environmental remediation and an efficient low-cost electrode material for supercapacitor applications. Using PET waste-based nanoporous carbon, a pathway to deal with a variety of environmental problems, such as trace metals, pharmaceutical and pesticides contaminations [19–21], among others, might be a possibility.

This chapter, therefore, describes the synthesis strategies, alongside important properties of PET waste-derived nanoporous carbon materials that were discussed prior to their application on the removal of various environmental contaminants.

2. Synthesis strategies for PET waste conversion into nanoporous carbons

PET plastic bottles are among the most valuable types of waste, thus their valorisation into new adsorbent materials has been explored using a variety of methods, including direct carbonisation (physical or chemical activation), hydrothermal carbonisation, and pyrolysis [22]. Subsequently, the common methods responsible for the conversion of PET waste into nanoporous carbon have been briefly described.

2.1 Direct carbonisation

Literature findings have reported intensively that the physical (temperature treatment usually between 500–1000 °C) and chemical activation (using activation agents, such as KOH, NaOH, H_3PO_4 , $ZnCl_2$, and K_2CO_3) enhance the surface properties of carbon-based materials, thus producing highly porous structured carbon-based materials [17,22–24]. To this end, Kaur *et al.* [12] synthesised the O-enriched porous carbonaceous adsorbents by directly carbonising hacked smaller PET waste bottle pieces with high carbon content at different temperatures (500–800 °C) in a tubular furnace under inert atmosphere prior to chemical activation using KOH. Figure 1 displays the SEM images of the adsorbent prepared by direct carbonisation without activation (Figure 1a) and the chemically activated carbon (Figure 1b–e). It can be noted that each carbon chemically activated with KOH displays better development of pores than the inactivated carbon. The best performing material for gas adsorption showed the best pore structure with a BET surface area of $1690 \text{ m}^2\text{g}^{-1}$ and micropore volume of $0.78 \text{ cm}^3 \text{ g}^{-1}$ is displayed in Fig. 1c. The authors ascribed the best performance of this materials to the higher microporosity and basic oxygen functionalities observed after KOH chemical activation.

2.2 Hydrothermal carbonisation

Hydrothermal carbonisation (HTC) has been described as a thermochemical conversion process usually carried out at temperatures between 150–250 °C for the conversion of organic waste to hydrochar with residence times between 0.5 and 8 hours [25,26]. However, this method has been modified for the synthesis of nanoporous carbon from PET waste into a two-step synthetic procedure as reported in the literature [6,12]. The initial step involves the depolymerisation of waste PET bottles that are first cut into small PET flakes, followed by their hydrolysis in a hydrothermal reactor (at 220 °C for 8 hours) with a given ratio of ethylene glycol and deionised water as described on the literature [6]. The product obtained is an organic linker called terephthalic acid (BDC) (shown in Figure 2), which

is then physically activated at temperatures around 700–850 °C to form nanoporous carbon in the second step of the synthesis [12,17].

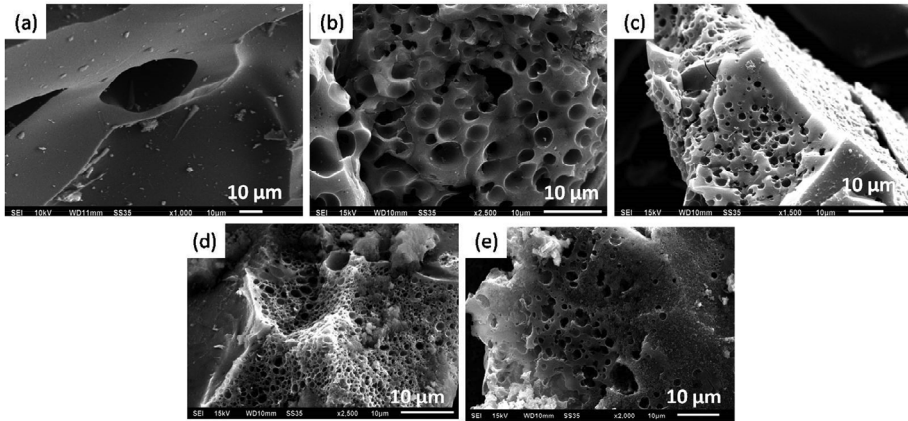


Figure 1: SEM images of nanoporous carbon derived from PET waste. Reprinted with permission from [12]. Copyright 2019, Elsevier.

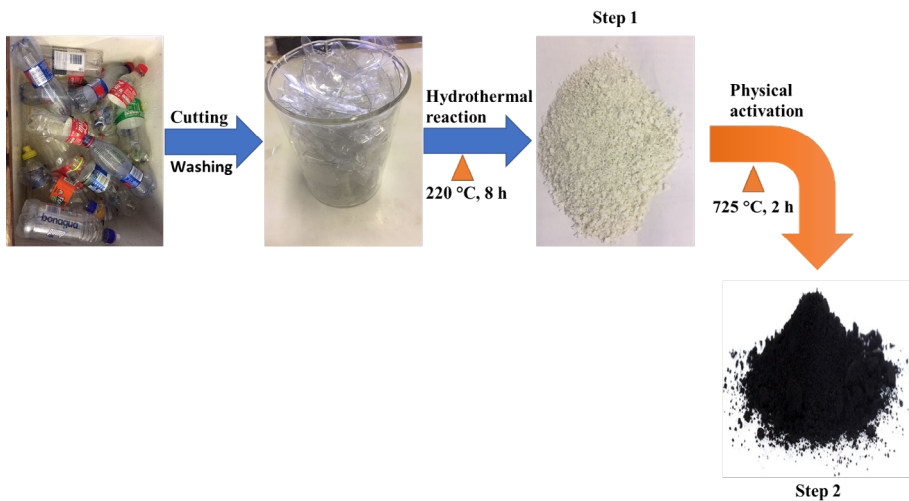


Figure 2: Hydrothermal synthesis and physical activation of PET waste bottles to porous carbon.

3. Properties of PET waste derived nanoporous carbon

Various structural, physical, and chemical properties of nanoporous carbon derived from PET waste have been outlined in the literature. For instance, Wenlong *et al.* [14] reported the nanoporous carbons (NPCs) with various pore structures and morphology control that were prepared

using MgO particles as nanotemplates and PET powders derived from waste PET bottles as a carbon precursor. The controllable porosity was very critical on the hybridisation with platinum particles, leading to the preparation of very small platinum particles. Yuan *et al.* [27] prepared an N-doped microporous carbon through the valorisation of waste PET plastic bottles through a one-pot synthesis. The Nitrogen doping did not only enhance the selectivity of the adsorbent, but also acted as active sites for the adsorption. Wei and Ali [28] proposed a two-steps strategy based on the controlled carbonisation and thermal oxidation in air to convert waste PET into porous carbon materials with high values of surface area and electrical conductivity. The PET- derived carbon materials prepared at different temperatures were found to exhibit an interesting combination of properties, including a high surface area of 644 m²/g, and electron conductivity of 37 S/m observed for the best performing adsorbent material. Subsequently, the structural, physical, and chemical properties observed from these literature studies were summarised in Figure 3.

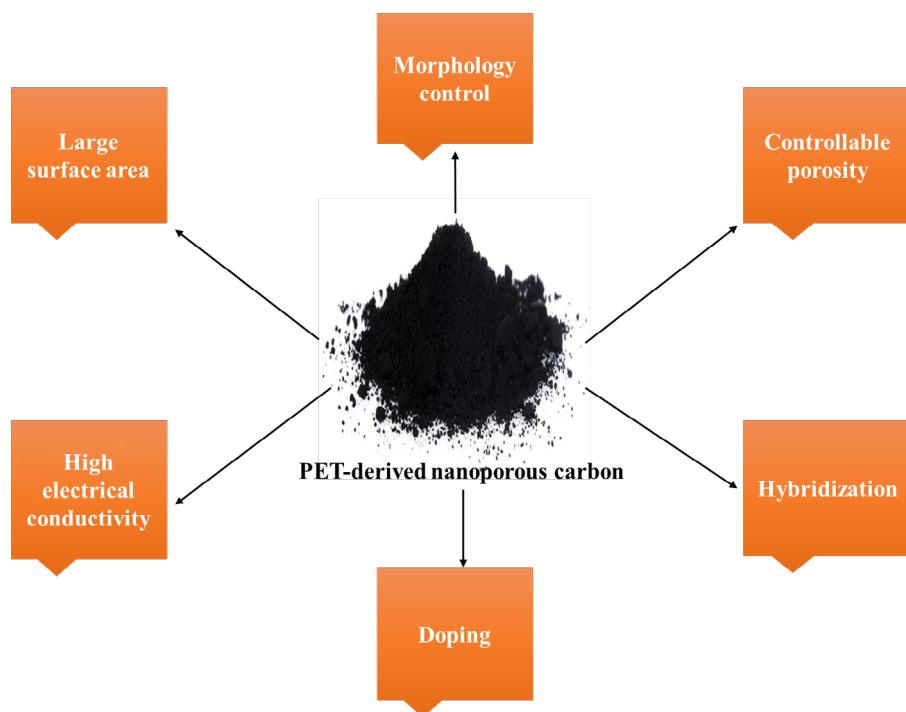


Figure 3: Key properties of PET-derived nanoporous carbon.

4. Application of nanoporous carbon as adsorbents

The global availability of PET waste in large quantities is unsurprisingly visual within the environment. Thus, the valorisation of PET waste as an efficient waste beneficiation strategy leading to the reduction of environmental pollution has attracted interest [6,7,10,27]. Due to the high content of carbon, negligible amounts of inorganic matter in its chemical constitution, high chemical, mechanical, and thermal stability, PET waste has advanced as an excellent porous carbon adsorbent in many gas adsorption applications, specifically in CO₂ adsorption [12,16,22,27,29]. Furthermore, PET waste has been converted to nanoporous carbon adsorbents for various environmental remediation applications ranging from organic dye removal to pesticides and pharmaceuticals removal in wastewater [15,30]. Although very few studies have been conducted for the removal of trace/heavy metals in aqueous environments using PET waste derived nanoporous adsorbents, their interesting structural, physical, and chemical properties seem to be attractive for these studies. To this end, Mendoza-Carrasco et al. [31] developed a waste-treats-waste approach enabling the waste PET to be used as the precursor for the preparation of activated carbons (ACs) by physical activation with steam and chemical activation with potassium hydroxide. Although the SEM images in Figure 4 show that the physically activated carbon (Figure 4a) is agglomerated and appears less porous than the chemically activated carbon (Figure 4b), the BET surface areas reached 1235 m² g⁻¹ with physical activation and 1002 m² g⁻¹ with chemical activation. The authors declared the formation of micro to mesoporous structures with physical activation and microporous structures with chemical activation. The selected AC samples were used to study the adsorption process for both p-nitrophenol and Fe(III) in aqueous solution, individually and simultaneously from the kinetic and equilibrium standpoint. Concerning the simultaneous adsorption of p-nitrophenol and Fe(III) in aqueous solution, both the PET derived ACs exhibited a better adsorption behaviour towards p-nitrophenol than commercial AC, both in terms of adsorption rate and adsorption capacity. Thus, the PET waste-derived AC adsorbents did not perform well for the adsorption of Fe(III) ions due to the p-nitrophenol already taking the active sites within the adsorbent, indicating that Fe(III) ions needs to be studied without the presence of their organic counterpart.

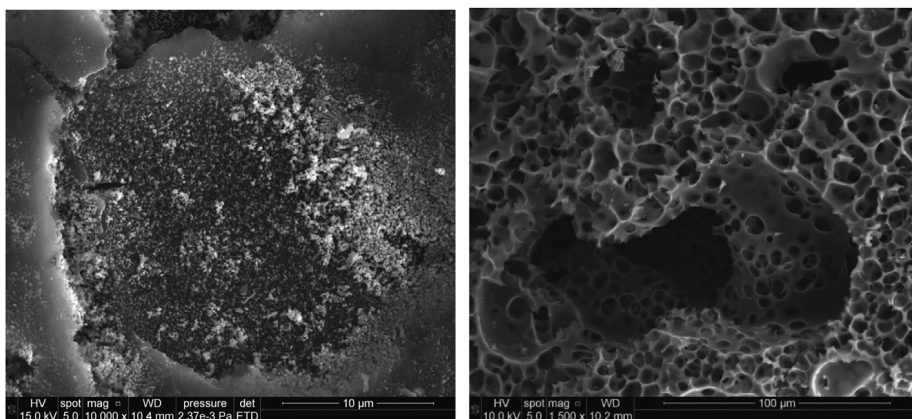


Figure 4: SEM images of PET waste-derived activated carbon prepared using (a) physical activation and (b) chemical activation. Reprinted with permission from [31]. Copyright 2016, Elsevier.

5. Challenges and future prospects

- Due to its high carbon contents, low nitrogen and sulfur contents, PET waste appears to be a suitable material to be used as the precursor in the preparation of nanoporous carbon materials, however, problems occur when mixing PET bottles by colour, as these introduce unwanted organic compounds during the synthesis procedures.
- The caps of PET bottles are usually made from polyolefins and have to be recycled separately, adding to the problems of coloured bottles in the mix.
- Considering that there have been very few studies utilising the structural, physical, and chemical properties of PET waste-derived nanoporous carbon for the removal of metals in aqueous systems (river water, wastewater, drinking water, etc.), this area paves new avenues for solving some of the environmental problems the world faces.

6. Conclusion

This chapter highlights the potential of utilising PET waste-derived nanoporous carbon adsorbents for the removal of environmental contaminants in aqueous environments. The subsequent literature discussed shows that the waste-treats-waste concept might be viable for the removal of contaminants from the environmental viewpoint. It is evident that the locally available PET waste can act as inexpensive precursor materials for the preparation of porous carbon adsorbents for the aqueous environment remediation. However, it is also evident that

more investigations are needed in order to assess the effectiveness of the PET waste-derived porous carbon materials as adsorbents for the removal of various environmental pollutants, thus proving if this is a sustainable concept to pursue.

7. Acknowledgements

This study received financial support from the Department of Science and Innovation/National Research Foundation South African Research Chairs Initiative (DSI/NRF SARChI) grant no. 91230.

References

1. Čolnik, M.; Pečar, D.; Knez, Ž.; Goršek, A.; Škerget, M. Kinetics Study of Hydrothermal Degradation of PET Waste into Useful Products. *Processes* **2022**, *10*, 24. <https://doi.org/10.3390/pr10010024>
2. Eriksen, M.K.; Christiansen, J.D.; Daugaard, A.E.; Astrup, T.F. Closing the loop for PET, PE and PP waste from households: Influence of material properties and product design for plastic recycling. *Waste Manag.* **2019**, *96*, 75–85. <https://doi.org/10.1016/j.wasman.2019.07.005>
3. Siracusa, V.; Blanco, I. Bio-Polyethylene (Bio-PE), Bio-Polypropylene (Bio-PP) and Bio-Poly(ethylene terephthalate)(Bio-PET): recent developments in bio-based polymers analogous to petroleum-derived ones for packaging and engineering applications. *Polymers (Basel)*. **2020**, *12*, 1641. <https://doi.org/10.3390/polym12081641>
4. Bonsu, P. The Impact and Development of handling PET bottles waste: Case Kasapreko Ltd in Ghana. **2020**.
5. Bashir, N.H.H. Plastic problem in Africa. *Jpn. J. Vet. Res.* **2013**, *61*, S1–S11.
6. Dyosiba, X.; Ren, J.; Musyoka, N.M.; Langmi, H.W.; Mathe, M.; Onyango, M.S. Preparation of value-added metal-organic frameworks (MOFs) using waste PET bottles as source of acid linker. *Sustain. Mater. Technol.* **2016**, *10*, 10–13. <https://doi.org/10.1016/j.susmat.2016.10.001>
7. Ren, J.; Dyosiba, X.; Musyoka, N.M.; Langmi, H.W.; North, B.C.; Mathe, M.; Onyango, M.S. Green synthesis of chromium-based metal-organic framework (Cr-MOF) from waste polyethylene terephthalate (PET) bottles for hydrogen storage applications. *Int. J. Hydrogen Energy* **2016**, *41*, 18141–18146. <https://doi.org/10.1016/j.ijhydene.2016.08.040>
8. Wu, S.; Montalvo, L. Repurposing waste plastics into cleaner asphalt pavement materials: A critical literature review. *J. Clean. Prod.* **2021**, *280*, 124355. <https://doi.org/10.1016/j.jclepro.2020.124355>

9. Cho, M.; Yang, J.; Noh, S.; Joe, H.; Han, M. Production of PBT (polybutylene terephthalate) Oligomer from Recycled PET (polyethylene terephthalate). *Korean Chem. Eng. Res.* **2016**, *54*, 437–442. <https://doi.org/10.9713/kcer.2016.54.4.437>
10. Merkel, D.R.; Kuang, W.; Malhotra, D.; Petrossian, G.; Zhong, L.; Simmons, K.L.; Zhang, J.; Cosimbescu, L. Waste PET chemical processing to terephthalic amides and their effect on asphalt performance. *ACS Sustain. Chem. Eng.* **2020**, *8*, 5615–5625. <https://doi.org/10.1021/acssuschemeng.0c00036>
11. Shirvanimoghaddam, K.; Motamed, B.; Ramakrishna, S.; Naebe, M. Death by waste: Fashion and textile circular economy case. *Sci. Total Environ.* **2020**, *718*, 137317. <https://doi.org/10.1016/j.scitotenv.2020.137317>
12. Kaur, B.; Gupta, R.K.; Bhunia, H. Chemically activated nanoporous carbon adsorbents from waste plastic for CO₂ capture: Breakthrough adsorption study. *Microporous Mesoporous Mater.* **2019**, *282*, 146–158. <https://doi.org/10.1016/j.micromeso.2019.03.025>
13. Al-Enizi, A.M.; Ubaidullah, M.; Ahmed, J.; Ahamad, T.; Ahmad, T.; Shaikh, S.F.; Naushad, M. Synthesis of NiOx@ NPC composite for high-performance supercapacitor via waste PET plastic-derived Ni-MOF. *Compos. Part B Eng.* **2020**, *183*, 107655. <https://doi.org/10.1016/j.compositesb.2019.107655>
14. Wenlong, Y.; Zhe, C.; Shitao, Y.; Junwei, D.; Yuling, S.; Fusheng, L.; Ming, L. Highly dispersed Pt catalyst supported on nanoporous carbon derived from waste PET bottles for reductive alkylation. *RSC Adv.* **2019**, *9*, 31092–31101. <https://doi.org/10.1039/C9RA04976B>
15. Zhang, H.; Pap, S.; Taggart, M.A.; Boyd, K.G.; James, N.A.; Gibb, S.W. A review of the potential utilisation of plastic waste as adsorbent for removal of hazardous priority contaminants from aqueous environments. *Environ. Pollut.* **2020**, *258*, 113698. <https://doi.org/10.1016/j.envpol.2019.113698>
16. Kaur, B.; Singh, J.; Gupta, R.K.; Bhunia, H. Porous carbons derived from polyethylene terephthalate (PET) waste for CO₂ capture studies. *J. Environ. Manage.* **2019**, *242*, 68–80. <https://doi.org/10.1016/j.jenvman.2019.04.077>
17. Moura, P.A.S.; Vilarrasa-Garcia, E.; Maia, D.A.S.; Bastos-Neto, M.; Ania, C.O.; Parra, J.B.; Azevedo, D.C.S. Assessing the potential of nanoporous carbon adsorbents from polyethylene terephthalate (PET) to separate CO₂ from flue gas. *Adsorption* **2018**, *24*, 279–291. <https://doi.org/10.1007/s10450-018-9943-4>

18. Ubaidullah, M.; Al-Enizi, A.M.; Ahamad, T.; Shaikh, S.F.; Al-Abdrabalnabi, M.A.; Samdani, M.S.; Kumar, D.; Alam, M.A.; Khan, M. Fabrication of highly porous N-doped mesoporous carbon using waste polyethylene terephthalate bottle-based MOF-5 for high performance supercapacitor. *J. Energy Storage* **2021**, *33*, 102125. <https://doi.org/10.1016/j.est.2020.102125>
19. Mnyipika, S.H.; Munonde, T.S.; Nomngongo, P.N. MnO₂@ Reduced Graphene Oxide Nanocomposite-Based Electrochemical Sensor for the Simultaneous Determination of Trace Cd (II), Zn (II) and Cu (II) in Water Samples. *Membranes (Basel)*. **2021**, *11*, 517. <https://doi.org/10.3390/membranes11070517>
20. Nyaba, L.; Munonde, T.S.; Mpupa, A.; Nomngongo, P.N. Magnetic Fe₃O₄@ Mg/Al-layered double hydroxide adsorbent for preconcentration of trace metals in water matrices. *Sci. Rep.* **2021**, *11*, 1–15. <https://doi.org/10.1038/s41598-021-81839-8>
21. Munonde, T.S.; Nomngongo, P.N. Nanocomposites for Electrochemical Sensors and Their Applications on the Detection of Trace Metals in Environmental Water Samples. *Sensors* **2021**, *21*, 131. <https://doi.org/10.3390/s21010131>
22. Hussin, F.; Aroua, M.K.; Kassim, M.A. Transforming Plastic Waste into Porous Carbon for Capturing Carbon Dioxide: A Review. *Energies* **2021**, *14*, 8421. <https://doi.org/10.3390/en14248421>
23. Yuan, X.; Lee, J.G.; Yun, H.; Deng, S.; Kim, Y.J.; Lee, J.E.; Kwak, S.K.; Lee, K.B. Solving two environmental issues simultaneously: Waste polyethylene terephthalate plastic bottle-derived microporous carbons for capturing CO₂. *Chem. Eng. J.* **2020**, *397*, 125350. <https://doi.org/10.1016/j.cej.2020.125350>
24. Adibfar, M.; Kaghazchi, T.; Asasian, N.; Soleimani, M. Conversion of poly (ethylene terephthalate) waste into activated carbon: chemical activation and characterization. *Chem. Eng. Technol.* **2014**, *37*, 979–986. <https://doi.org/10.1002/ceat.201200719>
25. Pauline, A.L.; Joseph, K. Hydrothermal carbonization of organic wastes to carbonaceous solid fuel—A review of mechanisms and process parameters. *Fuel* **2020**, *279*, 118472. <https://doi.org/10.1016/j.fuel.2020.118472>
26. Berge, N.D.; Ro, K.S.; Mao, J.; Flora, J.R. V; Chappell, M.A.; Bae, S. Hydrothermal carbonization of municipal waste streams. *Environ. Sci. Technol.* **2011**, *45*, 5696–5703. <https://doi.org/10.1021/es2004528>

27. Yuan, X.; Li, S.; Jeon, S.; Deng, S.; Zhao, L.; Lee, K.B. Valorization of waste polyethylene terephthalate plastic into N-doped microporous carbon for CO₂ capture through a one-pot synthesis. *J. Hazard. Mater.* **2020**, *399*, 123010. <https://doi.org/10.1016/j.jhazmat.2020.123010>
28. Wei, S.; Kamali, A.R. Dual-step air-thermal treatment for facile conversion of PET into porous carbon particles with enhanced dye adsorption performance. *Diam. Relat. Mater.* **2020**, *107*, 107914. <https://doi.org/10.1016/j.diamond.2020.107914>
29. Ungureanu, O.I.; Bulgariu, D.; Mocanu, A.M.; Bulgariu, L. Functionalized PET waste based low-cost adsorbents for adsorptive removal of Cu (II) ions from aqueous media. *Water* **2020**, *12*, 2624. <https://doi.org/10.3390/w12092624>
30. Jung, K.-W.; Kim, J.-H.; Choi, J.-W. Synthesis of magnetic porous carbon composite derived from metal-organic framework using recovered terephthalic acid from polyethylene terephthalate (PET) waste bottles as organic ligand and its potential as adsorbent for antibiotic tetracycline hydrochloride. *Compos. Part B Eng.* **2020**, *187*, 107867. <https://doi.org/10.1016/j.compositesb.2020.107867>
31. Mendoza-Carrasco, R.; Cuerda-Correa, E.M.; Alexandre-Franco, M.F.; Fernández-González, C.; Gómez-Serrano, V. Preparation of high-quality activated carbon from polyethyleneterephthalate (PET) bottle waste. Its use in the removal of pollutants in aqueous solution. *J. Environ. Manage.* **2016**, *181*, 522–535. <https://doi.org/10.1016/j.jenvman.2016.06.070>

Chapter 11

Techno-economic feasibility assessment on the viability of using waste PET (trays and coloured bottles) to produce Metal-Organic Frameworks (MOFs)

Jianwei Ren ^{a,*}, Tien-Chien Jen ^a, Wojciech Starosta ^b,
Bożena Sartowska ^b, Philiswa Nosizo Nomngongo ^c

^aUniversity of Johannesburg, Johannesburg, Kingsway and University Road,
Auckland Park, 2092, P.O. Box 524, Auckland Park, 2006,
Johannesburg, South Africa

^bLaboratory of Materials Research, Institute of Nuclear Chemistry and
Technology, Dorodna 16, 03-195 Warsaw, Poland

^cDepartment of Chemical Sciences, University of Johannesburg,
Doornfontein Campus, P.O. Box 17011, Johannesburg, 2028, South Africa

*Corresponding author. Tel: +27 11 559 2103. Email: jren@uj.ac.za (J. Ren)

Abstract

This work reviewed the business model of waste PET-to-MOFs from technical feasibility, economic appraisal, commercial viability, and risk assessment. A process model was developed to cover the mass balance, which considered material flows, chemical build-up, and energy requirements. The balance was based on a case of 1 kg/day, and the scalability was proved at a later stage. A financial model was then developed, and the analysis of economic appraisal and commercial viability showed that investing in MOFs will generate roughly a 5% internal rate of return (IRR) on a production capacity of 10 kg daily. Given the fact that these results are positive at a small scale, it is therefore recommended that this investment should proceed. The environmental and opportunity cost that is avoided has not been considered in the financial analysis. This can further strengthen the revenue side of this production. While a return of 5% is not the most attractive, the PET waste that would be redirected to this production contributes to the South African waste management strategy and climate change objectives. In addition, since the South

African government bond of ten years yields a return of 8.52% return, this initiative is competitive with a 5% IRR.

Keywords: Techno-economic Feasibility, Trays and Coloured Bottles, Metal-organic frameworks, Viability

1. Introduction

Polyethylene terephthalate (PET), as a dominant packing material, has impacted our lives since the 1960s with its global consumption reaching over 24 million tons per year. The present common practice of PET waste landfilling has led to serious environmental problems, and chemical recovery faces a huge challenge as a result of the complexity associated with the recycling methods coupled with low efficiency. On one hand, the current low-value market of the downstream products from recycled PET and the low prices of the virgin PET are the two main factors responsible for the low recycling rate of waste PET in South Africa. The PET recycling industry requires new processes to gain more value out of the PET wastes. On the other hand, governmental sectors in different countries have started to set penalties on non-recycled plastics, for instance, France has created a new penalty system where items packaged in non-recycled plastic could cost up to 10% more, and taxes on rubbish buried in landfills will also be increased. In this regard, an attractive and high-value recycling option for depolymerising PET bottles to obtain terephthalic acid (BDC) which is used as a linker for producing high value metal-organic frameworks (MOFs) has been demonstrated (Figure 1) as a promising PET recycling strategy.

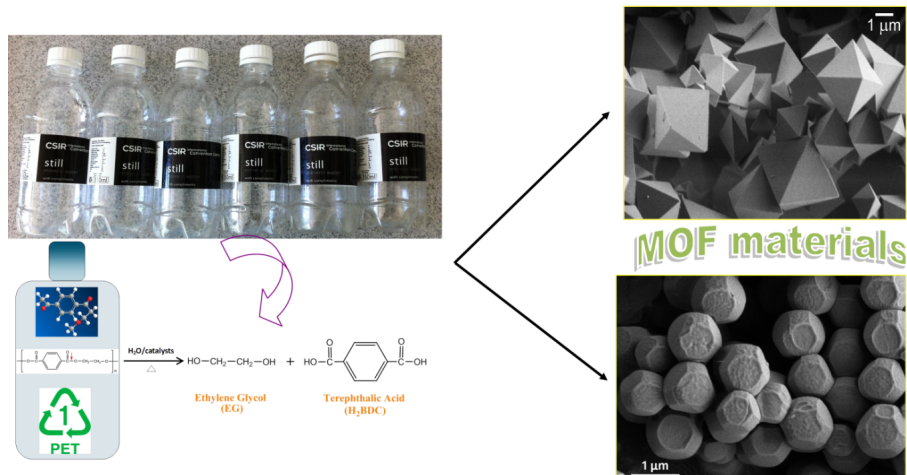


Figure 1: Conversion of waste PET into high value-added MOFs materials

MOFs as a new generation of porous materials are expected to solve real problems and challenges, and offer better performance than conventional materials, such as zeolites and activated carbons. MOFs have been reported to have wide industrial applications, such as gas storage, separation, purification, catalyst, sensor, drug delivery, etc. Although many bench scale experimental work on MOFs synthesis has been conducted, the biggest barrier to their wide-scale commercialisation has been due to the high cost of the constituent chemical feedstocks, of which the organic linkers are the most expensive. Therefore, for MOFs to advance towards large-scale commercial production and applications, there is a need to develop production technologies that will reduce their cost. In this regard, funded by the South African Department of Science and Innovation (DSI) HySA Infrastructure programme, the Council for Scientific and Industrial Research (CSIR) has built up the capabilities to develop the synthesis strategies for different types of MOFs. Of particular interest, our studies have shown that it is possible to produce high quality MOFs, such as those containing Cr, Fe and Zr metal centre. The developed MOFs (UiO-66, MIL-101-(Fe), MIL-101(Cr)) are known for their attractive properties and are applicable in many industrial processes.

The initial focus of our research was on the use of clear PET bottles and work was conducted on a small-batch scale level. Coloured bottles and food PET trays are currently considered as a problematic PET waste stream in South African PET recycling industries. Therefore, our preliminary research experiments proved successful with regards to the depolymerisation process of coloured bottles and food PET trays as well as MOFs synthesis. To complete the evaluations and leverage, the high potential for PET recycling into high-valuable MOF materials, there is a need to conduct further focussed research that integrates all aspects of PET-to-MOFs recycling technology so as to facilitate decision-making for the pre-commercialisation phase. In order to advance the proof of concept and move PET-to-MOF technology towards commercialisation, there is also a need to conduct a techno-economic feasibility study on the viability of converting waste PET to MOFs. In such a manner, the requisite information for making important decisions can be derived in the transition of the research towards the pre-commercialisation phase.

This work aims to review the proposed solution, and determine if the business idea of PET-to-MOFs has a potential of success by taking into account the technical feasibility, economical appraisal, commercial viability, and risk assessment. In the course of the project implementation, a process model was developed to cover the mass balance, which considered material flows, chemical build-up, and energy requirements. The balance was based on a case of 1 kg/batch, and the scalability was proved at a later

stage. A financial model was then developed to analyse the economic appraisal and commercial viability.

The result of this study will provide sufficient information and reveal whether this technology is worth further investment. More importantly, the outcomes of this study would provide the government sectors and other stakeholders with sufficient information to serve as a basis for consideration of this business model for increasing the current recycling/reprocessing of waste PET in South Africa.

2. Methodology

2.1. KG-scale depolymerisation of coloured PET bottles and PET food trays

A laboratory-scale crusher (model PC-180) was used to crush the coloured PET bottles and PET food trays (Figure 2a). Then a solvothermal approach was employed to depolymerise the coloured PET bottles and PET food trays in a 5 L high-pressure reactor as shown in Figure 2b. The following is the typical procedure:

1. The coloured PET bottles (green and brown) and PET food trays were collected and cleaned. Bottle caps, rings, and labels were removed accordingly.
2. The cleaned coloured PET bottles and PET food trays were crushed using the above-mentioned crusher.
3. The crushed waste PET (coloured PET bottles and PET food trays) and the calculated amount of water were put into the reactor.
4. The reactor was heated up to a temperature of 200 °C and maintained for 8 to 20 h at an autogenous pressure.
5. The solid product was separated from the mother liquid by centrifugation and dried after being washed twice in N,N-dimethylformamide (DMF).

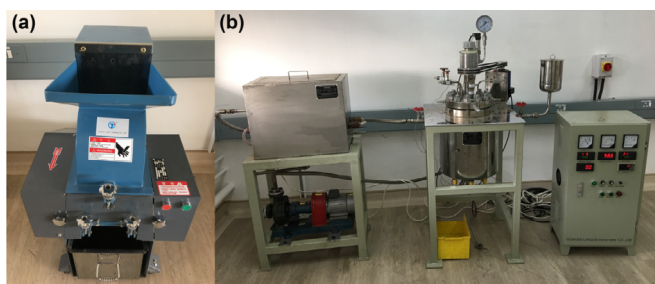


Figure 2: Digital pictures of: (a) Crusher for PET bottles, and (b) the 5 L reactor used in this project

The depolymerisation process for the baseline cost assessment is defined in Figure 3.

Steps of KG-scale depolymerisation of coloured bottles & PET food trays		
Process steps	Production principles	Key parameters for step
Recycling of coloured bottles & PET food trays	Classification and clean the recycled waste PET materials	Cost of manpower, Time efficiency
Crush the recycled raw PET materials	Safe operation, Energy efficiency, Time efficiency	Cost of crusher and manpower, Energy consumption
Reactant preparation 0.5 h/batch	Safer chemicals, Safer solvent and auxiliaries, Prevention of hazardous reactions	Cost of waste PET materials, solvent, and manpower
Depolymerisation 8–20 h/batch	Renewable energy, Less hazardous synthesis, Accident prevention, Energy efficiency, Real time analysis, Catalysis	Depolymerisation time, Energy consumption, Cost of manpower
Filtration & Washing, 2 h/batch	Safer solvent and auxiliaries, Solvent recycling	Costs of solvent, solvent recycling and manpower
Oven drying 8–12 h/batch	Energy efficiency, Time efficiency	Costs of electricity and drying equipment
Packaging of BDC products	MSDS, Green packaging options	Costs of MSDS tests and packaging
Market & Sales	Profitability, Commercial viability, Risk assessment	Costs of market survey, products marketing and sales

Figure 3: Process steps, production principles and key parameters of KG-scale depolymerisation of the coloured PET bottles and PET food trays (MSDS – Material Safety Data Sheets)

2.2. Deduced industrial-scale depolymerisation of coloured PET bottles and PET food trays

With the know-how of the laboratory-scale depolymerisation of coloured PET bottles and PET food trays, the industrial-scale depolymerisation can be deduced based on the assumptions below: firstly, the de-labelling, cleaning, and crushing processes of the recycled PET raw materials

can be combined with higher energy efficiency, time efficiency, and higher automation. The reactor used to depolymerise the recycled PET materials will have big capacity with higher volume availability, energy efficiency as well as time efficiency. At the industrial-scale process, the depolymerisation process can be standardised to take 8 h. The filtration, solvent recycling and vacuumdrying steps can be combined. This combination has the potential to shorten the total filtration, solvent recycling, washing, and drying time from 16 h to 4 h. A comparison of generalised laboratory-scale depolymerisation conditions and our assumed industrial-scale depolymerisation conditions is summarised in Table 1.

Table 1: Laboratory-scale vs Industrial-scale depolymerisation conditions

Process steps	Unit	Laboratory values	Industrial assumptions
Depolymerisation rate	%	85	85
Raw material	/	Waste PET	Waste PET
Solvent	/	Water	Water
Reactor autogenous pressure	bar	2	2
Reactor temperature	°C	200	200
Reaction time	h	12	8
Washing times	/	4	4
Wash fluid	/	DMF/methanol	DMF/methanol
Recycling	%	90	90
Drying time	h	12	4
Powder loss during processing	%	5	5

2.3. KG-scale of MOFs synthesis

The same laboratory-scale solvothermal synthesis was used to produce KG-scale MOF UiO-66(Zr) in a 5 L high-pressure reactor. The process steps were as follows:

1. The waste PET (coloured PET bottles and PET food trays)-derived BDC and Zr-metal salt were put into the reactor.

2. The calculated amount of DMF was poured into the reactor as a solvent.
3. The calculated amount of formic acid was poured into the reactor as a modulator.
4. MOF UiO-66(Zr) materials were obtained after 8 h at an elevated temperature of 120 °C and an autogenous pressure.
5. The MOF UiO-66(Zr) products were separated from the mother liquid by centrifugation.
6. Products were washed twice in methanol and dried after being separated from the solvents.

The production process for the baseline cost assessment for the representative MOF UiO-66(Zr) is defined in Figure 4.

Steps of KG-scale Zr-MOFs production from waste PET-derived BDC		
Process steps	Production principles	Key parameters for step
Reactant preparation 1 h/batch	Renewable feedstocks, Safer chemicals, Safer solvent and auxiliaries, Prevention of hazardous reactions	Cost of waste PET-derived BDC, solvent, modulator, Zr-metal salt and manpower
Precipitation 8 h/batch	Renewable energy, Atom economy, Less hazardous synthesis, Accident prevention, Energy efficiency, Real time analysis, Catalysis	Synthesis time Energy consumption Cost of manpower
Filtration & Washing, 5 h/ batch	Safer solvent and auxiliaries, Solvent recycling	Costs of solvent, solvent recycling and manpower
Oven drying 8 - 12 h/batch	Energy efficiency, Time efficiency	Costs of electricity and drying equipment
Shaping of Zr-MOFs 50 KG/h	Production volume, Energy efficiency, Time efficiency	Costs of shaping facilities and manpower
Packaging of Zr-MOFs products	MSDS of Zr-MOFs products, Green packaging options	Costs of MSDS tests and packaging
Market & Sales	Profitability, Commercial viability, Risk assessment	Costs of market survey, products marketing and sales

Figure 4: Process steps, production principles and key parameters of KG-scale MOF UiO-66(Zr) production from waste PET-derived BDC.

2.4. Deduced industrial-scale MOFs production

An industrial-scale MOFs production from the waste PET was deduced based on the reaction conditions and process steps demonstrated at a laboratory scale as described above. However, based on engineering judgement, the laboratory procedures are not suitable for high production rates, so some variations on the laboratory procedures need to be examined as the Industrial Baseline Process. The process' steps, production principles, and key parameters are listed accordingly. This process is based on laboratory-scale synthesis but has been modified to translate the steps to standard operations conducted in large production facilities. Thus, the Industrial Baseline Process is intended to represent the cost if the proven laboratory-scale synthesis were transferred directly to scale-appropriate unit operations. This section will describe the assumptions that were made to scale up laboratory-demonstrated synthesis.

At the industrial-scale production, it is assumed that the reaction temperature can be raised to 160 °C to shorten the reaction time from 8 h to 6 h and improve the yield of the MOF UiO-66(Zr) products. The filtration, drying and vacuum activation steps can be combined using a rotary dryer, which has the potential to shorten the total washing and driving time from 16 h to 6 h, and meanwhile remove the excess organic ligands that might remain in the framework pores after the filtration/wash step. This contaminant cleaning effect is expected to be more effective than that achievable in a spray dryer or belt dryer due to the much longer residence time at temperature. A comparison of generalised laboratory-scale solvothermal reaction conditions and our assumed industrial-scale solvothermal reaction conditions are summarised in Table 2. Zr-metal precursors and reaction modulators were generally selected for scale-up from demonstrated laboratory-scale solvothermal synthesis.

Table 2: Laboratory-scale vs Industrial-scale Process Conditions

Process steps	Unit	Laboratory values	Industrial assumptions
Molar yield	%	85	85
Metal salt	/	ZrCl ₄	ZrCl ₄
Organic linker	/	Waste PET-derived BDC	Waste PET-derived BDC
Waste PET-derived BDC: metal salt molar ratio	/	0.5:1	1:1
Solvent	/	DMF	DMF

Process steps	Unit	Laboratory values	Industrial assumptions
Modulator	/	Formic acid	Formic acid
Reactor autogenous pressure	bar	1	1
Reactor temperature	°C	120	160
Reaction time	h	8	6
Washing times	/	4	2
Wash fluid	/	methanol	methanol
Recycling	%	90	90
Drying time	h	12	4
Powder loss during processing	%	5	5

The above are expected to be valid assumptions because of the similarities between the laboratory-scale and industrial-scale process conditions of producing MOF UiO-66(Zr) products.

2.5. Technical feasibility of converting coloured waste PET and food trays to BDC

In the experimental trials, different PET sources including green PET bottles, brown PET bottles, PET food trays, and PETCO PET beads were converted to BDC products. Meanwhile, the characterisation results of the derived-BDC samples were compared with those of the commercial BDC purchased from Sigma-Aldrich, as illustrated in Figure 5.

Figure 5a shows the X-ray diffraction (XRD) patterns of the BDC products from different PET sources. Compared to the commercial Sigma-Aldrich BDC sample with a purity of 98%, the crystallinity of PETCO PET Beads-derived BDC is very close to that of the commercial BDC, as evidenced by the similar acid number of 448 mg NaOH/g against 450 mg NaOH/g. As indicated by the XRD patterns, the crystallinity of the Brown PET Bottles derived-BDC sample is similar to that of the PET Food Trays-derived BDC sample, and the containing acid numbers are also nearly the same. In contrast, the crystallinity of the Green PET Bottles-derived BDC is the lowest, with an acid number of only 192 mg NaOH/g. It can be seen from Figure 5b that the purities of the different BDC samples are slightly different.

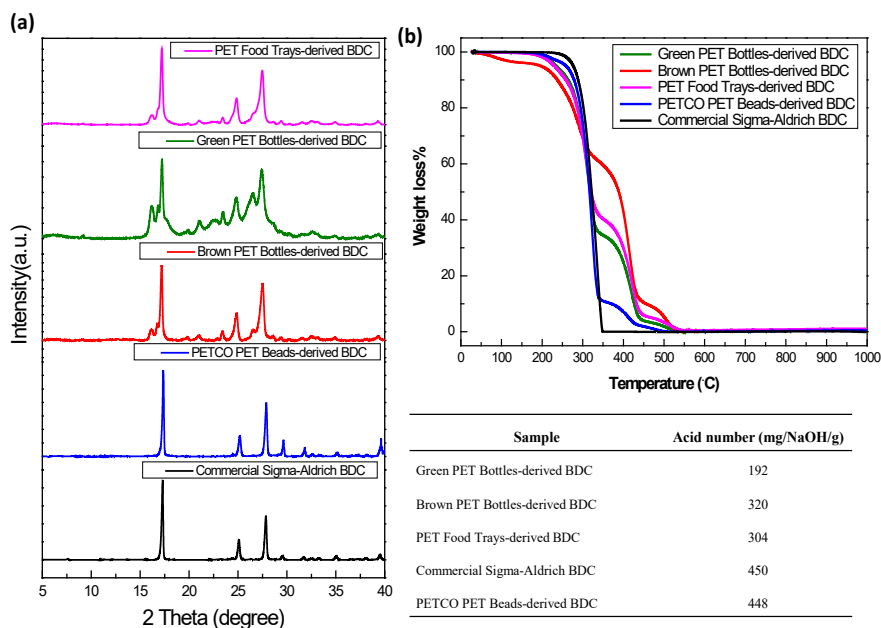


Figure 5: (a) PXRD patterns, and (b) TGA curves of the BDC samples derived from different PET sources. Right bottom Table: the titration results of the acid numbers from different BDC samples

2.6. Technical feasibility of converting coloured waste PET and food trays-derived BDC to MOF UiO-66(Zr)

Several characteristic reflection signals in Figure 6a confirmed the successful synthesis of MOF UiO-66(Zr) from different PET-derived BDC when compared to the simulated XRD pattern. The relative crystallinities of the obtained MOF UiO-66(Zr) samples are comparable to that from commercial BDC feedstock from Sigma-Aldrich. However, the Zr-MOF sample synthesised from Green PET Bottles-derived BDC shows the lowest relative crystallinity. The scanning electron microscope (SEM) images in Figure 6b-f show the quite different morphologies of the obtained MOF UiO-66(Zr) samples.

Figure 7a shows the thermogravimetric analysis (TGA) properties of the obtained MOF UiO-66(Zr) prepared from different BDC sources. The N_2 and H_2 sorption isotherms presented in Figure 7b, respectively, indicate that all the PET-derived MOF UiO-66(Zr) materials have relatively lower N_2 and H_2 adsorption levels, but the obtained values (as listed at the bottom of Figure 7b) are comparable to that from the commercial feedstock as well as other previously developed MOF UiO-66(Zr) materials. As MOF

UiO-66(Zr) samples were also synthesised from the coloured PET bottles-derived BDC, where the effects of additives and colourants should be taken into account on the textural properties of the prepared MOF UiO-66(Zr). The experimental results suggested that the MOF UiO-66(Zr) samples from the clear PET food trays-derived BDC have lower textural properties than those from a clear PET beads-derived BDC. The reason could be the effects of additives and colourants from the green and brown coloured bottles.

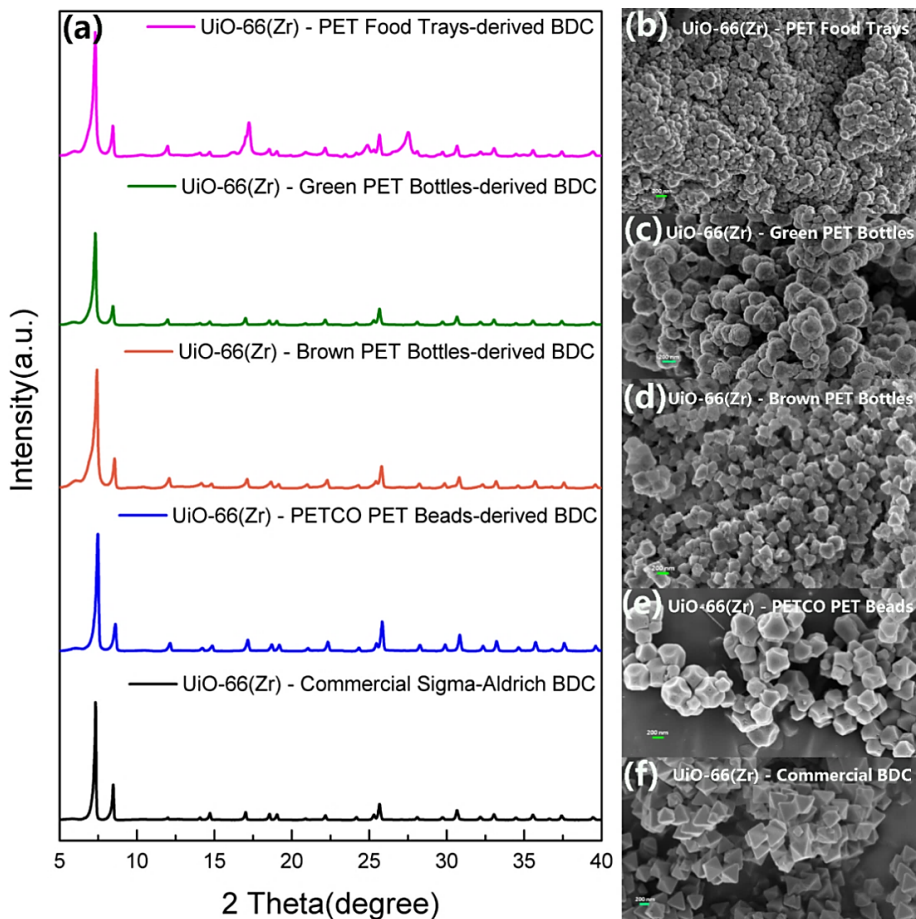


Figure 6: (a) XRD patterns and (b-f) SEM images of the Zr-MOF samples prepared from different BDC sources

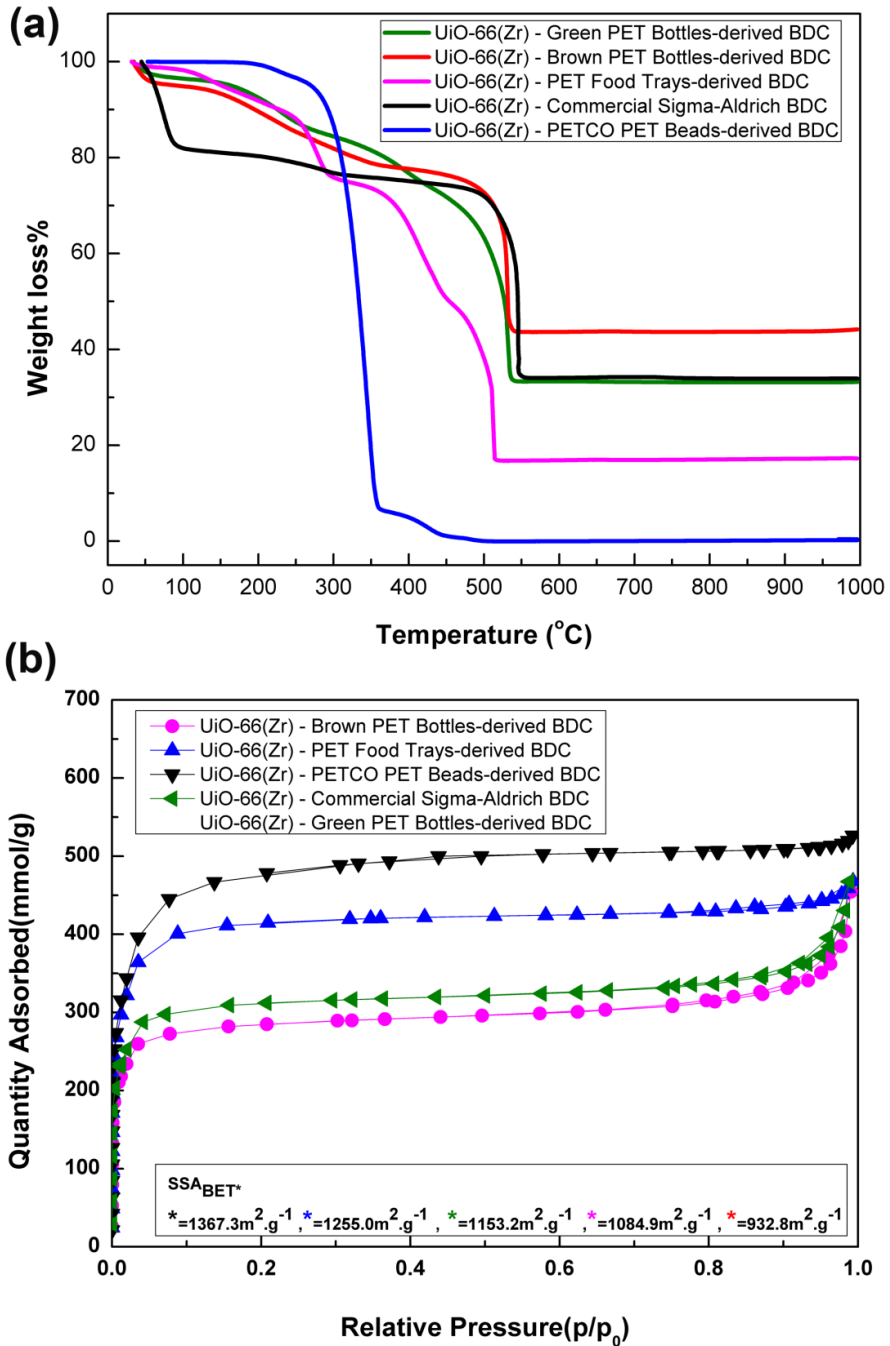


Figure 7: (a) TGA curves and (b) N₂ sorption of the MOF UiO-66(Zr) samples prepared from different BDC sources. Bottom: BET and H₂ uptake results of the prepared MOF UiO-66(Zr) samples

2.7. Economic appraisal and commercial viability on the business model: converting coloured waste PET and food trays to MOFs

2.7.1 Costing factors and assumptions in KG-scale

The cost results of KG-scale depolymerisation of coloured bottles and PET food trays are presented in Table 3.

The cost was calculated based on the respective materials, process conditions, and times presented in Figure 4. For the KG-scale experiments on depolymerisation of the waste-coloured bottles and food trays, the samples were 'home collected' by the researchers. The costs of chemicals were calculated based on the usage and prices available on the Sigma-Aldrich website. The cost of electricity was calculated based on the Eskom charges of R1.94/kWh. The cost of labour was calculated based on the rate of a PhD candidate working at the CSIR. The market price for waste PET-derived BDC was referred to as the commercial BDC price. In Table 3, material costs reflect the costs of raw materials (recycled PET, solvents and additives), while manufacturing costs reflect the cost of machinery amortised over equipment lifetime as well as process energy, utilities, labour, and facility costs. As seen, the machinery costs dominate the total costs for the KG-scale depolymerisation of coloured bottles and PET food trays to produce BDC. Apparently, the profitability of this case is very low, and there is potential to lower the manufacturing costs by scaling-up the process. The cost results of KG-scale MOF UiO-66(Zr) production from waste PET-derived BDC trays are presented in Table 4.

MOF UiO-66(Zr) product serves as a representative MOF to illustrate cost trends. Costs are divided between materials and manufacturing costs and are further segregated by the processing steps shown in Figure 5. The cost was calculated based on the respective materials, process conditions, and times.

For the KG-scale experiments of Zr-MOF production, the BDC acid was derived from the recycled coloured bottles and food trays in the previous step. The costs of chemicals were calculated based on the usage and prices available on the Sigma-Aldrich website (on 25 March 2019). The cost of electricity was calculated based on the Eskom charges of R1.94/kWh. The cost of labour was calculated based on the rate of estimated labour h (based on an hourly rate of a salary of R500k annually) for three technicians requested. A levelised price of ZAR198240/kg was taken by averaging the prices of several available MOFs products in Table 5. However, a late quotation on MOF UiO-66(Zr) was received from Strem Chemicals Inc. at ZAR283, 638/kg, and the formal quotation sheet was attached in Annexures (II). In Table 4, the material costs reflect the costs

Table 3: Cost calculations of KG-scale depolymerisation of coloured bottles and PET food trays

Process steps	Facilities		Raw materials		Cost of electricity (ZAR)*	Cost of labour (ZAR)#	Sub-Total (ZAR)
	Description	Cost (ZAR)	Description	Cost (ZAR)&			
Recycling of coloured bottles & PET food trays	-	-	-	-	-	200	200
Crush the recycled raw PET materials 0.5 h/batch	Crusher	32,000	-	-	4	65	32,069
Reactant preparation 0.5 h/batch	-	-	D.I.H ₂ O	100	-	65	165
Depolymerisation 8 - 20 h/batch	5L reactor	200,000	Ethylene glycol	368	14	1,040	202,665
			D.I.H ₂ O	100	103	1,040	
Filtration & Washing, 3.5 h/batch	Overhead stirrer	11 264	D.I.H ₂ O	100	0.48	455	29,219
	Vacuum pump	14 500	Filter paper	2900	0.40		
Oven drying 8 - 12 h/batch	Oven	15,000	-	-	14	1040	16,054
Yield of BDC (kg)							
Market Price (ZAR/kg)							
1							
2,000							

Cost as per Sigma Aldrich website; *Calculations based on Eskom charges = R1.94/kWh; #Calculations based on CSIR's PhD Candidate rates = R130/h

Table 4: Cost calculations of KG-scale MOF UiO-66(Zr) production from waste PET-derived BDC

Process steps	Facilities		Raw materials		Cost of electricity (ZAR)	Cost of labour (ZAR)	Sub-Total (ZAR)
	Description	Cost (ZAR)	Description	Cost (ZAR)			
Reactant preparation, 1 h/ batch	Sonicator bath	9,430	D.I.H ₂ O	100	13	130	9,673
	Hot plate/ Magnetic stirrer	2,000	ZrCl ₄	536	8	650	
PET-derived BDC			2,000				
Formic acid			1,614				
Precipitation, 5 h/batch	5L reactor	200,000	DMF	2,960	64	650	
			Conical centrifuge tubes	50			
Filtration & Washing, 5 h/ batch	Centrifuge	68,000	D.I.H ₂ O	100	8	650	72,173
			Paraffin liquid	99			
Oven drying 8-12 h/batch	Oven	15,000	Ethanol	1200	14	1,040	16,054
			-	-			
Yield of Zr-MOF (kg)							1
Market Price (ZAR/kg)*							198,240

*Average price took from Sigma-Aldrich website on MOFs products.

of raw materials (salts, linkers, and solvents), while manufacturing costs reflect the cost of machinery amortised over equipment lifetime as well as process energy, utilities, labour, and facility costs. Still, the machinery costs dominate the entire manufacturing costs for the solvothermal synthesis of the representative MOF UiO-66(Zr). The profitability for this case still reflects negative, and the potential to make a turnover can be expected from the scale-up of the manufacturing process of the representative MOF UiO-66(Zr). This would offer potential cost reductions through the advantage of economies of scale as well as removing a layer of cost mark-up. Material costs also contribute more to the total production cost than manufacturing costs for all cases.

2.7.2. Costing factors and assumptions in 10KG-scale

Table 6 lists the cost calculations of semi-industrial-scale (10KG/day) depolymerisation of coloured bottles and PET food trays, and the following assumptions have been considered: the recycled PET beads will be purchased directly from the local PET recycling companies such as PETCO at approximately R20/ton. Given a depolymerisation rate of 85% and 5% powder loss during processing, to produce 10KG of BDC, 12.5KG recycled PET will be required. As the recycled PET can be delivered in the bead form, there is no need to crush in the laboratory anymore. The size of the reactor will be scaled-up to 50 L, and the prices of the reactants will be at 50% discount compared to the 1KG-scale experiments. The energy efficiency at 10KG-scale production can be improved by 50% compared to the 1KG-scale. The cost of labour will be paid annually at ZAR600,000 in total. When coming to the semi-industrial-scale operation, three employees will be hired, including one for marketing and Sales, a technician, and an accountant with annual salary packages of R310399, R261641, and R282413, respectively.

Table 7 lists the cost calculations of industrial-scale (10KG/day) MOF UiO-66(Zr) production from waste PET-derived BDC, and the following assumptions have been considered: the BDC acid linker will use the waste PET-derived BDC products. A conversion rate of 85% and 5% powder loss during processing was considered to produce 10KG of MOF UiO-66(Zr). The size of the reactor will be scaled-up to 50 L, and the prices of the reactants will be at 50% discount compared to the 1KG-scale experiments. The energy efficiency at 10KG-scale MOF UiO-66(Zr) production can be improved by 50% compared to the 1KG-scale. Regarding the industrial-scale operation, three employees will be hired, including one for marketing and sales, a technician and an accountant with annual salary packages of R310399, R261641, and R282413, respectively.

Table 5: Prices of the example MOFs products from Sigma-Aldrich.

Supplier	MOFs	Synonym	Empirical formula	Price (ZAR/ KG)	Note
Sigma-Aldrich	Basolite® Z1200	2-Methylimidazole zinc salt, ZIF-8	$C_8H_{10}N_4Zn$	186,000	
Sigma-Aldrich	Basolite® F300	Fe-BTC, Iron 1,3,5-benzenetricarboxylate	$C_9H_3FeO_6$	117,600	
Sigma-Aldrich	Basolite® A100	Aluminum terephthalate, MIL- 53(Al)	$C_8H_5AlO_5$	174,000	
Sigma-Aldrich	Basolite® C 300	Copper benzene-1,3,5- tricarboxylate, Cu-BTC MOF, HKUST-1	$C_{18}H_6Cu_3O_{12}$	297,600	
Sigma-Aldrich	Basolite® Z377	MOF 177	$C_{54}H_{30}O_{13}Zn_4$	216,000	
Strem Chemicals	Zr-MOF	UiO-66(Zr)	$Zr_6O_4(OH)_4(BDC)_6$	283,638*	USD20000/KG

*The exchange rate was: 1 USD = ZAR14.1815 on 04/04/2019.

Table 6: Cost calculations of semi industrial-scale (10KG/day) depolymerisation of coloured bottles and PET food trays

Process steps	Facilities		Raw materials		Cost of electricity (ZAR)*	Cost of labour (ZAR)#	Sub-Total (ZAR)
	Description	Cost (ZAR)	Description	Cost (ZAR)&			
Recycling of coloured bottles & PET food trays	-	-	-	-	-	200	200
Crush the recycled raw PET materials 0.5 h/batch	Crusher	0	-	-	0	0	0
Reactant preparation 0.5 h/batch	-	-	D.I.H2O	100	-	82	182
Depolymerisation 8 h/batch	50L reactor	500,000	E.G.	368	14	1308	501893
			D.I.H2O	100	103		
Filtration & Washing, 3.5 h/batch	Presser	68,000	Filtration	50	1	573	68724
			D.I.H2O	100			
Oven drying 8 - 12 h/batch	Oven	15,000	Paraffin liquid	99	5	0	15014
			-	-			
Packaging of BDC products	-	-	Plastic bags	20	-	130	150
Yield of BDC (KG)							
Market Price (ZAR/KG)							
&Cost as per Sigma Aldrich website; *Calculations based on Eskom charges = R1.94/kWh; #Calculations based on CSIR's PhD Candidate rates = R130/h							
2,000							

Table 7: Cost calculations of semi- industrial -scale (10KG/day) MOF UiO-66(Zr) production from waste PET-derived BDC

Process steps	Facilities		Raw materials		Cost of electricity (ZAR)	Cost of labour (ZAR)	Sub-Total (ZAR)
	Description	Cost (ZAR)	Description	Cost (ZAR)			
Reactant preparation, 1 h/ batch	Sonicator bath	9,430	D.I H ₂ O	100	13	163.5	9,673
	Stirrer/ heating block	2,000	ZrCl ₄	536	8	1308	
PET-derived BDC			2,000				
50L reactor			500,000	Formic acid			1,614
	DMF	2,960					
Filtration & Washing, 5 h/ batch	Vacuum filtration system	68,000	Conical centrifuge tubes	50	1	817.5	70,973
			D.I H ₂ O	100			
			Paraffin liquid	99			
Oven drying 8 -12 h/batch	Oven	15,000	-	-	14	0	16,054
Yield of Zr-MOF (KG)							
Market Price (ZAR/KG)*							
							10
							198,240

2.7.3. Financial Viability

The theory of financial viability measures two outputs, namely;

- Financial profitability and solvency of the planned investments
- The viability of a new project or enterprise.

A sound investment is one that generates enough revenue to meet all financial obligations on a timely basis and command an adequate level of working capital for continued operations. Usually, it implies the ability to earn a reasonable rate of return on capital employed. The extent of the success of a project is determined by a review of its financial structure, liquidity trends, and profitability over time. For a new project, the main objective of the analysis is to demonstrate that the financial cash flows expected to be generated are attractive to prospective investors, encouraging them to contribute equity funds to the particular project rather than to employ them elsewhere. Contributing equity investments to a project lessens the burden of raising project finance. Development financial institutions generally fund projects that are co-financed through an equity investment. The analyses on which investment decisions are based are driven by the net present value (NPV) and the internal rate of return (IRR).

$$NPV = \sum_{t=0}^n \frac{Rt}{(1+i)^t}$$

The NPV method consists of discounting all future cash flows to the present value by means of some appropriate rate of interest. The rate of interest to be used should reflect the minimum rate of return which is acceptable to the firm for a given investment. It works on the simple but fundamental principle that an investment is worth undertaking only if the present value of the cash inflows is at least equal to, if not greater than the present value of the cash outflows arising from an investment. To put it another way, companies should make investments in projects with a zero or positive net present value. The calculated NPV for this study is shown in Table 8.

Table 8: Net Present Value for the MOFs project

Year	2019	2020	2021	2022	2023	2024	2025	2026	2027	2028	2029
Index	0	1	2	3	4	5	6	7	8	9	10
Subsidies	0										
Equity	130439										
Private Withdrawal											
Loan	521755										
Total Investment Payout	652194										
CASH POSITION	236400	1286315	998916	1051663	1106213	1166277	1229912	1303203	1391078	1505309	1670124
Cash position cumulated; negative values compensated by current account	236400	1049915	2048831	3099895	4206108	5371385	6601297	7904500	9295578	10800887	12471012
Cash Flow after Dept Service, after tax	236400	1266315	998916	1051063	1106213	1165277	1229912	1303203	1391078	1505309	1670124
Cash Flow after Dept, before tax	236400	1641502	1373085	1445148	1521316	1602803	1691814	1792452	1912590	2067839	2308548
Equity	130439										
Free Cash - Flow (before tax) to Equity	366839	1641502	1373085	1445148	1521316	1602803	1691814	1792452	1912590	2067839	2308548

$$IRR = NPV = \sum_{t=1}^T \frac{C_t}{(1+r)^t} - C_0 = 0$$

An investor would be interested in the IRR after tax which he would compare with returns from alternative investment opportunities at similar risk levels before committing funds to a particular project. If the IRR after the tax of a project is greater than the cost of capital, it can be concluded that the project is financially viable. Besides, the production machinery is to recover funds and the terms of repayment loans have to be adjusted to take any cash flow requirements. IRR does not provide any information on the requirements for phasing short-term bridging finance or grace periods on the loan required to accommodate delayed benefits. As shown in Table 9, the calculated IRR for producing MOFs in this study is estimated at 4.35% with the assumption of 5.5 annual increases. An annual increase cost of 7.5% on the products offer an IRR of 4.49%.

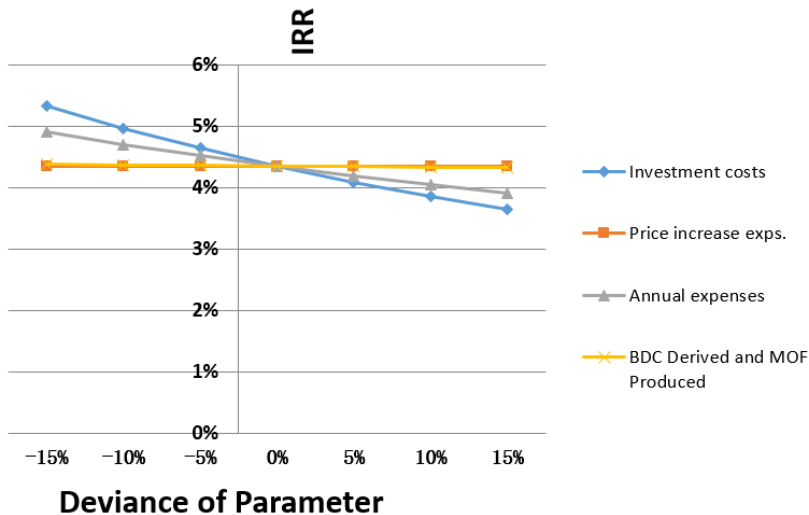


Figure 8: Estimated internal rate of return

Figure 8 shows the estimated internal rate of return. The investment expenditures, including the incremental working capital needs of a project/enterprise need to be met on a well-timed basis with a minimum cost. In setting up the financing plan, consideration for the most effective capital cost requirement is decided in order to satisfy the financial requirements of the business. These requirements are carefully determined by budgeting forecasts as a mechanism to avoid extreme expenditure and over- or under-capitalisation. In a continuing business where a budgetary control

system is in operation, the forecasting of requirements presents no difficulty. For new projects, more has to be left to estimates. While costs can be estimated, the generated revenue is solely dependent on demand, which, in turn, is influenced by a number of economic indicators, such as the domestic economic performance that is independent of any business operations. In both new and existing businesses, funds may be raised from external sources but in a continuing business, internal resources can be mobilised by reinvesting profits.

Certain factors need to be taken into account when external financing is considered. These include, a Memorandum of Agreement (MoA) that might be in place before a project funding is concluded, the projected financial condition and performance of the investment, and the inherent risk of business operations. The nature of the need for funds influences the type of financing that should be used. If there is a seasonal component to the business, it offers itself to short-term financing and bank loans in particular. The financial condition and performance of the plant will influence the type of financing that should be utilised. The larger the liquidity position of a plant, the stronger the overall financial condition and the greater the profitability of the firm. On the contrary, the basic business risk faced by any plant has an important bearing on the type of financing that should be used. The desirable debt financing usually becomes less relative to equity financing when the business risk is greater. Equity financing is safer in that there is no contractual obligation to pay interest and repay the principal as there is with a loan.

2.7.4. The financial and economic analysis

Two ways are used to assess the desirability of undertaking a project: financial and economic analysis. These primary tools are used for carrying out financial and economic analyses, and both types of analyses are required for project screening and selection. However, there is a difference in application since financial analysis deals with the cost and benefit flows from the point of view of a plant's financial viability while economic analysis deals with the costs and benefits to society. In this instance, PET waste would have other climate and social negative impacts. Economic analysis, in this regard, takes a broader view of costs and benefits as well as financial analysis. The methods, nonetheless, differ in several important ways. An enterprise is interested in financial profit and the stability of that profit, while society or government is concerned with much wider objectives such as waste management new economic opportunities, poverty alleviation, and resulting net benefits to society as a whole. Therefore, the objectives of the two types of analysis are different. The cost-benefit analysis for the purposes of this study has not

been quantified. Only a financial analysis for a project plant that would produce MOFs has been considered. This means that the cost of landfilling PET waste has not been measured and the potential incomes stream for climate change mitigation have not been calculated.

2.7.5. MOFs financial modelling results

Production costs have been evaluated by adding up fixed costs (depreciation rates), operating and maintenance (O&M), and variable operating and maintenance (VOMs). Data utilised have been collected from literature sources and calculations for the infrastructure energy and water usage have been estimates using utility tariffs, respectively. The estimation of capital investment cost comprised seven parameters that represent the total cost of the infrastructure. The combined parameters for the balance sheet are as follows:

- Crusher
- Overhead stirrer
- Vacuum Pump
- Oven
- Sonicator bath
- Hot plate/Magnetic stirrer
- Centrifuge

These assets have a total capital cost of **R652 194**. The estimated revenue from a 10kg MOF production is **R1 585 920** with additional revenue from PET-derived BDC that is approximately **R2000** per kg. The operations and maintenance costs have been considered as a percentage of capital cost that is shown in Figure 9. The variable fixed operations and maintenance have been represented by 2.5% of the capital cost.

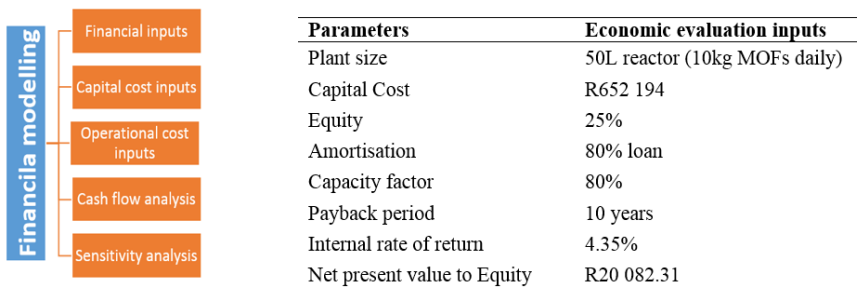


Figure 9: Modelling input and results

The calculated financial results from the data shown in Figure 10 are based on a yearly production of MOFs and the derived BDC that generates a total revenue of **R1 601 920**. The cost of the depreciation rate has an impact

of **R65 2193** per annum for MOFs produced. Figure 11 shows the different parameters utilised into the overall MOFs production costs. Under the above assumption, the production cost is estimated to be **R270 286** for 10kg of MOFs produced.

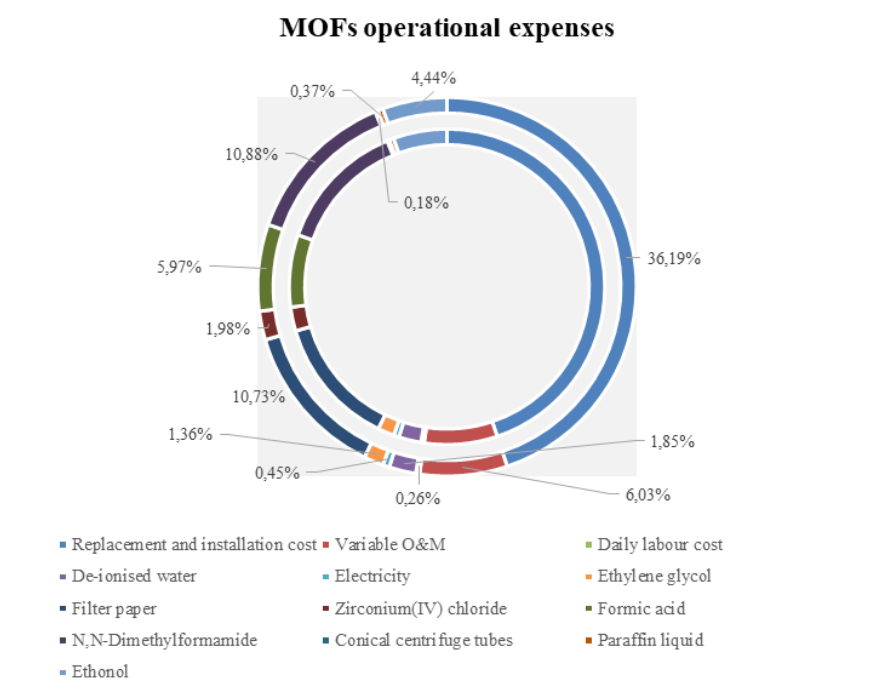


Figure 10: MOFs operational expenses

The depreciation of this evaluation was evaluated over ten years for this plant, while the amortisation estimates have been calculated over a duration of 11 years with a 10% interest rate. This is equivalent to the South African lending rate. The operational expenses show that about 36% of the OPEX cost is used for replacement parts and this is followed by electricity and N,N-Dimethylformamide costs that are about 11% of the operational costs.

Table 10: Revenue generated

Revenue Parameters	
MOFs UiO-66(Zr)	R1 585 920
PET-derived BDC	R16 000

The revenue generated per annum is shown in Table 10 while escalation rates are shown in Figure 11. The revenues from produced MOFs show an overall escalation rate of approximately 18% over the lifespan of the projects. The investment cost slope is normal and corresponds with initial investment costs. The operational costs increase with an estimate of 10% over the project life cycle. This is confirmed on the annual expenses slope shown in Figure 11.

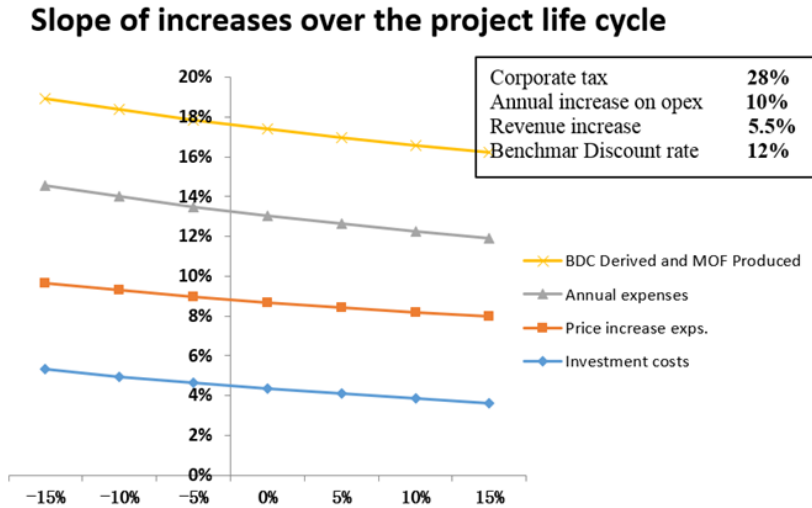


Figure 11: Project costs escalation rate slopes

2.7.6. Commercial viability

Investing in MOFs will generate roughly a 5% IRR on a production capacity of 10kg daily. Given the fact that these results are positive at a small-scale, it is therefore recommended that this investment should proceed. The environmental and opportunity cost that is avoided has not been considered in the financial analysis. This can further strengthen the revenue side of this production. While a return of 5% is not the most attractive, the PET waste that would be redirected to this production contributes to the South African waste management strategy and climate change objectives. In addition, the South African government bond of 10 years yields a return of 8.52% return and this initiative is competitiveness with a 5% IRR.

2.8. Risk assessment of converting of coloured waste PET and food trays to MOFs

Table 11. Risks and risk mitigation

Risk	Risk mitigation
Barriers to entry, that is, highly technical expertise on MOFs materials	Employ technical expertise
High set-up costs for a MOF producing facility	Partner with other industries
Engineering knowledge towards the scaling-up of MOFs production	Involve quality chemical engineers
Usage of organic solvents, that is, DMF	Recycle and reuse the organic solvents
Handling and disposal of the hazardous substances	Follow the standard handling and disposal arrangements

As listed in Table 11, the overall assessment of risks and strategies to minimise those risks are provided. The safety, health, and environmental aspects with regards to the handling and disposal of the hazardous substances can be arranged in compliance with national/international standards. There are no other clearances and objection certificates required.

3. Conclusions

This study focused on the coloured bottles and food PET trays as they have been identified as the problematic stream from the current waste PET recycling industries in South Africa.

Firstly, the results of this study revealed the technical feasibilities of lab-scale and KG-scale depolymerisation of coloured bottles and PET food trays to BDC were quite high. The lab-scale and KG-scale production from coloured bottles and PET food trays-derived BDC have also proved technically feasible. The production costs can be significantly reduced at an industrially relevant scale. Given the different BDC-based MOFs, the selection of a manufacturing method will be determined by the suitability of a method for a particular MOF, and it is recognised that a fully continuous synthesis operation has an opportunity to further bring down the production costs. For direct comparison and extension from laboratory-scale, the scope of this analysis was based on a KG-scale batch synthesis with certain steps that could be implemented with a pseudo-continuous operation such as drying and shaping. A future study should

be conducted to evaluate each process step to determine the most suitable approach between continuous and batch processing since certain batch process operations may still be optimal. As solvent cost is a significant cost contributor, high solvent recycle rates ($\geq 90\%$) are crucial to achieving moderate to high-cost projections made within the analysis for solvothermal syntheses. This will be particularly important for MOFs that may not be amenable to aqueous or mechanochemical syntheses. Studies to minimise solvent usage are also recommended. Similarly, a reduction of material costs and sizes of reactors could also contribute in the reduction of MOF manufacturing costs.

Secondly, through the analysis of the built-up financial model, the results of economic appraisal and commercial viability showed that investing in MOFs will generate roughly a 5% IRR on a production capacity of 10kg daily. Given the fact that these results are positive at a small-scale, it is therefore recommended that this investment should proceed. The environmental and opportunity cost that is avoided has not been considered in the financial analysis. This can further strengthen the revenue side of this production. While a return of 5% is not the most attractive, the PET waste that would be redirected to this production contributes to the South African waste management strategy and climate change objectives. In addition, the South African government bond of 10 years yields a return of 8.52% return and this initiative is competitiveness with a 5% IRR.

Finally, the results of this analysis are expected to be generally valid for other BDC-based MOFs from other waste PET materials.

References

- Al-tamimi, R.K., Khalaf, M.N., Sabri, M., Sabri, L. (2011) Postconsumer poly(ethylene terephthalate) de-polymerization by waste of battery acid hydrolysis. *J Mater Environ Sci*, 2, 88.
- Awaja, F. and Pavel, D. (2005) Recycling of PET. *Euro. Poly. J.*, 41, 1453. <https://doi.org/10.1016/j.eurpolymj.2005.02.005>
- Chen, J.Y., Shen, K., Li, Y.W. (2017) Greening the processes of metal-organic framework synthesis and their use in sustainable catalysis. *ChemSusChem*, 10, 3165. <https://doi.org/10.1002/cssc.201700748>
- Deleu, W.P.R., Stassen, I., Jonckheere, D., Ameloot, R., De Vos, D.E. (2016) Waste PET (bottles) as Resource or Substrate for MOF Synthesis. *J. Mater. Chem. A*, 4, 9519. <https://doi.org/10.1039/C6TA02381A>

- DeSantis, D., Mason, J.A., James, B.D., Houchins, C., Long, J.R., Veenstra, M. (2017) Techno-economic analysis of metal-organic frameworks for hydrogen and natural gas storage. *Energy Fuels*, 31, 2024. <https://doi.org/10.1021/acs.energyfuels.6b02510>
- Dyosiba, X., Ren, J., Musyoka, N.M., Langmi, H.W., Mathe, M., Onyango, M.S. (2016) Preparation of value-added metal-organic frameworks (MOFs) using waste PET bottles as source of acid linker. *Sustainable Materials and Technologies*, 10, 10. <https://doi.org/10.1016/j.susmat.2016.10.001>
- Huang, Y.T., Lai, Y.L., Lin, C.H., Wang, S.L. (2011) Direct use of waste PET as unfailing source of organic reagents in the synthesis of intrinsic white/yellow luminescent nanoporous zincophosphates. *Green Chem*, 13, 2000. <https://doi.org/10.1039/c1gc15427c>
- Jacoby, M. (2008) For metal-organic frameworks, lab-scale research is brisk as commercialization begins. *Chem Eng News*, 86:13. <https://doi.org/10.1021/cen-v086n038.p013a>
- Julien, P.A., Mottillo, C., Friščić, T. (2017) Metal-organic frameworks meet scalable and sustainable synthesis. *Green Chem.*, 19, 2729. <https://doi.org/10.1039/C7GC01078H>
- Lo, S., Raja, D.S., Chen, C., Kang, Y., Chen, J., Lin, C. (2016) Waste polyethylene terephthalate (PET) materials as sustainable precursors for the synthesis of nanoporous MOFs, MIL-47, MIL-53(Cr, Al, Ga) and MIL-101(Cr). *Dalton. Trans.*, 45, 9565. <https://doi.org/10.1039/C6DT01282E>
- Musyoka, N.M., Ren, J., Langmi, H.W., North, B.C., Mathe, M., Bessarabov, D. (2017) Synthesis of rGO/Zr-MOF composite for hydrogen storage application. *J. Alloys Compd.*, 724, 450. <https://doi.org/10.1016/j.jallcom.2017.07.040>
- Quaresma, S., André, V., Fernandes, A., Teresa Duarte, M. (2017) Mechanochemistry-A green synthetic methodology leading to metallodrugs, metallopharmaceuticals and bio-inspired metal-organic frameworks. *Inorganica Chimica Acta*, 455, 309. <https://doi.org/10.1016/j.ica.2016.09.033>
- Ren, J., Dyosiba, X., Musyoka, N.M., Langmi, H.W., Mathe, M., Liao, S. (2017) Review on the current practices and efforts towards pilot-scale production of metal-organic frameworks (MOFs). *Coord. Chem. Rev.*, 352, 187. <https://doi.org/10.1016/j.ccr.2017.09.005>

- Ren, J., Dyosiba, X., Musyoka, N.M., Langmi, H.W., North, B.C., Mathe, M. (2016) Green synthesis of chromium-based metal-organic framework (Cr-MOF) from waste polyethylene terephthalate (PET) bottles for hydrogen storage applications. *Inter. J. Hydrogen Energy*, 41, 18141. <https://doi.org/10.1016/j.ijhydene.2016.08.040>
- Ren, J., Langmi, H.W., North, B.C., Mathe, M. (2015) Review on processing of metal-organic framework (MOF) materials towards system integration for hydrogen storage. *Int. J. Energy Research*, 2015b, 39, 607. <https://doi.org/10.1002/er.3255>
- Ren, J., Musyoka, N.M., Langmi, H.W., Mathe, M., Liao, S. (2017) Current research trends and perspectives on materials-based hydrogen storage solutions: a critical review. *Int. J. Hydrogen Energy*, 42, 289. <https://doi.org/10.1016/j.ijhydene.2016.11.195>
- Ren, J., Musyoka, N.M., Langmi, H.W., Mathe, M., Liao, S., Pang, W. (2017) Structural defects in metal-organic frameworks (MOFs): Formation, detection and control towards practices of interests. *Coord. Chem. Rev.*, 349, 169. <https://doi.org/10.1016/j.ccr.2017.08.017>
- Ren, J., Musyoka, N.M., Langmi, H.W., Swartbooi, A., North, B.C., Mathe, M. (2015) A more efficient way to shape metal-organic framework (MOF) powder materials for hydrogen storage applications. *Int. J. Hydrogen Energy*, 40, 4617. <https://doi.org/10.1016/j.ijhydene.2015.02.011>
- Ren, J. and North, B.C. (2014) Shaping porous materials for hydrogen storage applications: a review. *J. Technol. Innov. Renew. Energy*, 3, 12. <https://doi.org/10.6000/1929-6002.2014.03.013>
- Rubio-Martinez, M., Avci-Camur, C., Thornton, A.W., Imaz, I., MasPOCH, D., Hill, M.R. (2017) New synthetic routes towards MOF production at scale. *Chem. Soc. Rev.*, 46, 3453. <https://doi.org/10.1039/C7CS00109F>
- Wang, S., Wang, C., Wang, H., Chen, X., Wang, S. (2015) Sodium titanium tris(glycolate) as a catalyst for the chemical recycling of poly(ethylene terephthalate) via glycolysis and repolycondensation. *Polym. Degrad. Stab.*, 114, 105. <https://doi.org/10.1016/j.polymdegradstab.2015.02.006>
- Welle, F. (2011) Twenty years of PET bottle to bottle recycling—An overview. *Resources, Conservation and Recycling* 55, 865. <https://doi.org/10.1016/j.resconrec.2011.04.009>
- Zhang, J.F., White, G.B., Ryan, M.D., Hunt, A.J., Katz, M.J. (2016) Dihydrolevoglucosenone (Cyrene) as a green alternative to N,N-Dimethylformamide (DMF) in MOF synthesis. *ACS Sustainable Chem. Eng.*, 4, 7186. <https://doi.org/10.1021/acssuschemeng.6b02115>

